EUR 5294 e

COMMISSION OF THE EUROPEAN COMMUNITIES

VIBRATION AND NOISE ANALYSIS IN NUCLEAR POWER PLANTS

1974

Report prepared by

Allianz-Zentrum für Technik Gmbh (AZT), Ismaning — Deutschland

Electricité de France (EdF), Paris — France
Ente Nazionale per l'Energia Elettrica (ENEL), Roma — Italia
Laboratoire belge de l'Industrie Electrique (LABORELEC), Linkebeek — Belgique
Lehrstuhl und Institut für Kerntechnik, TU, Hannover — Deutschland
Lehrstuhl für Reaktordynamik und Reaktorsicherheit, T.U. München — Deutschland

EURATOM Contract No. 47-72-12 ECIC

LEGAL NOTICE

This document was prepared under the sponsorship of the Commission of the European Communities.

Neither the Commission of the European Communities, its contractors nor any person acting on their behalf:

make any warranty or representation, express or implied, with respect to the accuracy, completeness, or usefulness of the information contained in this document, or that the use of any information, apparatus, method or process disclosed in this document may not infringe privately owned rights; or

assume any liability with respect to the use of, or for damages resulting from the use of any information, apparatus, method or process disclosed in this document.

This report is on sale at the addresses listed on cover page 4

at the price of B.Fr. 600,—

Commission of the
European Communities
D.G. XIII - C.I.D.
29, rue Aldringen
L u x e m b o u r g

December 1974

This document was reproduced on the basis of the best available copy.

EUR 5294 e

VIBRATION AND NOISE ANALYSIS IN NUCLEAR POWER PLANTS

Commission of the European Communities
Report prepared by
Allianz-Zentrum für Technik GmbH (AZT) — Ismaning (Deutschland)
Électricité de France (EdF) — Paris (France)
Ente Nazionale per l'Energia Elettrica (ENEL) — Roma (Italia)
Laboratoire belge de l'Industrie Électrique (LABORELEC) — Linkebeek (Belgique)
Lehrstuhl und Institut für Kerntechnik, TU Hannover — Deutschland
Lehrstuhl für Reaktordynamik und Reaktorsicherheit, TU München — Deutschland
Contract Euratom No. 047-72-12 ECIC
Luxembourg, December 1974 - 288 Pages - 161 Figures - B.Fr. 600.—

Results of the investigations on noise and vibration analysis are presented as a follow-up study of the work published in "On-load Surveillance of Nuclear Power Plant Components by Noise and Vibration Analysis" EUR 5036 e.

EUR 5294 e

VIBRATION AND NOISE ANALYSIS IN NUCLEAR POWER PLANTS

Commission of the European Communities
Report prepared by
Allianz-Zentrum für Technik GmbH (AZT) — Ismaning (Deutschland)
Électricité de France (EdF) — Paris (France)
Ente Nazionale per l'Energia Elettrica (ENEL) — Roma (Italia)
Laboratoire belge de l'Industrie Électrique (LABORELEC) — Linkebeek (Belgique)
Lehrstuhl und Institut für Kerntechnik, TU Hannover — Deutschland
Lehrstuhl für Reaktordynamik und Reaktorsicherheit, TU München — Deutschland
Contract Euratom No. 047-72-12 ECIC
Luxembourg, December 1974 - 288 Pages - 161 Figures - B.Fr. 600.—

Results of the investigations on noise and vibration analysis are presented as a follow-up study of the work published in "On-load Surveillance of Nuclear Power Plant Components by Noise and Vibration Analysis" EUR 5036 e.

EUR 5294 e

VIBRATION AND NOISE ANALYSIS IN NUCLEAR POWER PLANTS

Commission of the European Communities
Report prepared by
Allianz-Zentrum für Technik GmbH (AZT) — Ismaning (Deutschland)
Électricité de France (EdF) — Paris (France)
Ente Nazionale per l'Energia Elettrica (ENEL) — Roma (Italia)
Laboratoire belge de l'Industrie Électrique (LABORELEC) — Linkebeek (Belgique)
Lehrstuhl und Institut für Kerntechnik, TU Hannover — Deutschland
Lehrstuhl für Reaktordynamik und Reaktorsicherheit, TU München — Deutschland
Contract Euratom No. 047-72-12 ECIC
Luxembourg, December 1974 - 288 Pages - 161 Figures - B.Fr. 600.—

Results of the investigations on noise and vibration analysis are presented as a follow-up study of the work published in "On-load Surveillance of Nuclear Power Plant Components by Noise and Vibration Analysis" EUR 5036 e.

The state of the art in on-load surveillance techniques of light water reactors is given by extending the preceding studies to investigations of boiling water reactors and by summarizing the latest results of pressurized water reactors, the basis being experimental and theoretical work performed by the different organizations involved in preparing this report. Finally, some developments with respect to measurement- and identification methods are discussed.

The state of the art in on-load surveillance techniques of light water reactors is given by extending the preceding studies to investigations of boiling water reactors and by summarizing the latest results of pressurized water reactors, the basis being experimental and theoretical work performed by the different organizations involved in preparing this report. Finally, some developments with respect to measurement- and identification methods are discussed.

The state of the art in on-load surveillance techniques of light water reactors is given by extending the preceding studies to investigations of boiling water reactors and by summarizing the latest results of pressurized water reactors, the basis being experimental and theoretical work performed by the different organizations involved in preparing this report. Finally, some developments with respect to measurement- and identification methods are discussed.

EUR 5294 e

COMMISSION OF THE EUROPEAN COMMUNITIES

VIBRATION AND NOISE ANALYSIS IN NUCLEAR POWER PLANTS

1974

Report prepared by

Allianz-Zentrum für Technik Gmbh (AZT), Ismaning — Deutschland

Electricité de France (EdF), Paris — France
Ente Nazionale per l'Energia Elettrica (ENEL), Roma — Italia
Laboratoire belge de l'Industrie Electrique (LABORELEC), Linkebeek — Belgique
Lehrstuhl und Institut für Kerntechnik, TU, Hannover — Deutschland
Lehrstuhl für Reaktordynamik und Reaktorsicherheit, T.U. München — Deutschland

EURATOM Contract No. 47-72-12 ECIC

ABSTRACT

Results of the investigations on noise and vibration analysis are presented as a follow-up study of the work published in "On-load Surveillance of Nuclear Power Plant Components by Noise and Vibration Analysis" EUR 5036 e. The state of the art in on-load surveillance techniques of light water reactors is given by extending the preceding studies to investigations of boiling water reactors and by summarizing the latest results of pressurized water reactors, the basis being experimental and theoretical work performed by the different organizations involved in preparing this report. Finally, some developments with respect to measurement- and identification methods are discussed.

Foreword

This report was prepared under Study Contract No. 47-72-12 ECIC between the European Communities (EC) and

- Allianz-Zentrum für Technik GmbH (AZT), Germany
- Electricité de France (EdF), France
- Ente Nazionale per l'Energia Elettrica (ENEL), Italy
- Laboratoire Belge de l'Industrie Electrique, Belgium
- Lehrstuhl und Institut für Kerntechnik, TU Hannover, Germany
- Lehrstuhl für Reaktordynamik und Reaktorsicherheit, TU München, Germany

It was initiated by the EC as a consequence of the results of a previous study /1/. A series of interesting investigations was performed at the time, when this study was at its end, so that it was impossible to include the associated results. In addition it seemed to be worthwhile to take also due note of the various noise measurements taken recently on BWRs, and the various efforts in the work dealing with models, which try to explain the noise and vibration signal spectra. The main aim of investigations concerning the turbines was to make accessible for the operator the results of the vibration measurements in order to increase the availability and safety of nuclear

power plant turbines.

Part one "Reactor Components" was prepared by

R. Baeyens, Laborelec
W. Bastl, TU München (acting as coordinator)
M. Calcagno, ENEL
F. Cioli, ENEL
P. Gebureck, TU Hannover
B. Raible, AZT
R. Roche, EdF
E. Sädtler, TU München
W. Seifritz, TU Hannover
S. Sighicelli, EdF
D. Wach, TU München

Part two "Turbines" was prepared by

H.J. Bohnstedt, AZT (acting as coordinator)
A. Jaudet, EdF
G. Pleeck, Laborelec
G. Possa, CISE*

---

*CISE (Centro Informazioni Studi Esperienze, Milan) is working, jointly with ENEL, on the development of surveillance techniques for power stations.

Acknowledgements

The parties to this Study Contract wish to express their gratitude to Mr. M. Siebker of the European Commission, who assisted them to continue - with this second report - the activities of reviewing the development of on-load surveillance techniques in the European Community and thus making it possible to take care of the latest progress in the field.

The valuable suggestions and stimulating comments of Mr. J.W. Ehrentreich of the European Commission, who has closely followed the various phases in the preparation of this report, are acknowledged.

The participants are grateful to the managements of those utilities which granted permission to perform surveillance tests on their power plants and to the operating personnel for their assistance in the data collection phase of such tests. Finally the various informations provided by the manufacturers are also acknowledged.

Table of Contents

Part Two: TURBINES

PART I: REACTOR COMPONENTS

I.1 Introduction

The main aspects of on-load surveillance techniques, the involved measurements and analyses and the methods of interpreting the noise and vibration signals taken from various sensors have been discussed in the preceding report*. This study is based on the information given there and does not recall the principles, problems and ideas behind the analysis techniques, which are necessary to understand when reading this paper. In this context we refer specially to the chapters "Measurement Techniques" and "Analysis Techniques" of the previous report.

Therefore we start immediately with the presentation of results gained from actual measurements and analyses. The first part deals with signals measured at the GARIGLIANO and LINGEN boiling water reactors. The investigations concentrate on the interpretation of the boiling noise present in the various neutron flux chamber currents.

The second part is devoted to pressurized water reactors. Following previous results* a direct proof of the core barrel/pressure vessel pendular movement could be given by a special measurement technique. Further on new measurements performed at BR3, JOSE CABRERA and SENA power stations are discussed. In STADE thorough investigation of pressure and displacement signals taken during the pre-operational phase lead to a better understanding of noise sources and of the pressure signal as a means for vibration detection.

In the last part we have summarized those items, which are not typical for the one or the other reactor type, but still are of great interest for noise and vibration analysis from the principle point of view. Thus it is dealt with the use of self-powered detectors for noise analysis purposes, the application of identification theory for the interpretation

of the signals and theoretical models used to predict the vibration behaviour of structural parts.

---

*On-load Surveillance of Nuclear Power Plant Components by Noise and Vibration Analysis
Status Report on work performed for the Commission of the European Communities under Euratom Study Contract No. 043-71-10 ECIC (F), April 1972

I.2 Boiling Water Reactors

I.2.1 GARIGLIANO Nuclear Power Plant

Garigliano is a dual cycle water reactor with 150 MW_{el}. Based on the results gained by means of noise analysis at the TRINO, JOSE CABRERA and SENA pressurized water reactors it was decided to perform noise measurements at a boiling water reactor. For the pressurized water reactors mentioned before characteristic peaks in the neutron noise frequency spectra could be found, which evidently stem from the pendulum oscillations of the reactor internals package. It was hoped to get a further proof for this interpretation by means of BWR neutron noise analysis, because due to the configuration of the internals the spectra should not show the peaks mentioned before.

I.2.2.1 Measurements

A sequence of 10 groups of neutron noise recordings was performed at the GARIGLIANO station in March 1972 /1/. Each group consisted of four or five simultaneous recordings. In table I.2.1/1 are listed the nine pairs of the most meaningful recordings considered, and the characteristics of detectors which were used.

I.2.2.2 Analysis

The analysis was carried out with the CISE computer (IBM 1800) equipped with an analog-digital converter. The plotting of calculated noise spectra was performed with an automatic plotter (BENSON 411).

In figs. I.2.1/1 through I.2.1/10 the normalized noise spectra

NO.	NOISE SIGNAL KIND	DETECTOR NAME	DETECTOR DISTANCE FROM THE CENTRE OF THE CORE	DETECTOR AXIAL POSITION	MUTUAL RADIAL POSITION OF THE TWO DETECTORS
1	NEUTRON	C7	OUT-OF-CORE		OPPOSITE
	NEUTRON	C8	OUT-OF-CORE		(160°)
2	NEUTRON	C9	OUT-OF-CORE		OPPOSITE
	NEUTRON	C2	OUT-OF-CORE		(170°)
3	NEUTRON	C8	OUT-OF-CORE		0°
	NEUTRON	101-A	IN-CORE AT PREIFERY	BOTTOM QUARTER	
4	NEUTRON	C8	OUT-OF-CORE		
	PRESSURE	GE-MAC	VESSEL		
5	NEUTRON	C8	OUT-OF-CORE		0°
	NEUTRON	101-D	IN-CORE, PERIFERY	TOP QUARTER	
6	NEUTRON	118-A	IN-CORE, PERIFERY	BOTTOM QUARTER	OPPOSITE
	NEUTRON	101-A	IN-CORE, PERIFERY	BOTTOM QUARTER	(135°)
7	NEUTRON	115-A	IN-CORE, PERIFERY	BOTTOM QUARTER	OPPOSITE
	NEUTRON	109-A	IN-CORE, PERIFERY	BOTTOM QUARTER	(160°)
8	NEUTRON	111-B	IN-CORE, NEAR CENTRE		0° (in the same
	NEUTRON	111-C	IN-CORE, NEAR CENTRE		string)
9	NEUTRON	111-A	IN-CORE, NEAR CENTRE	BOTTOM QUARTER	0° (in the same
	NEUTRON	111-D	IN-CORE, NEAR CENTRE	TOP QUARTER	string)

Table I.2.1/1: Detectors used for noise recordings

are reported. The first figure shows the the trend of neutron spectra of all considered out-of-core detectors. The most evident features are the peaks at 8.8 and 25.0 Hz, showed by all the spectra. In figs. I.2.1/2 and I.2.1/3 are reported the same neutron spectra (out-of-core) plotted two by two. They are originated by detectors diametrically opposite located in front of the subcooled zone of the core.

The coherence between the noise signals is very high, therefore the reactivity noise is dominant through the whole core, moreover the phase is 0^{o} through the entire frequency range. The coherence is not negligible also at 35 Hz, so the Campbell noise becomes the most important component at higher frequencies.

Fig. I.2.1/4 shows the neutron noise spectrum (out-of-core) compared with the pressure noise spectrum of the vessel. The 8.8 and 25.0 Hz peaks are confirmed by the pressure noise, too, with a high coherence and a 0^{o} phase.

In fig. I.2.1/5 the spectra of an in-core and an adjacent out-of-core sensor are compared. The in-core detector is located in the bottom quarter of the active core region, its noise spectrum shows smaller peaks, but the coherence is still good. In fig. I.2.1/6 the comparison is done between the same out-of-core and an in-core detector located in the same string but at the top quarter of the core. At low frequency the spectra nearly coincide and the coherence is good, then the in-core spectrum diverges, due to the boiling noise, while the phase swings. The variance in the range 5-20 Hz might be taken as a void index.

In fig. I.2.1/7 two in-core detectors located in the

same string near the centre of the core, at bottom and top axial quarter, are compared together. The coherence is low, because the boiling noise hides every other information in the in-core chamber located in the upper part of the core.

In fig. I.2.1/8 the comparison is done between the remaining two in-core sensors of the preceding string. They are at intermediate height, but the boiling noise is already strong. The anomalous behaviour of the phase is probably due to an instrumentation effect. A further check should be done between a high and an intermediate in-core detector.

In figs. I.2.1/9 and I.2.1/10 are reported the neutron noise spectra of incore detectors, located at the same axial level (bottom quarter), but at different radial distances from the centre of core. The coherence is rather low, in contrast with the behaviour of the out-of-core sensors, and some strange peaks appear.

In fig. I.2.1/11 the normalized RMS - noise amplitude is reported versus the axial position. This amplitude increases linearly up to the middle of the core and remains constant in the upper half of the core.

Finally the same recordings analysed in the frequency range 2-35 Hz (see figs. I.2.1/3 and I.2.1/5) have been analysed in the range 0.2-3.5 Hz. The obtained spectra are reported in figs. I.2.1/12 and I.2.1/13.

At the time being no final conclusions on the phenomena causing the various peaks were obtained. The analysis and interpretation of noise recordings and spectra will continue.

Literature, Section I.2.1

/1/ Trino Vercellese Nuclear Power Plant
Research Program for the Development of Closed-Cycle
Water Reactor Technology
ENEL-EURATOM Contr. No. 071-66-6 TEEI(RD)
Quaterly Progress Report No. 22-23 (Oct. 1971 - March 1972)
Quaterly Progress Report No. 24 (April - June 1972)

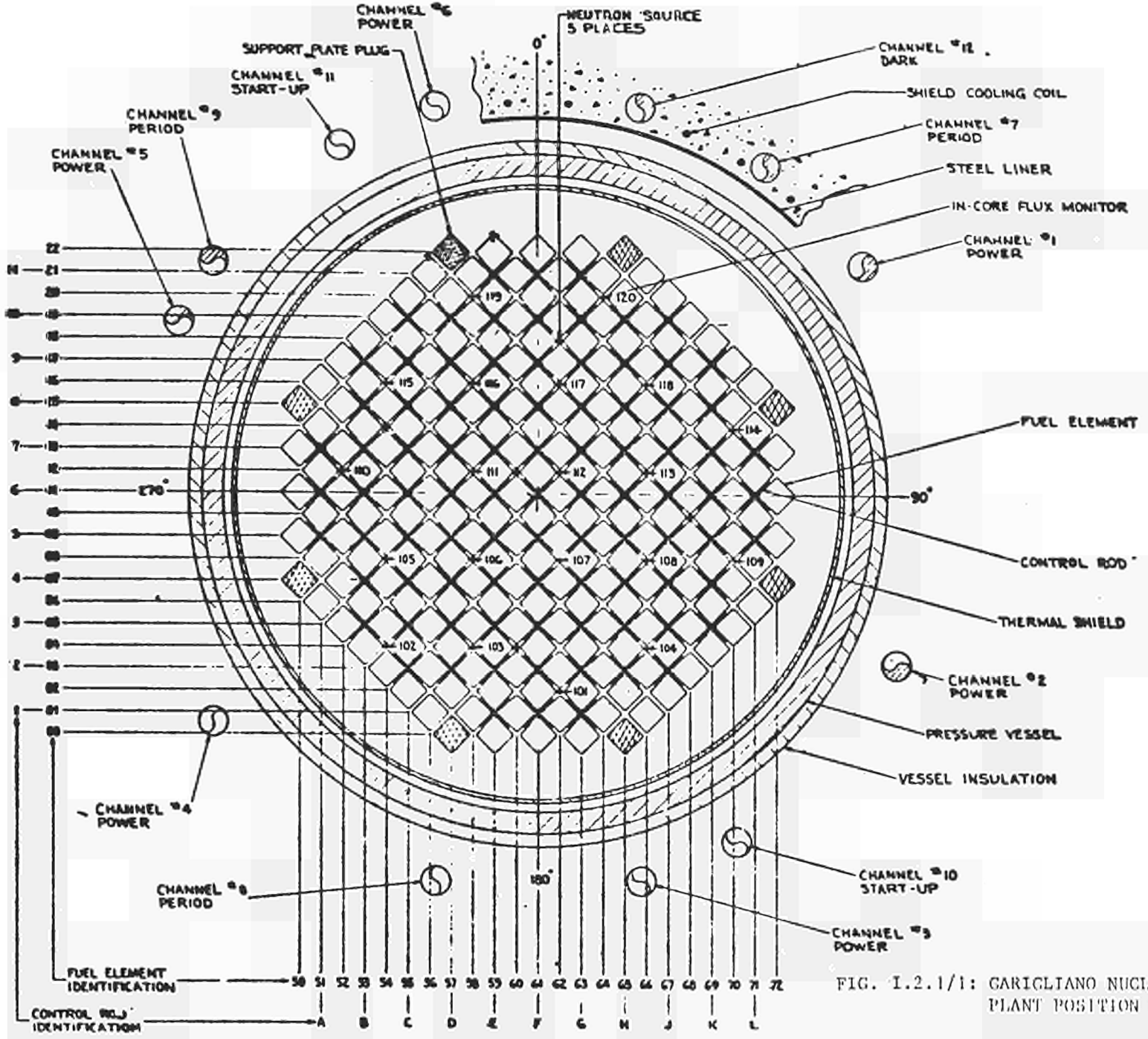

FIG. I.2.1/1: GARIGLIANO NUCLEAR POWER PLANT POSITION OF SENSORS

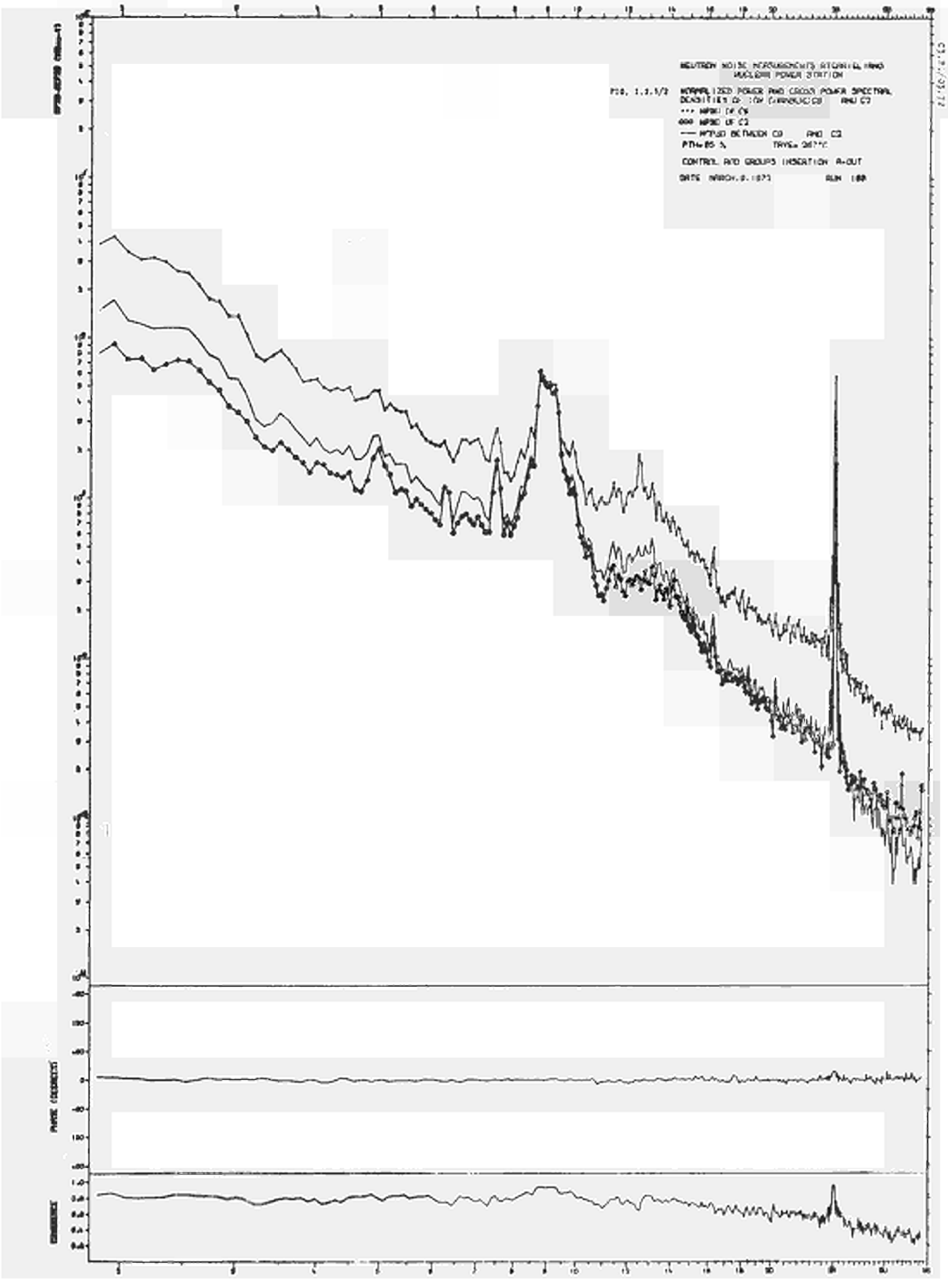
NEUTRON NOISE MEASUREMENTS AT BIBLIS NPP
NUCLEAR POWER STATION
FIG. 1.2.1/2
NORMALIZED POWER AND CROSS POWER SPECTRAL
DENSITIES OF THE CHANNELS C2 AND C3
*** NPSD OF C2
000 NPSD OF C3
—— MPSD BETWEEN C2 AND C3
P(T)=85 %
CONTROL ROD GROUPS INSERTION A-OUT
DATE MARCH,8.1975 RUN 188
PHASE (DEGREES)
COHERENCE

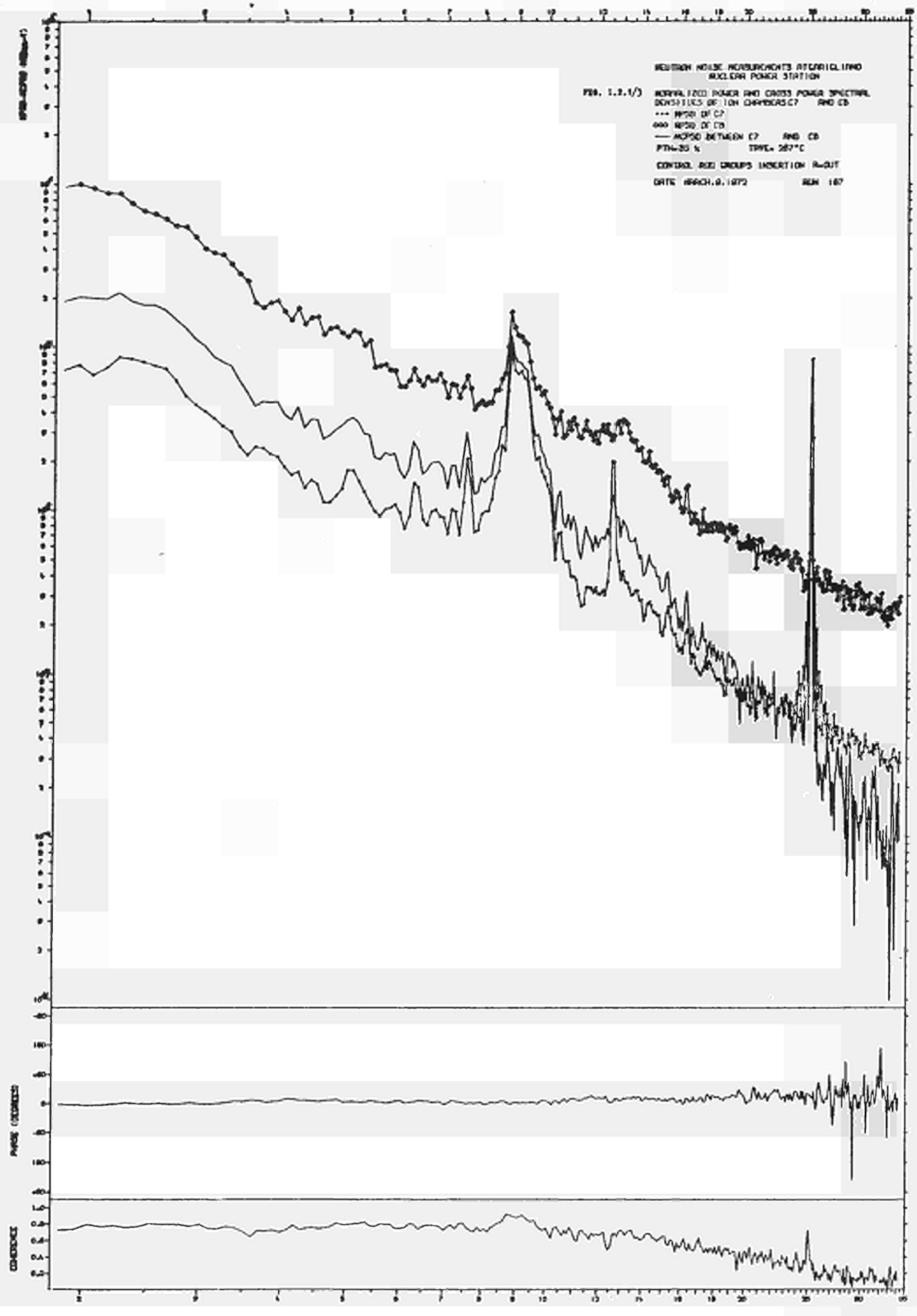
NEUTRON NOISE MEASUREMENTS AT ARIELLINO
NUCLEAR POWER STATION
FIG. 1.3.1/1
NORMALIZED POWER AND CROSS POWER SPECTRAL
DENSITIES OF ION CHAMBERS C7 AND C8
--- NPSD OF C7
000 NPSD OF C8
—— MCPSD BETWEEN C7 AND C8
POW=85 % TAVE= 287°C
CONTROL ROD GROUPS INSERTION A-OUT
DATE MARCH.8.1972 REN 187
PHASE (DEGREES)
COHERENCE

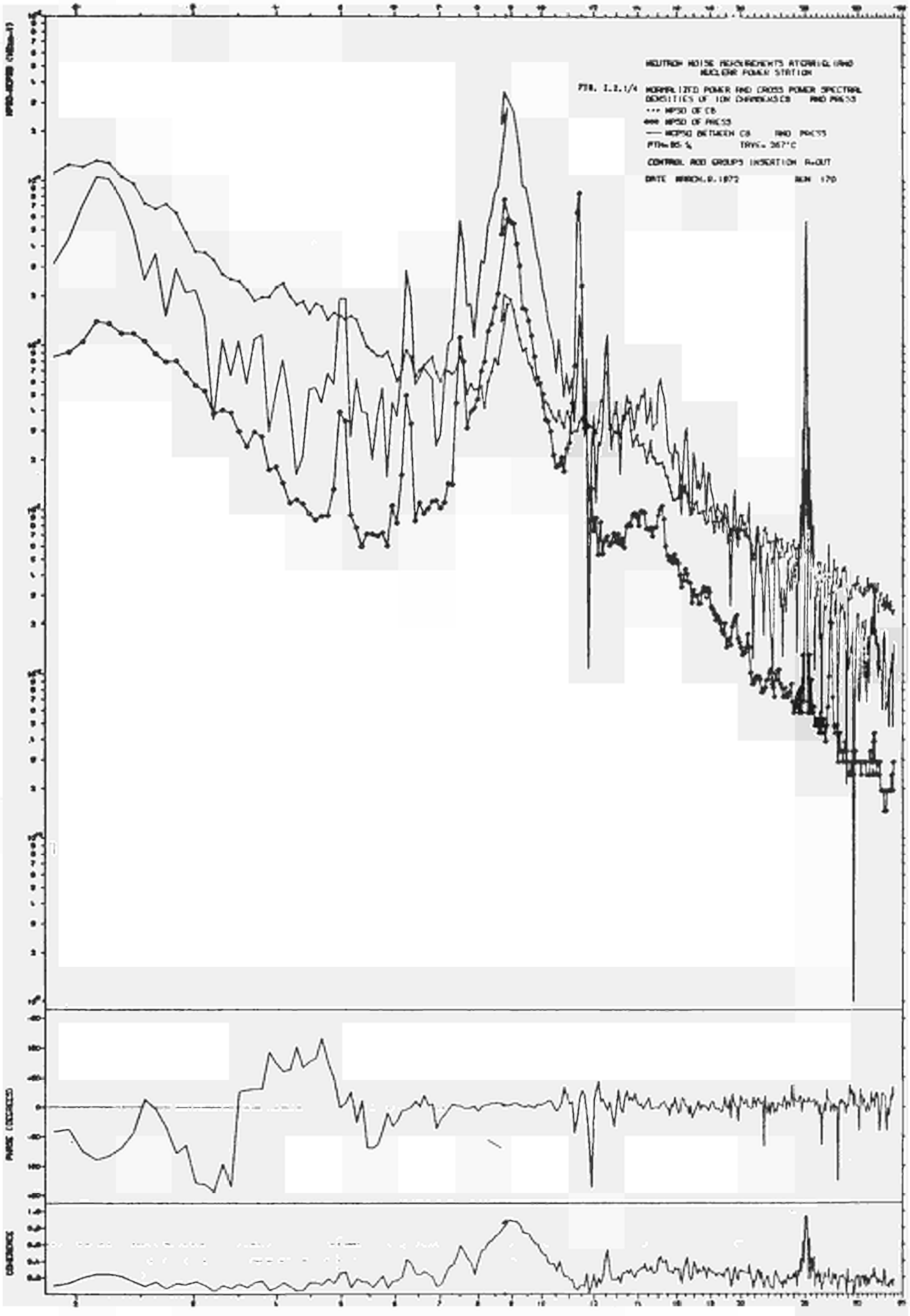
NEUTRON NOISE MEASUREMENTS AT ORRIL (AND NUCLEAR POWER STATION
FIG. I.2.1/4 NORMALIZED POWER AND CROSS POWER SPECTRAL DENSITIES OF ION CHAMBERS CB AND PRESS
*** NPSD OF CB
000 NPSD OF PRESS
—— NCPSD BETWEEN CB AND PRESS
PTH= 86 %
TAVG= 287°C
CONTROL ROD GROUPS INSERTION R-OUT
DATE MARCH.8.1972
RUN 170
NPSD-NCPSD (%DK/K)**2/HZ
PHASE (DEGREES)
COHERENCE
FREQUENCY (HZ)

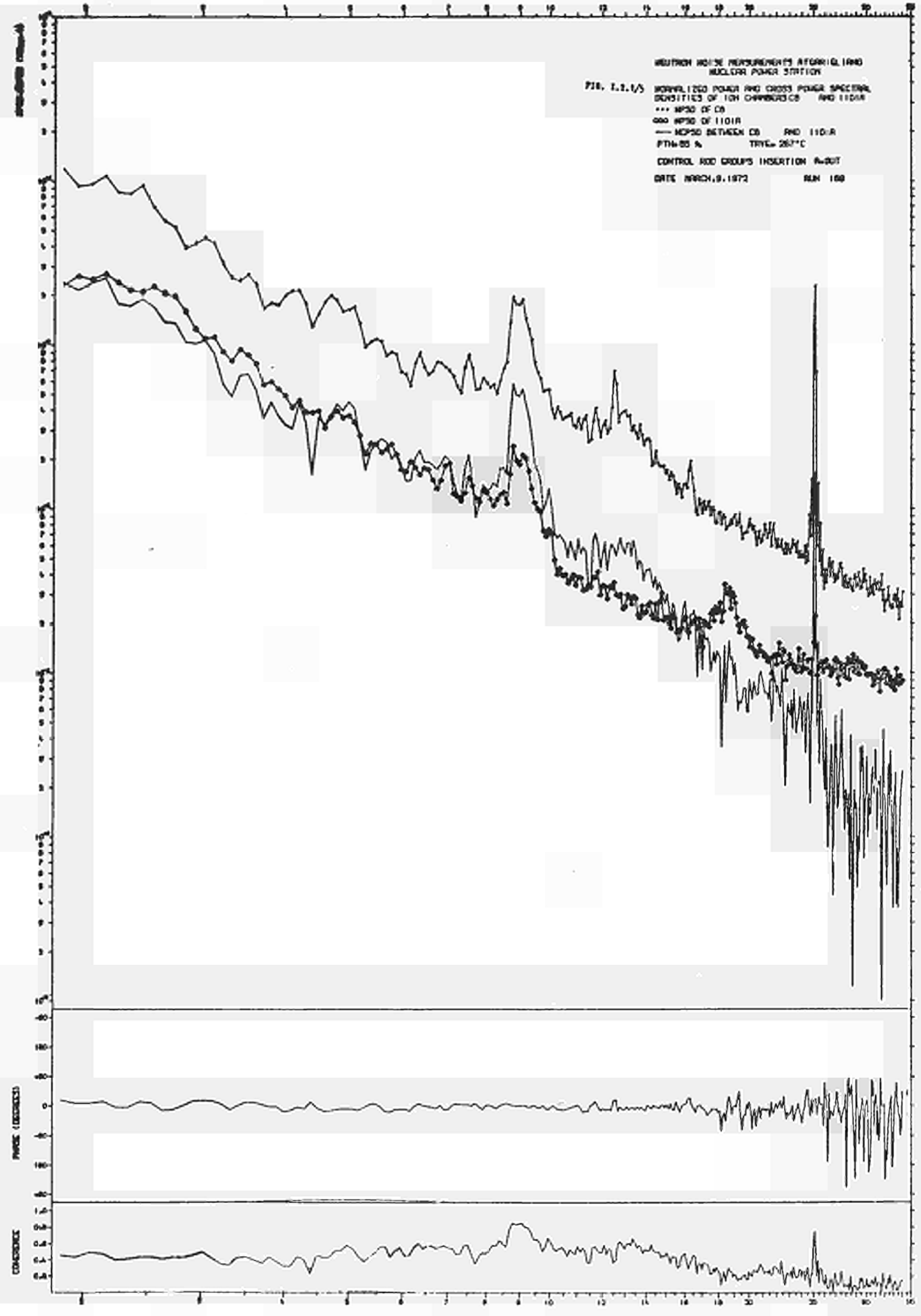
NEUTRON NOISE MEASUREMENTS AT GARIGLIANO NUCLEAR POWER STATION
FIG. 2.2.1/5
NORMALIZED POWER AND CROSS POWER SPECTRAL DENSITIES OF 10H CHAMBERS C8 AND 110A
*** NPSD OF C8
000 NPSD OF 110A
—— MCPSD BETWEEN C8 AND 110A
PTH=85 %
TAVE= 287°C
CONTROL ROD GROUPS INSERTION A=80%
DATE MARCH,9.1972
RUN 168
PHASE (DEGREES)
COHERENCE

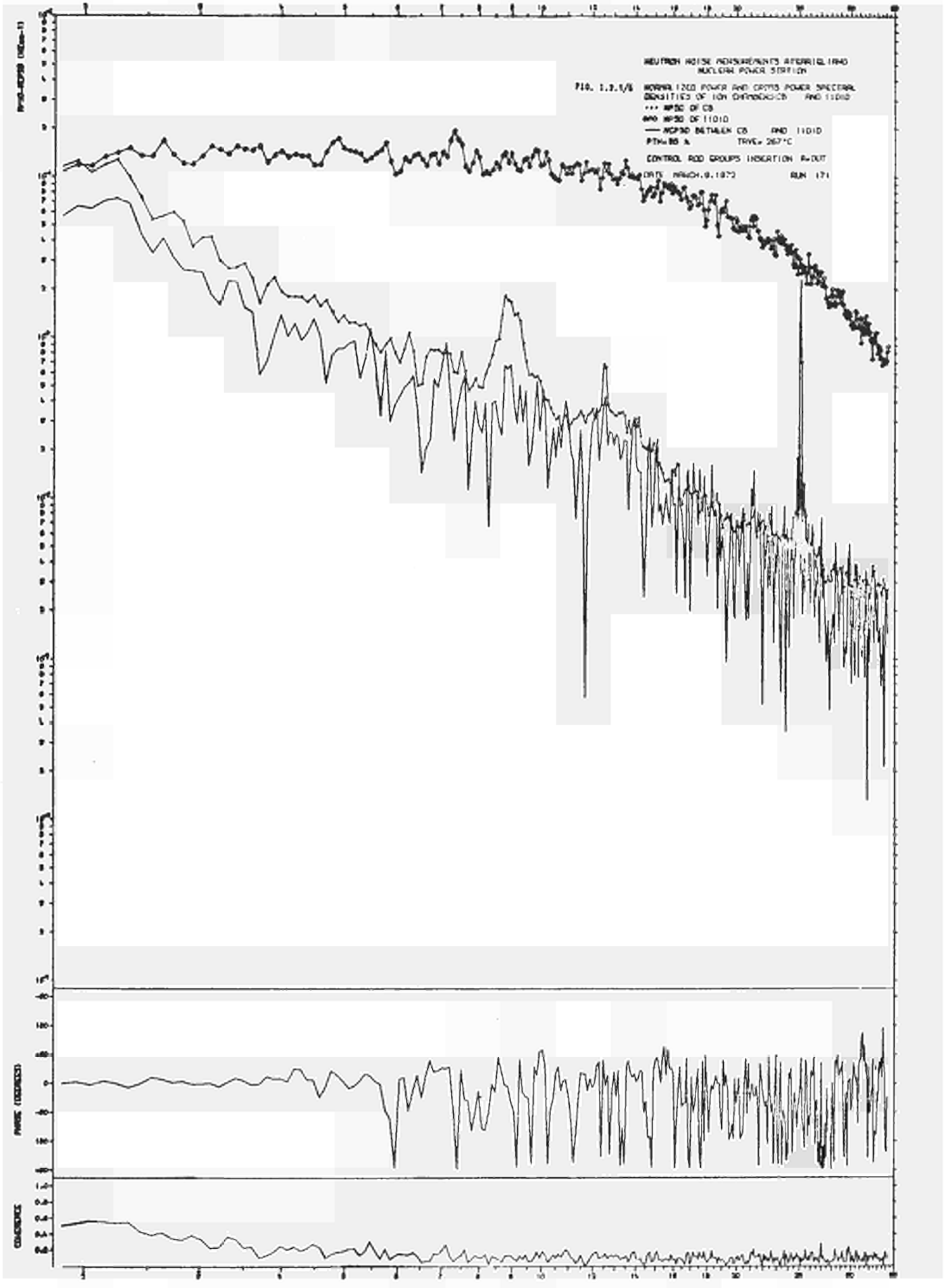
NEUTRON NOISE MEASUREMENTS AT TARRAGONA NUCLEAR POWER STATION
FIG. 3.3.1/6
NORMALIZED POWER AND CROSS POWER SPECTRAL DENSITIES OF ION CHAMBERS CB AND 11D10
··· WPSD OF CB
··· WPSD OF 11D10
— WCPSD BETWEEN CB AND 11D10
PTN=86 %
TAVE= 267°C
CONTROL ROD GROUPS INSERTION A-OUT
DATE MARCH.8.1972
RUN 171
PHASE (DEGREES)
COHERENCE

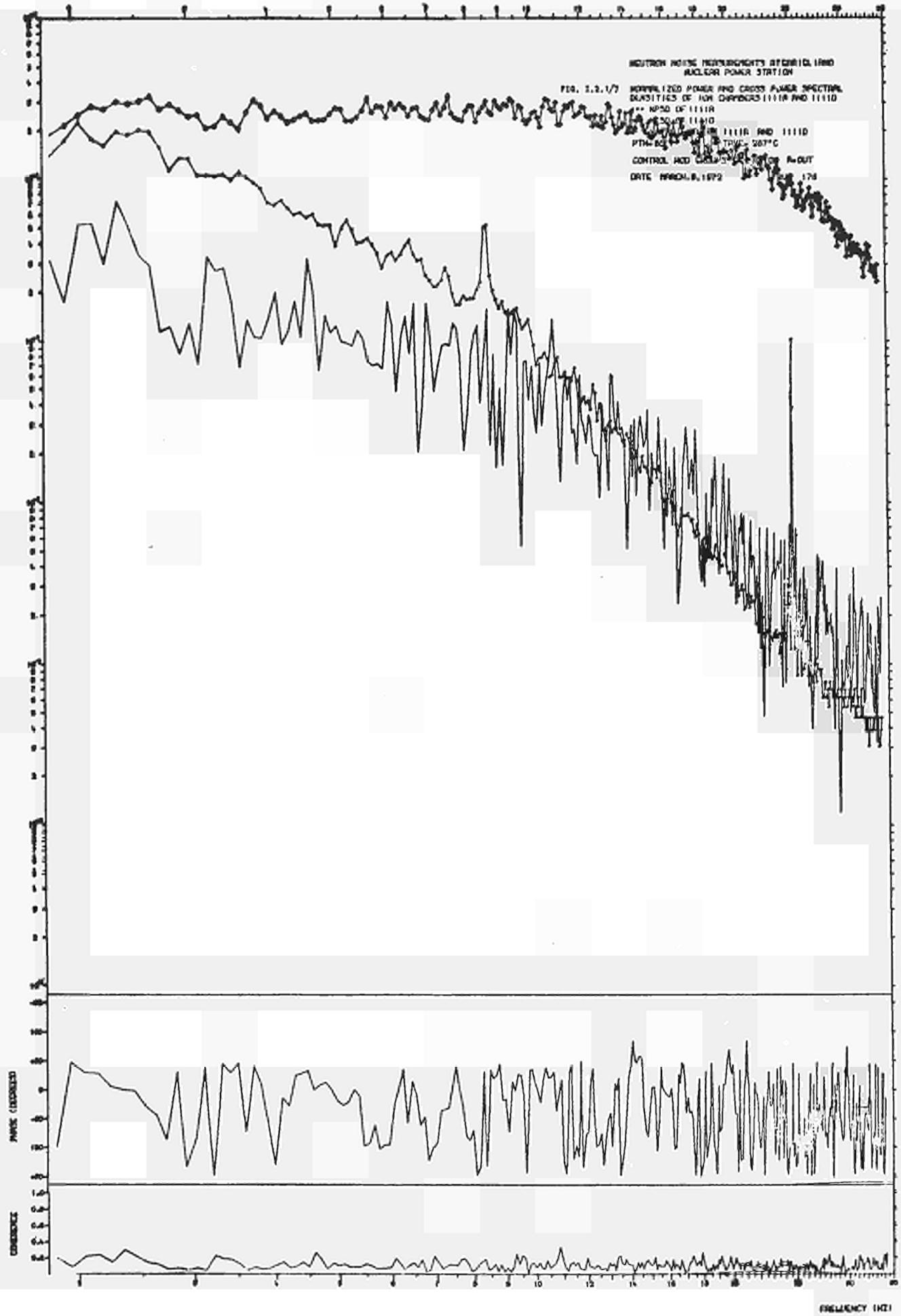
NEUTRON NOISE MEASUREMENTS AT DUNGENESS B
NUCLEAR POWER STATION
FIG. 3.2.1/7
NORMALIZED POWER AND CROSS POWER SPECTRAL
DENSITIES OF ION CHAMBERS 1111A AND 1111D
*** KPSD OF 1111A
KPSD OF 1111D
CROSS POWER SPECTRUM 1111A AND 1111D
PTH= 80
TAVE= 287°C
CONTROL ROD CONFIGURATION R-OUT
DATE MARCH 8, 1972
178
PHASE (DEGREES)
COHERENCE
FREQUENCY (HZ)

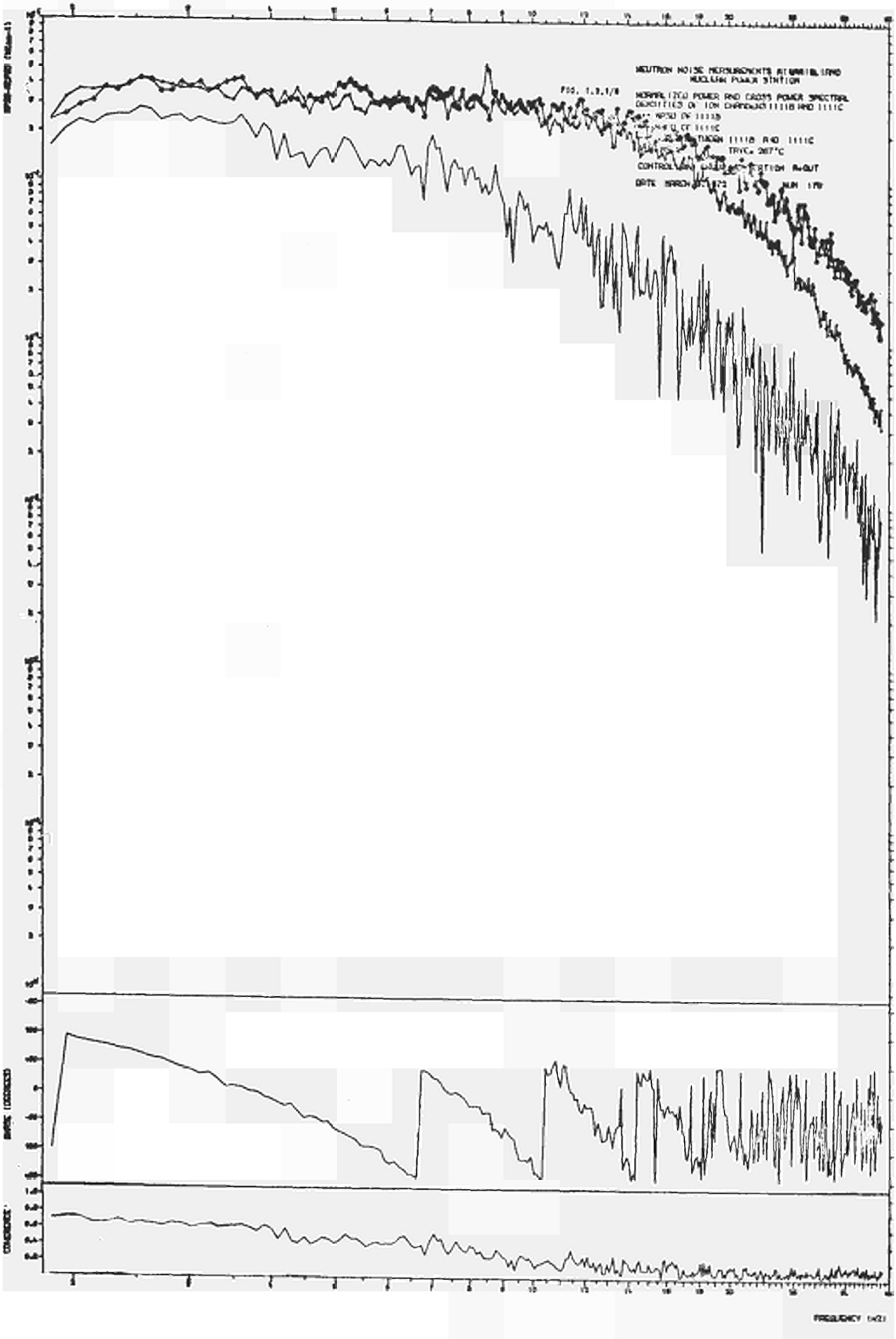
NEUTRON NOISE MEASUREMENTS AT WINFRITH
NUCLEAR POWER STATION
FIG. 1.3.1/8
TRYC= 267°C
FREQUENCY (HZ)

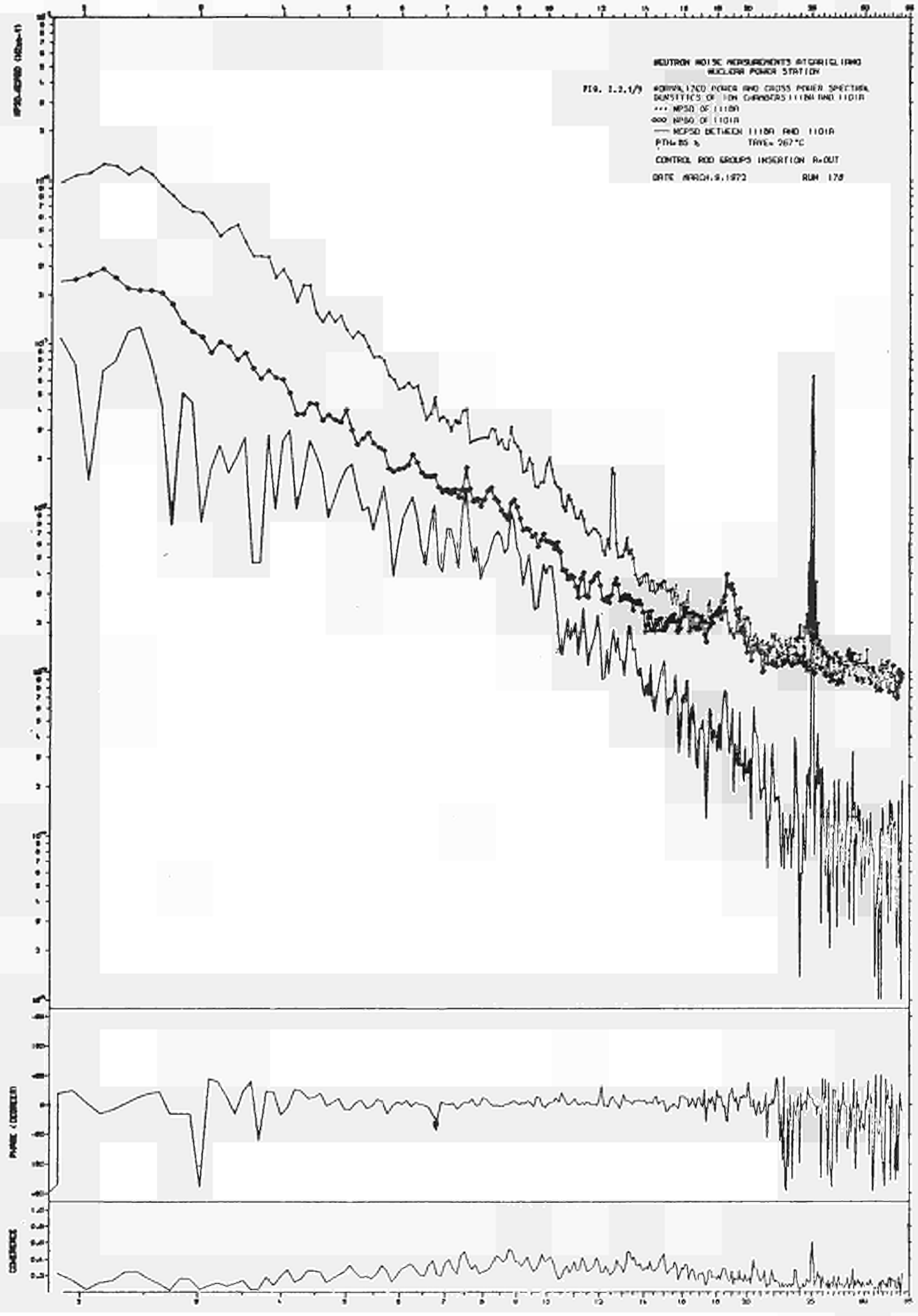
NEUTRON NOISE MEASUREMENTS AT GARIGLIANO
NUCLEAR POWER STATION
FIG. 3.2.1/9
NORMALIZED POWER AND CROSS POWER SPECTRAL DENSITIES OF ION CHAMBERS 1118A AND 1101A
*** NPSD OF 1118A
ooo NPSD OF 1101A
—— XCPSD BETWEEN 1118A AND 1101A
PTH=85 %
TAVE= 267°C
CONTROL ROD GROUPS INSERTION A-OUT
DATE MARCH.9.1972
RUN 178
PHASE (DEGREES)
COHERENCE
FREQUENCY (HZ)

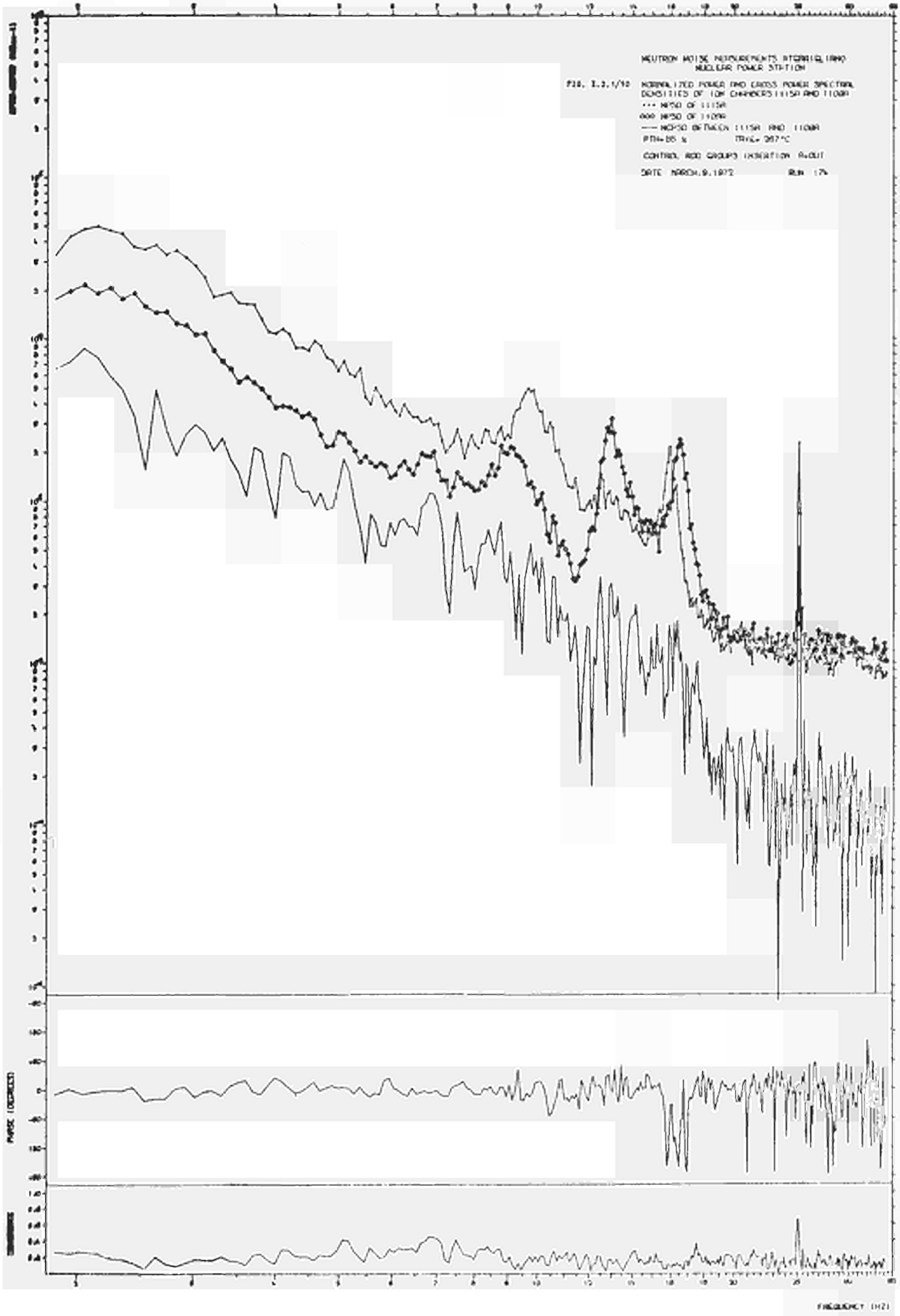
NEUTRON NOISE MEASUREMENTS AT BRUNSBÜTTEL NUCLEAR POWER STATION
FIG. 3.3.1/10
NORMALIZED POWER AND CROSS POWER SPECTRAL DENSITIES OF 10M CHAMBERS 11150 AND 11080
+++ NPSD OF 11150
000 NPSD OF 11080
—— NCPSD BETWEEN 11150 AND 11080
POWER 85 %
TRIVEL= 287°C
CONTROL ROD GROUP 3 INSERTION 4=OUT
DATE MARCH.9.1972
RUN 174
PHASE (DEGREES)
COHERENCE
FREQUENCY (HZ)

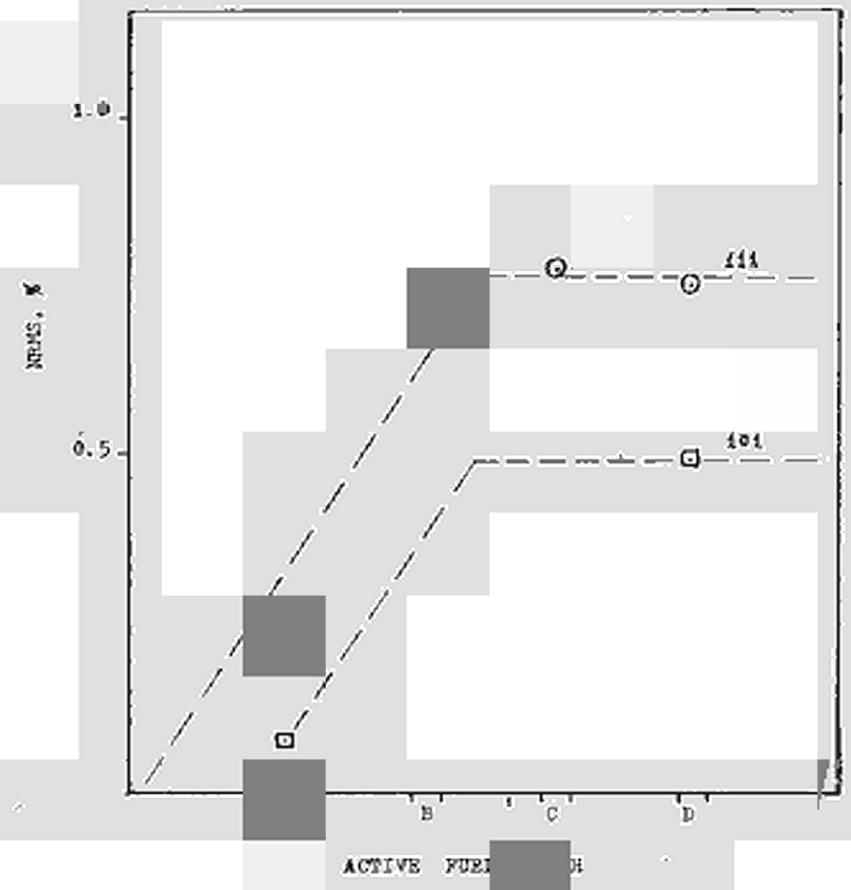

FIG. I.2.1/11 - NRMS - N . IN-C N

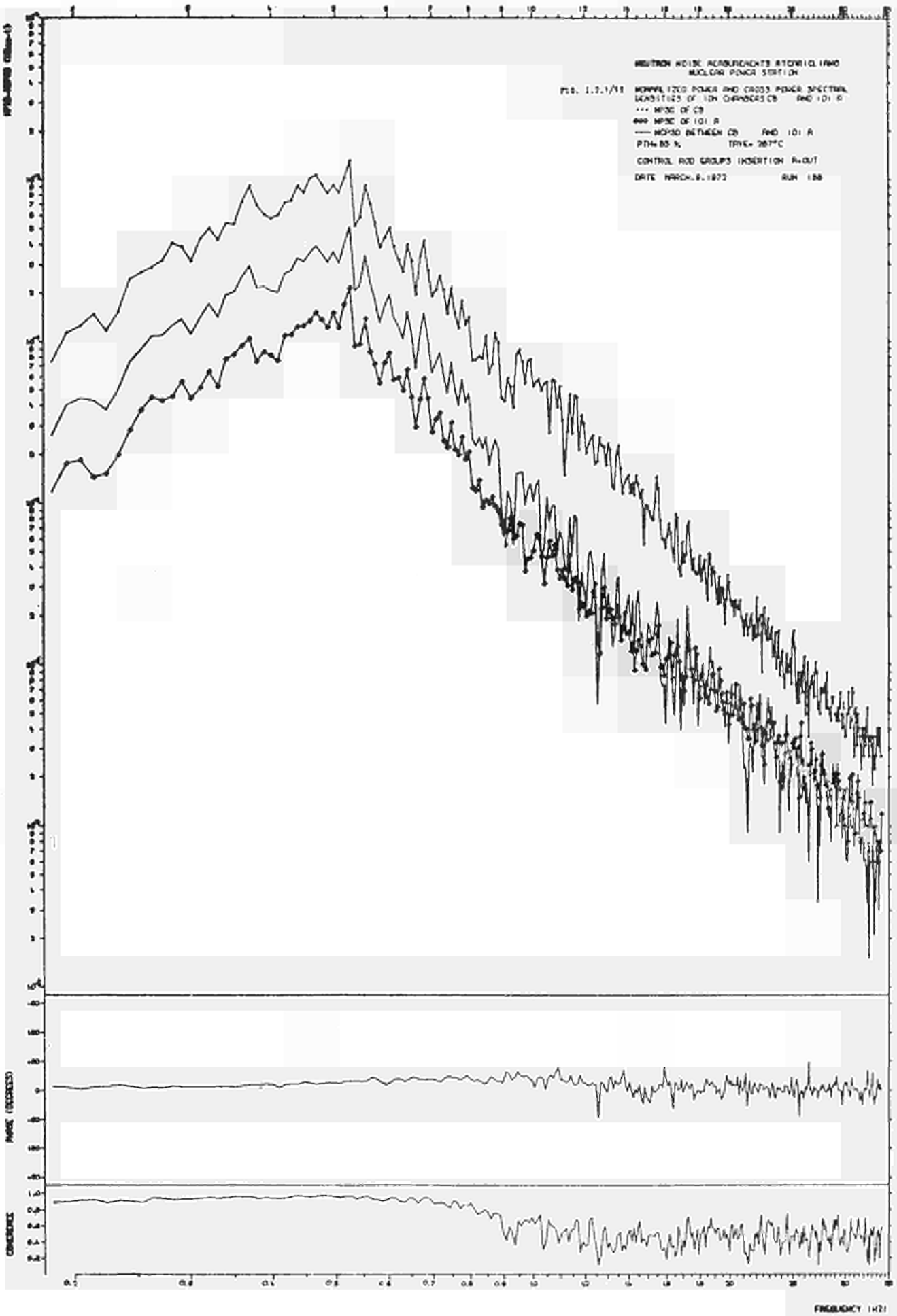
NEUTRON NOISE MEASUREMENTS AT KRŠKO NUCLEAR POWER STATION
FIG. 1.3.1/11 NORMALIZED POWER AND CROSS POWER SPECTRAL DENSITIES OF ION CHAMBERS CB AND 101 A
--- NPSD OF CB
--- NPSD OF 101 A
—— NCPSD BETWEEN CB AND 101 A
P(%) 85 %
TAVE= 287°C
CONTROL ROD GROUPS INSERTION A-OUT
DATE MARCH.8.1972
RUN 188
PHASE (DEGREES)
COHERENCE
FREQUENCY (HZ)

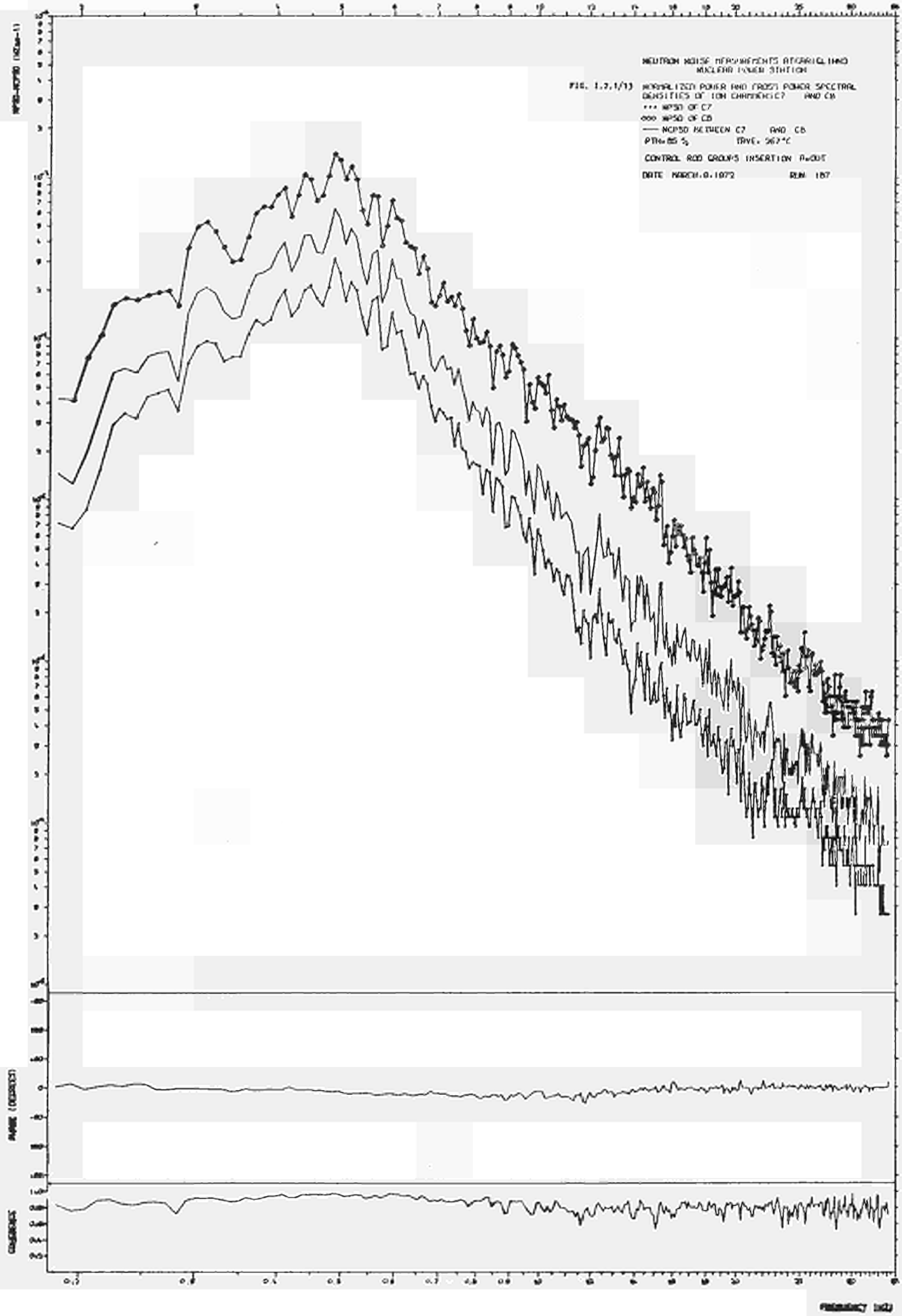
NEUTRON NOISE MEASUREMENTS AT GRIFLINHO
NUCLEAR POWER STATION
FIG. 1.2.1/13 NORMALIZED POWER AND CROSS POWER SPECTRAL DENSITIES OF ION CHAMBERS C7 AND C8
*** NPSD OF C7
ooo NPSD OF C8
—— NCPSD BETWEEN C7 AND C8
PTN=85 % TAVE. 567°C
CONTROL ROD GROUPS INSERTION A+OUT
DATE MARCH.8.1972 RUN 187
PHASE (DEGREES)
COHERENCE
FREQUENCY (HZ)

I.2.2 LINGEN Nuclear Power Plant

I.2.2.1 Measurements

The LINGEN nuclear power plant (KWL) is one of the first commercial BWRs of Germany. It is equipped with an AEG two-loop reactor. Power operation started in May 1968. The thermal reactor power is 520 MW. Together with a fossil overheating system the plant delivers 252 MW electrical power.

Noise measurements at KWL have been performed by AEG and T.U. München in April 1971 /1/, /2/, /3/. Several noise signals have been tape-recorded during two operating conditions (72 ata, 106% and 30 ata, 50%) as long time series (ca 3 hours) in order to have a good statistical confidence in the low frequency range (down to 0.01 Hz). In addition, there have been shorter noise measurements of the in-core neutron flux signals (ca 5 minutes) with the aim to get information about space-dependent effects (e.g. steam void generation and velocity) and the mechanical behaviour of the core in the frequency range above 1Hz. During these measurements a movable in-core-chamber could be positioned at different core heights.

The most important recorded signals, which are discussed in this paper, were received from the following sensors:

- 1 ionisation chamber (NF) out-of-core. γ-compensated, sensitive length 150 mm, radial position see fig. I.2.2/1, axial position ca middle of core height
- 3 in-core ionisation chambers (J28/1, J28/2, J28/4), sensitive length 25 mm,

all in the same radial position M28 (see fig. I.2.2/1), different axial positions:

2269 mm for J28/1
1735 mm for J28/2 (only available at 72 ata)
667 mm for J28/4

(all measures are refferred to the lower core edge)

- 1 axial movable miniature ionisation chamber (TIP), radial position M25 (see fig. I.2.2/1), during the 30 ata measurement below the lower core edge
- differential pressure over the core (DPK)
- reactor primary pressure (PR)
- differential pressure over one of the two forced circulation pumps (FH2)

I.2.2.2 Analysis

Since some years at the T.U. München investigations are performed as to what extent useful information can be obtained from the fluctuations of the plant instrumentation signals of nuclear power reactors. When starting the KWL-noise measurements similar measurements had already been performed at the PWR of Obrigheim and had shown very promising results /4/. In the meantime further vibration and noise measurements at the STADE nuclear power plant have shown concrete and practically useful results for the pressurized water reactor (see I.3.3). Now, two years after the measurements, the KWL-noise signals were investigated in order to check also the possibilities at a boiling water reactor.

I.2.2.2.1 Normalized Power Spectral Densities (NPSDs)

At first the NPSDs of all neutron flux signals were

computed and figured by an incremental plotter using double logarithmic scales. For this purpose the dynamic component of the signal was normalized to the mean value which has been compensated before amplifying and tape-recording. The calculations were performed in two frequency ranges with two resolutions:

0 Hz to 12.5 Hz with Δf = 0.125 Hz
0 Hz to 3.6 Hz with Δf = 0.031 Hz

In fig. I.2.2/2 the NPSDs of the neutron flux signals during the 106% power operation (72 ata) are shown.

There are two striking frequency ranges to discuss:

- from 0 Hz to ca 1.6 Hz a strong broad peak at 0.5 Hz (or rather the behaviour of a band-limited white noise). The NPSDs of the ionisation chambers inside and outside the core are nearly identical
- from 1.6 Hz to 12.5 Hz a band-limited white noise with a power density some decades lower. The levels are different for detectors in different core heights. Signal NF has the lowest, signal J28/1 (on the upper core edge) the highest noise power density.

In the NPSDs of the 30 ata-measurement (fig. I.2.2/3) the resonance peak at 0.58 Hz now appears clearly and narrow (0.18 Hz broad at the half of the peak maximum). In the range above 0.75 Hz the NPSDs of NF and TIP (positioned below the core) decrease nearly identically corresponding to the 72 ata-measurement. On the contrary the NPSDs of the in-core chambers are greater by factors between 20 and 100.

Looking at the NPSDs of TIP at different axial positions

(Pos. 2 = 400 mm, Pos. 4 = 930 mm, Pos. 8 = 2000 mm, Pos. 10 = 2540 mm) again an increasing of the power spectral density can be observed with increasing core height in the range above 0.75 Hz (fig. I.2.2/4).

I.2.2.2.2 Coherence Functions

Generally it can be said that only in the lower frequency range of the powerful peak good coherences do exist (for 72 ata see figs. I.2.2/5 and I.2.2/6, for 30 ata see fig. I.2.2/7). In the higher frequency range the coherences between the two lower chambers are better than between the two upper ones though the distance is twice the distance of the upper chambers. It is remarkable that in this frequency range the coherence functions show a characteristic dip-behaviour whilst the NPSDs are continuous. Following the experience obtained from the investigations of neutron noise signals in pressurized water reactors /4/ such a behaviour indicates the co-acting of noise driving sources with different phase relations.

I.2.2.2.3 Phase Functions

Phase functions of two noise signals can be considered as true only in these frequency ranges, in which as well sufficient noise power as good coherences do exist.

At first especially the mutual phase relations of the in-core-chambers are of the greatest interest. Noise signals of three in-core-chambers, which are positioned one above the other in the same cooling channel, are only available from the 72-ata-measurement. From figs. I.2.2/8 and I.2.2/9 it can be seen that linear relations exist between phase angles and frequency of axially adjacent chambers.

I.2.2.2.4 Relations Between Neutron Flux NF and Pressure Signals

Fig. I.2.2/10 shows the PSDs of the out-of-core ionisation chamber NF, the core differential pressure DPK, the reactor pressure PR and the differential pressure over a forced circulation pump FH2, fig. I.2.2/11 the coherences between NF and the pressure signals in the frequency range up to 3.6 Hz. Especially in the low range correlations up to 90% exist.

I.2.2.2.5 Interpretations

In this paper the interpretation is restricted to the most important result: the identification of those noise sources which are generated by the moved steam bubbles.

Concerning the powerful peak at 0.5 Hz it should be only referred to the following points:

- Supposing that only one noise driving source is acting in this frequency range, it would be possible to calculate a velocity of the disturbance (noise source) from the phase relation of the noise signals of axially adjacent in-core chambers. This velocity would be ca 40 m/sec for the 72-ata-measurement and ca 9 m/sec for the measurement at 30 ata and half power. From the signum of the phase it would result in the disturbance travelling through the core from bottom to top. But it is not physically reasonable to assume a disturbance of this velocity. Therefore, the supposition made above is not correct and the phase behaviour has to be explained by the co-acting of different noise sources.

- The peak becomes small and marked at 30 ata.
- The peak is very well correlated with the core differential pressure.

As a consequence the 0.5 Hz peak is mainly due to an integral void effect, which is confirmed especially by the good correlation with the pressure. It is not referable to the transit time of the bubble through the core. This result is in accordance with measurements obtained during a campaign with self-powered detectors, which was performed by the T.U. Hannover. There one had tried to correlate the coherence function phase shifts in the frequency range below 1 Hz with the local steam velocities, because the brake point at 1 Hz seemed to indicate that no useful information was to be expected above this value. Again too high figures (20 to 30 m/sec) resulted. Unfortunately, a later investigation of the higher frequencies was not possible because of the bad signal resolution in this range (see I.4.1).

On the contrary, the spectra of ion chamber signals discussed in this chapter, show the well expressed band limited white noise above 1.6 Hz mentioned before (fig. I.2.2/2). Though some decades lower it contains evidently the wanted information on steam void velocity. For this frequency range where the power spectral densities of the core neutron flux signals increase with increasing core height, the following considerations can be made:

With increasing core height the proportion of steam bubbles and therefore the local steam void fraction $\alpha(z)$ increase. As the distribution density of the number of steam bubbles is nearly a Poisson-distribution (where the variance is equal to the mean value) it can be shown that the variance of the fluctuations of the water density is

proportional to the local steam void fraction $\alpha(z)$. These fluctuation of the moderator density causes perturbations in k_∞ (and therefore in the neutron flux signals) immediately via the macroscopic cross sections. Another - may be not neglectible - fact is, that a steam bubble between the fuel elements (the neutron sources) and an in-core-detector causes a variation in the detected neutron flux signal due to the displacing of water (attenuation effect). In this case a positive contribution would be given to the detector current as a consequence of the existence of the bubble, in the case of the local reactivity distortion a negative one.

For the following it is not important to clarify which contribution is dominant. In both cases the detector current is influenced in a pulse-type way and we have to take into consideration that for each in-core-detector a certain effective sensitivity volume has to be observed, defined as this region around the detector in which steam bubbles contribute to the detector signal.

Such a smoothed impulse corresponds to band limited spectrum:

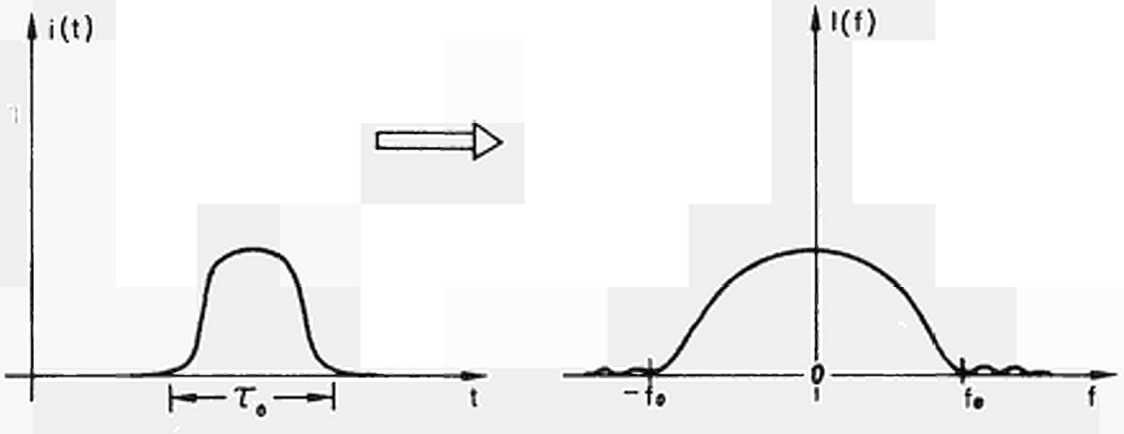

The pulse length τ_o in the time domain corresponds to the corner frequency f_o in the frequency domain and can be estimated by the transit time of the bubble when travelling through the effective sensitivity range of the detector. Let be l_s the effective sensitivity lenght in z-direction and v_B the bubble velocity we apply:

$$f_o = \frac{1}{\tau_o} = \frac{v_B}{l_s}$$

The coherence between the lower in-core chamber J28/4 and the other neutron flux signals decrease with increasing distance (fig. I.2.2/5). The coherence between the two closed situated ion chambers J28/1 and J28/2 in the upper core range is comparatively bad. These facts mean that only in the lower core range the shape of the bubbles is nearly constant while in the upper range the shape is largely changed by whirling and collapsing. The assertion that the observed power spectral densities are referable to local flux perturbations caused by the moved bubbles and detected from axially adjacent detectors delayed by the transit time of the bubbles, can be proved by the phase functions of the in-core signals. A dead time behaviour is characterized by the linear growing-on of the phase difference with frequency. Fig. I.2.2/8 and fig. I.2.2/9 show that these conditions are quite well satisfied for the phase function J28/4 → J28/2 and for the phase function J28/2 → J28/1. Differences are explained either by missing coherences or by additional deterministic noise terms (e.g. from the magnetic tape). In the lower frequency range (0.5-Hz-Peak) where the coherence is extremely good both curves show a deviation from a straight line in direction to smaller

phase angles. An explanation of this behaviour can be given by the assumption that in this frequency range the noise generated by the bubble transport is present, but is covered by an additional strong noise source simultaneously acting upon all detectors.

The mean transit time τ of the bubbles can be evaluated from the slope m of the straight line representing the fitted curve of the measured phase values.

We apply $\varphi = m\ f$

$$\varphi = \omega \cdot \tau = 2\pi\ \tau\ f = 360^{\circ}\ \tau\ f$$

$$\tau = \frac{m}{2\pi} = \frac{m}{360^{\circ}}$$

With $m_1 = -\ 101^{\circ}/Hz$ for the phase function J28/4 - J28/2 we get

$$\tau_1 = 0.280 \text{ sec}$$

For the phase function J28/2 - J28/1 with $m_2 = -\ 35.4^{\circ}/Hz$ we get

$$\tau_2 = 0.098 \text{ sec}$$

Using the geometrical distances of the detectors (1068 mm and 534 mm) and τ_1, τ_2, two mean values of the steam bubble velocity can be calculated

$$v_{B1} = 3.81\ \frac{m}{sec}$$

$$v_{B2} = 5.45\ \frac{m}{sec}$$

In the KWL-safety report the following mean velocities are given

$v_{\text{water inlet}} = 2.24$ m/sec
$v_{\text{water outlet}} = 4.5$ m/sec
$v_{\text{steam outlet}} = 7.1$ m/sec

With the equation

$$F_w \rho_w v_w + F_s \rho_s v_s = \dot{m}_T$$

$$v_s = s\, v_w$$

$$\alpha = \frac{F_s}{F_T} = \frac{F_s}{F_s + F_w}$$

where: ρ_w, ρ_s = density of water and steam
v_w, v_s = velocity of water and steam
F_w F_s = area of water and steam
F_T = total area
$\dot{m}_T$ = total mass flow
s = slip ratio
α = local steam void fraction

it can be written

$$v_w(z) = \frac{\dot{m}_T / F_T}{(1-\alpha(z))\ \rho_w + \alpha(z)\ \rho_s\ s(z)}$$

$$v_s(z) = s(z)\ v_w(z)$$

Fig. I.2.2/12 shows these two theoretically derived velocities versus the core height z. The bubble velocities v_{B1} and v_{B2} are drawn with dotted lines. It can be seen that the values resulting from the phase shift of the cross power spectral densities are in very good accordance with the theoretical expected mean velocities.

I.2.2.3 Conclusions

Up to now it seems to be impossible to extract information about the mechanical behaviour of the core structure (vibrations) from the neutron noise at the KWL. On the

contrary, with regard to surveillance techniques, it seems to be possible to detect irregularities (partial obstructions) within a cooling channel by the control of the phase function of in-core ion chambers (positioned one above the other) in the frequency range above 1.6 Hz. The possibility to determine the local steam void velocities in the whole core region may be of general interest. This could be done by a two-detector-system consisting of two miniature in-core ionisation chambers which are moveable in z-direction and positioned one above the other with constant distance (maximum 60 cm). Attention has to be paid when using sensors near the boiling boundary. The relevant frequencies range up to a frequency f_o, which depends on the mean bubble velocity and an effective sensitivity length of the detector.

To improve the measurements of the local steam void velocities at KWL it is proposed to filter the signals of the in-core detectors with a high-pass-filter at 1.6 Hz before amplifying and recording on magnetic tapes.

Literature, Section I.2.2

/1/ Lembcke, R.
Spektren von Rauschsignalen im KWL und Vergleich mit theoretischen Vorstellungen
Reaktortagung, Hamburg, April 1972

/2/ Wach, D.
Ermittlung lokaler Dampfblasengeschwindigkeiten aus den Rauschsignalen von Incore-Ionisationskammern
Atomwirtschaft, Dezember 1973

/3/ Lembcke, R., Wach, D.
Noise measurements in the BWR-Lingen at different power levels and different times
to be published

/4/ Wach, D.
Der Informationsgehalt der Rauschsignale von Druckwasserreaktoren in Hinblick auf das Schwingungsverhalten der Druckgefäßeinbauten (Voruntersuchungen am KWO)
MRR-111, April 1972

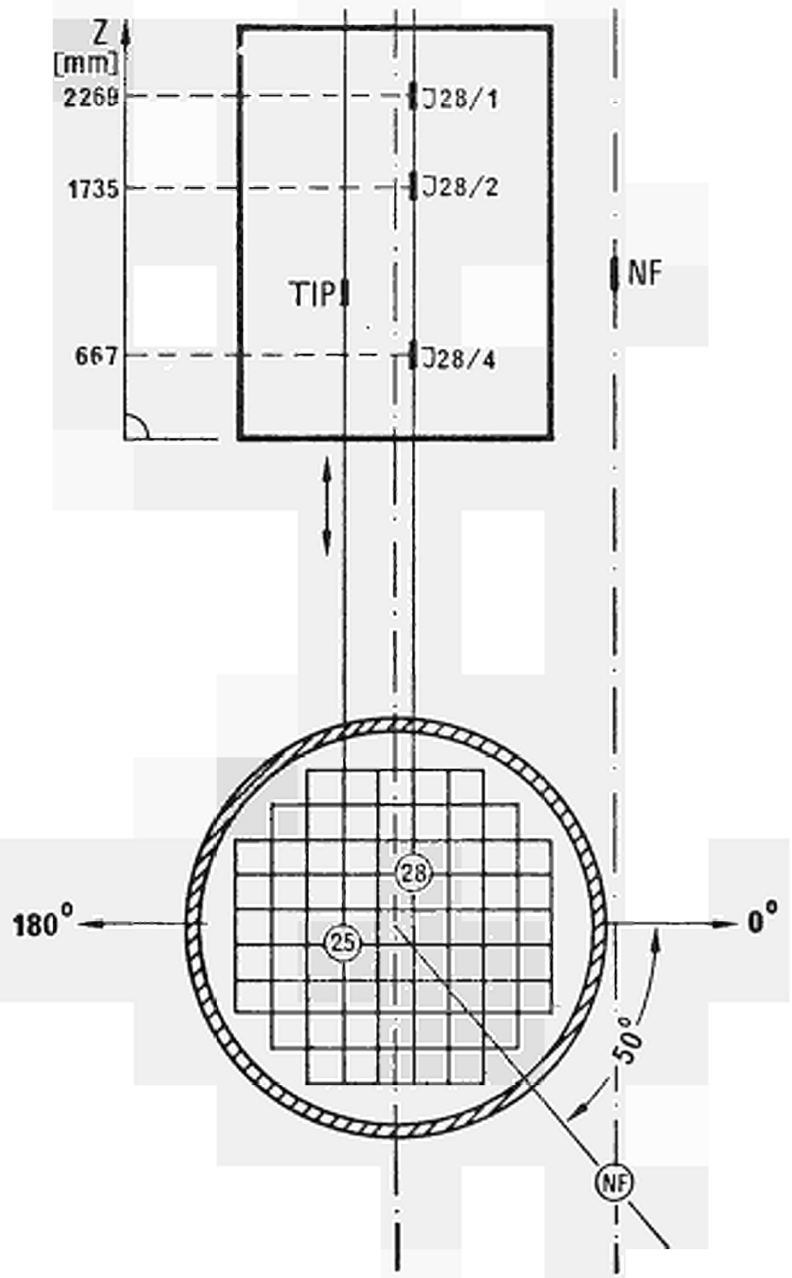

Fig. I.2.2/1: Position of neutron flux sensors
(KWL noise measurements, April 1971)

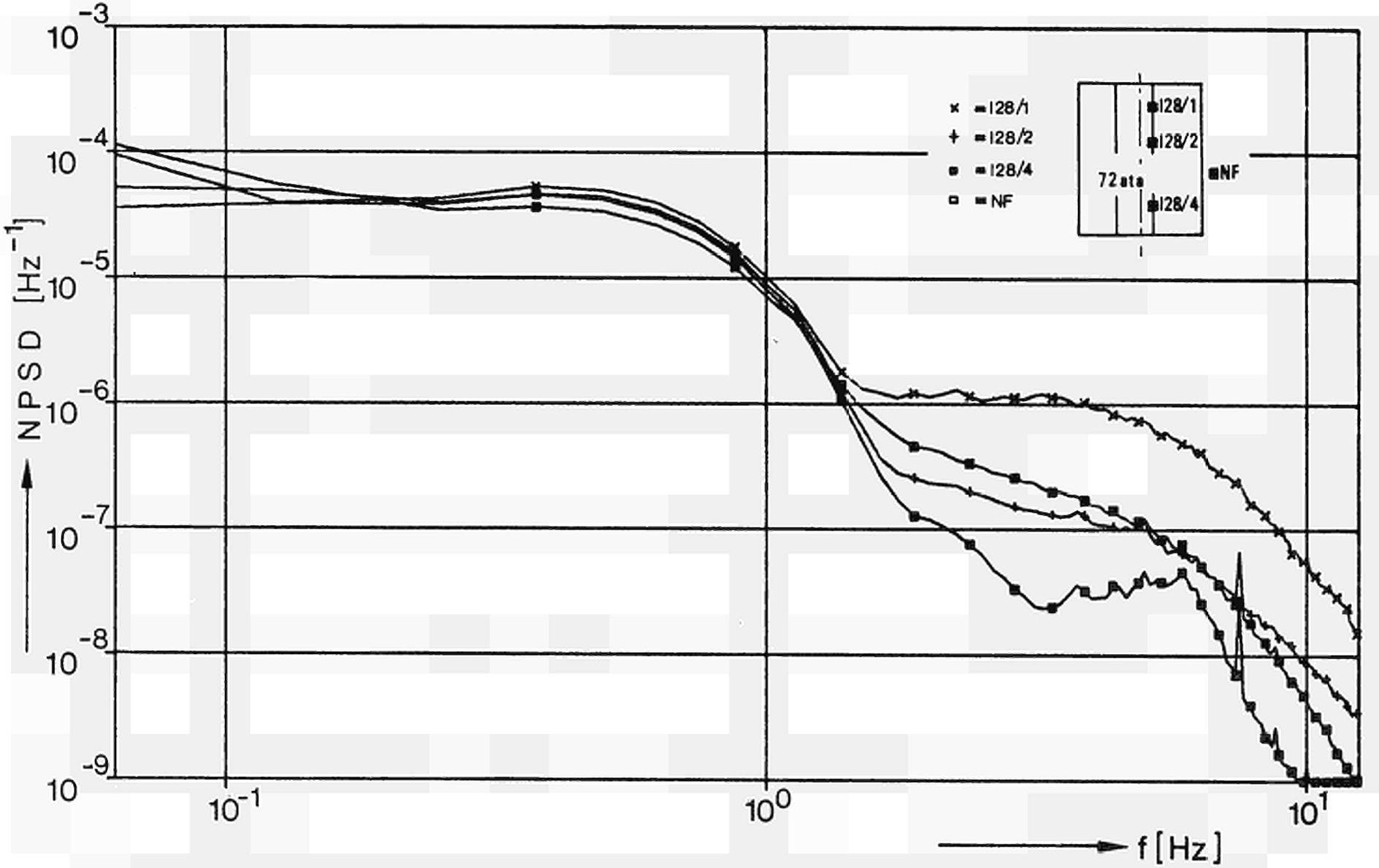

Fig. I.2.2/2: Normalized power spectral densities of the ion chambers NF, J28/1, J28/2 and J28/4 at full power (KWL: 72 ata, 106%, April 1971)

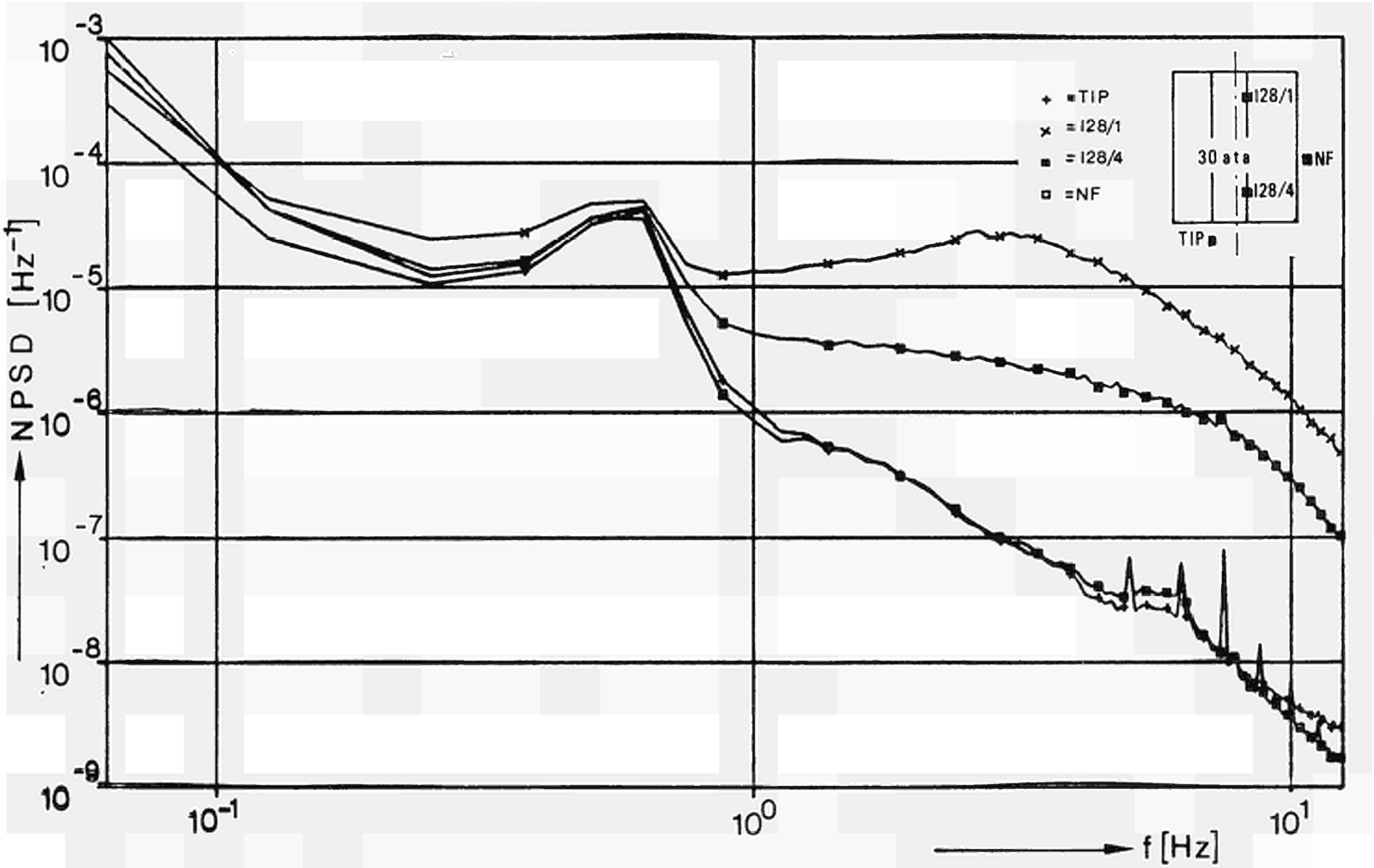

Fig. I.2.2/3: Normalized power spectral densities of the ion chambers NF, TIP, J28/1 and J28/4 at half power (KWL: 30 ata, 50%, April 1971)

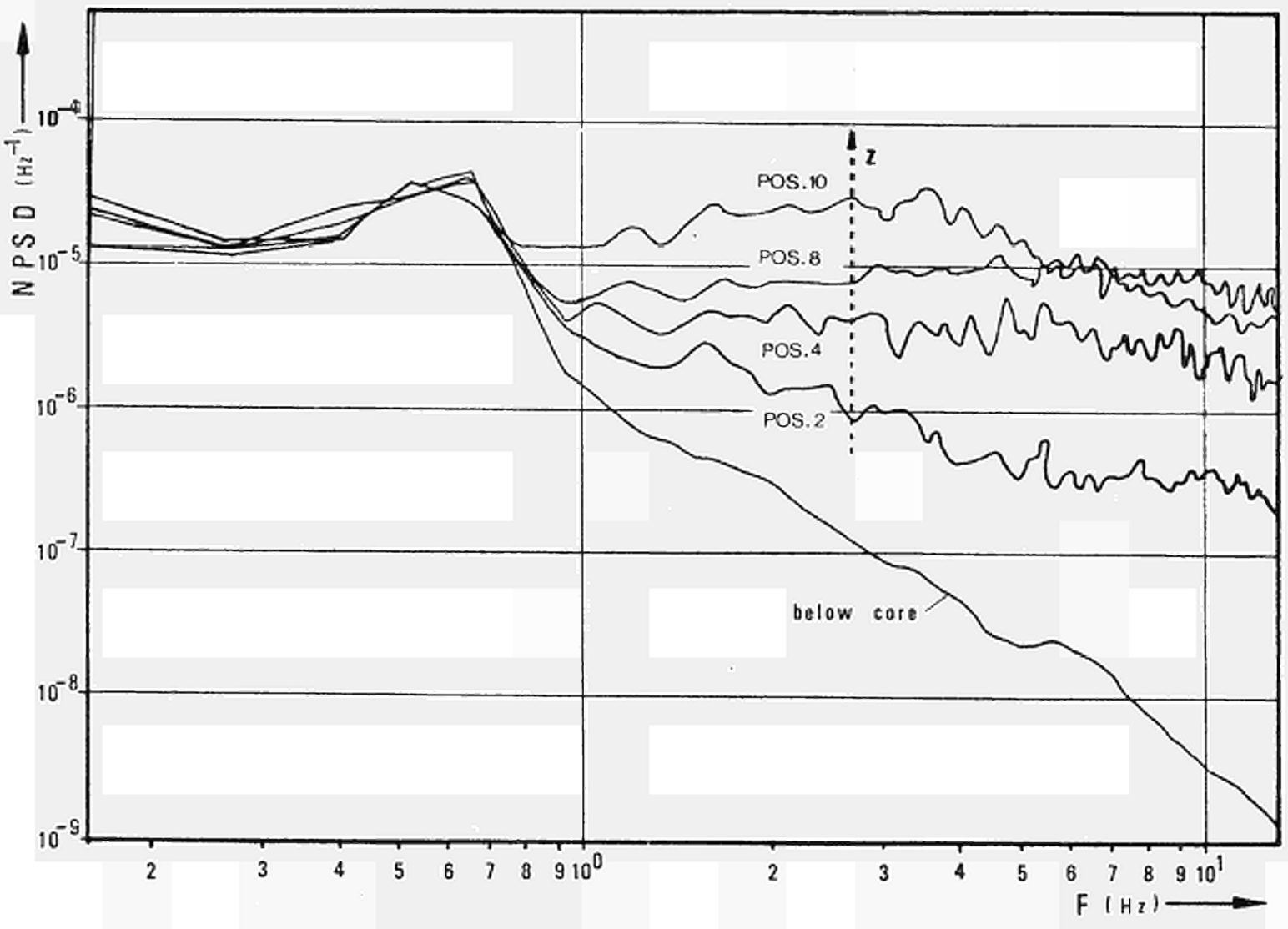

Fig. I.2.2/4: Normalized power spectral densities of the moveable ion chamber TIP at different core height positions (KWL: 30 ata, 50%, April 1971)

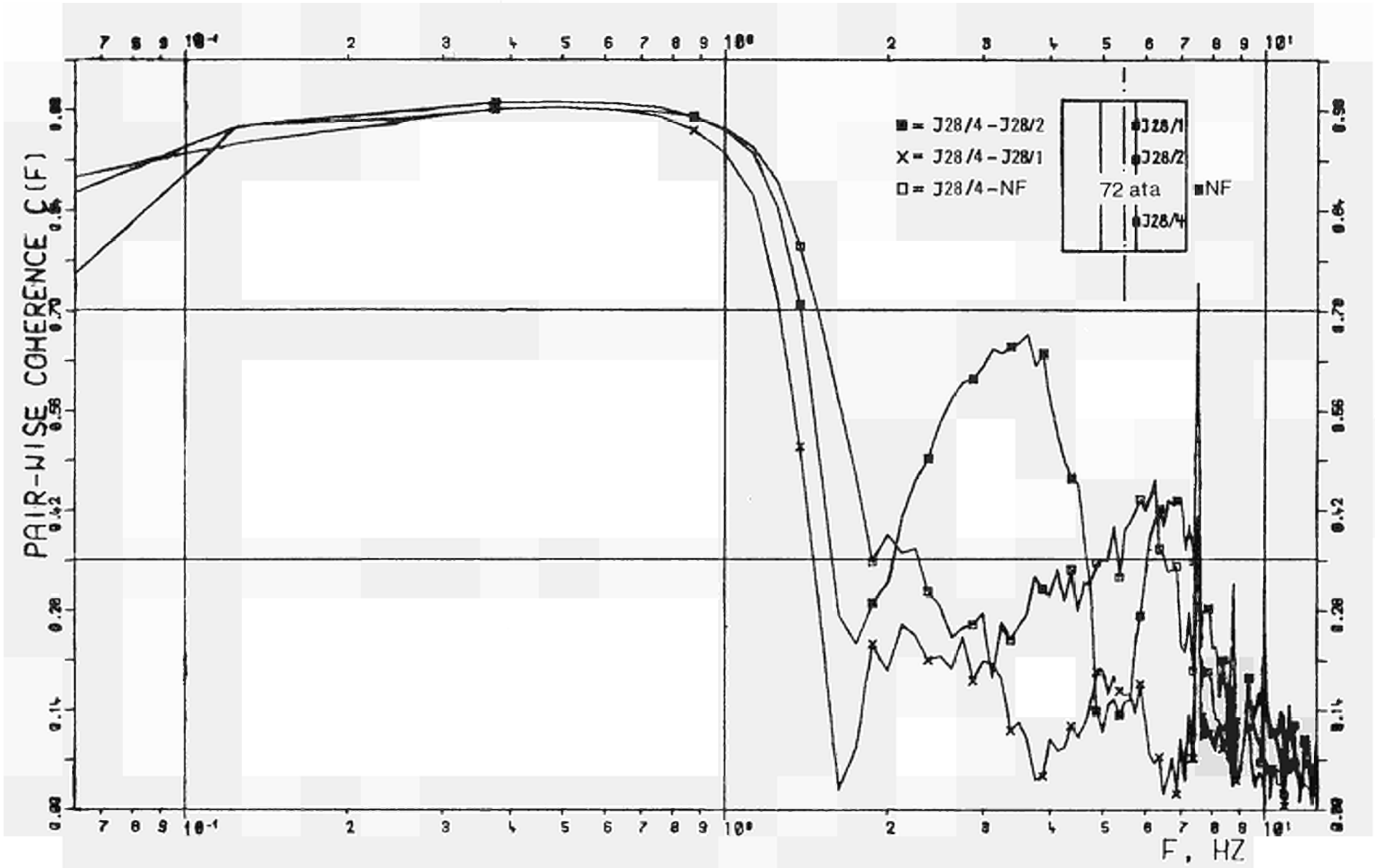

Fig. I.2.2/5: Coherence functions between the incore ion chamber J28/4 and the other available neutron flux signals at full power (KWL: 72 ata, 106%, April 1971)

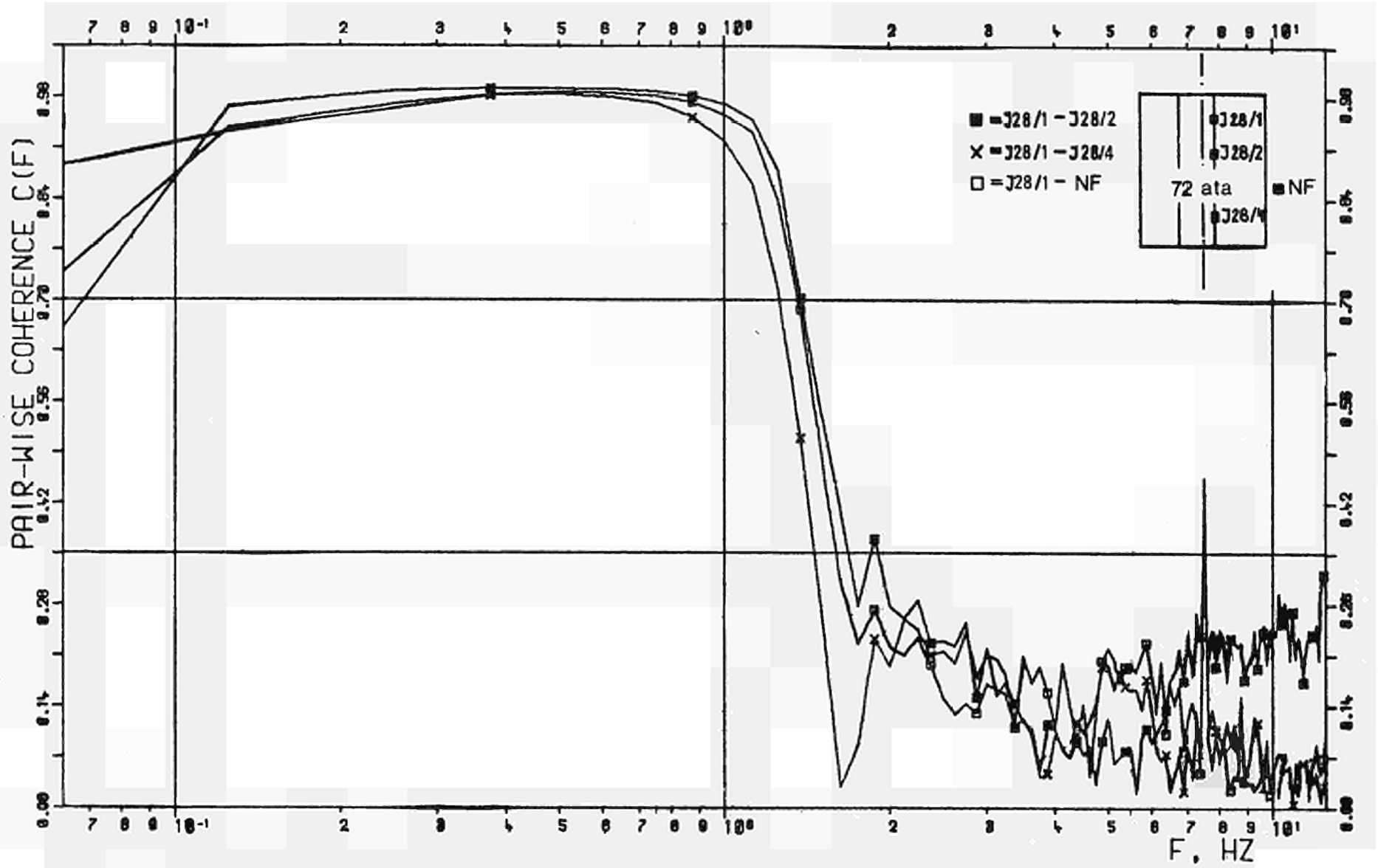

Fig. I.2.2/6: Coherence functions between the incore ion chamber J28/1 and the other available neutron flux signals at full power (KWL: 72 ata, 106%, April 1971)

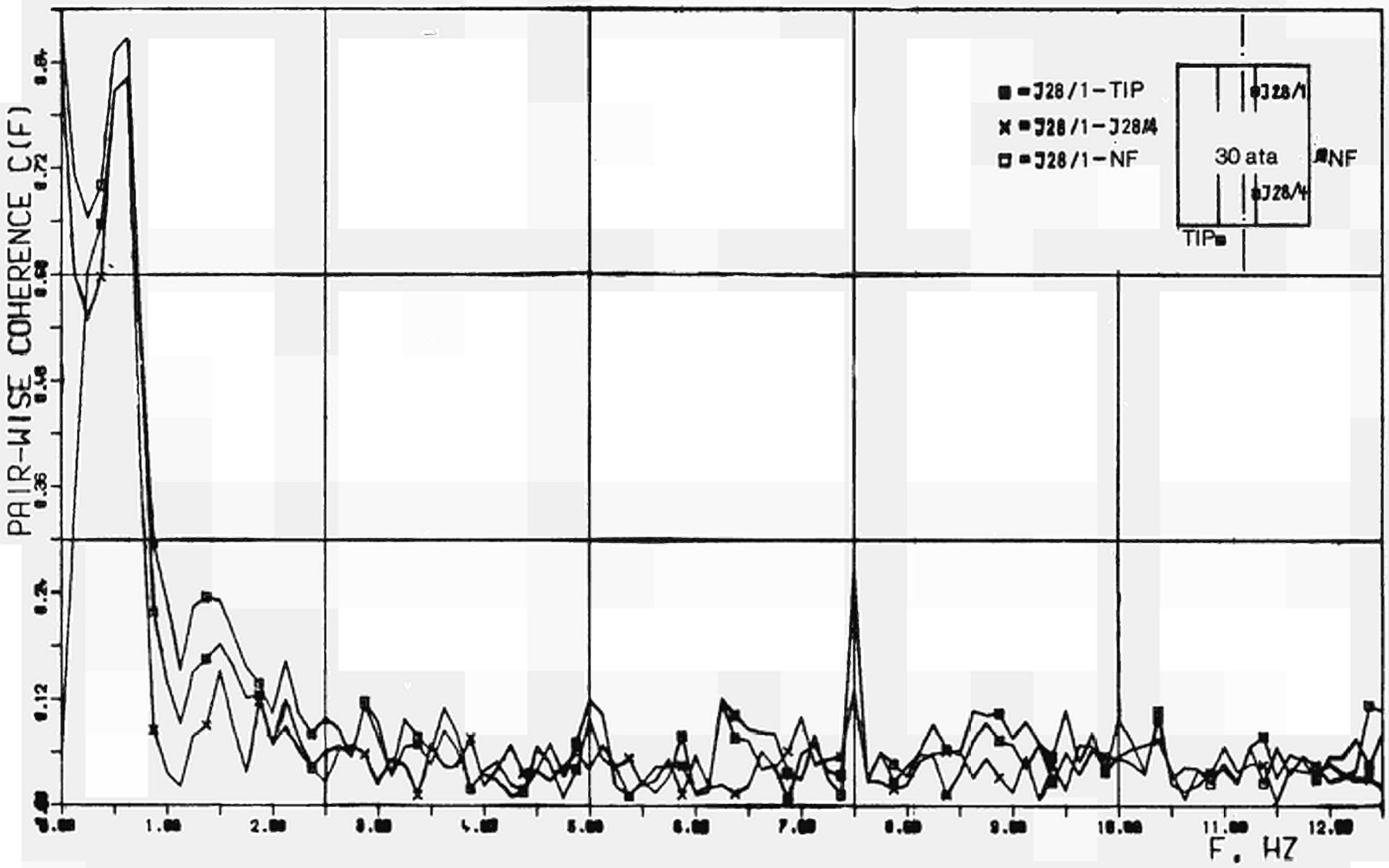

Fig. I.2.2/7: Coherence functions between the incore ion chamber J28/1 and the available neutron flux signals at half power (KWL: 30 ata, 50%, April 1971)

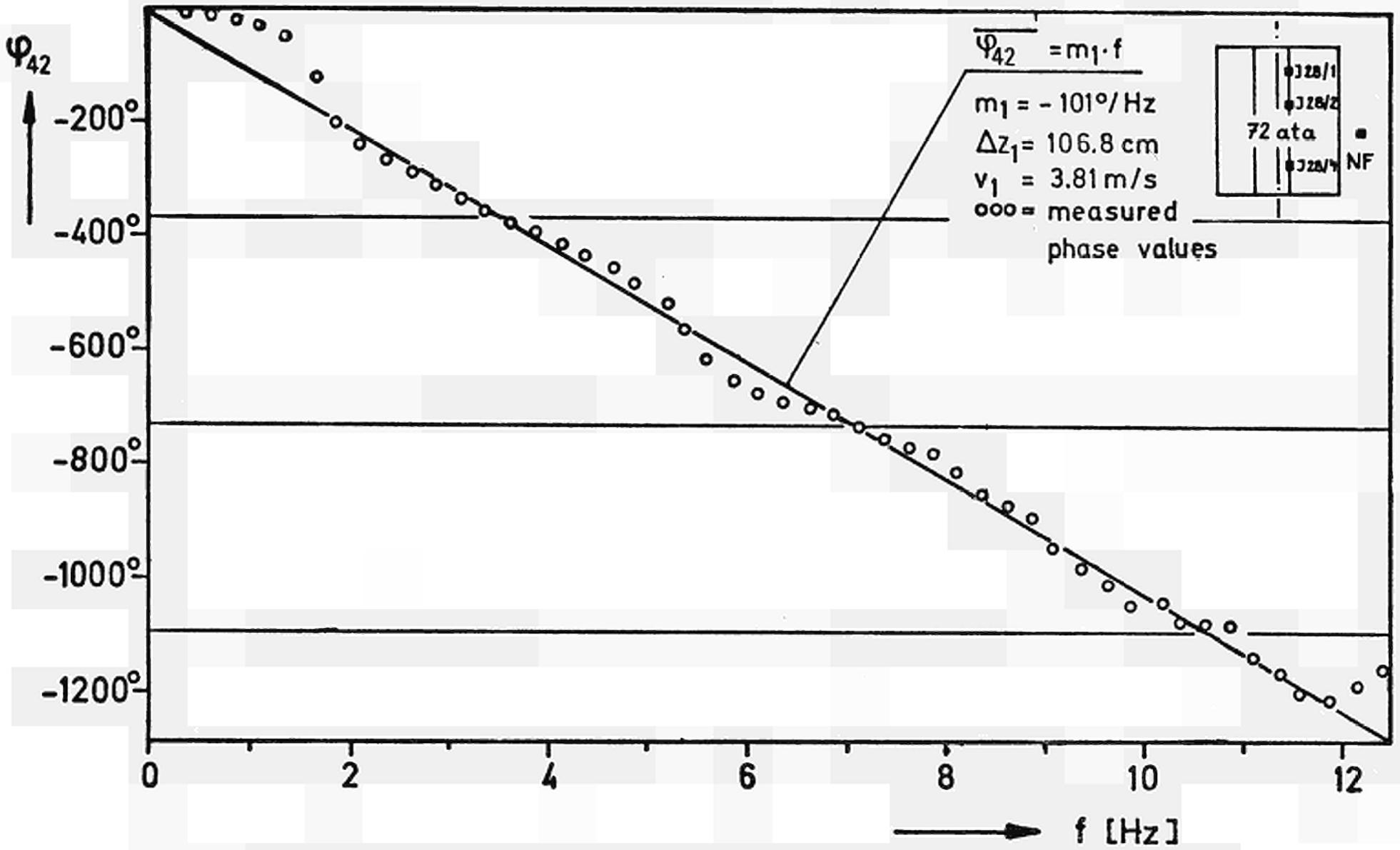

Fig. I.2.2/8: Phase of the CPSD of the incore ion chambers J28/4 and J28/2 at full power (KWL: 72 ata, 106%, April 1971)

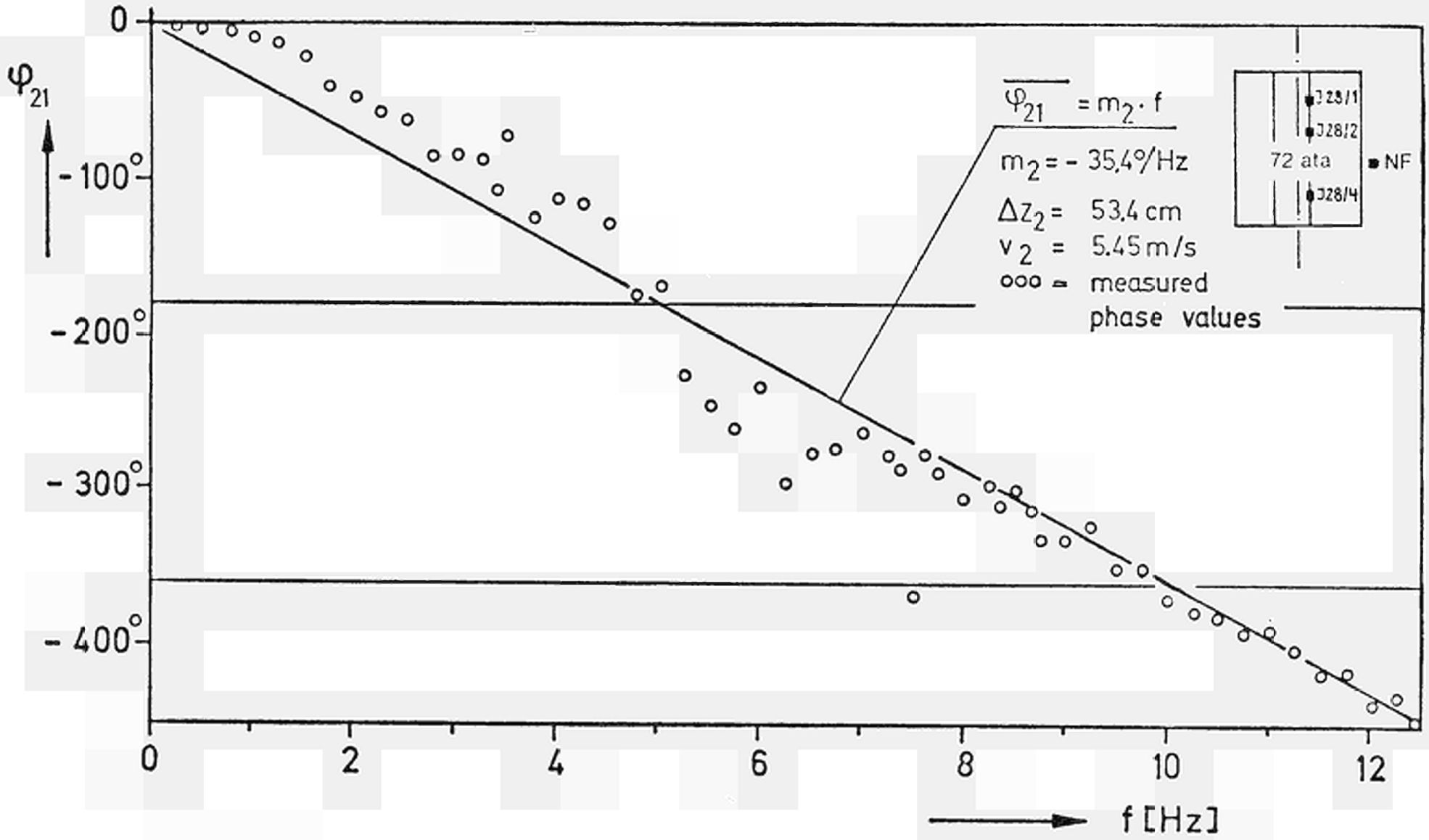

Fig. I.2.2/9: Phase of the CPSD of the incore ion chambers J28/2 and J28/1 at full power (KWL: 72 ata, 106%, April 1971)

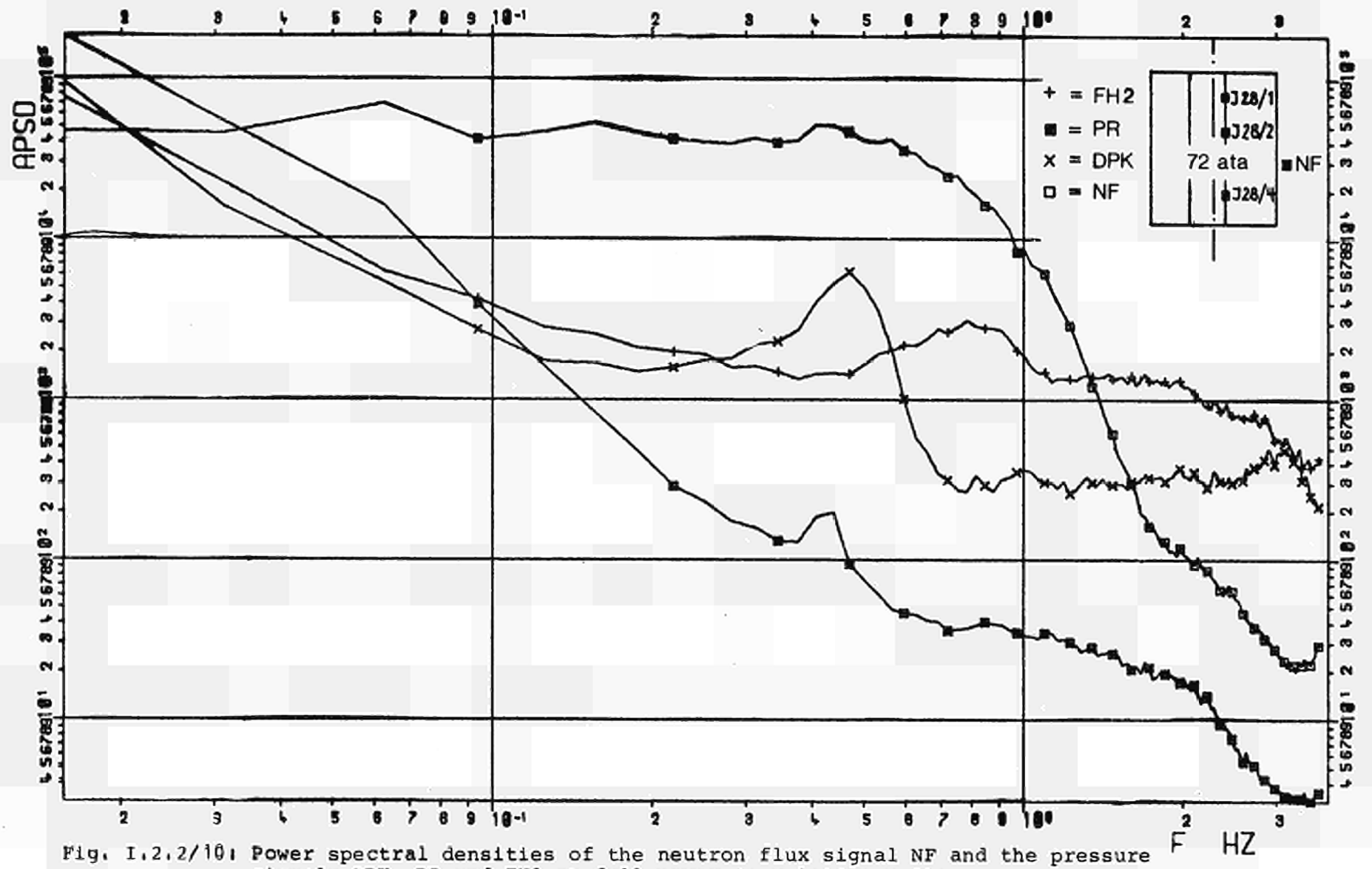

Fig. I.2.2/10: Power spectral densities of the neutron flux signal NF and the pressure signals DPK, PR and FH2 at full power in relative units (KWL: 72 ata, 106%, April 1971)

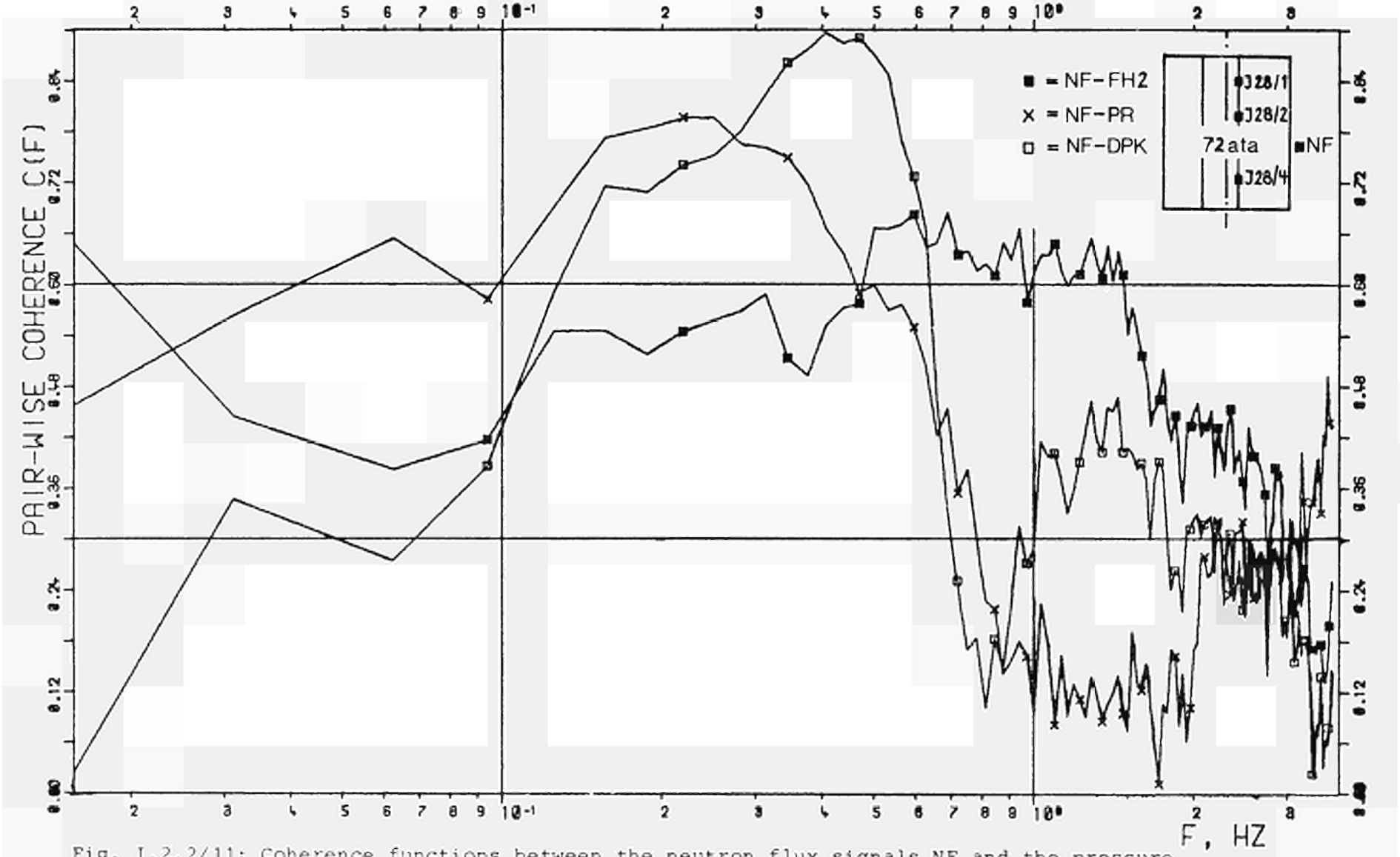

Fig. I.2.2/11: Coherence functions between the neutron flux signals NF and the pressure signals DPK, PR and FH2 at full power (KWL: 72 ata, 106%, April 1971)

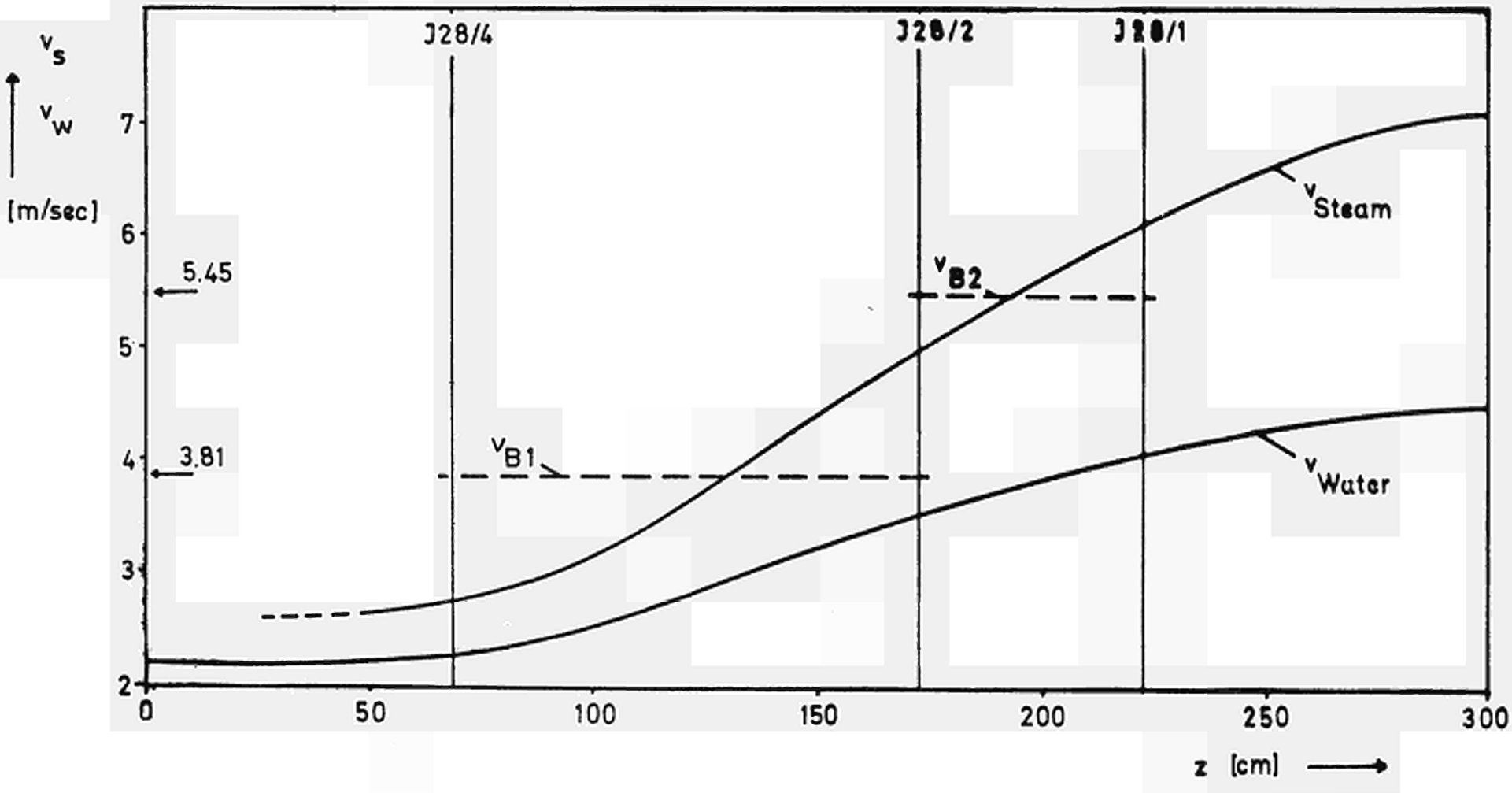

Fig. I.2.2/12: Local mean velocities of water (v_w) and steam (v_s) versus core height z at full power and mean bubble velocities (v_{B1} and v_{B2}, dotted lines) resulting from incore noise analysis at 106% (KWL, April 1971)

I.2.3 WÜRGASSEN Nuclear Power Plant

WÜRGASSEN is a 2-loop boiling water reactor plant with an output of 670 MW_{el}. It went in operation in 1972. Accelerometers were installed at several positions of the reactor vessel wall and the two recirculation pumps. The aim of the investigations was to get further information of that type of sensors for on-line surveillance purposes.

I.2.3.1 Measurements

At the pressure vessel 4 X-ray resistant accelerometers were installed. Both the recirculating pumps are also equipped with an accelerometer (figs. I.2.3/1 and I.2.3/2). The signals were digitized on line and stored by means of a transportable digital data reducing system.

I.2.3.2 Analysis

Lower frequency range (1 cps up to 50 cps): It is interesting to see, that only in the upper range at the pressure vessel close to the steam outlet and to the inlet of the core sparger a vibration of 30 cps can be found. It is possible, that this is a vibration of a tube or of a construction unit (fig. I.2.3/3).

Middle frequency range (100 cps up to 3000 cps): At the recirculating pumps one can measure characteristic frequencies of the pump noise in the range of 2000 cps up to 3000 cps. In addition to this frequencies one can find at the pressure vessel special peaks of 700 cps and 870 cps. This points to vibrations which are produced in the pressure vessel in addition to the noise of the pumps (figs. I.2.3/4 and I.2.3/5).

Upper frequency range (above 3000 cps): In the range above the noise of the pumps there exists a sharp peak at 4176 cps. This frequency is particularly found in the upper region of the pressure vessel. The reason is unknown (fig. I.2.3/6).

In normal operation of the WÜRGASSEN plant no burst of noise could be found until now. For detecting and finding of loose parts it is important to know the delay of bursts within the water and the wall of the pressure vessel. For that reason knock tests were made during the shut-down of the plant. The delay between the individual measuring points is in the range of 5 ms up to 20 ms (figs. I.2.3/7 and I.2.3/8). By regard of these delays it should be possible to find loose parts /1/.

Literature, Section I.2.3

/1/ Moravek, I., Raible, B.
Körperschallmessungen an Reaktordruckbehältern
Vortragstagung 1973: Zerstörungsfreie Materialprüfung
Salzburg, Oct. 18-19, 1973

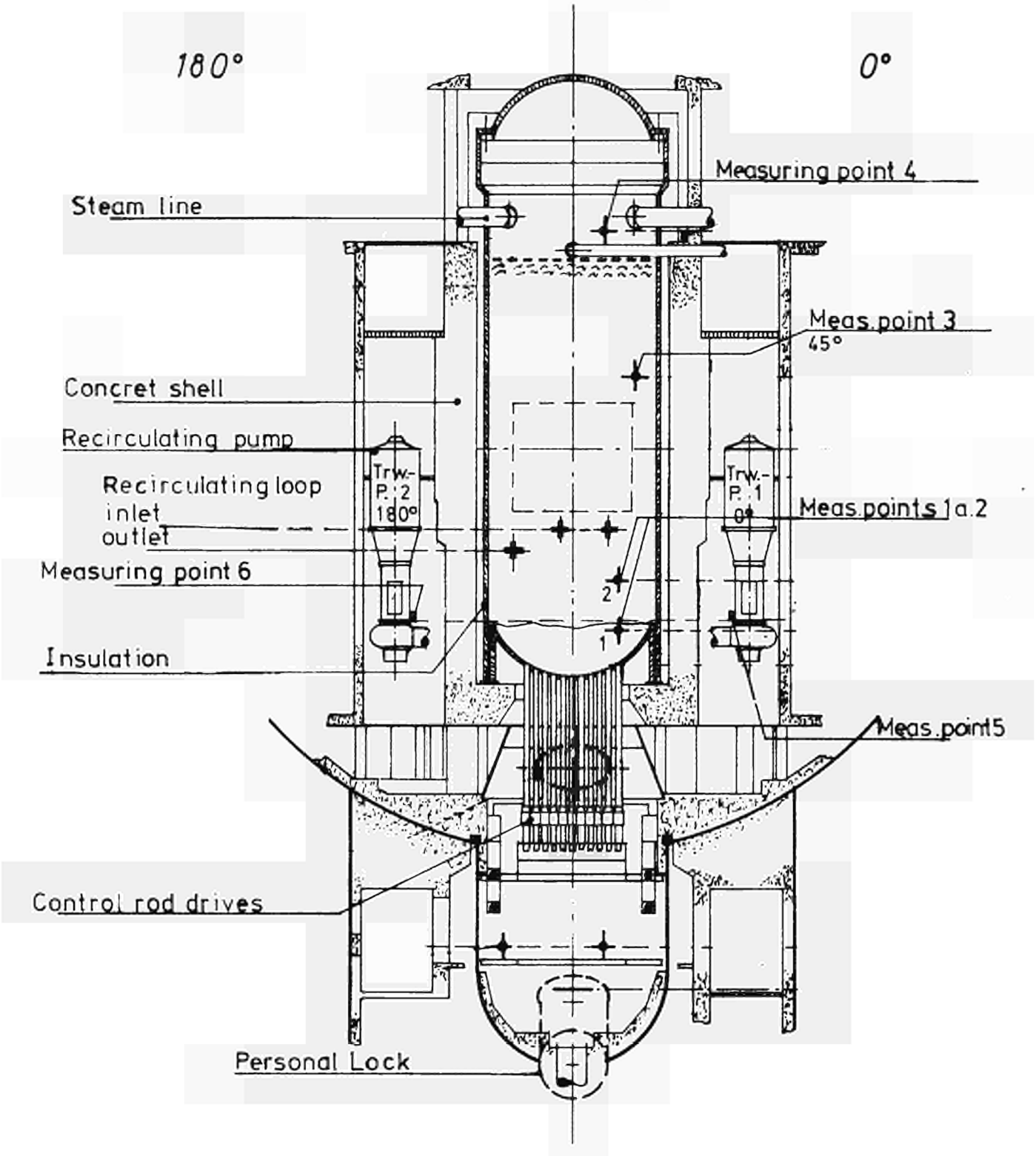

Fig. I.2.3./1 Measuring Points on the Reactor pressure vessel

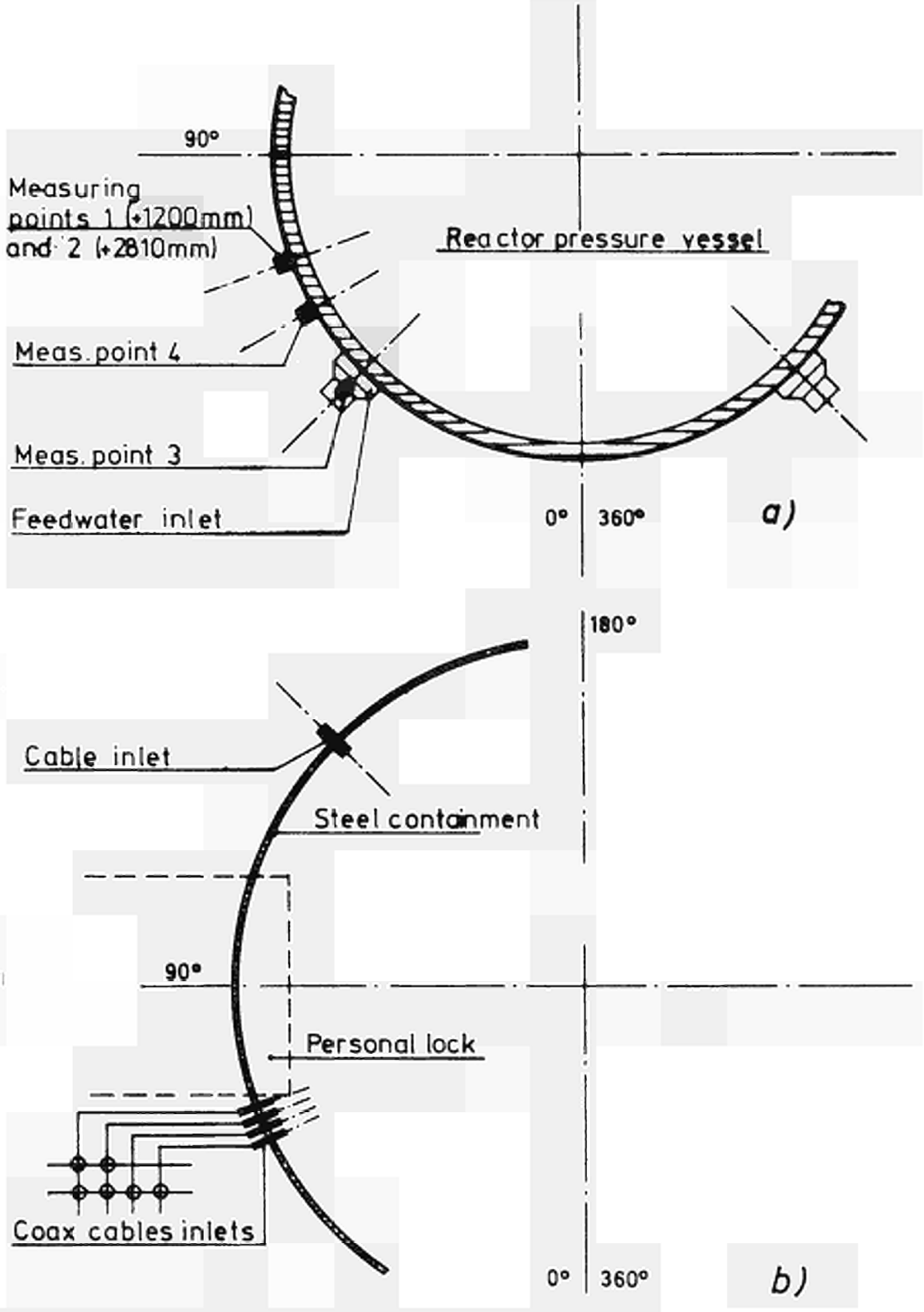

Fig. I.2.3/2 Measuring Points and Cables inlets

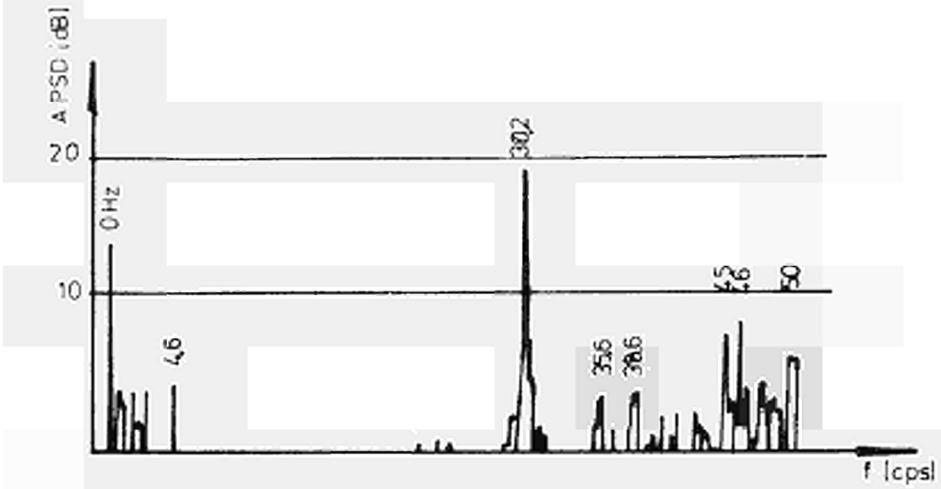

Fig I.2.3/3 Measuring point 4, Power Spectral Density (APSD)

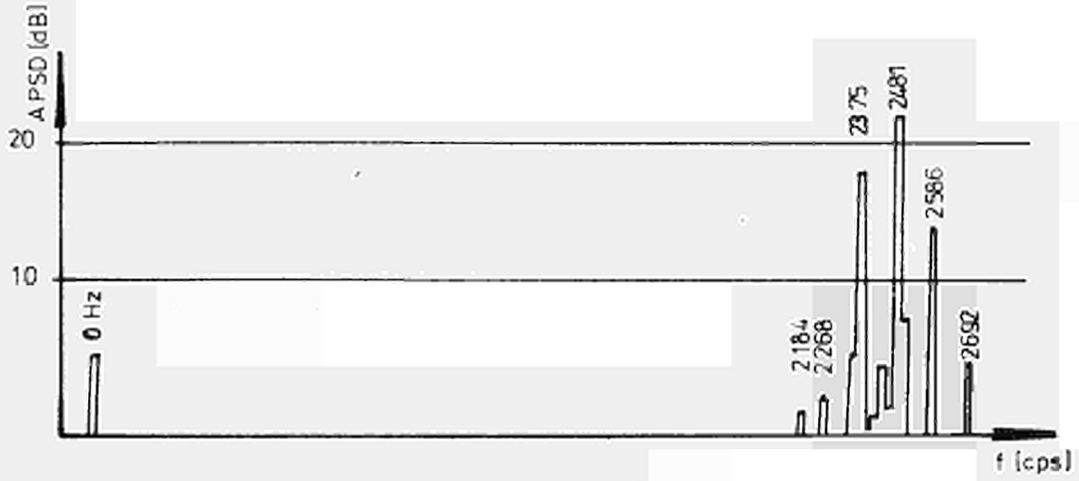

Fig.I.2.3./4 APSD of measuring point 5 (pump)

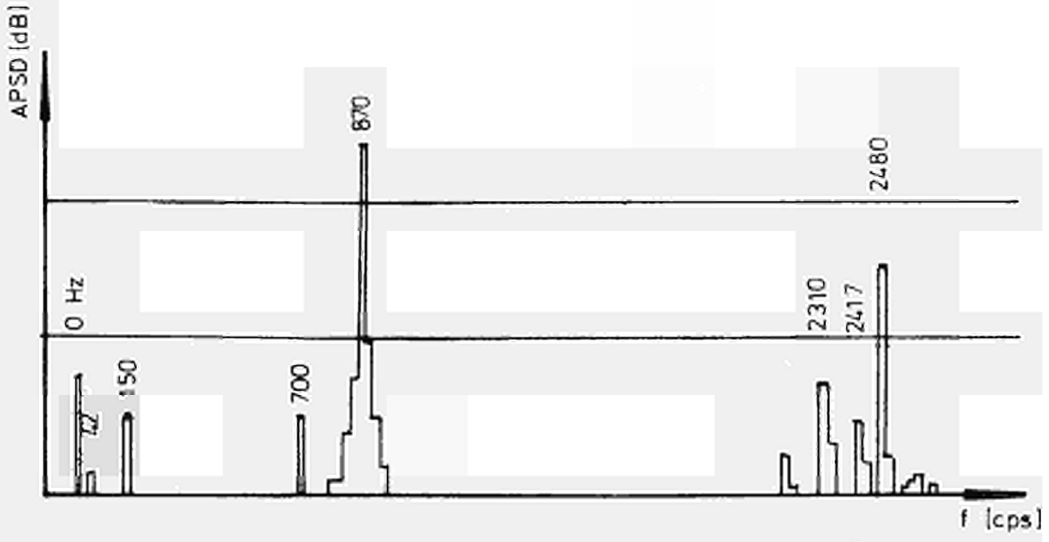

Fig. I.2.3./5 APSD of measuring point 1 (reactor pressure vessel)

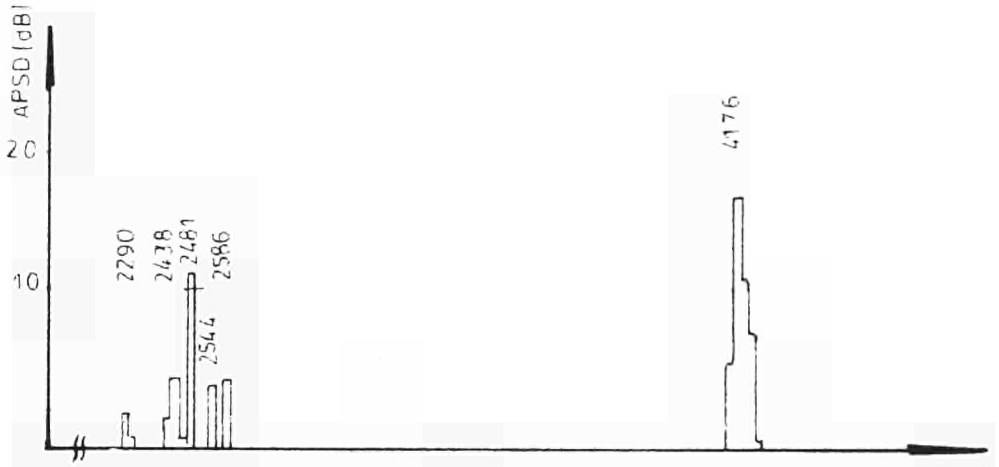

Fig. 1.2.3/6 APSD of measuring point 4

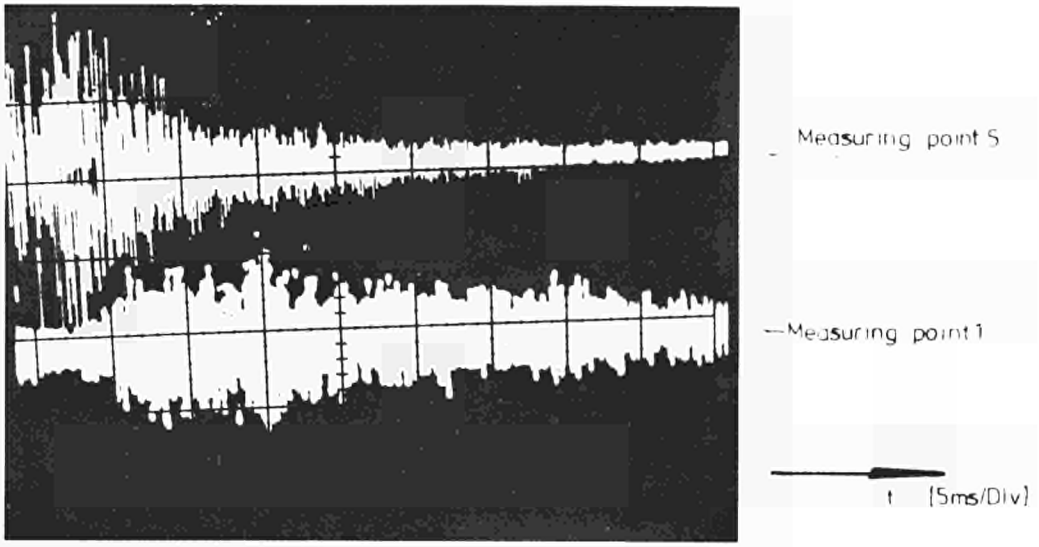

Fig. 1.2.3/7 Delay between measuring point 5 and 1

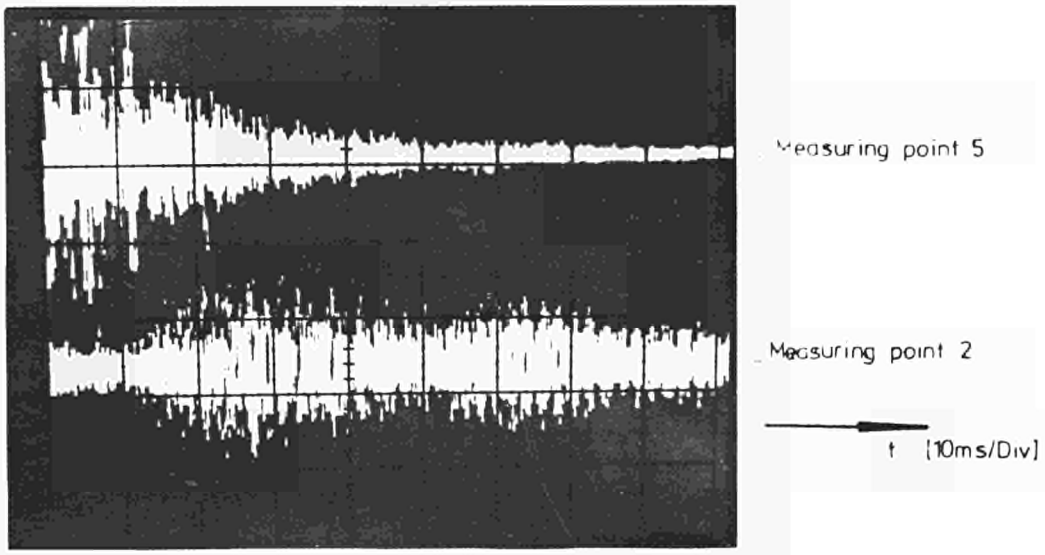

Fig. 1.2.3/8 Delay between measuring point 5 and 2

I.3 Pressurized Water Reactors

I.3.1 BR 3 Nuclear Power Plant

I.3.1.1 Measurements

BR 3 is a 12 MW_e pressurized water reactor located at Mol. Noise measurements were performed with the operating staff of BR 3, the Katholieke Universiteit Leuven and Laborelec in December 1972 and repeated regularly since then.

The neutron flux fluctuations were first analysed and later on accelerometers were placed on the upper side of the vessel, on the steam generator and on the two main coolant pumps and analysed, too.

Neutron flux fluctuations were measured by means of three power range ionization chambers. These were long (20 cm active length) uncompensated ionization chambers. Their location is shown in fig. I.3.1/1. Chambers ICA and ICB are opposite and ICC is located at 90° from the two others. The sensor current was converted by a series resistance of 1 KΩ to a voltage. This way of measuring introduces a low-pass filtering effect but was the only possible. The singal from which the DC component was substracted was amplified thousand times by a Preston floating differential amplifier, band-pass filtered (1Hz - 25 Hz) with a Krohn-Hite filter, and then directly analyzed by a Hewlett-Packard Fourier Analyzer (16 K memory).

In addition six accelerometers (Bruel and Kjaer) were installed on the primary circuit, i.e.

- on the reactor vessel (fig. I.3.1/1 and I.3.1/2). Three accelerometers were screwed on an inox patch soldered on the top of the pressure vessel in a horizontal position.
- on the steam-generator. One accelerometer was fixed in the same manner as on the pressure vessel near the water box.
- on the two main coolant pumps. They were fixed on a gripping collier fixed on the refrigerating circuit of the pumps close to the motor.

I.3.1.2 Analysis

The power spectral densities of the signals were computed with the Fourier Analyzer. A resolution of 512 points in frequency seemed sufficient and in order to have a good statistical confidence in the spectral estimates two hundred samples were taken. Normalisation for the ionization chamber signals was done afterwards.

The frequency range was for the neutron flux spectra 0 to 25 Hz, (~.1 Hz resolution) or 0 to 50 Hz (~.2 Hz resolution). For the accelerometer signals several ranges were used up to 10 kHz.

I.3.1.2.1 Ionization Chambers

A series of measurements was performed in March 1973. The power level was 38.6 MW_{th}. The correspondent dc level of the ionization chamber signals was at the 1 KΩ resistance 153 mV for ICA and ICC and 98 mV for ICB. Shown in the figs. I.3.1/4, I.3.1/5, I.3.1/6, I.3.1/7 are the NPSDs of ICA and ICB, the NCPSD of ICA and ICB.

A peak at 16 Hz is noticed, the width of which is about 3 Hz. On ICC the same peak is noticed. The phase of the NCPSD of ICA and ICB shows a small shift between ICA and ICB (fig. I.3.1/7). On the NCPSD of ICA and ICC the phase shift was zero (not shown on the figures). The coherence is fairly good at this 16 Hz peak (fig. I.3.1/8).

At frequencies above ca 30 Hz the coherence function had to be erased due to computational problems. These problems are noticed, too, on the NCPSD whose level is higher than each NPSD above 30 Hz.

Insertion of the control rods was slightly changed but no modification in the 16 Hz peak could be noticed, so that this peak could not be attributed to vertical movement of the core. Also horizontal movement had to be excluded since no 180^{o} phase shift between ICA and ICB was observable. So far no explanation could be given for this peak.

When investigating the reproducibility of the measurements the following behaviour of the spectra was observed:

The same tests as those of March 1973 were repeated afterwards and no noticeable change in the spectra was seen. However, the spectra obtained already in December 1972 showed a complete different shape (figs. I.3.1/9 to I.3.1/20). At that time the power level was lower, i.e. 30.2 MW_{th} against 38.6 MW_{th}. A huge peak at 7.7 Hz and two peaks at 13 and 16 Hz appeared on the different ionization chamber spectra (figs. I.3.1/9 - I.3.1/10). After two days the peak at 13 Hz was no more present and the peak at 7.7 Hz was not so important any more (figs. I.3.1/11 to I.3.1/14). After a week, only the

peak at 16 Hz remained (figs. I.3.1/15 to I.3.1/20). No change in operating conditions was noticed during this period.

I.3.1.2.2 Accelerometers

Spectra obtained on the two pumps are shown in the figs. I.3.1/21 and I.3.1/22 (relative scales). Two frequency ranges are shown. The first (0 - 100 Hz) is the most interesting. The second (0 - 10 kHz) only shows a difference in level between MC pump 1 and 2.

The pumps are rotating near 3000 rpm and have 7 blades and a diffuser with 8 blades. The motor is a double squirrel cage. The rotating frequency ($\sim$50 Hz) is clearly shown. Interesting is the 24 Hz peak on the MC pump 2 which indicates an excentricity of the rotor. On MC pump 1, this 24 Hz peak is not present but two important lateral bands can be noticed.

Another feature is that much more frequency lines are present on MC pump 1 than on MC pump 2. In fact MC pump 1 was malfunctioning and had to be stopped one month later. The damages were so important that the pump was unrepairable. This problem will be discussed in more detail in the second part (turbines) of this report.

The accelerometer at the steam generator is only intended to detect loose parts travelling through the primary circuit. The spectrum is of no interest up to this point.

The spectra of the three accelerometers attached to

the reactor vessel are shown in figs. I.3.1/23 and I.3.1/24 in arbitrary units. Accelerometers no. 1 and no. 2 have approximately the same spectra in the 0 to 25 Hz range. Several little peaks are noticed. Some are related to peaks discovered on the two pumps. The 13 and ~16 Hz peaks are not yet explained. On accelerometer no. 6 no peaks are discernible. Typical results between 0 and 10 kHz are also shown (figs. I.3.1/25 and I.3.1/26).

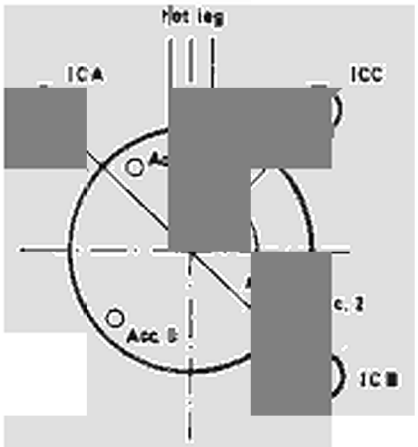

Accelerometers and ionization chambers location

FIG. I.3.1/1.

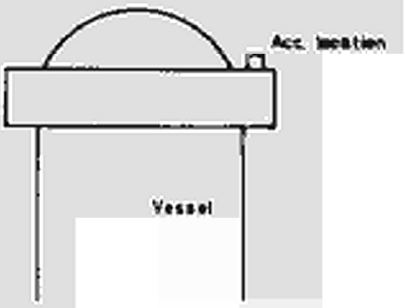

Schematic location of the accelerometers

FIG. I.3.1/2

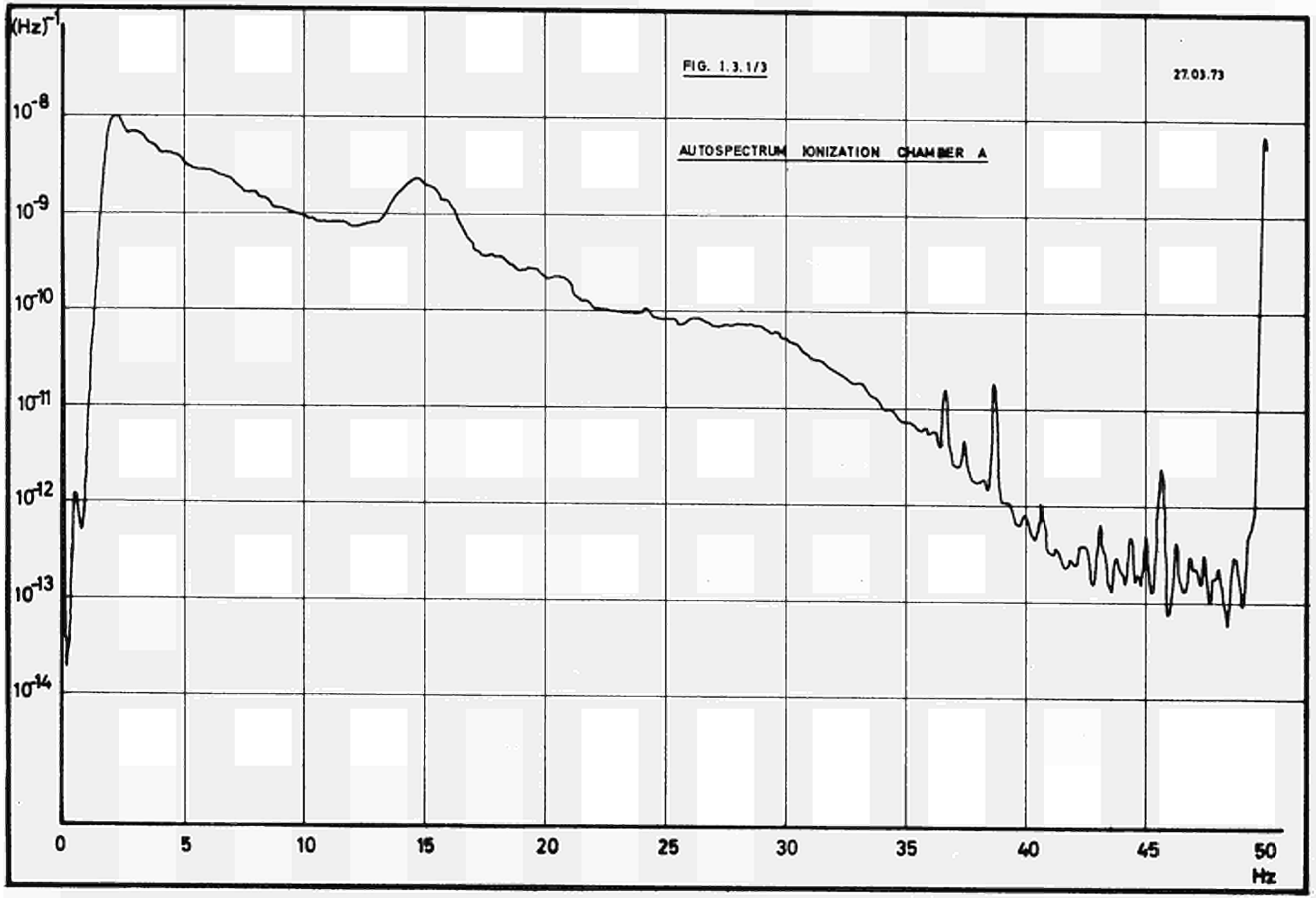
(Hz)$^{-1}$
10^{-8}
10^{-9}
10^{-10}
10^{-11}
10^{-12}
10^{-13}
10^{-14}
FIG. 1.3.1/3
27.03.73
AUTOSPECTRUM IONIZATION CHAMBER A
0
5
10
15
20
25
30
35
40
45
50
Hz

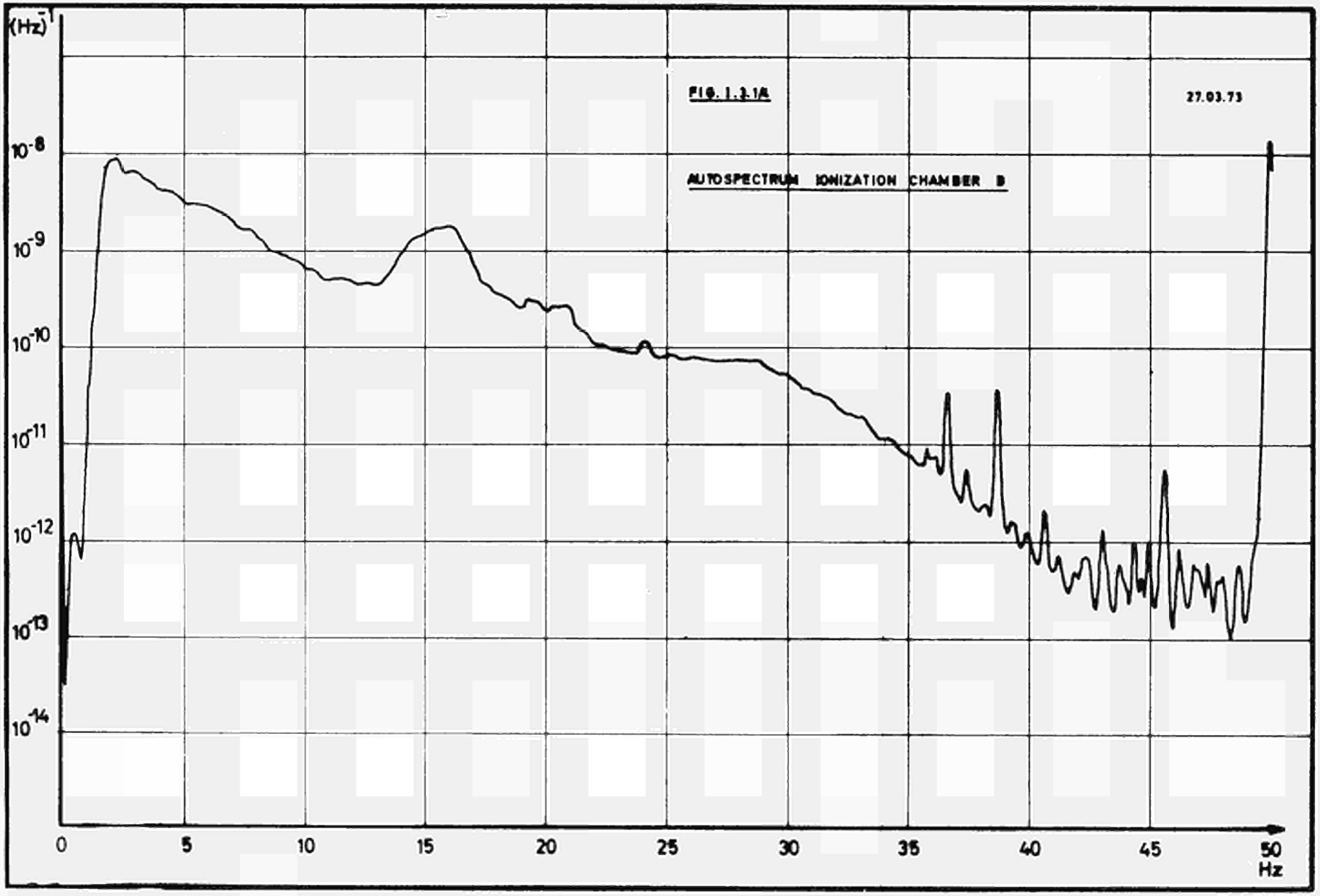
(Hz)⁻¹
FIG. 1.3.1A
27.03.73
AUTOSPECTRUM IONIZATION CHAMBER B
10⁻⁸
10⁻⁹
10⁻¹⁰
10⁻¹¹
10⁻¹²
10⁻¹³
10⁻¹⁴
0
5
10
15
20
25
30
35
40
45
50
Hz

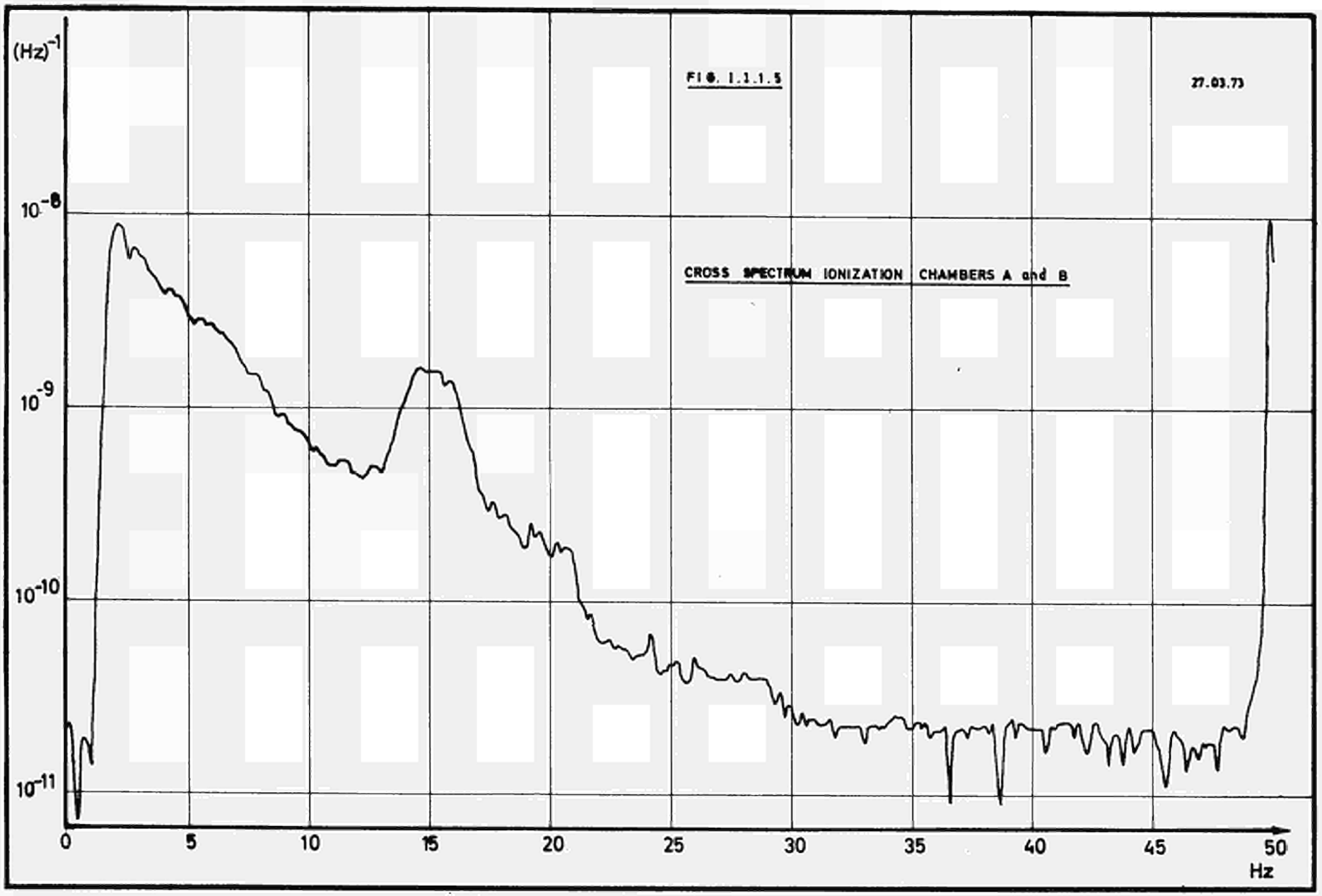
(Hz)$^{-1}$
FIG. 1.1.1.5
27.03.73
CROSS SPECTRUM IONIZATION CHAMBERS A and B
10^{-8}
10^{-9}
10^{-10}
10^{-11}
0
5
10
15
20
25
30
35
40
45
50
Hz

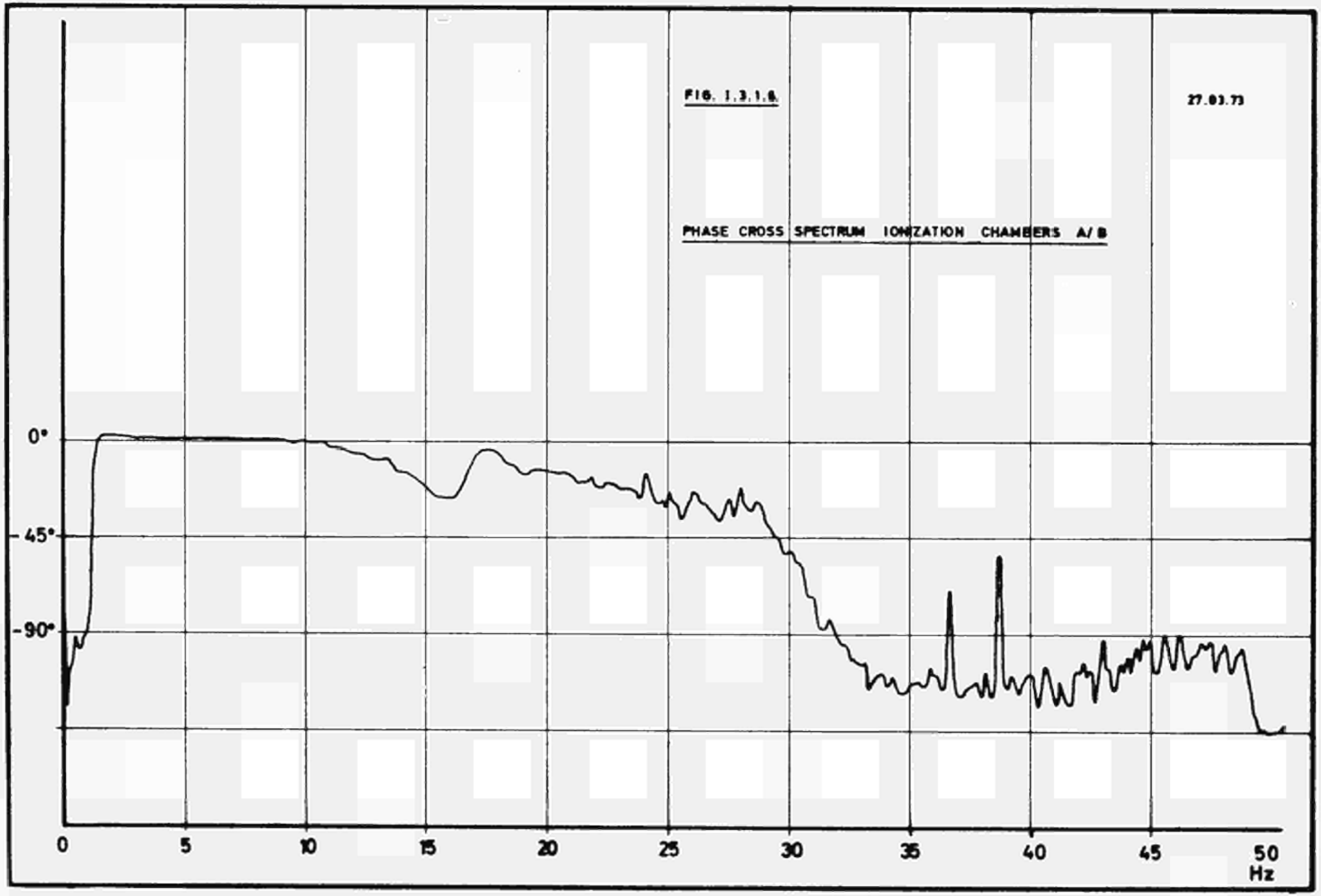
FIG. 1.3.1.8.
27.03.73
PHASE CROSS SPECTRUM IONIZATION CHAMBERS A/B
0°
-45°
-90°
0
5
10
15
20
25
30
35
40
45
50
Hz

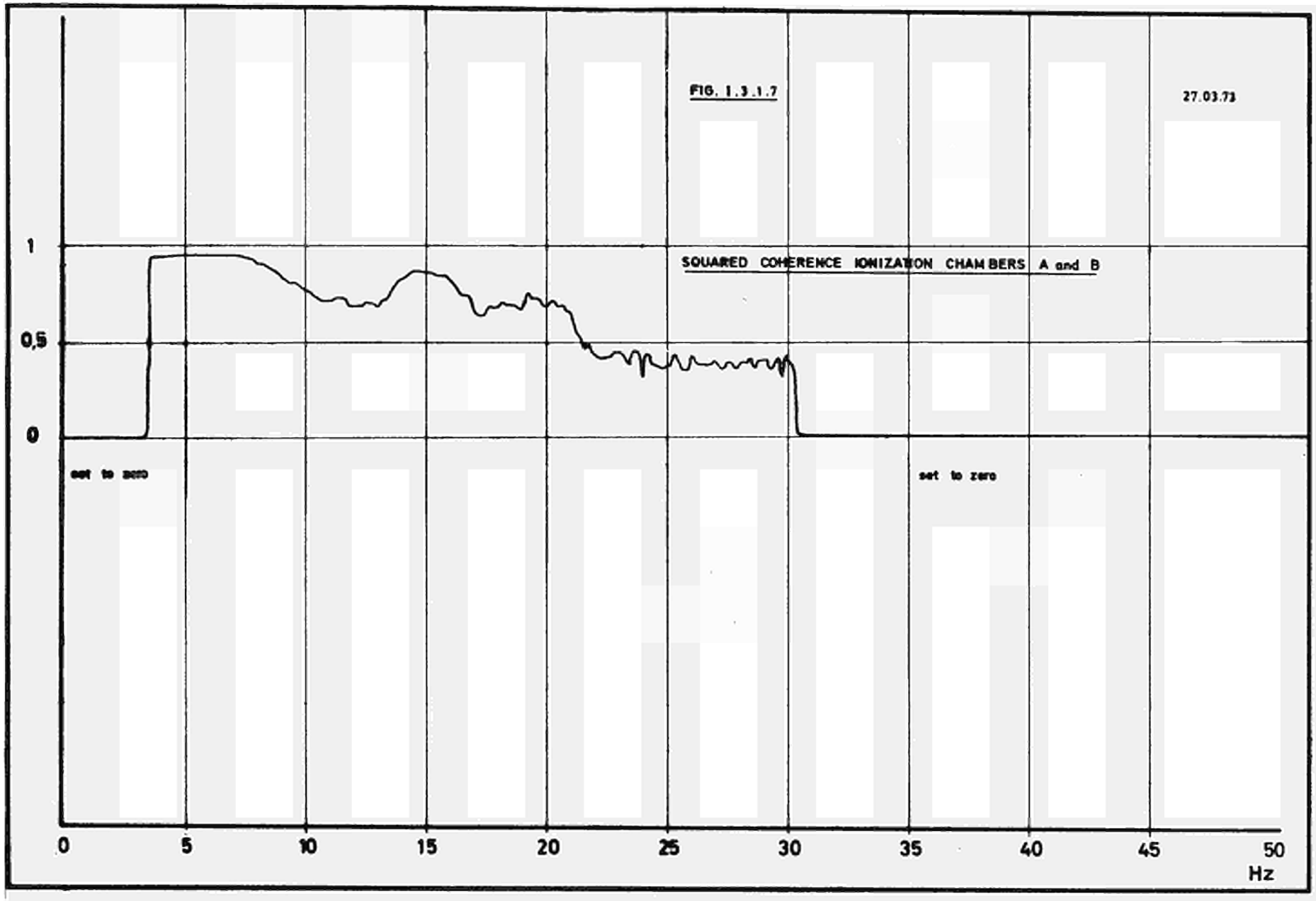
FIG. 1.3.1.7
27.03.73
SQUARED COHERENCE IONIZATION CHAMBERS A and B
1
0,5
0
set to zero
set to zero
0
5
10
15
20
25
30
35
40
45
50
Hz

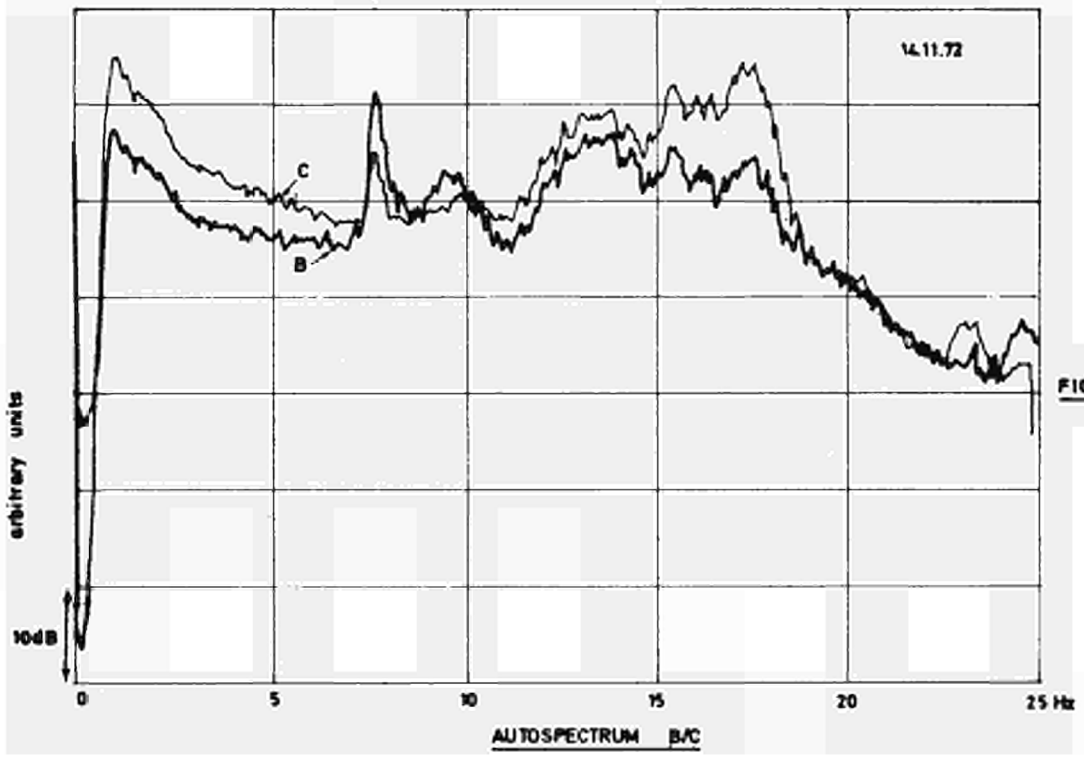

AUTOSPECTRUM B/C

FIG. I.3.1.8

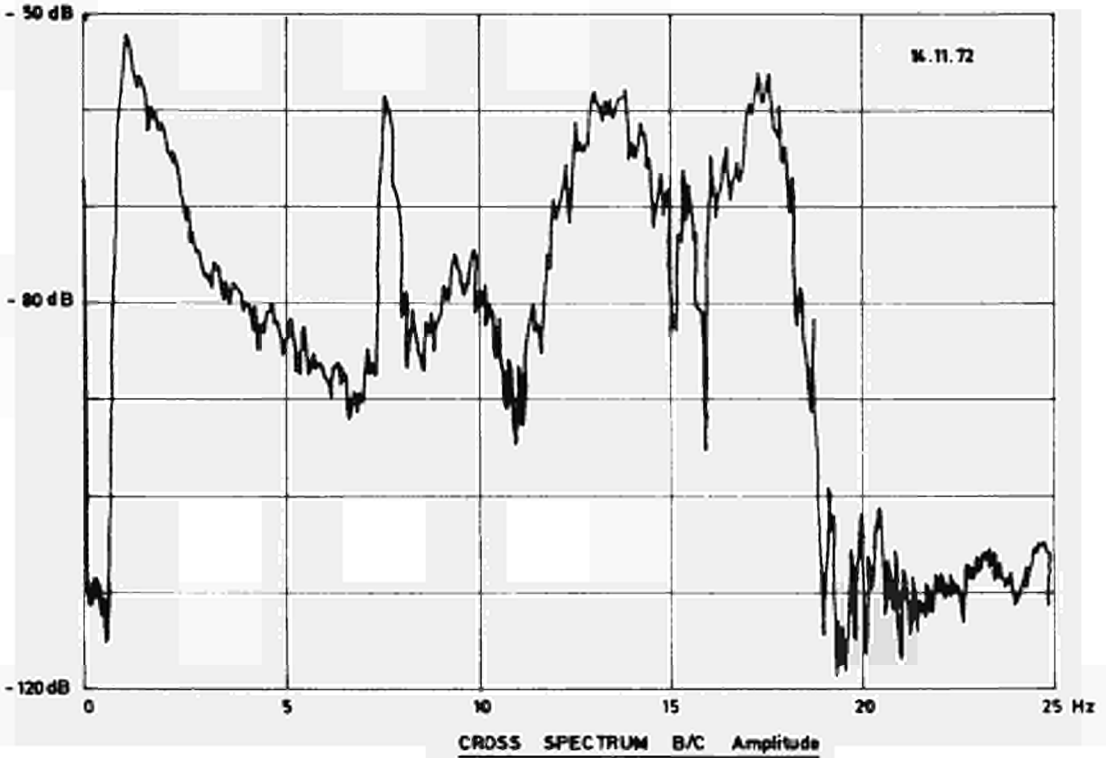

CROSS SPECTRUM B/C Amplitude

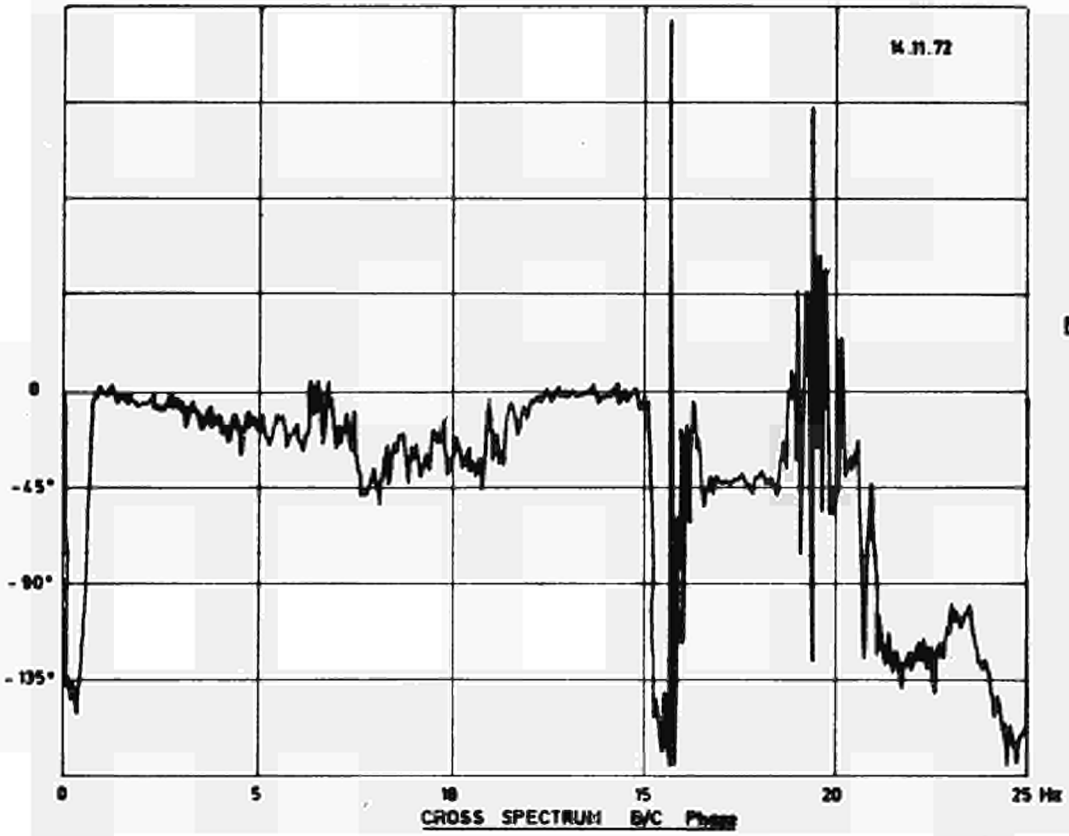

FIG. 1.3.19

CROSS SPECTRUM B/C Phase

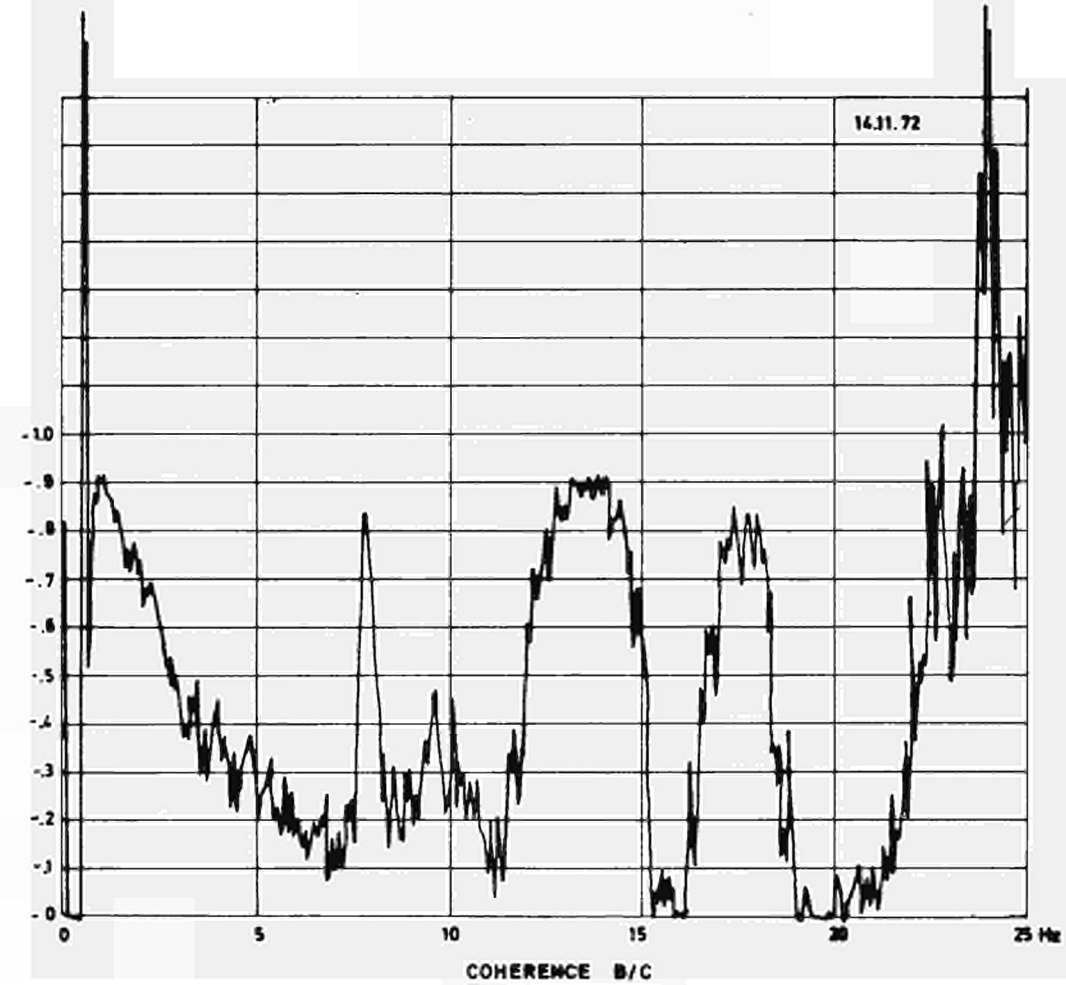

COHERENCE B/C

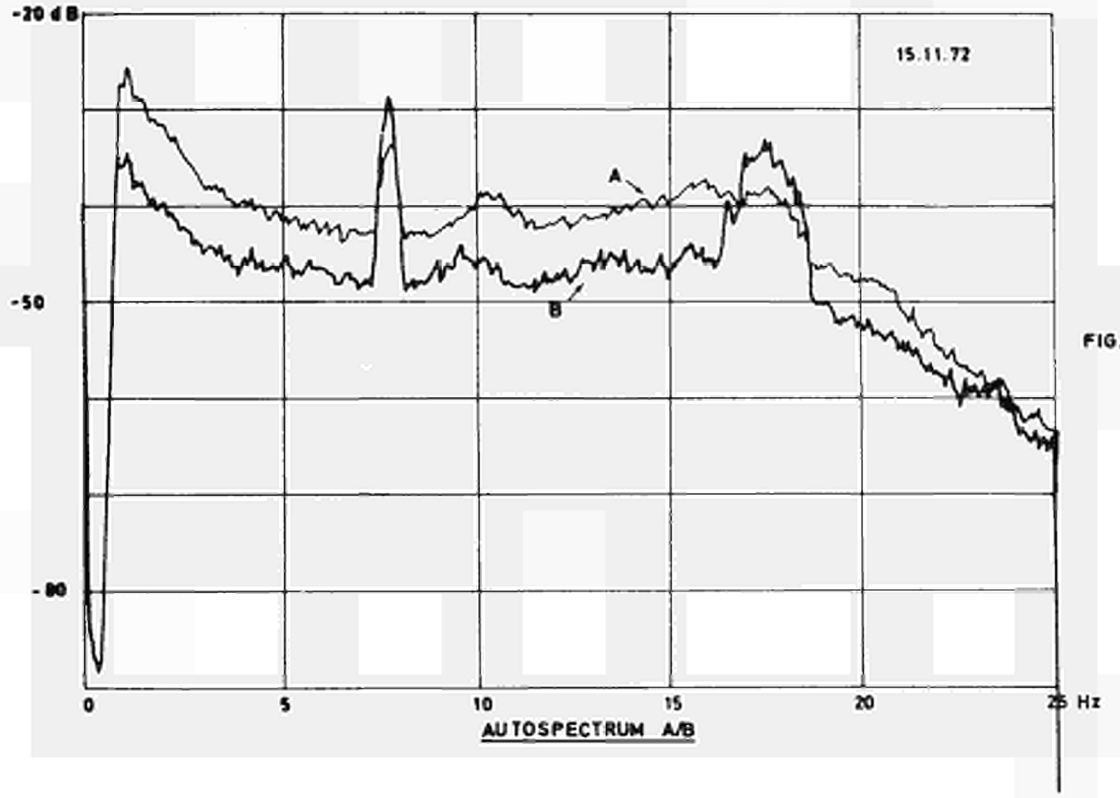
-20 dB
-50
-80
15.11.72
A
B
0
5
10
15
20
25 Hz
AUTOSPECTRUM A/B

FIG. I.3.1.10

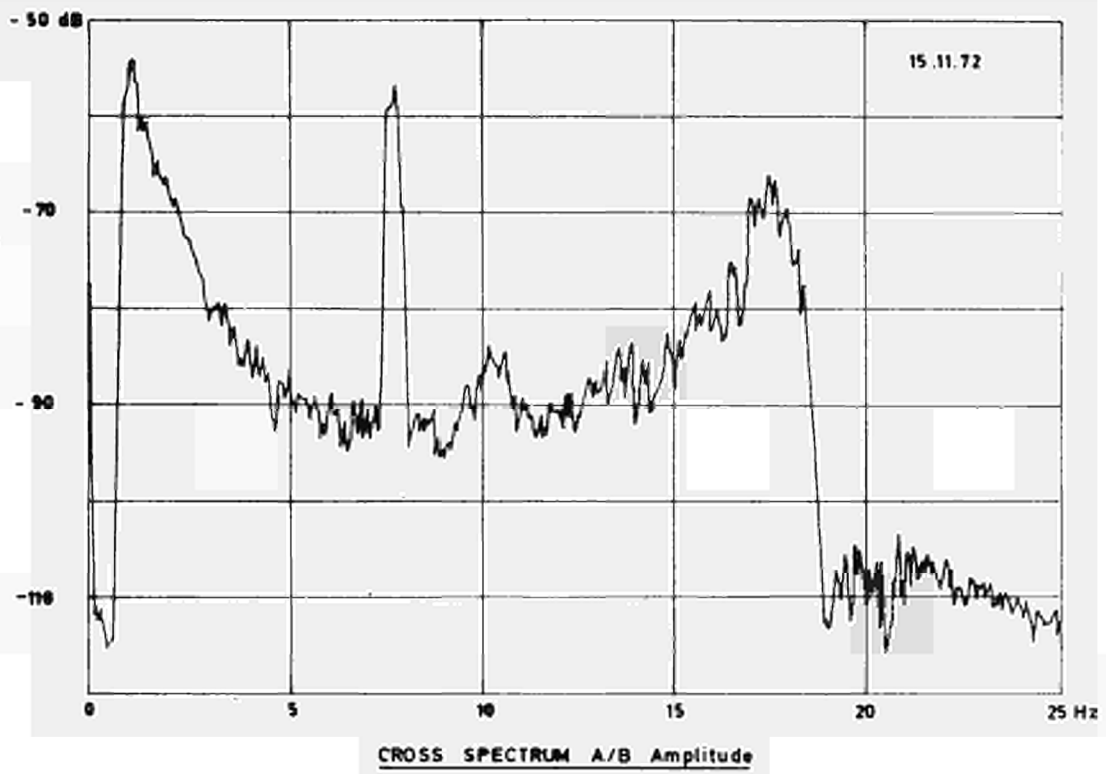
- 50 dB
-70
-90
-110
15.11.72
0
5
10
15
20
25 Hz
CROSS SPECTRUM A/B Amplitude

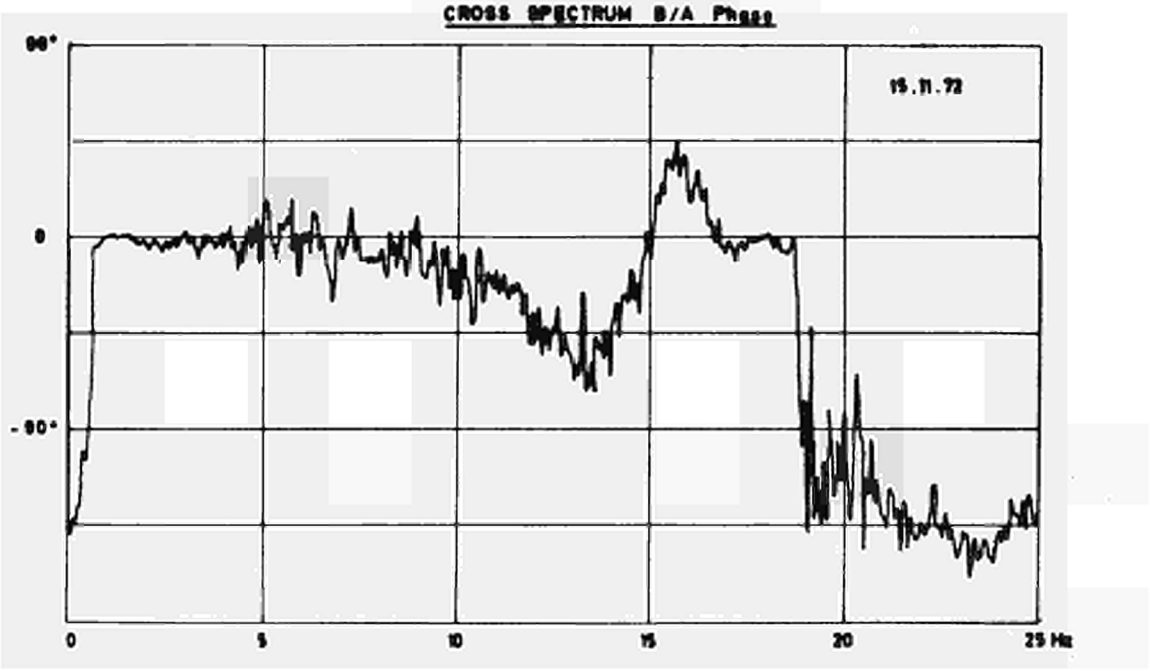

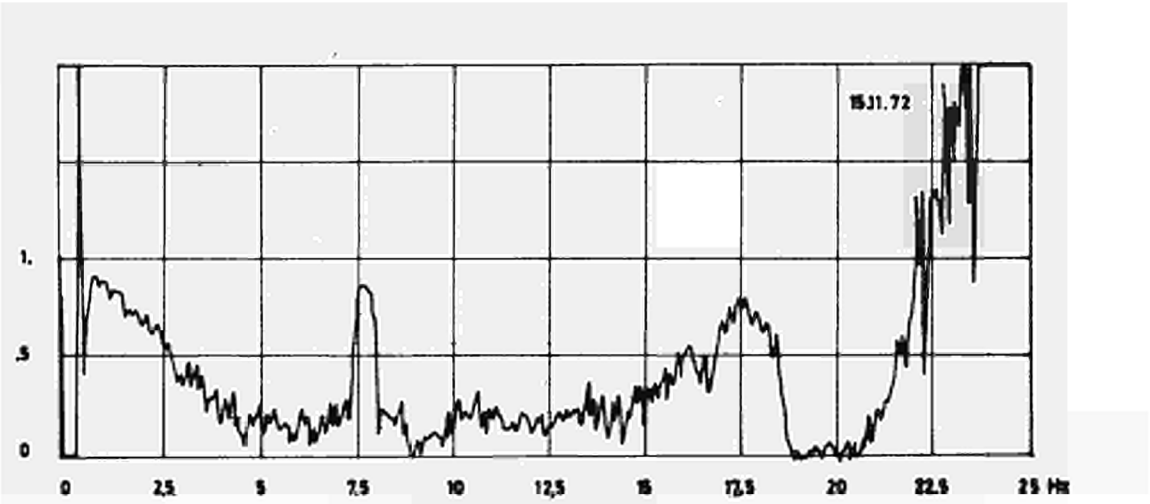

COHERENCE B/A

FIG. I.3.1.11

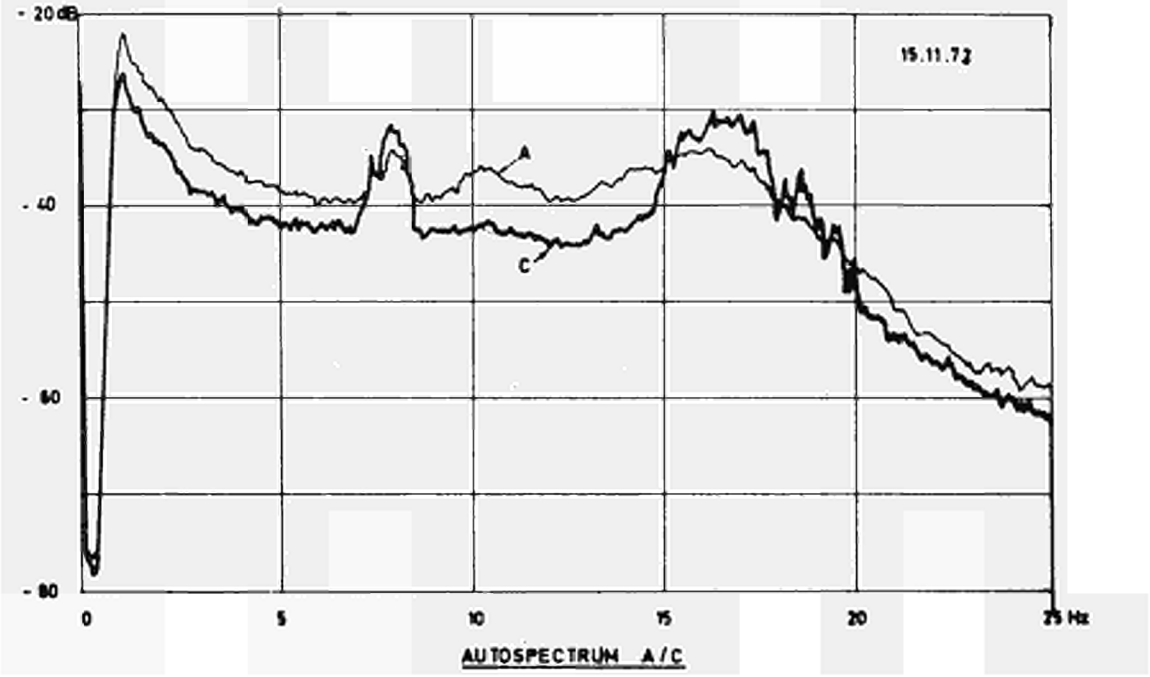

AUTOSPECTRUM A/C

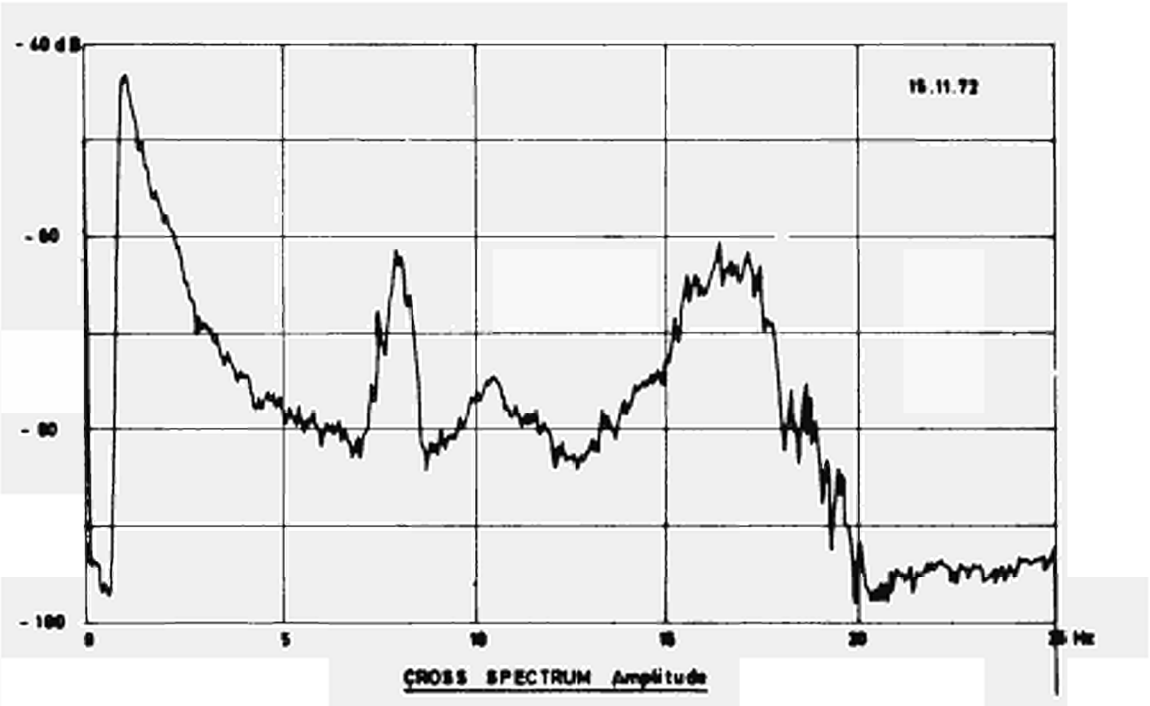

CROSS SPECTRUM Amplitude

FIG. I.3.1.12

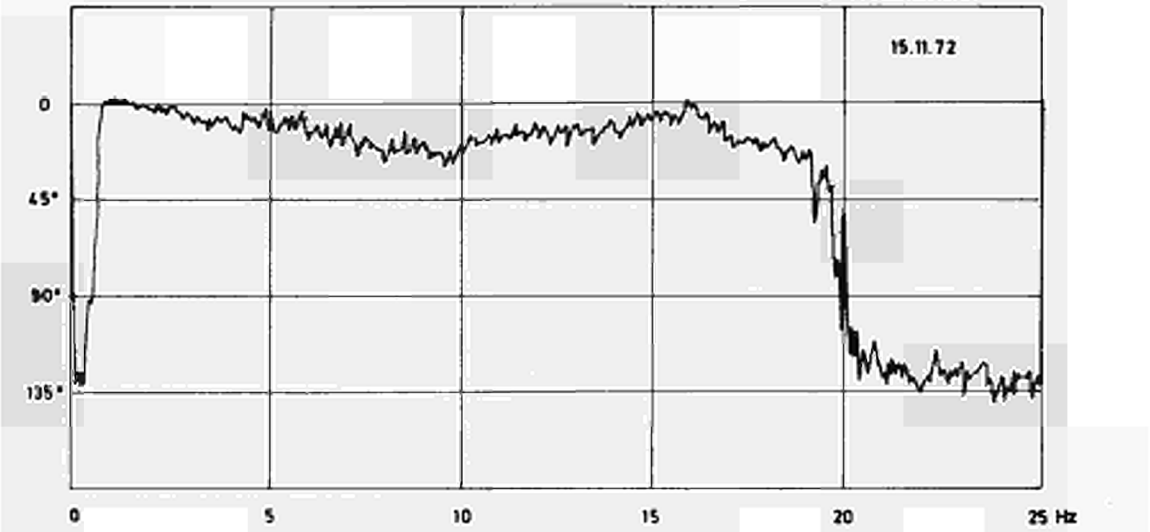

CROSS SPECTRUM Phase

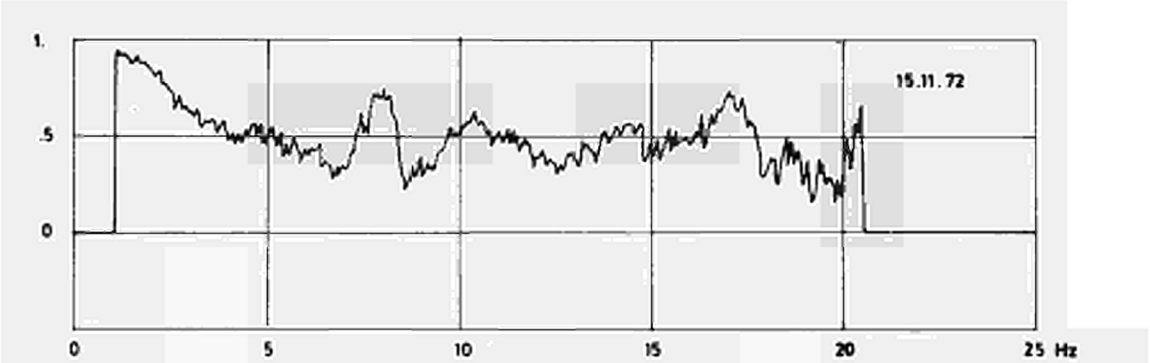

COHERENCE A/C

FIG. I.3.1.13

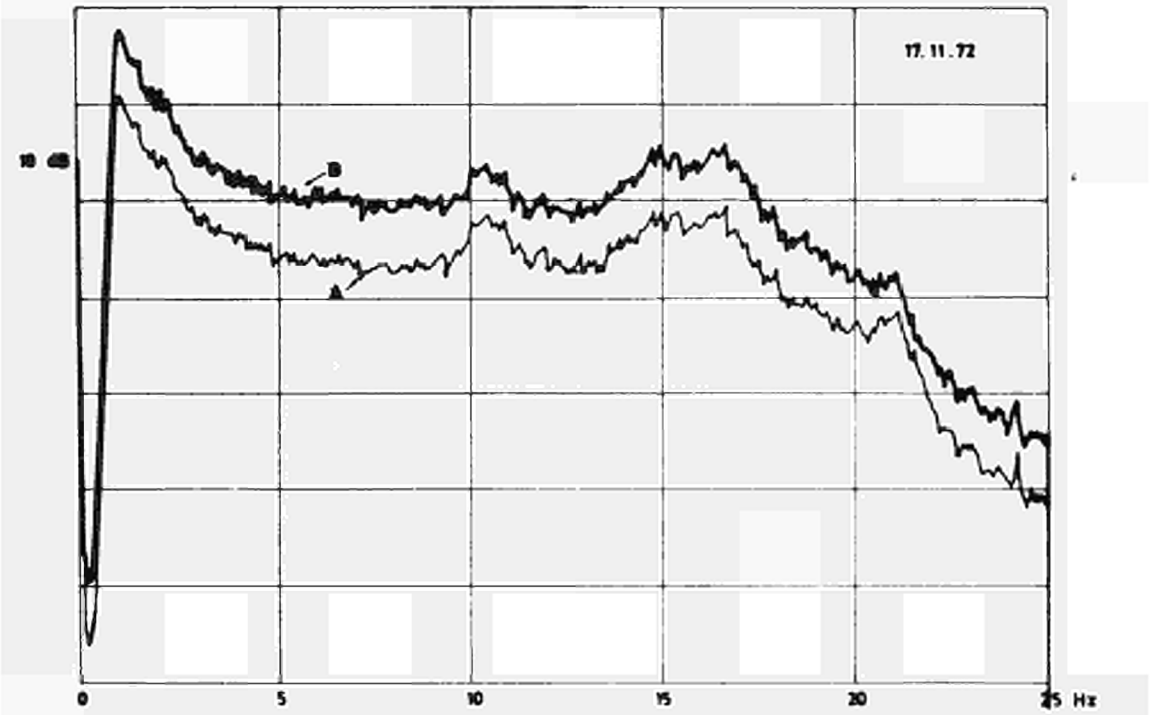

AUTOSPECTRUM A/C

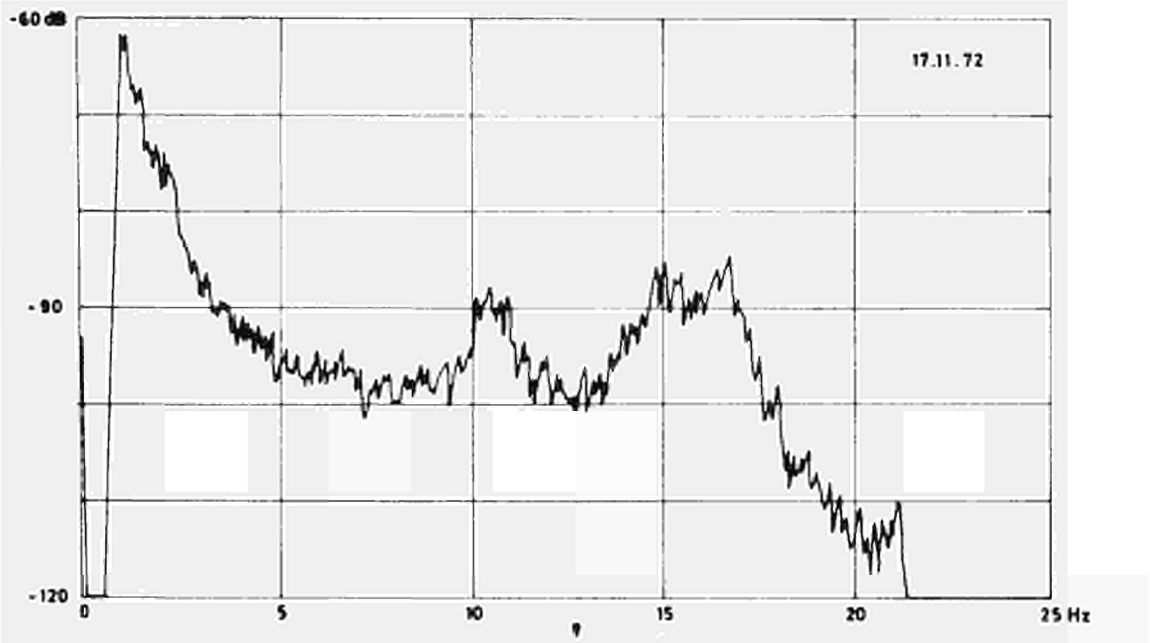

CROSS SPECTRUM A/C Amplitude

FIG. 1.3.1.14

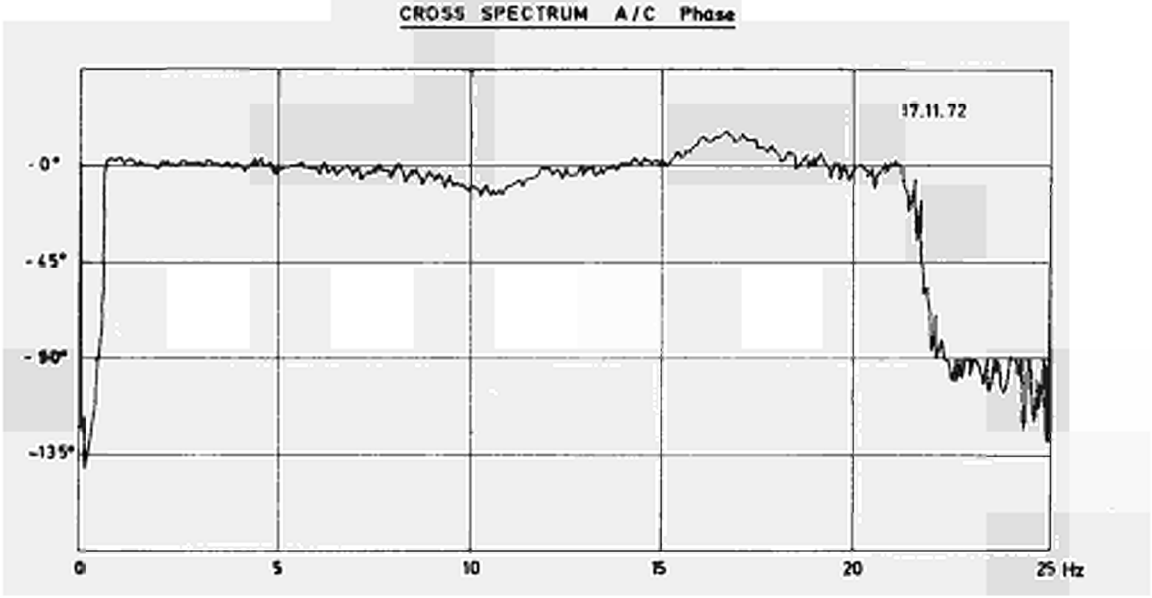
CROSS SPECTRUM A/C Phase
17.11.72
- 0°
- 45°
- 90°
-135°
0
5
10
15
20
25 Hz

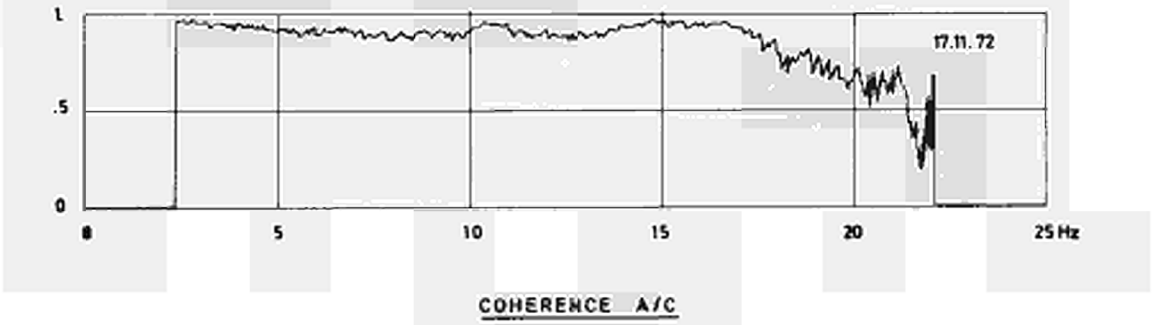
1
.5
0
17.11.72
0
5
10
15
20
25 Hz
COHERENCE A/C

FIG. I.3.1.15

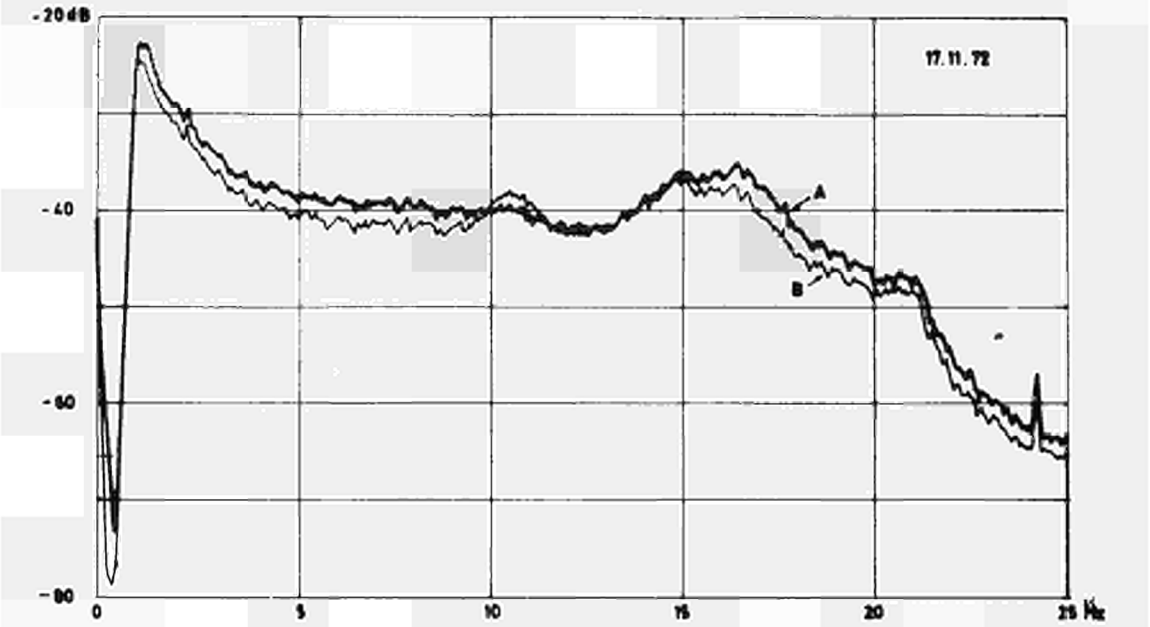

POWER SPECTRUM A / B

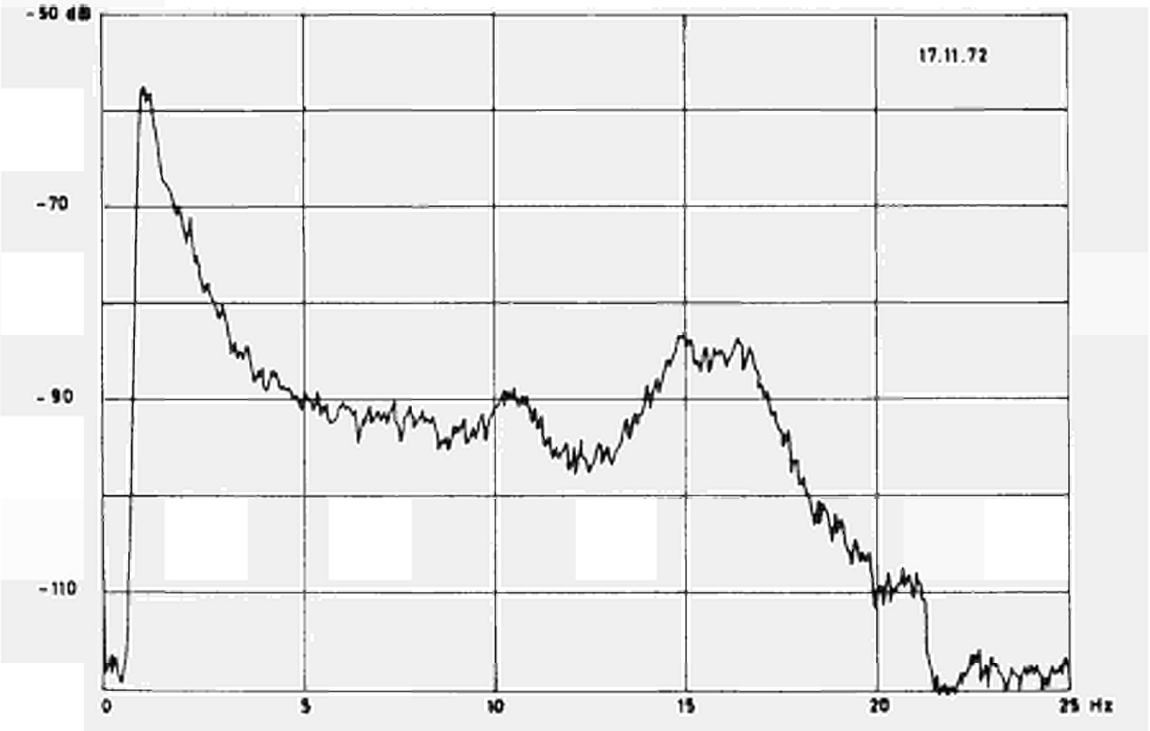

CROSS SPECTRUM A/B Amplitude

FIG. I.3.1.16

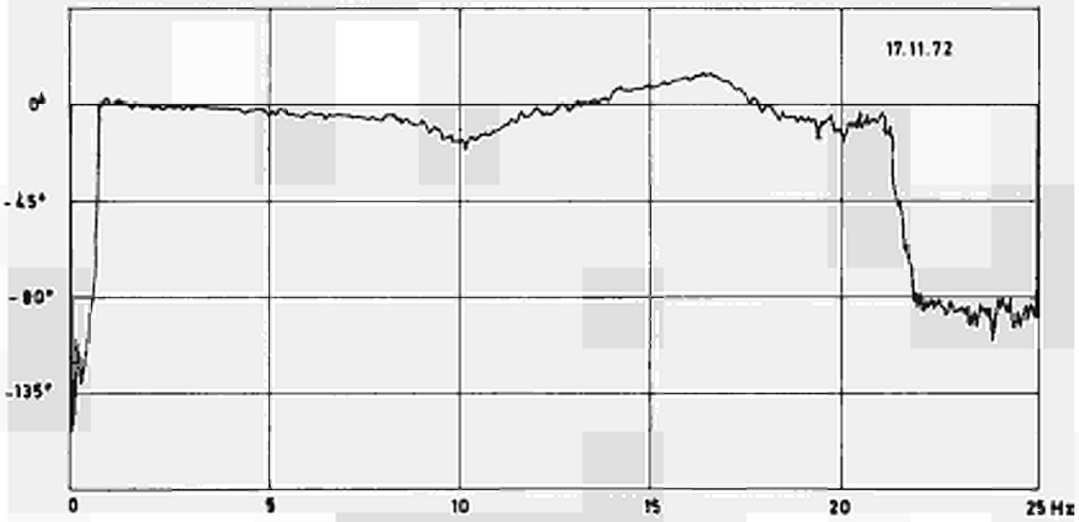

CROSS SPECTRUM A/B Phase

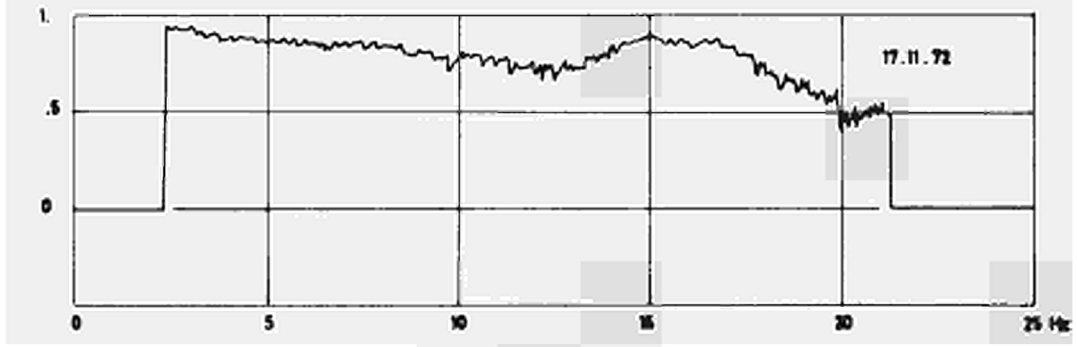

COHERENCE A/B

FIG. I.3.1.17

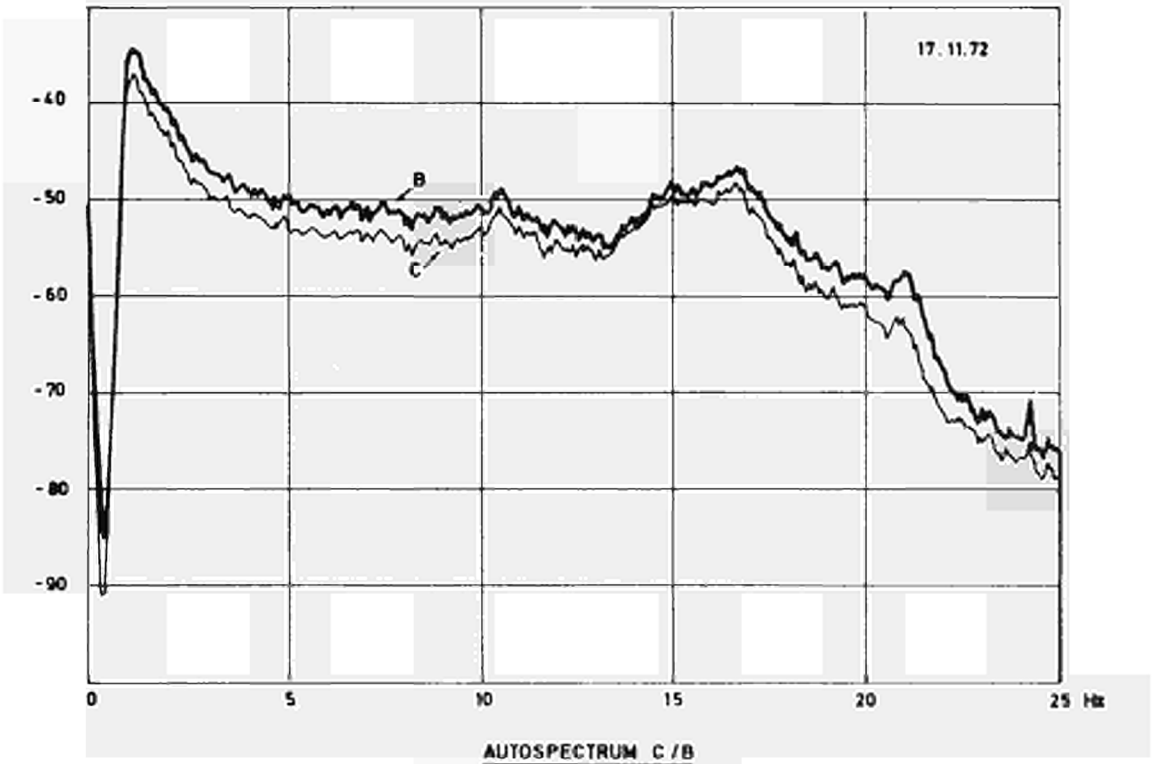

AUTOSPECTRUM C/B

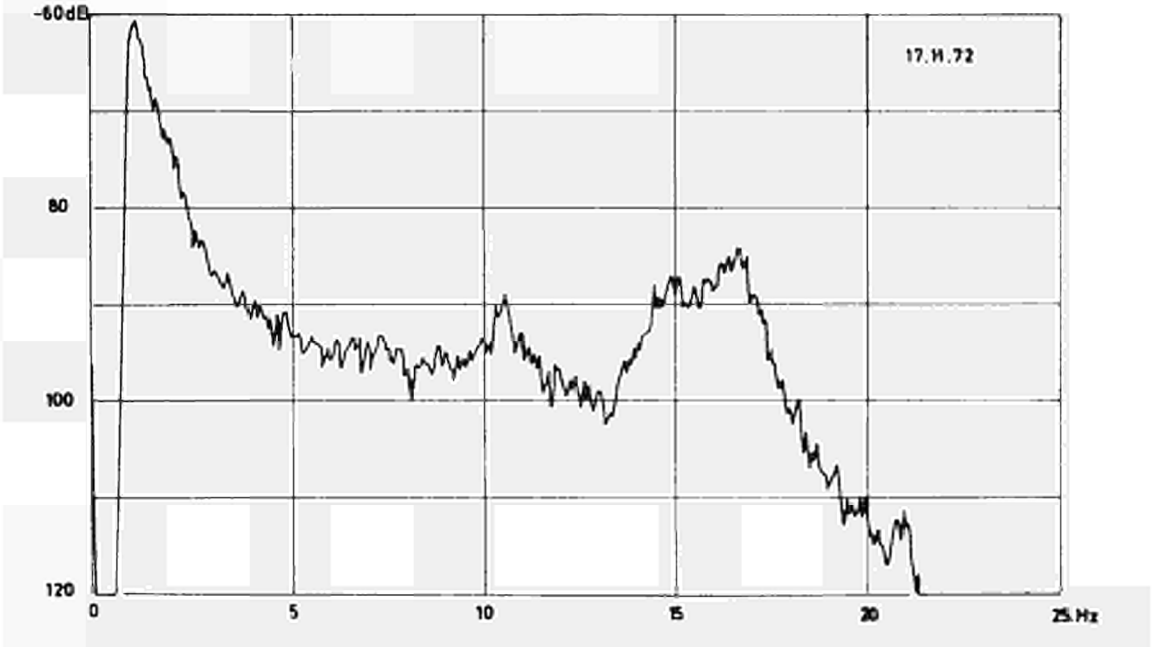

CROSS SPECTRUM C/B Amplitude

FIG. 1.3.1.48

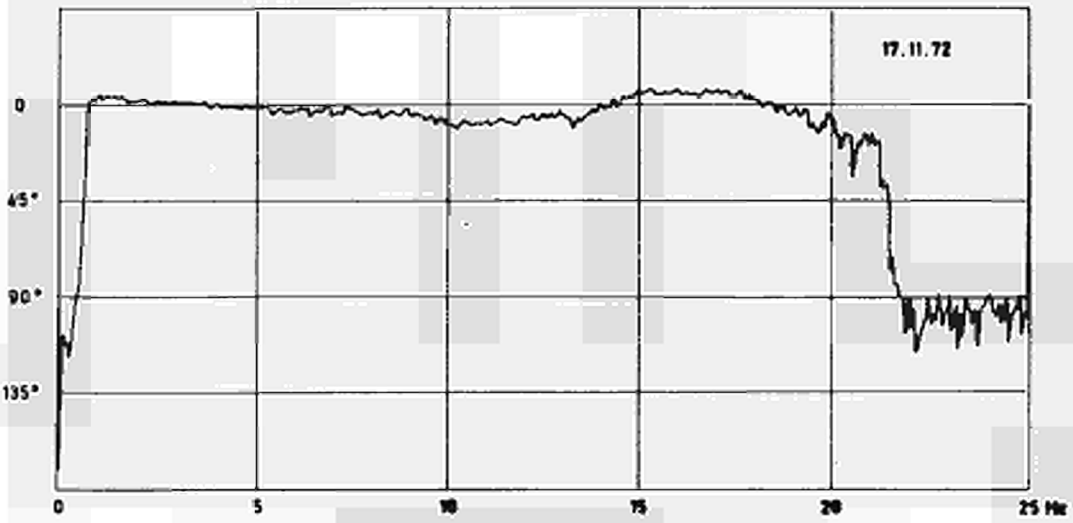

CROSS SPECTRUM C/B Phase

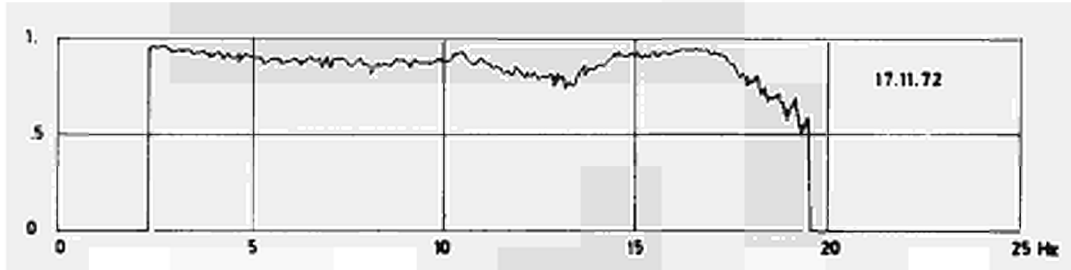

COHERENCE C/B

FIG. I.3.1.18

FIG. 1.3.1.20

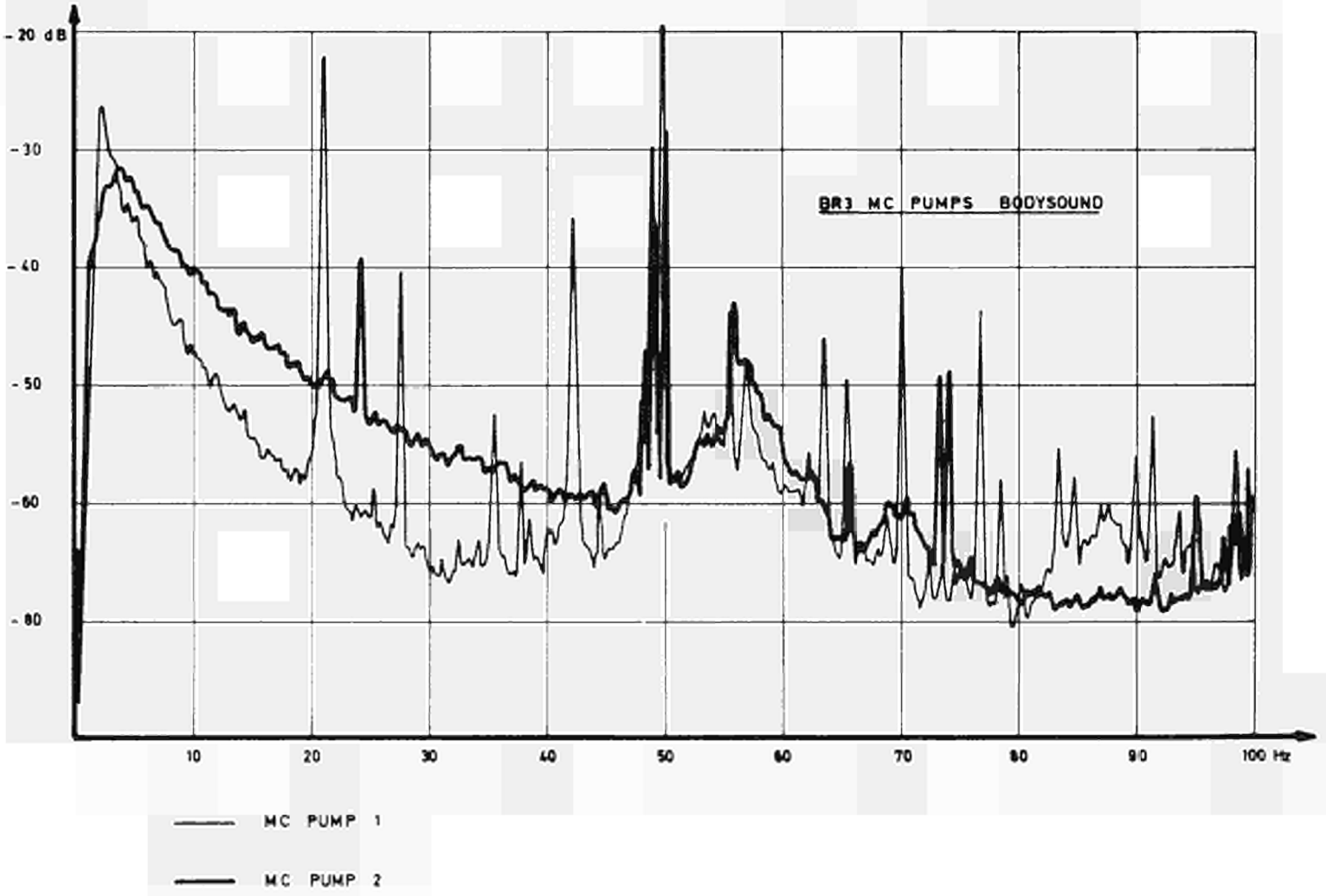
- 20 dB
- 30
- 40
- 50
- 60
- 80
BR3 MC PUMPS BODYSOUND
10
20
30
40
50
60
70
80
90
100 Hz
MC PUMP 1
MC PUMP 2

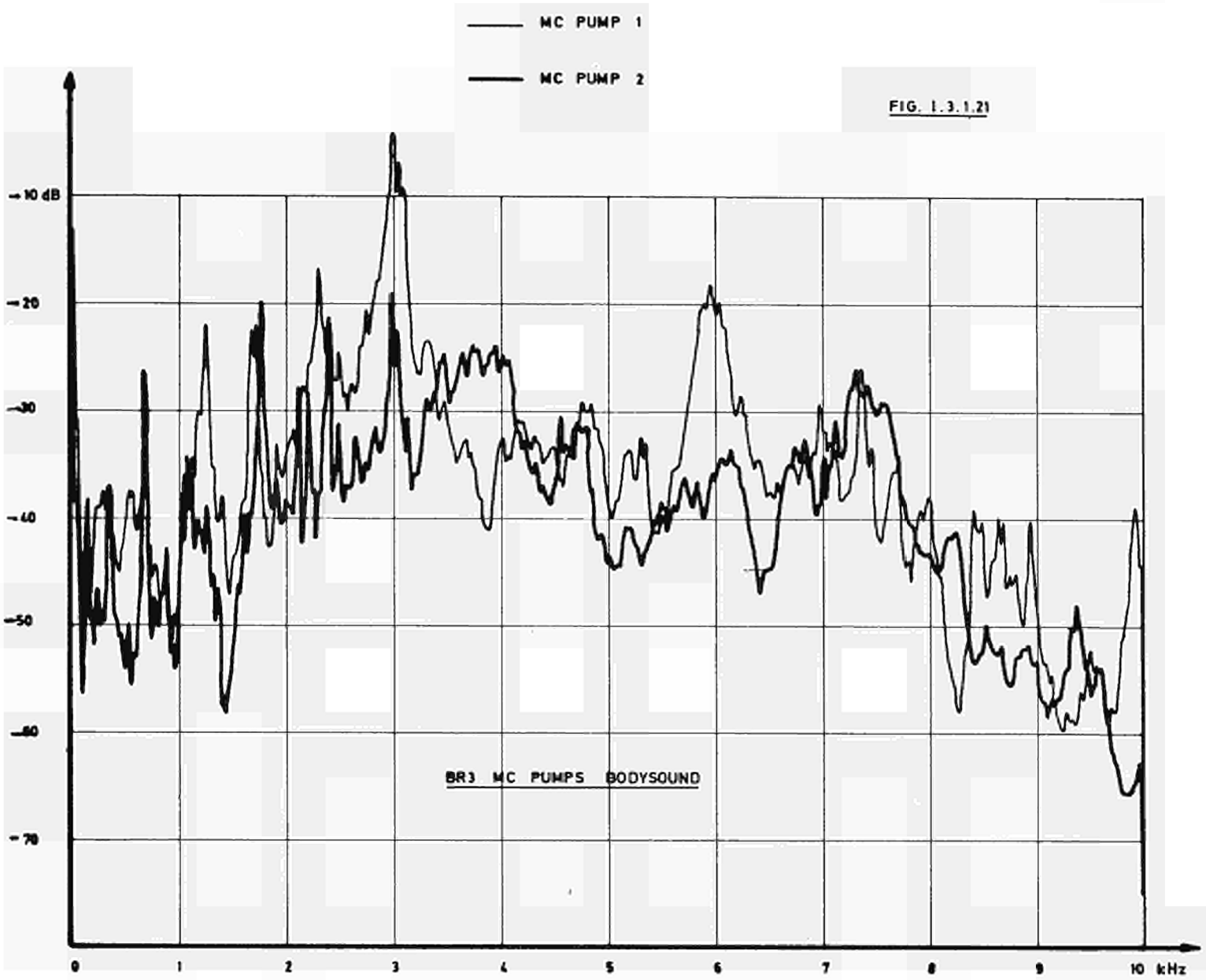
MC PUMP 1
MC PUMP 2
FIG. I.3.1.21
-10 dB
-20
-30
-40
-50
-60
-70
BR3 MC PUMPS BODYSOUND
0
1
2
3
4
5
6
7
8
9
10 kHz

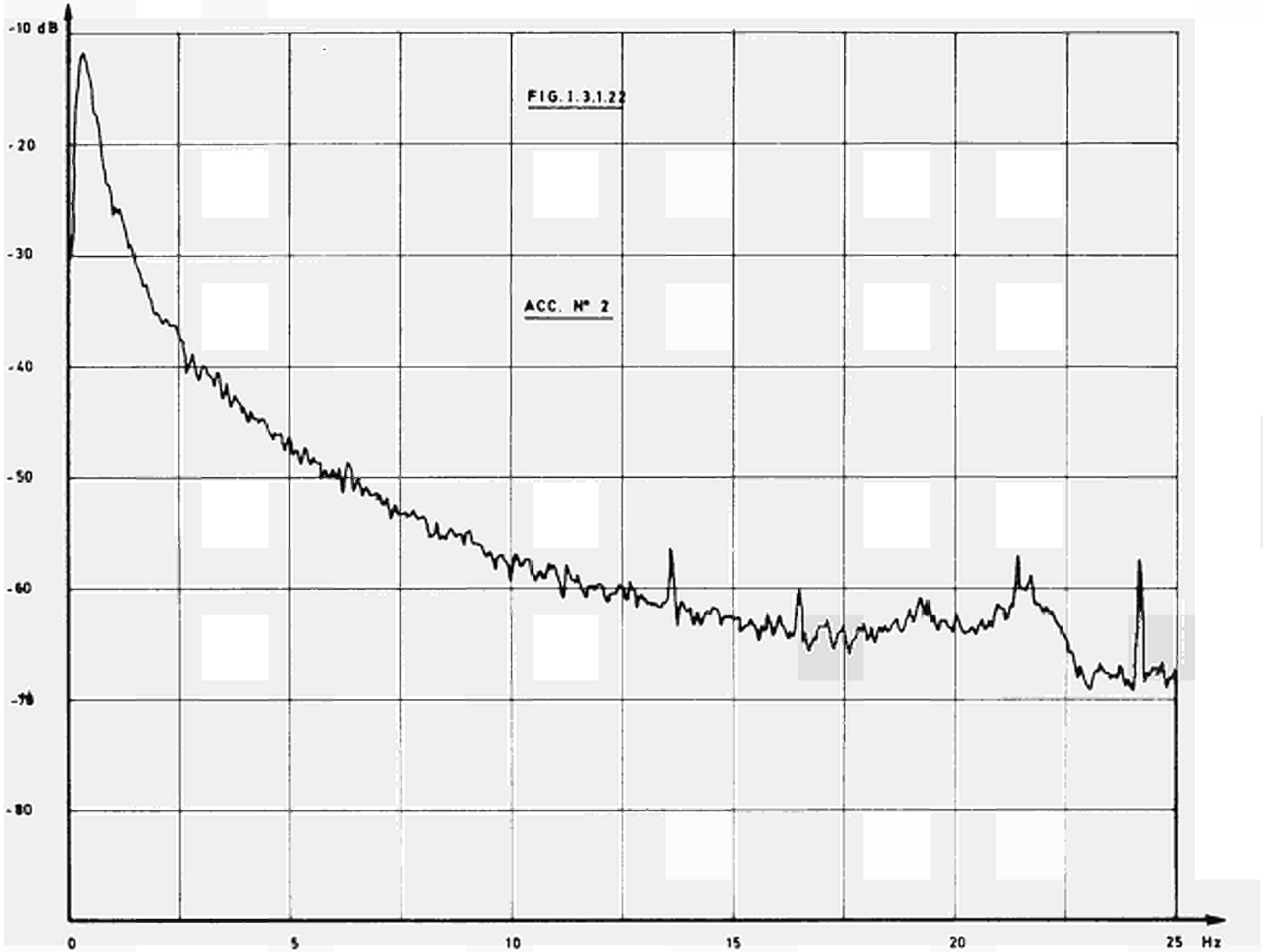
-10 dB
-20
-30
-40
-50
-60
-70
-80
FIG. 1.3.1.22
ACC. N° 2
0
5
10
15
20
25 Hz

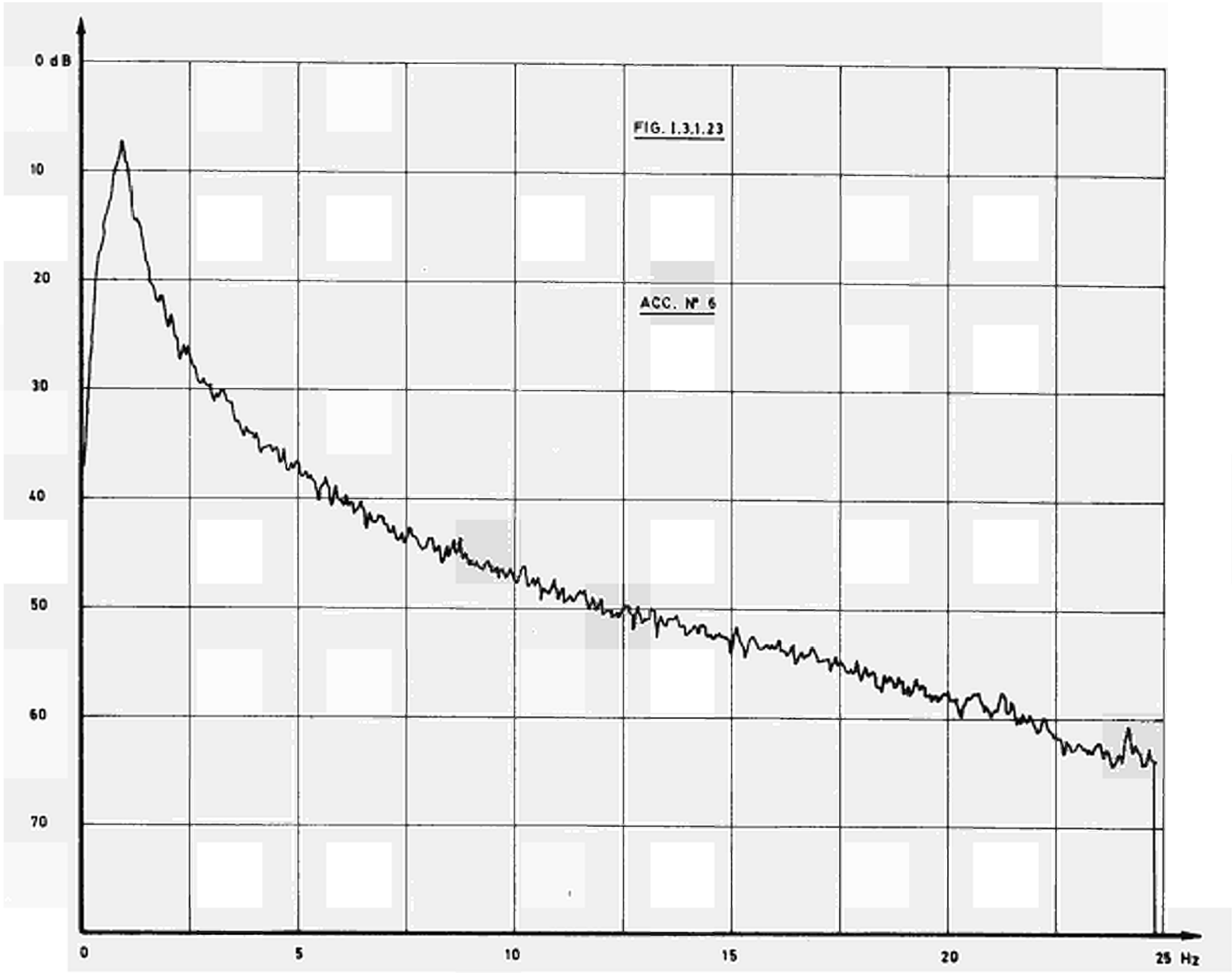
FIG. I.3.1.23
ACC. N° 6
0 dB
10
20
30
40
50
60
70
0
5
10
15
20
25 Hz

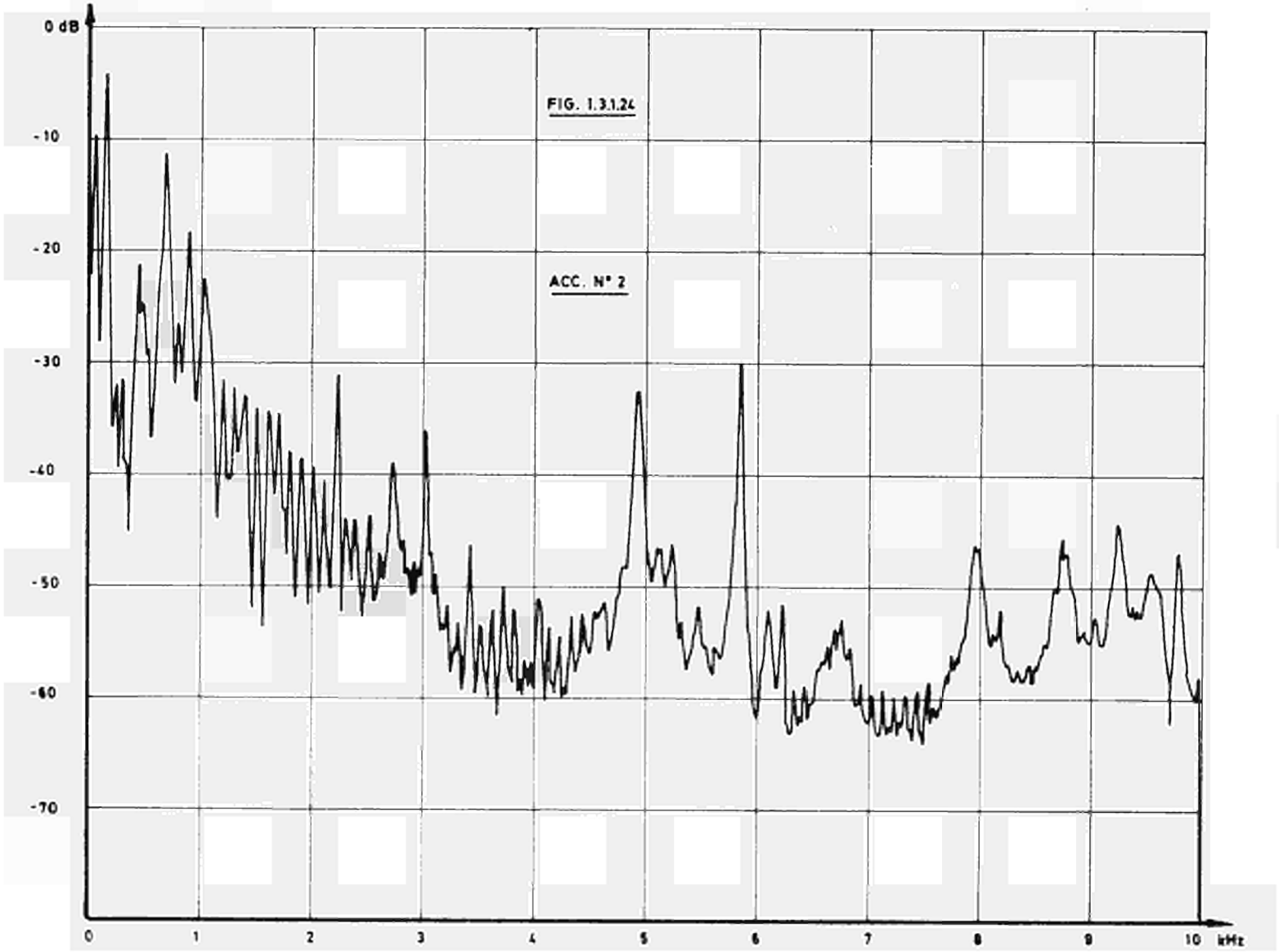
0 dB
-10
-20
-30
-40
-50
-60
-70
FIG. 1.3.1.24
ACC. N° 2
0
1
2
3
4
5
6
7
8
9
10 kHz

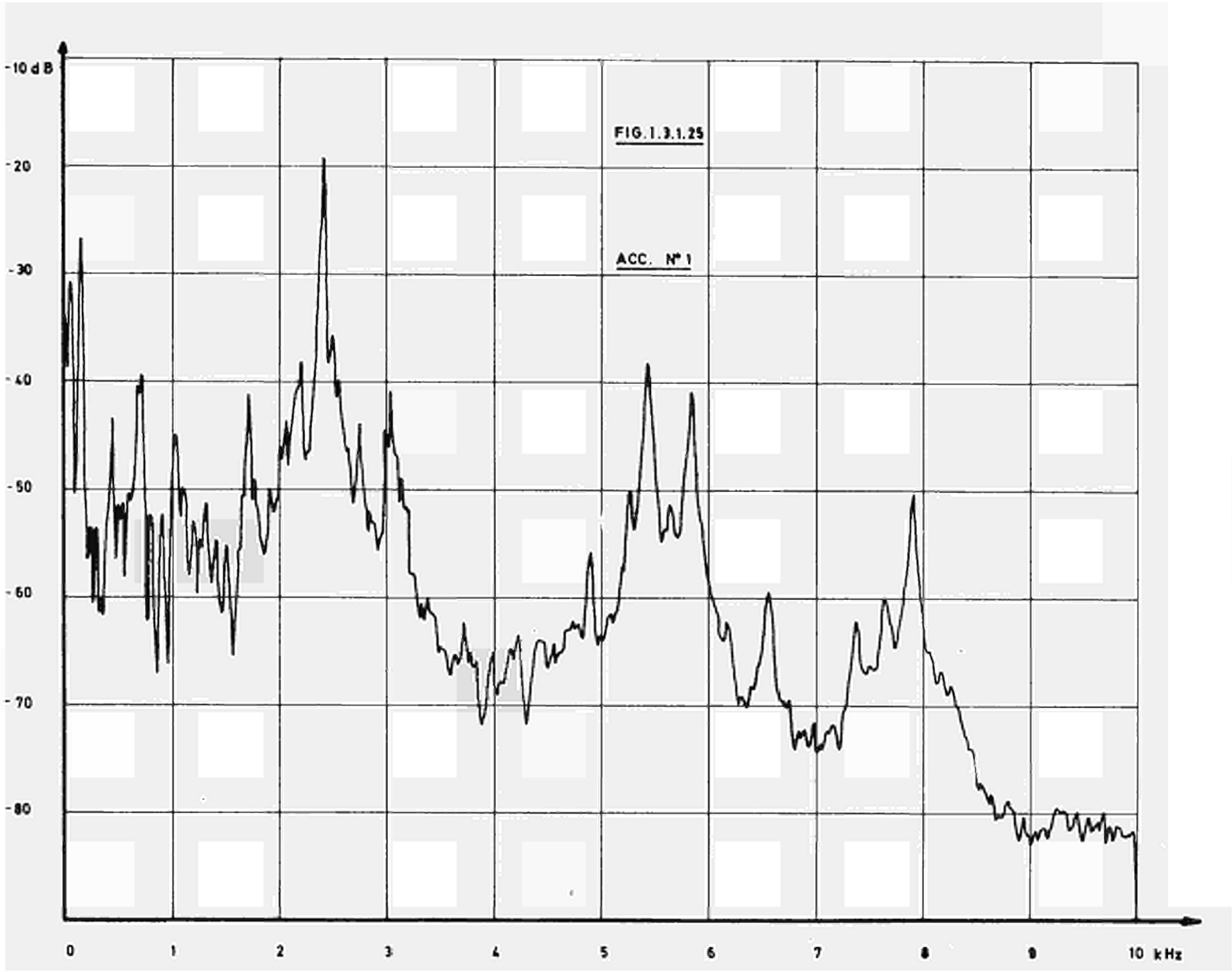
FIG. I. 3. 1. 25
ACC. N° 1
-10 d B
-20
-30
-40
-50
-60
-70
-80
0
1
2
3
4
5
6
7
8
9
10 kHz

I.3.2 JOSE CABRERA Nuclear Power Plant

I.3.2.1 Measurements

The JOSE CABRERA nuclear power plant is equipped with a Westinghouse one-loop pressurized water reactor having a thermal power of 510 MW to which corresponds a gross electrical output of 160 MW. The reactor vessel and internals, whose general arrangement is shown in fig. I.3.2/1, are of the up-dated design which utilizes control rods of cluster type.

Neutron noise measurements were performed in April 1971 at three power levels just before the shutdown for the first refuelling /1/. As the spectra of the neutron flux signals taken at the TRINO power plant show a resonance peak at 5.5 Hz caused by horizontal core movements, it was the purpose of the investigations to confirm these results, especially by means of in-core detectors which were not available at the TRINO reactor /2/. Due to the fact that the horizontal core movement modulates the neutron flux signal measured outside the vessel via the attenuation effect in-core signals should have no oscillations caused by that mechanism. Moreover, during the hot functional pre-operational tests of the JOSE CABRERA reactor, some accelerometers were installed on the upper core plate which provided some information about the oscillatory behaviour of the reactor internals package.

The nuclear detectors installed at the reactor and made available for the noise measurements, were the following:

- 4 long ion chambers installed in four thimbles equally spaced around the reactor vessel. Each long chamber is actually made up of an upper uncompensated ion chamber and a lower compensated ion chamber. The radial and axial location of these chambers are shown in fig. I.3.2/2. The four long chambers are identified by 31, 32, 33 and 34. "A" indicates the upper section, "B" the lower section. During normal operation in the power range, all the chambers are connected to the reactor protection system. However, it was possible to disconnect one long chamber at a time and to use it for neutron noise measurements. Fig. I.3.2/3 shows the typical electrical connections of the two sections of a long ion chamber.

- 1 short compensated ion chamber which is normally connected to a reactivity computer. This chamber, indicated in fig. I.3.2/2 by "R" was available at any time for neutron noise measurements.

- 2 movable miniature fission chambers of the core flux mapping system. The two detectors can be driven inside any one of the thimbles located at the centre of 20 selected fuel assemblies (fig. I.3.2/4).

The measurement runs are summarized in table I.3.1/1.
The five measuring channels were connected as follows:

- 2 to the two sections of the disconnected "long" chamber
- 1 to the chamber of the reactivity computer
- 2 to the in-core fission chambers

The differential values of the inserted control rods were estimated at about 3 pcm/cm (full power) and 6 pcm/cm (half power and "zero" power).

At the end of the measurements at full power, the two in-core chambers failed. Only one in-core chamber was replaced and then only four channels were used in the subsequent measurements. The in-core chambers were always positioned at the core height corresponding to the centre of the lower section of the long chambers, i.e. at 1/4 of core height towards the bottom. The only exception is Run 28 where the in-core chamber was positioned at the core height corresponding to the centre of the upper section of the long chambers. At half power, an attempt was made to perform noise measurements without disconnecting the ion chambers from the reactor protection system.

I.3.2.2 Analysis

The NPSDs of the four chambers 31B, 32B, 33B and 34B at 100, 50, and about 1% of rated power levels are shown in figs. I.3.2/5, I.3.2/6 and I.3.2/7. They are practically coincident except in the frequency range where a large peak occurs at about 11 Hz. In this range, the pair of chambers 32B and 34B, whose relative position is 180^{o} around the core periphery, have similar NPSD values. The same is true for the other pair of chambers 31B and 33B, whose relative position is also 180^{o} around the core periphery. In addition we notice from figs. I.3.2/8 and I.3.2/9 that the noise signals of chamber R and opposite chambers 33B and 34B are in opposition to phase.

The effect of the chamber vertical position in a thimble is shown in figs. I.3.2/10 and I.3.2/11. These figures show the normalized autospectra, the cross spectra (modulus and phase), and the coherence functions (root square) of sections A and B of a

same long chamber. The normalized autospectra of sections A and B appear quite similar.

Figs. I.3.2/12, I.3.2/13 and I.3.2/14 show the normalized auto and cross spectra, and the coherence functions of the in-core chamber in various core locations, at 100% power level. NPSDs, cross spectra and coherence functions between in-core and out-of-core chambers are given in figs. I.3.2/15 and I.3.2/16.

Interpreting the computed curves we can draw the following conclusions:

- The normalized power and cross power spectral densities of both out-of-core and in-core ion chambers show one distinct wide-band resonance peak at 11.5 Hz.

- The characteristics of this peak for out-of-core ion chambers diametrically opposed are those of the 5.5 Hz peak found in the TRINO reactor, i.e.:

  Equal height in the two autospectra of noise signals from ion chambers diametrically opposed.

  Opposition of phase, in the frequency range associated to the peaks.

  Peak height and frequency independent of the power level.

  As for the TRINO reactor, this peak can be satisfactorily explained by assuming a pendular oscillation of the internals package.

- The 11.5 Hz peak in the noise spectra of the in-core chamber in the various core locations can be explained by the movement of the chamber inside the thimble

due to the mentioned pendular oscillation of the internals package because of the neutron flux gradient across the thimble.

- The 16.5 Hz peak has a frequency equal to the rotational frequency of the main coolant pumps.

Literature, Section I.3.2

/1/ Calcagno, M., Castaldi, D., Cioli, F., Ottaviani, C.A.
Neutron Noise Measurements at the Jose Cabrera Reactor
ENEL C3.R1/06.72, Nov. 1972

/2/ Calcagno, M., Cioli, F., Gadola, A., Possa, G., Vanoli, G.
Trino Nuclear Power Station
In-Service Monitoring of Reactor Internals
Meeting on Vibration Phenomena Inside Light Water Reactor Vessels, Mol, Dec. 1970

RUN	CORE POWER LEVEL %	CORE AVERAGE TEMP. °C	INSERTION OF CONTROL GROUPS, %		DETECTORS EMPLOYED				
			GROUP A	GROUP B	OUT-OF-CORE			IN-CORE	
1	96	290	0	1.6	33A	33B	R	G-8	C-2
2	96	290	0	1.6	34A	34B	R	G-2	B-5
3	96	290	0	1.6	31A	31B	R	A-5	C-2
4	96	290	0	1.6	32A	32B	R	A-5	C-8
5	96	290	0	8.3	34A	34B	R	G-2	B-5
6	96	290	0	8.3	33A	33B	R	E-5	B-5
7	96	290	0	8.3	33A	33B	R	E-2	E-8
8	96	290	0	8.3	33A	33B	R	-	C-2
8 bis	96	290	0	8.3	33A	33B	R	-	G-7
9	52	283	0	33	31A	31B	R	B-3	-
10	52	283	0	33	33A	33B	R	B-3	-
11	52	283	0	33	33A	33B	R	G-8	-
12	52	283	0	33	33A	33B	R	A-5	-
13	52	283	0	33	32A	32B	R	B-6	-
14	52	283	0	33	34A	34B	R	B-6	-
15	52	283	0	33	34A	34B	R	G-2	-
16	52	283	0	33	34A	34B	R	A-5	-
24	4.6	273	30	100	32A	32B	R	B-6	-
25	6.0	273	30	100	34A	34B	R	B-6	-
26	0.5	272	38	100	34A	34B	R	G-2	-
27	0.4	272	38	100	34A	34B	R	A-5	-
28	0.45	272	38	100	34A	34B	R	G-2 (*)	-
29	0.3	274	35	100	33A	33B	R	B-6	-
30	0.7	273	35	100	33A	33B	R	G-2	-
31	0.6	274	35	100	33A	33B	R	A-5	-

(*) Positioned at the same height of the upper section centre of the long chambers.

Table I.3.2/1: Summary of neutron noise measurements

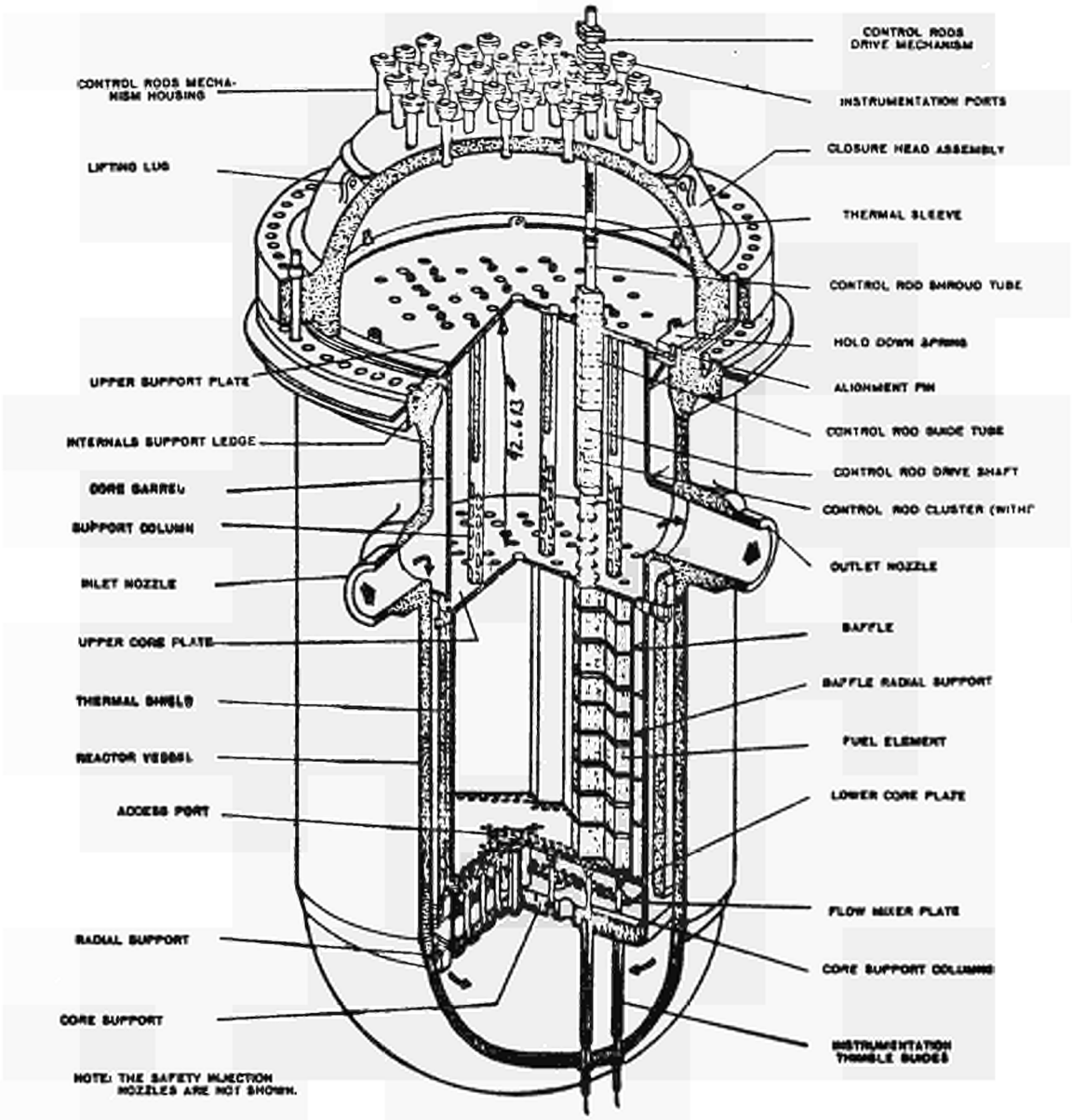

FIG. I.3.2/1: GENERAL ARRANGEMENT OF REACTOR VESSEL AND INTERNALS

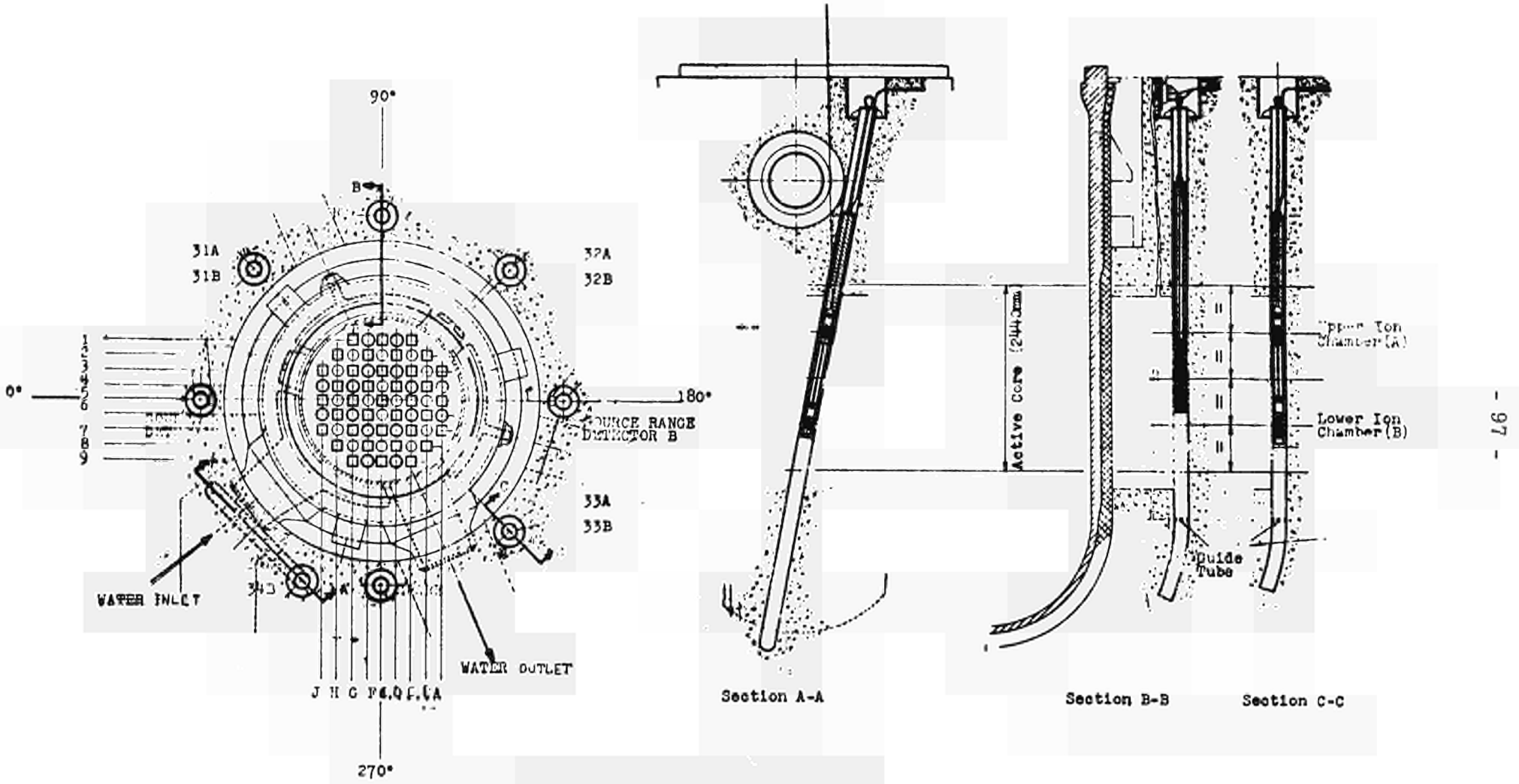

FIG. I.3.2/2: ION CHAMBER LOCATIONS

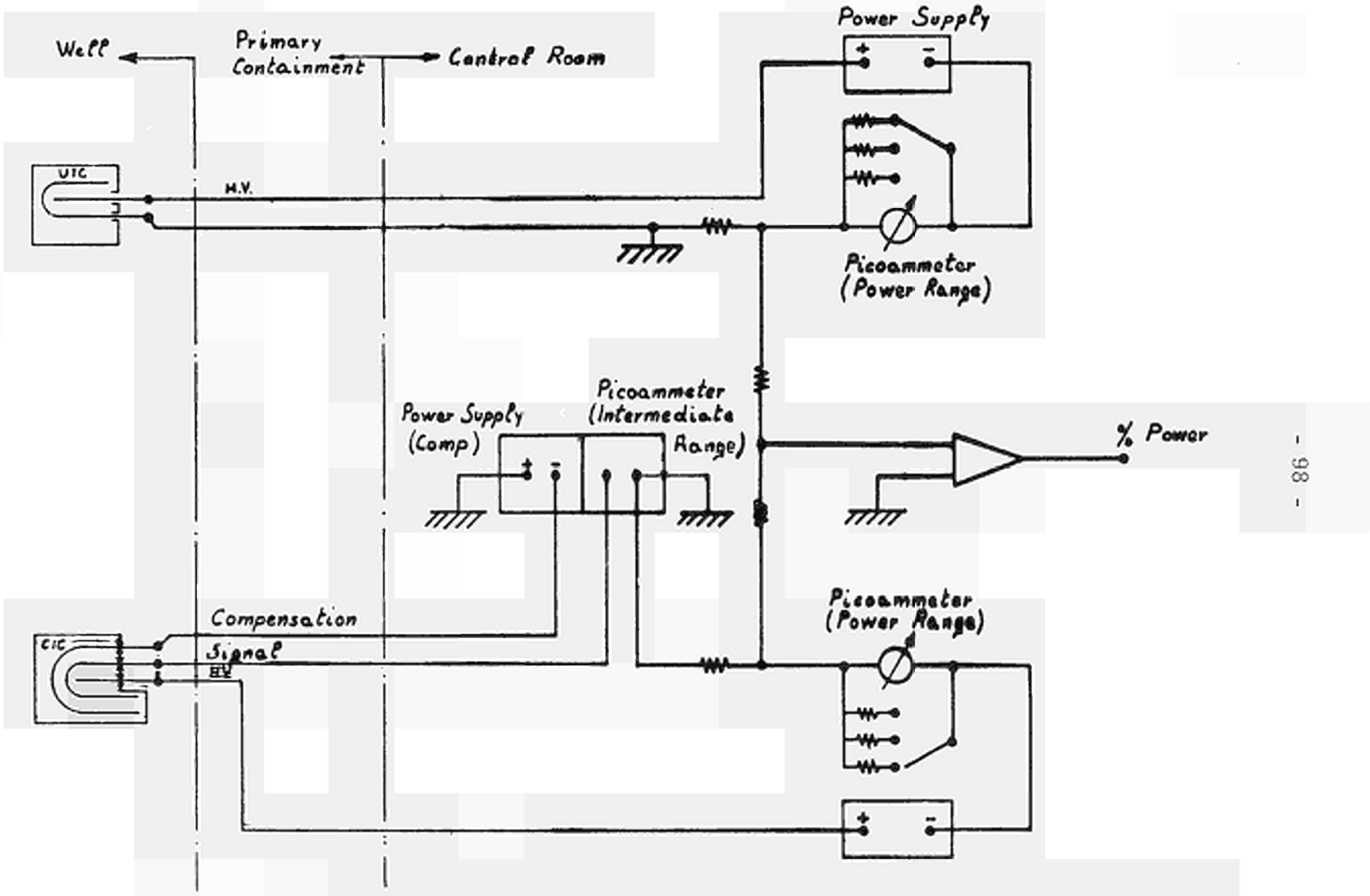

FIG. 1.3.2/3: TYPICAL ELECTRICAL CONNECTIONS OF A LONG ION CHAMBER

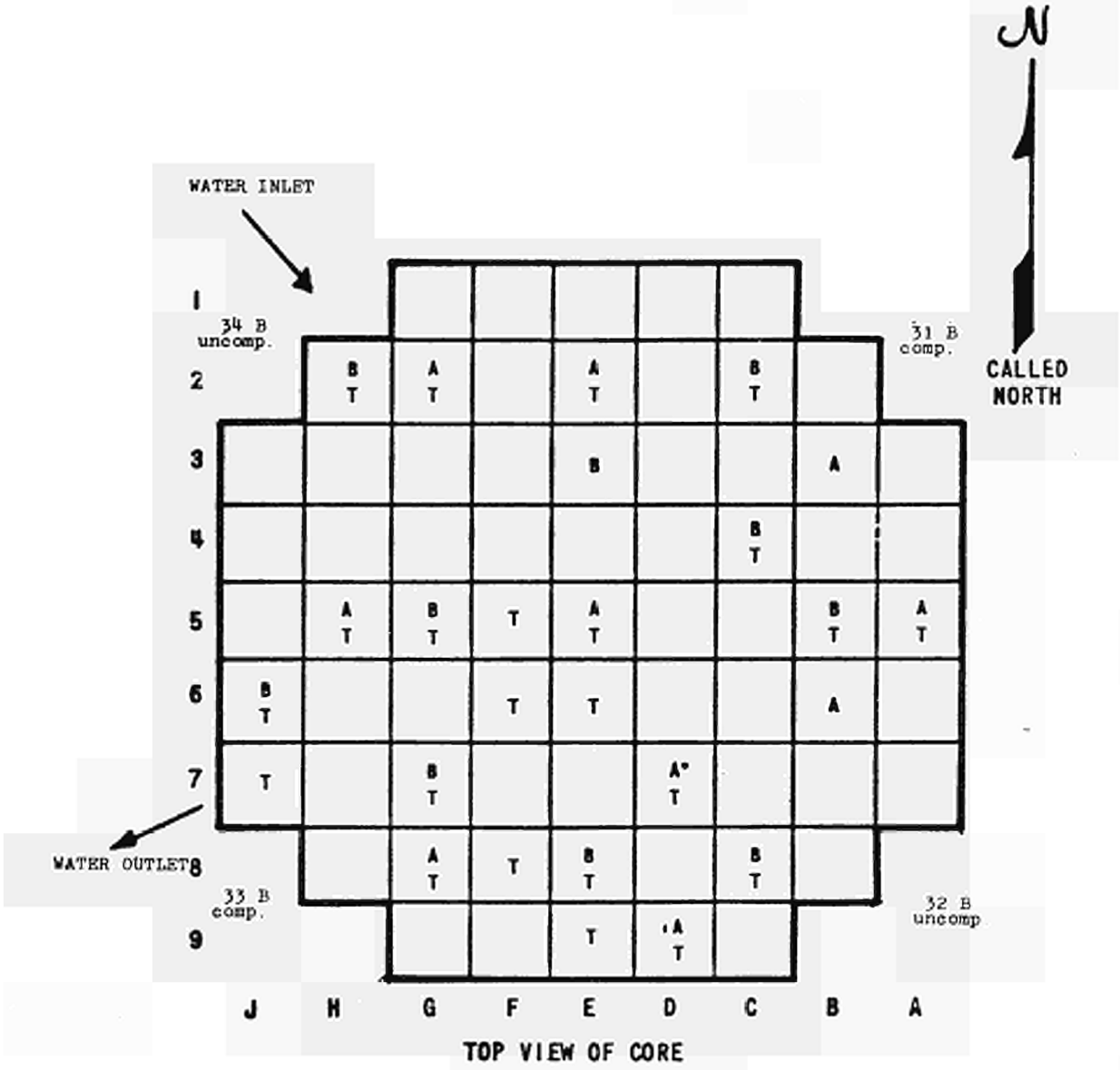

FIG. I.3.2/4: IDENTIFICATION OF THE INSTRUMENTED ASSEMBLIES

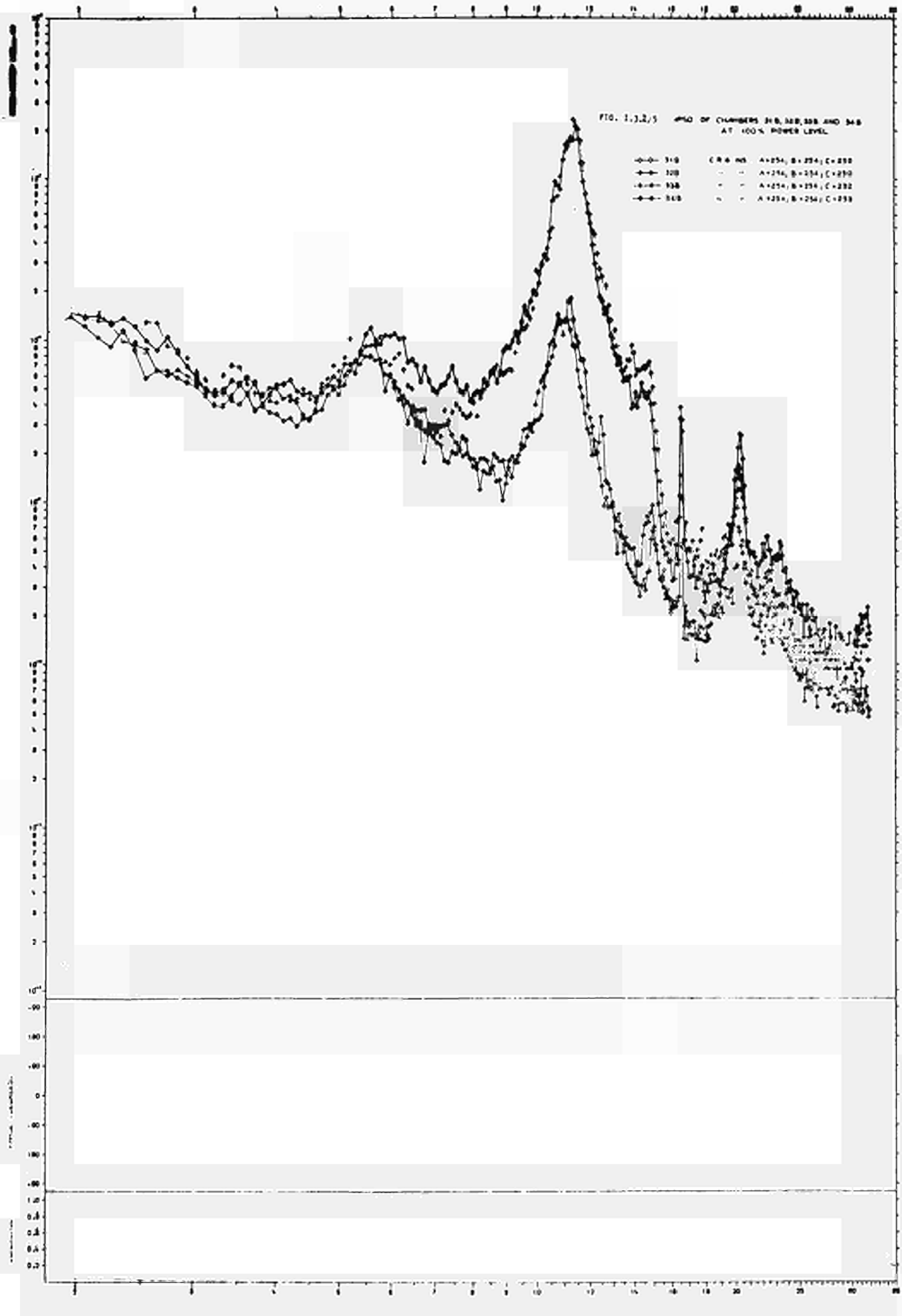
FIG. 3.3.2/5
AT 100% POWER LEVEL

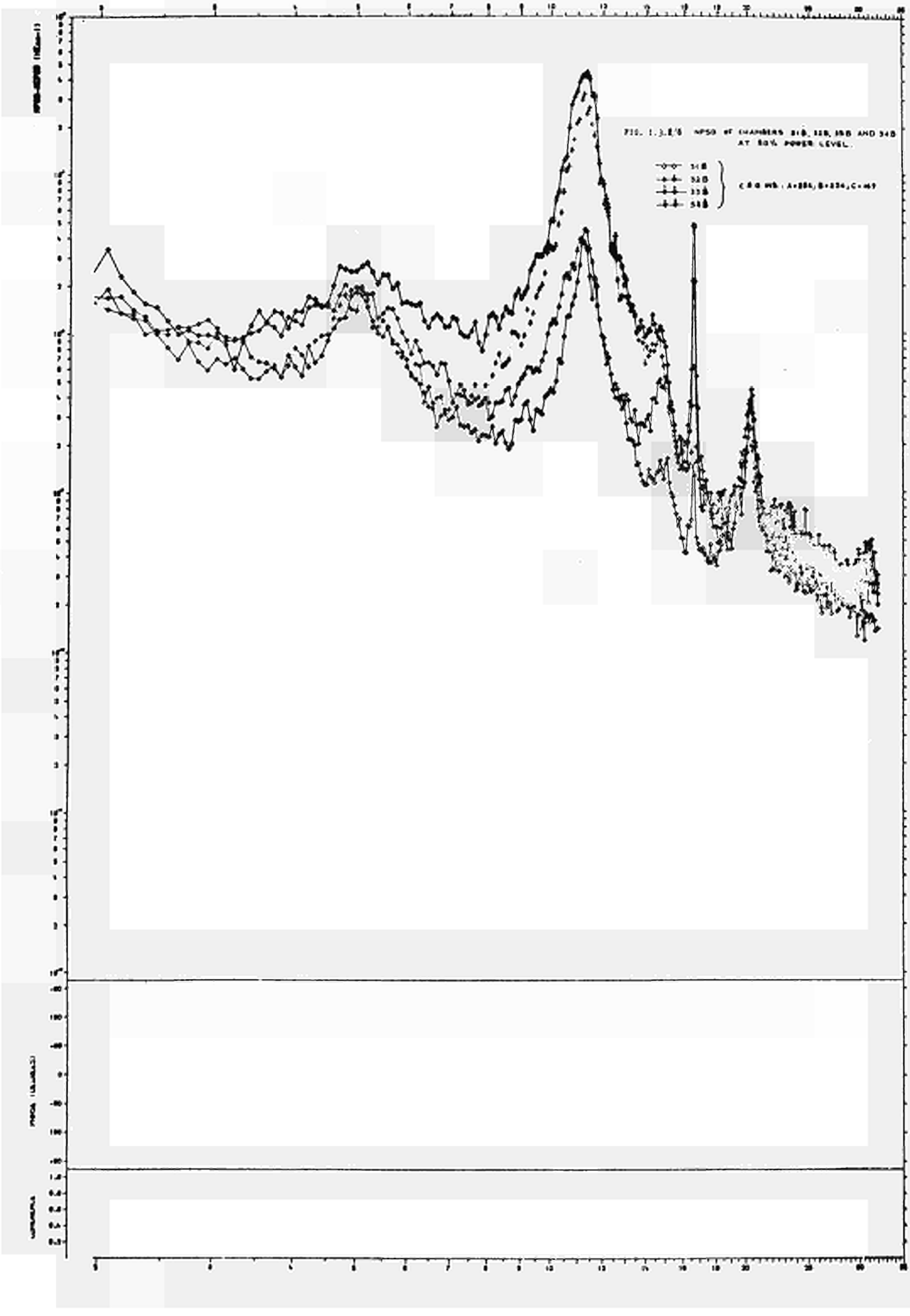
FIG. 1.3.E/5 NPSD AT CHAMBERS 31B, 32B, 33B AND 34B AT 80% POWER LEVEL.
34B
32B
33B
34B

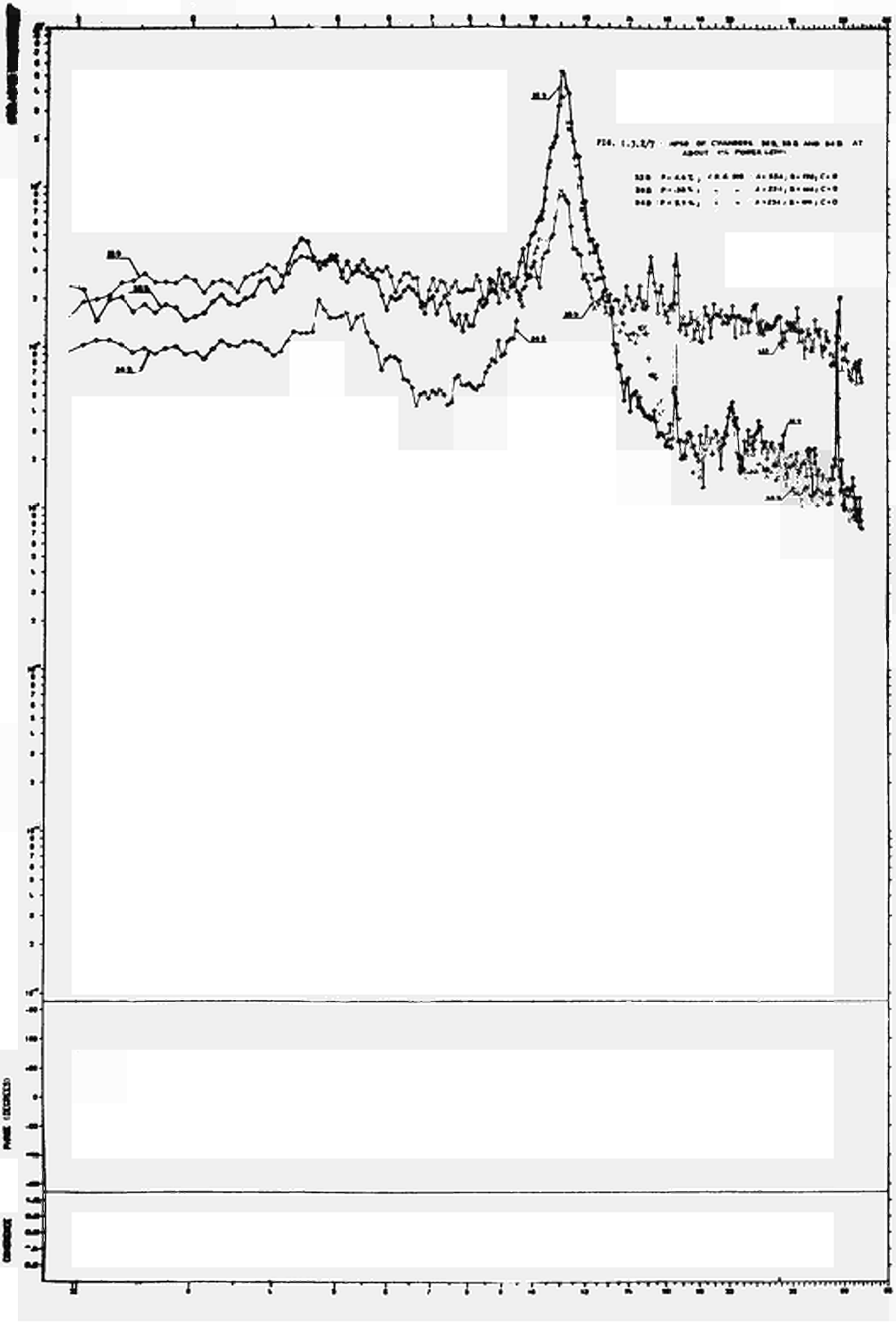

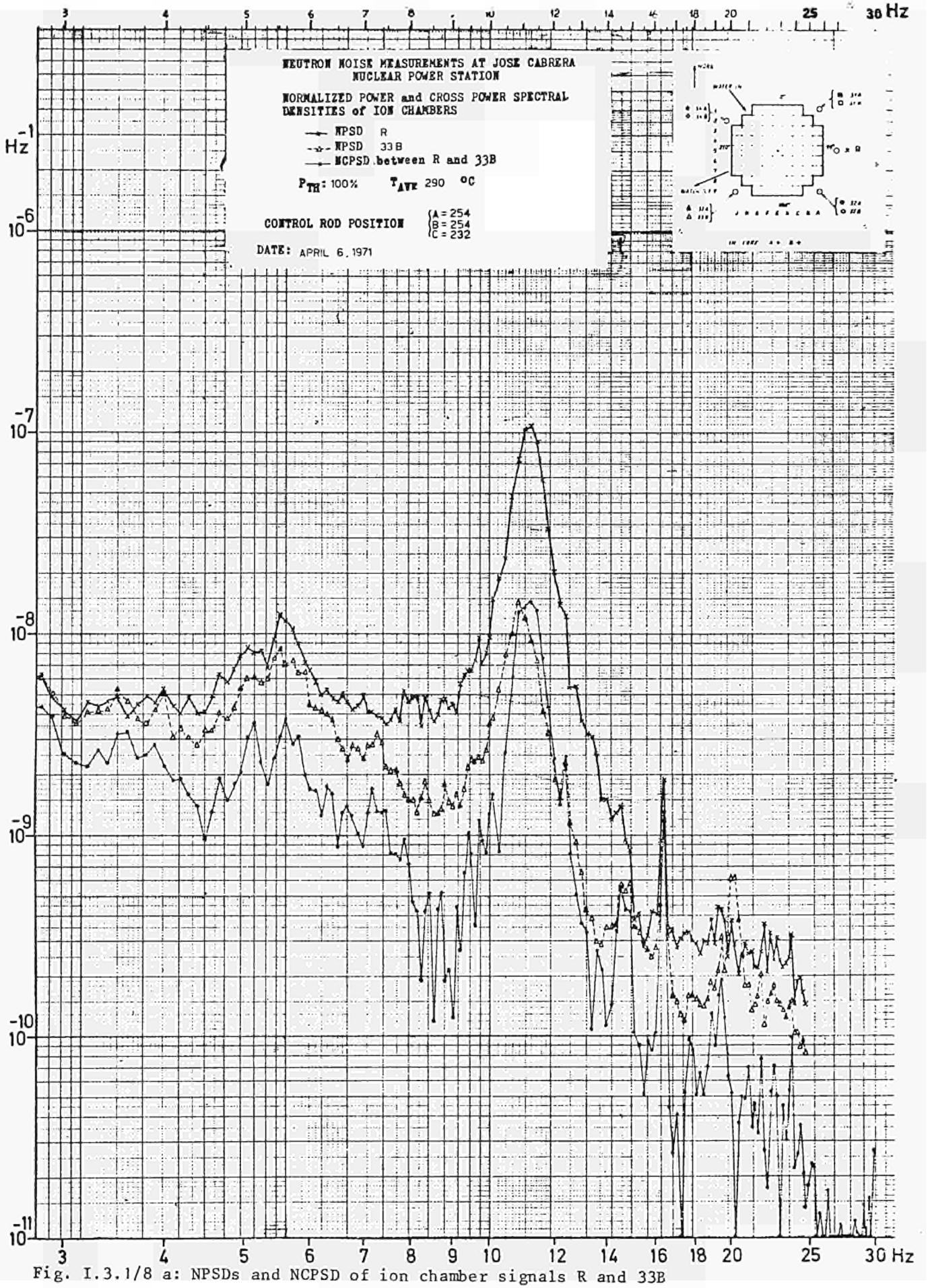

Fig. I.3.1/8 a: NPSDs and NCPSD of ion chamber signals R and 33B

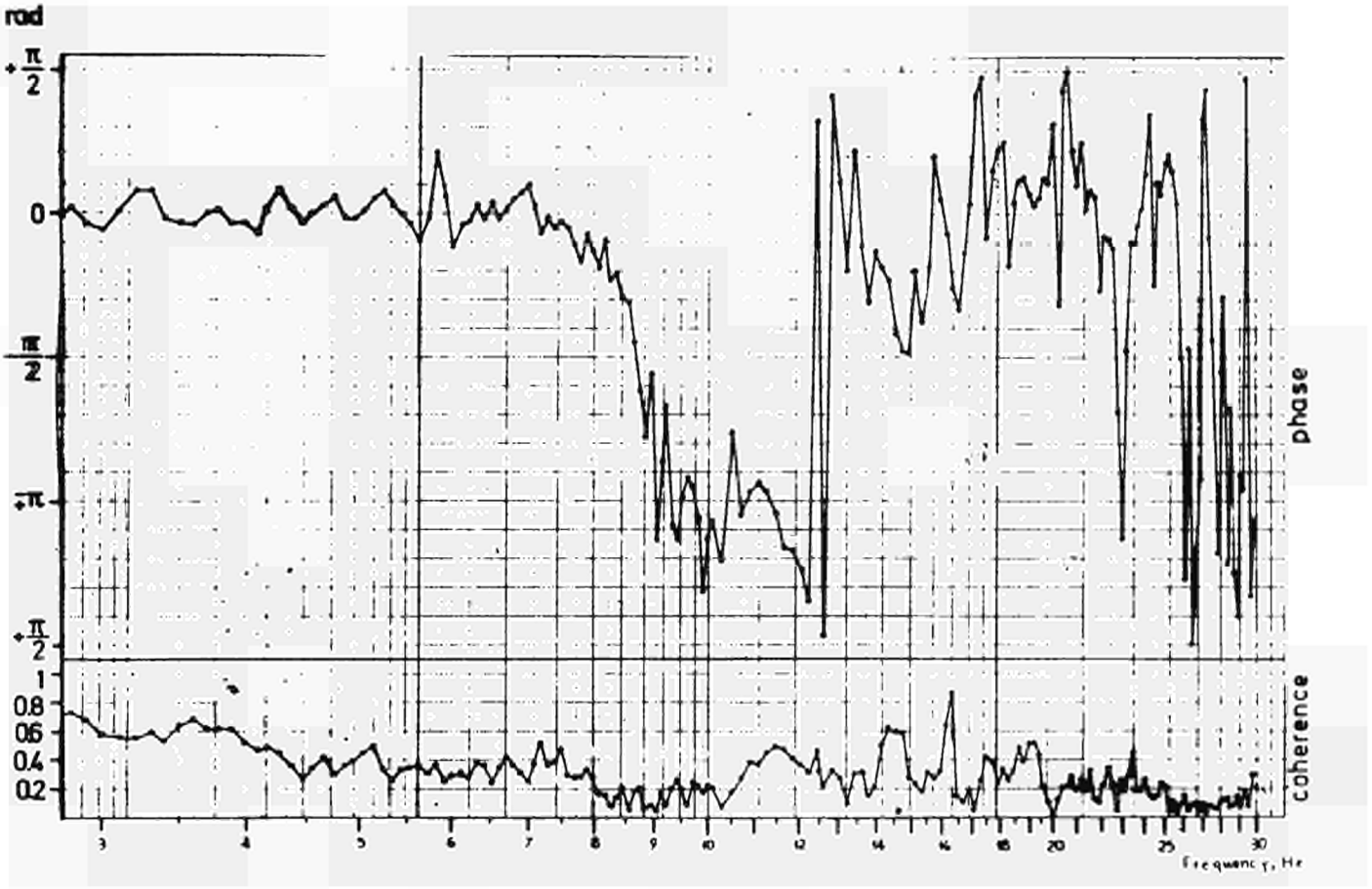

Fig. I.3.1/8 b: Phase and coherence function of ion chamber signals R and 33B

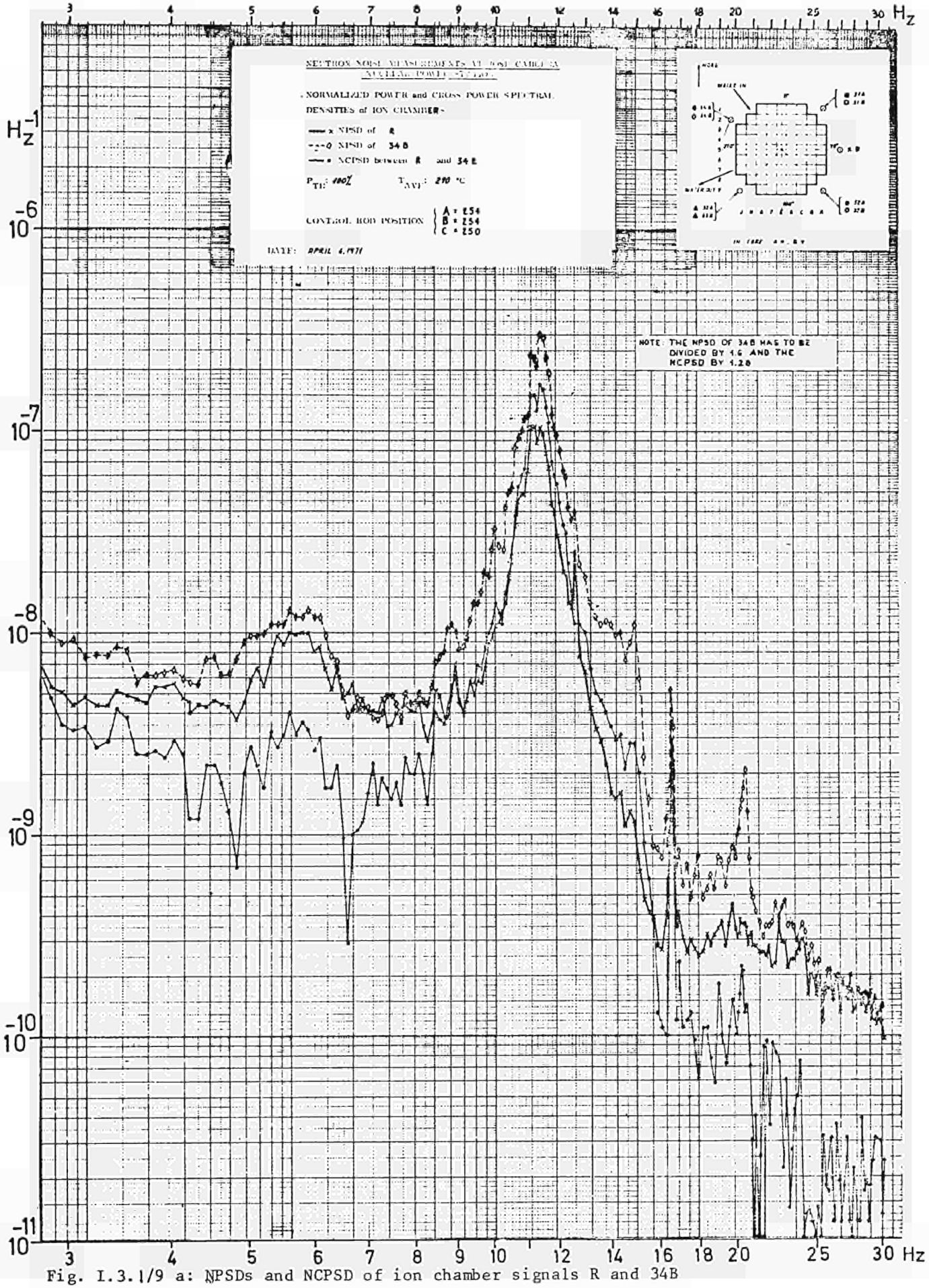

Fig. I.3.1/9 a: NPSDs and NCPSD of ion chamber signals R and 34B

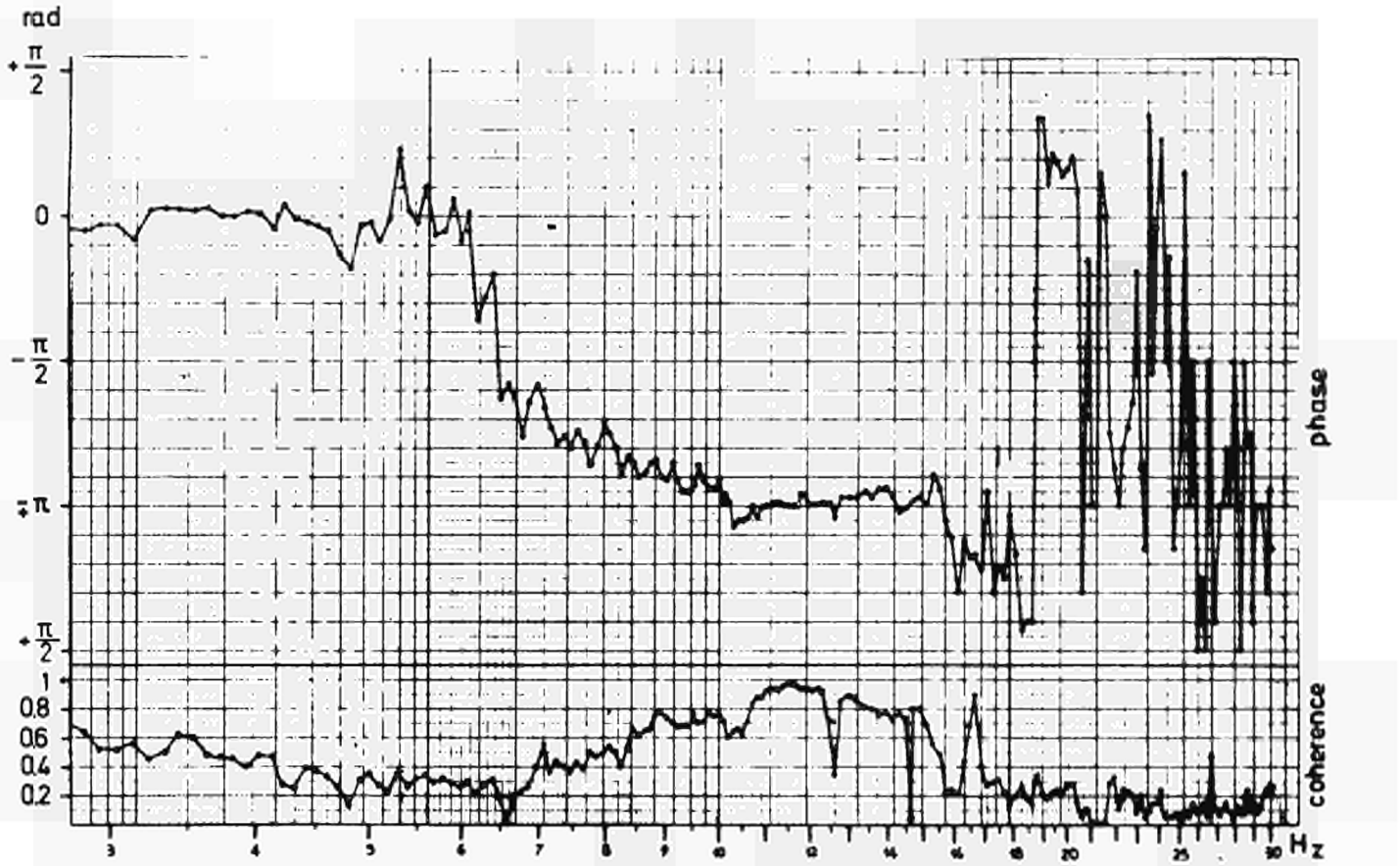

Fig. I.3.1/9 b: Phase and coherence function of ion chamber signals R and 34B

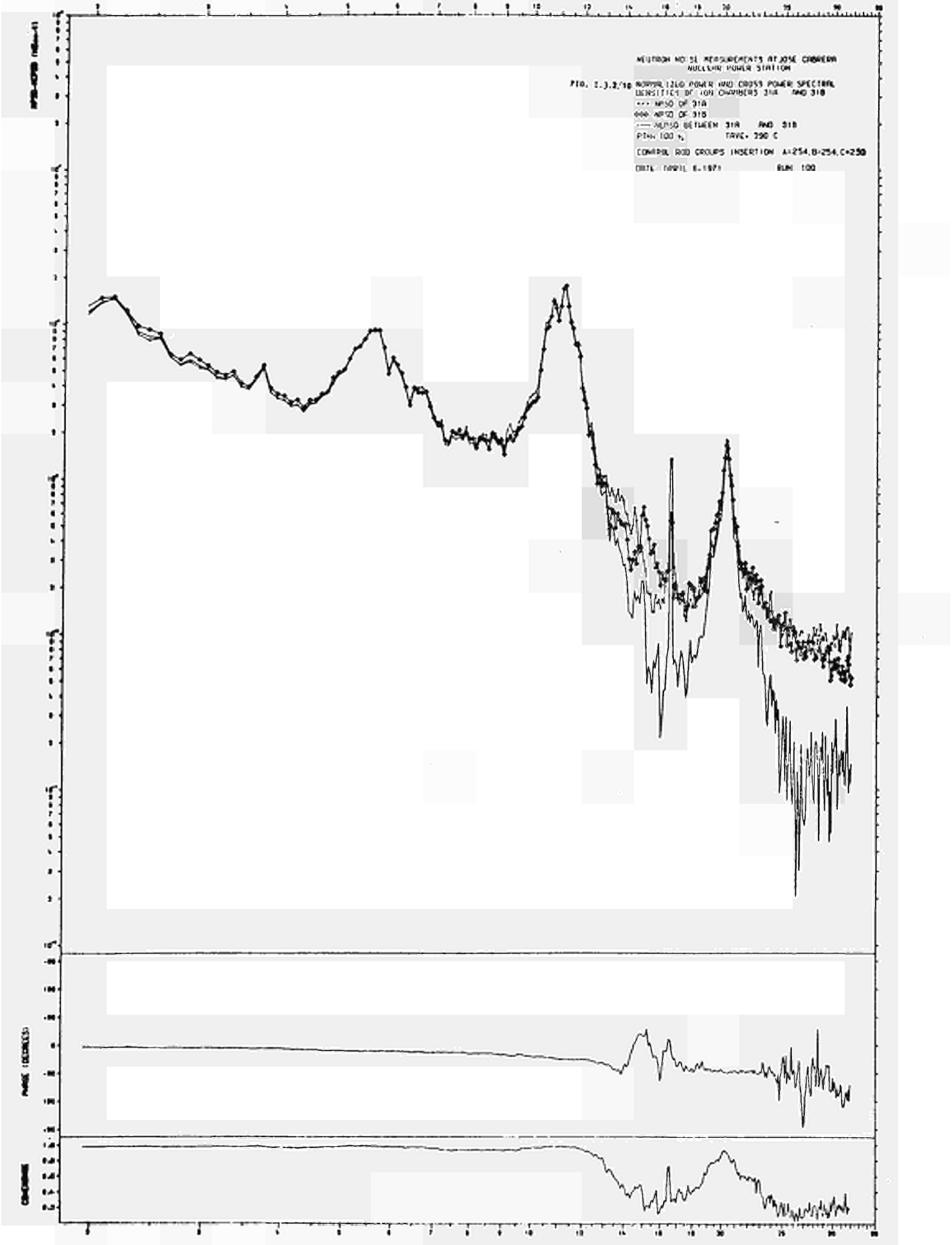
NEUTRON NOISE MEASUREMENTS AT JOSE CABRERA
NUCLEAR POWER STATION
FIG. I.3.3/16
NORMALIZED POWER AND CROSS POWER SPECTRAL
DENSITIES OF ION CHAMBERS 31A AND 31B
--- NPSD OF 31A
000 NPSD OF 31B
—— NPSD BETWEEN 31A AND 31B
POW: 100 %
TAVE: 290 C
CONTROL ROD GROUPS INSERTION A=254,B=254,C=250
DATE: APRIL 6,1971
RUN 100
PHASE (DEGREES)
COHERENCE

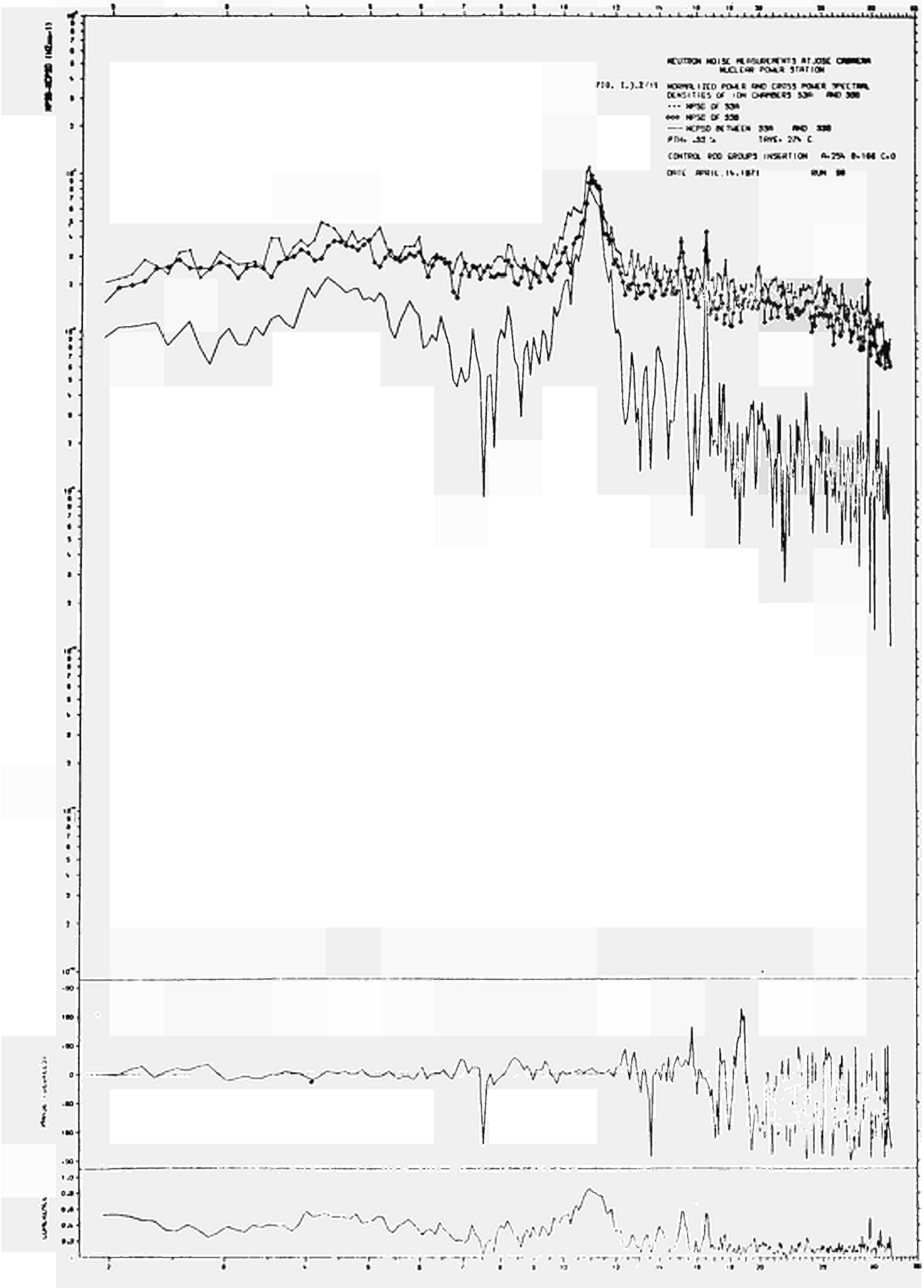
NEUTRON NOISE MEASUREMENTS AT JOSE CABRERA
NUCLEAR POWER STATION
FIG. I.3.2/11 NORMALIZED POWER AND CROSS POWER SPECTRAL
DENSITIES OF ION CHAMBERS 53A AND 53B
--- NPSD OF 53A
---- NPSD OF 53B
—— NCPSD BETWEEN 53A AND 53B
PTH= .33 % TMVS= 27% C
CONTROL ROD GROUPS INSERTION A=25A B=16B C=0
DATE APRIL 14,1971 RUN 88

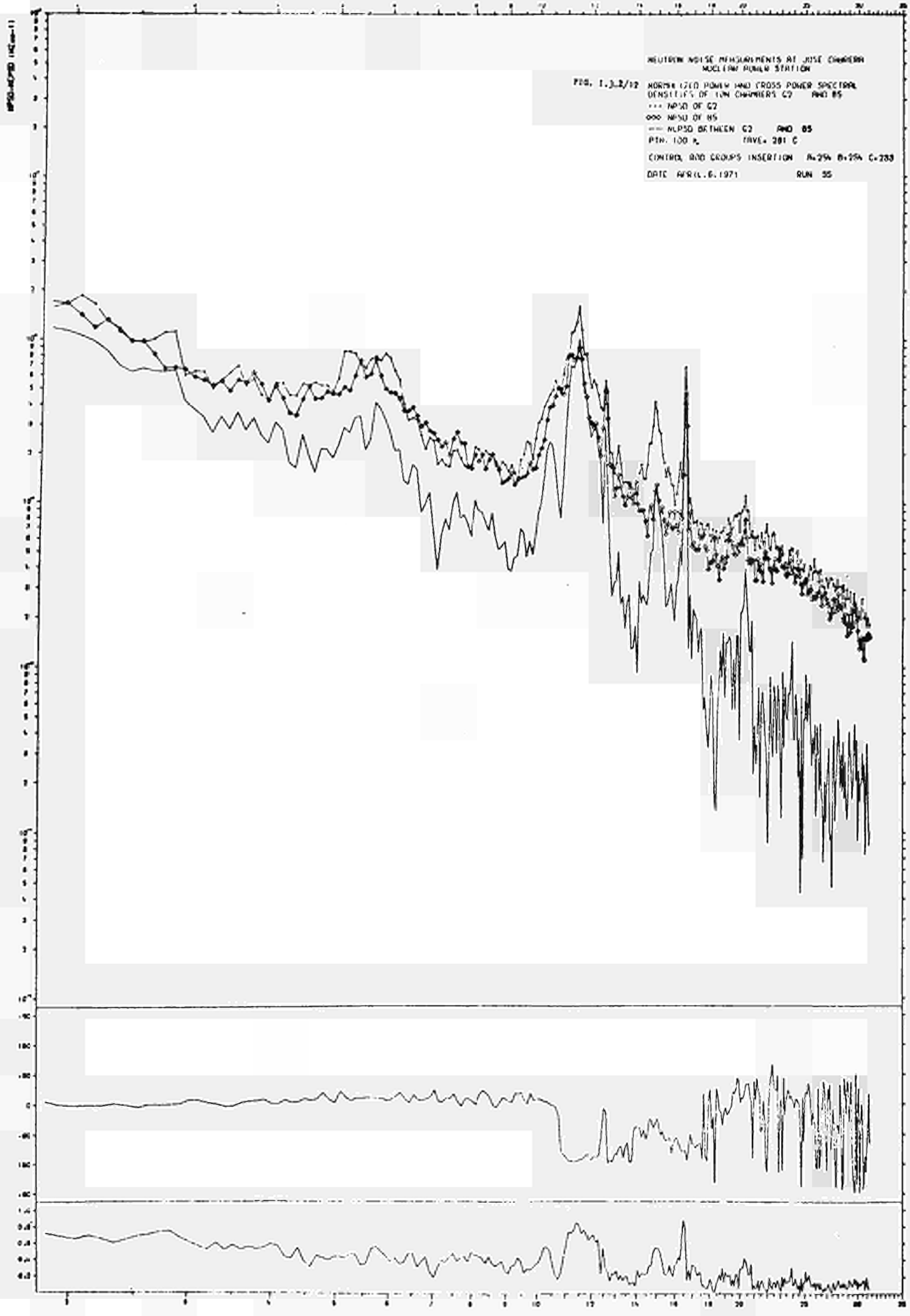
NEUTRON NOISE MEASUREMENTS AT JOSE CABRERA NUCLEAR POWER STATION
FIG. I.3.2/12 NORMALIZED POWER AND CROSS POWER SPECTRAL DENSITIES OF ION CHAMBERS C2 AND B5
··· NPSD OF C2
ooo NPSD OF B5
— NCPSD BETWEEN C2 AND B5
PTH. 100 %. TAVE. 281 C
CONTROL ROD GROUPS INSERTION A=25% B=25% C=25%
DATE APRIL.6.1971 RUN 55

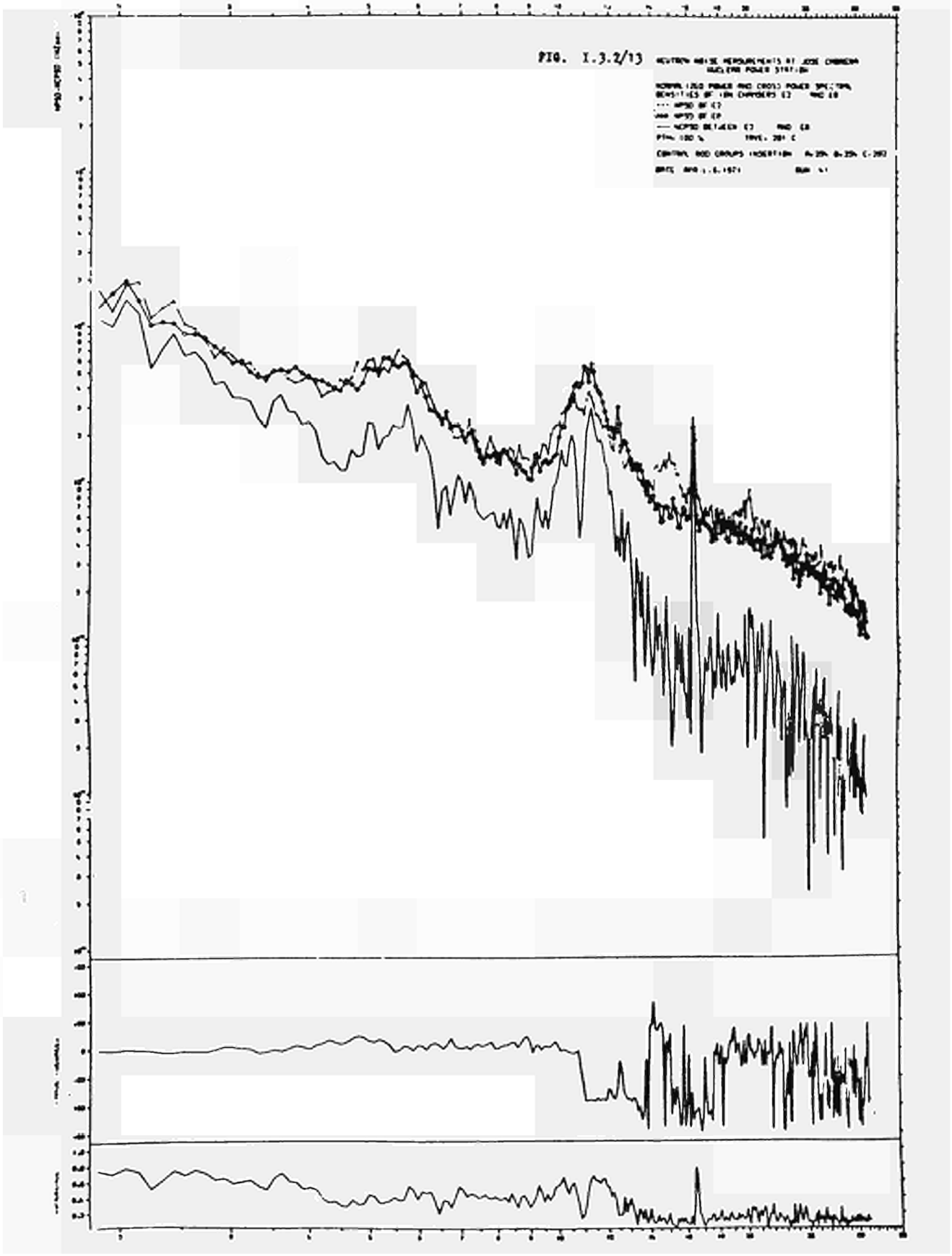

FIG. I.3.2/13

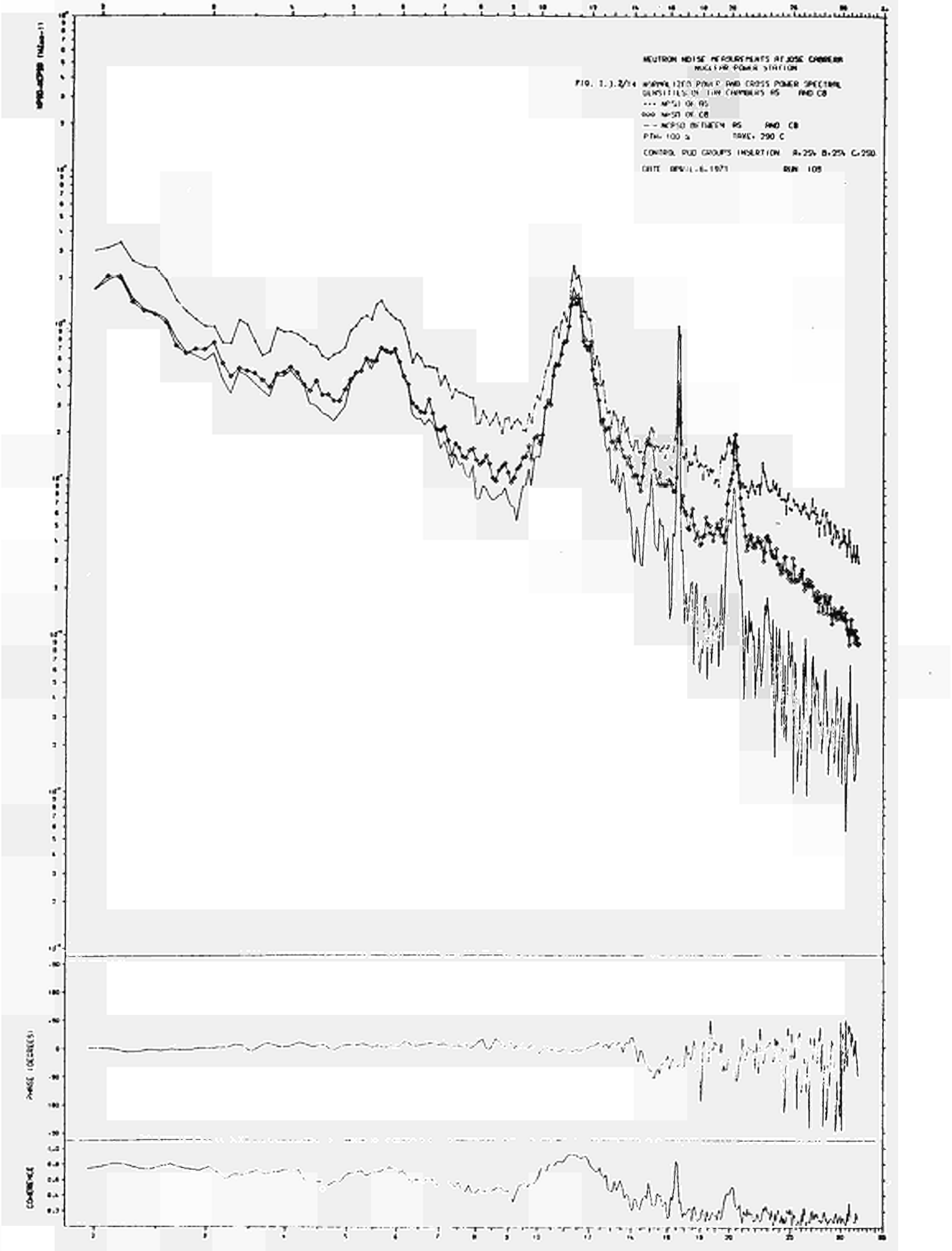
NEUTRON NOISE MEASUREMENTS AT JOSE CABRERA
NUCLEAR POWER STATION
FIG. 1.1.2/14 NORMALIZED POWER AND CROSS POWER SPECTRAL
DENSITIES ON TWO CHAMBERS RS AND CB
--- NPSD OF RS
000 NPSD OF CB
- - - NCPSD BETWEEN RS AND CB
PTH= 100 %
TAVE= 290 C
CONTROL ROD GROUPS INSERTION A=25% B=25% C=25%
DATE DEC/1.6.1971
RUN 105
PHASE (DEGREES)
COHERENCE

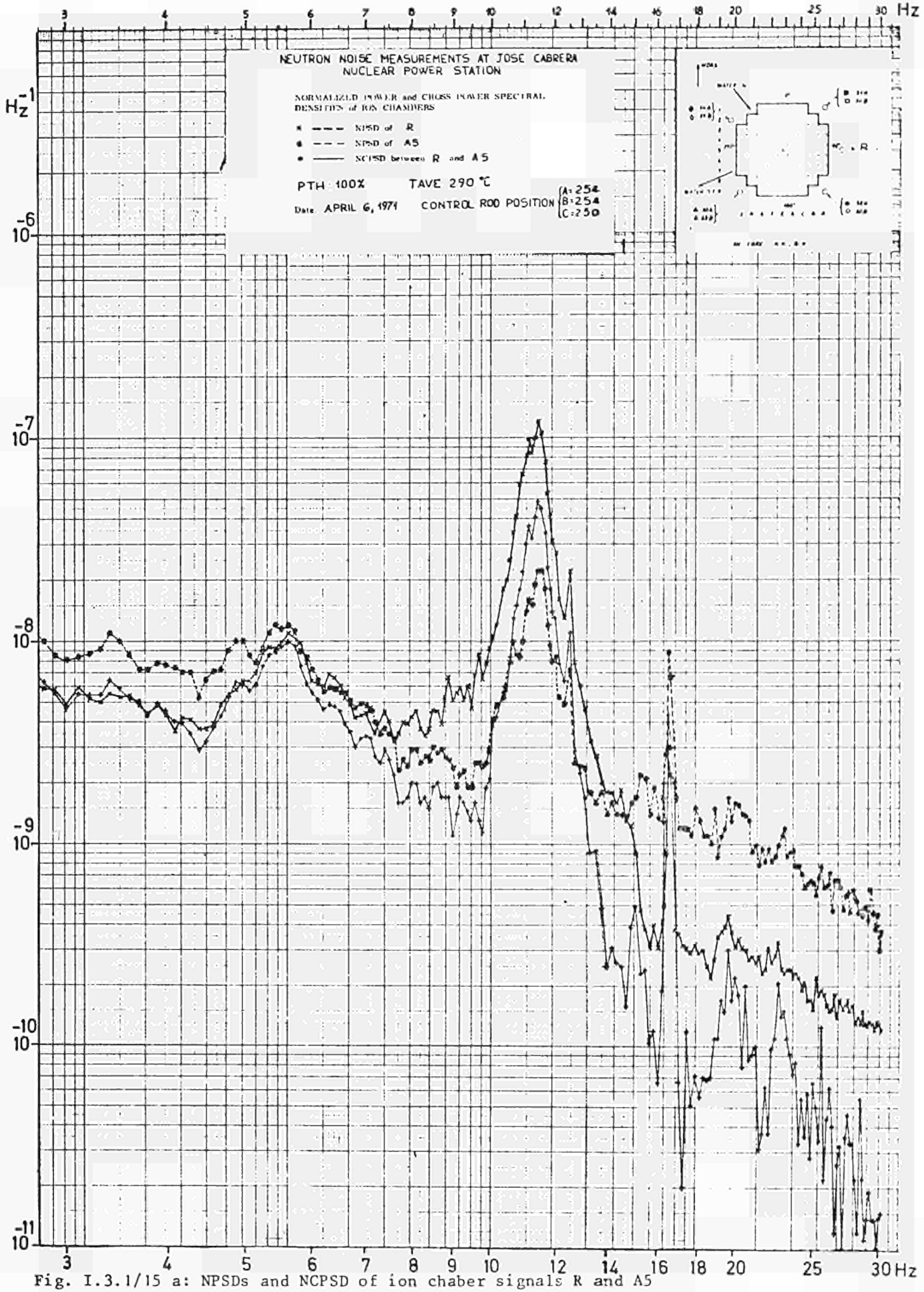

Fig. I.3.1/15 a: NPSDs and NCPSD of ion chaber signals R and A5

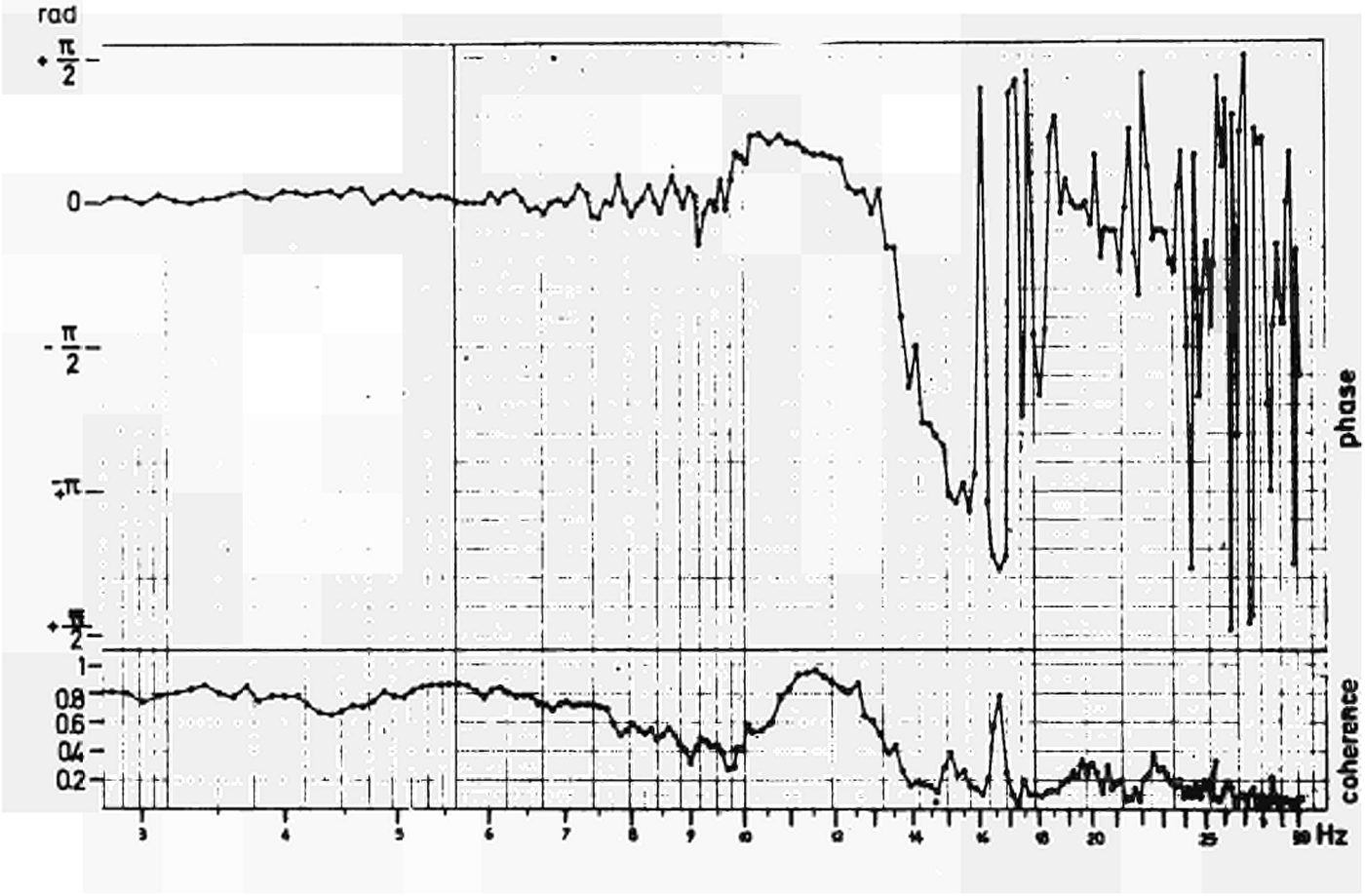

Fig. I.3.1/15 b: Phase and coherence function of ion chamber signals R and A5

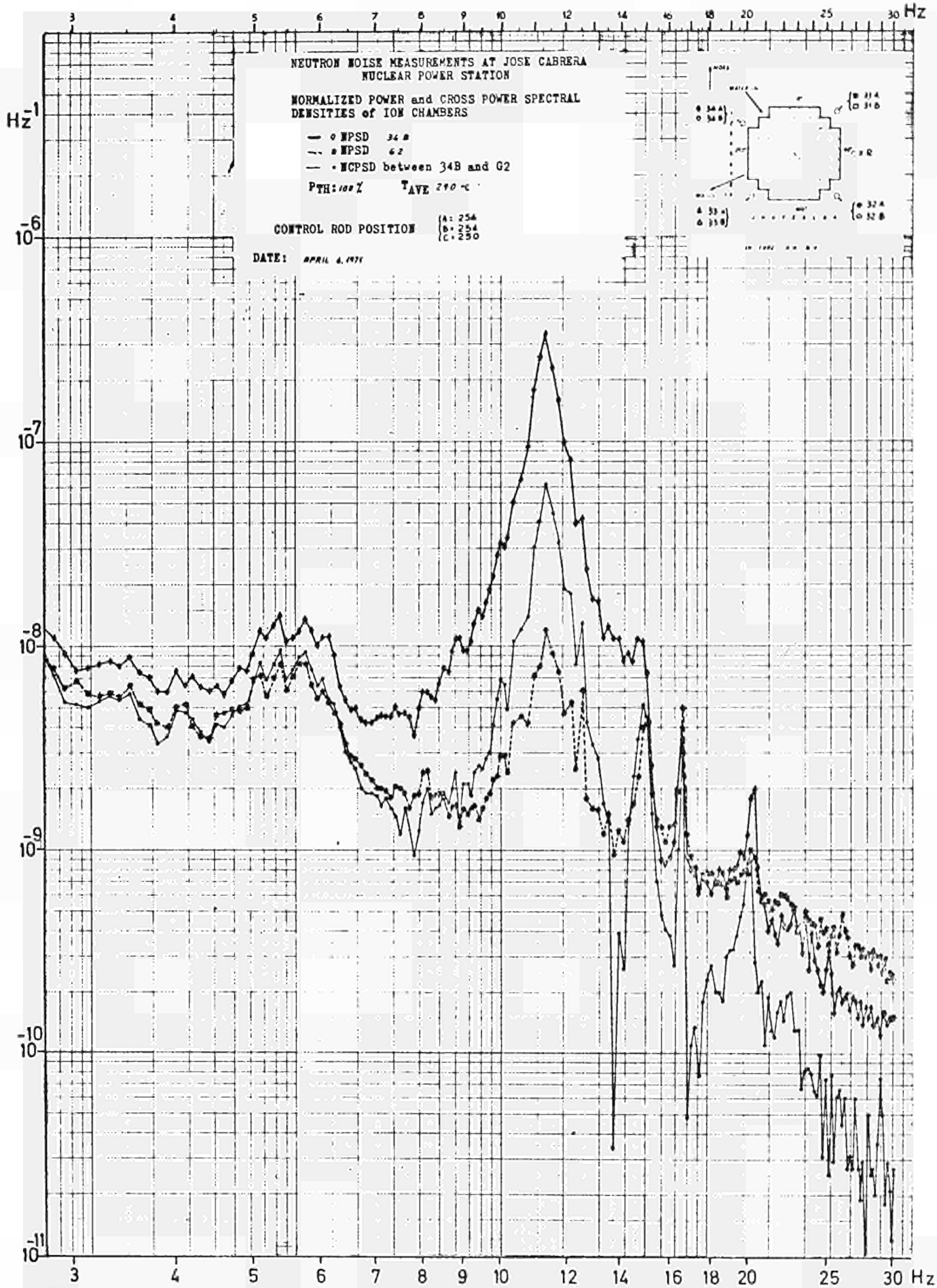

Fig. I.3.1/16 a: NPSDs and NCPSD of ion chamber signals 34B and G2

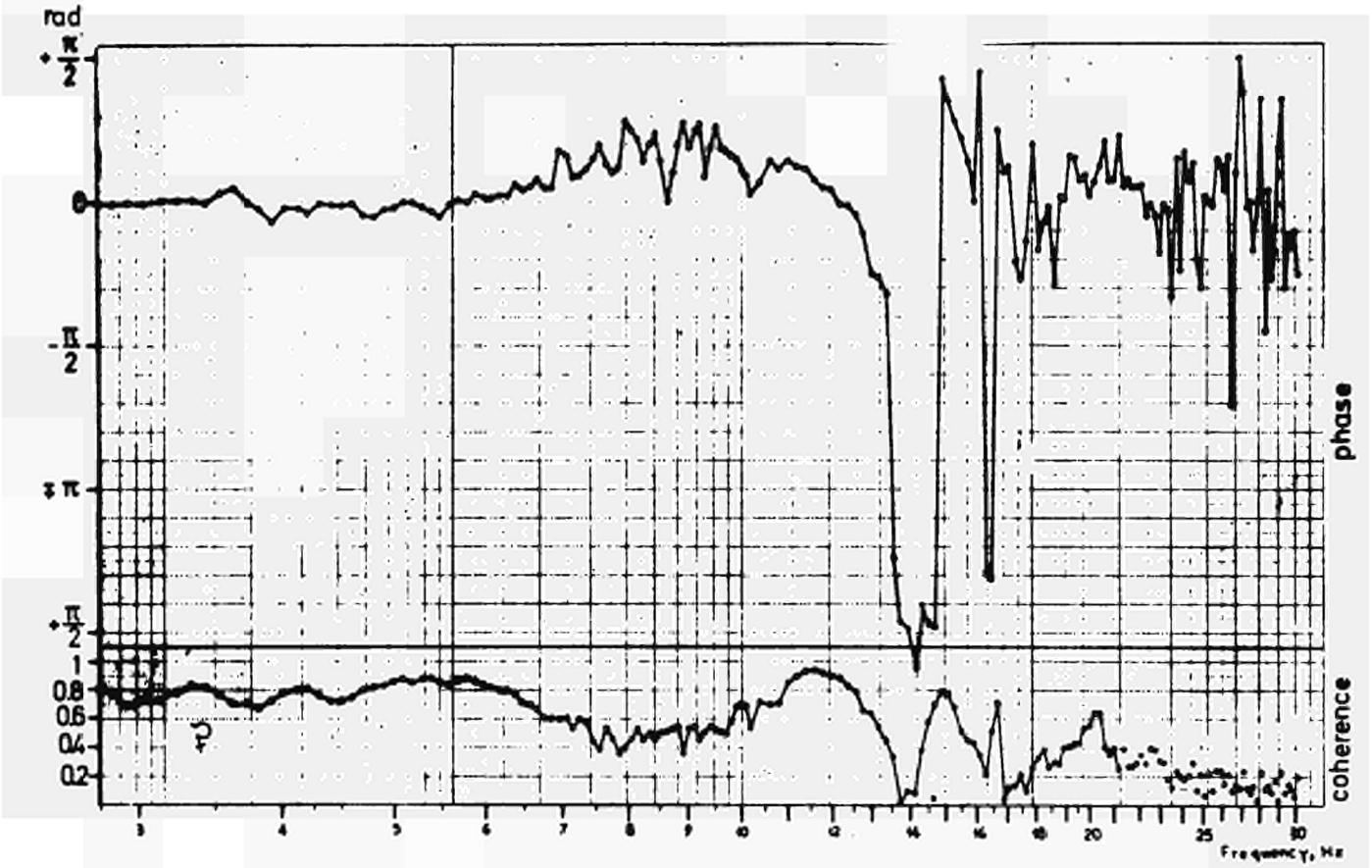

Fig. I.3.1/16 b: Phase and coherence function of ion chamber signals 34B and G2

I.3.3 SENA Nuclear Power Plant

I.3.3.1 Measurements

SENA is a 4 loop plant with an electrical output of 266 MW_e. In the course of neutron noise measurements performed in 1972 after refuelling at full power (905 MW_{th}) two significant peaks were found /1/ (for sensor positions see fig. I.3.3/1):
4.2 Hz in the LRP 3 - LRP 4 direction
5.5 Hz in the LRP 9 - LRP 11 direction
The analysis had been performed between 1 and 30 Hz.
The corresponding oscillation amplitudes peak to peak had been estimated as follows
250 µm for the 4.2 Hz frequency
70 µm for the 5.5 Hz frequency

In 1973 different kinds of tests were performed, whose nature and aims are hereunder indicated:

- Before refuelling at full power. Neutron noise measurements to compare the new behaviour of the core with the one it had last year after refuelling.
- After refuelling at full power. Neutron and pressure noise measurements to know the new behaviour of the core and try to correlate the two phenomena, and additional investigations of the frequencies below 1 Hz.

I.3.3.2 Analysis

In the chapters below noise analysis results are discussed as gained from measurement signals obtained during full power operation of the plant (905 MW_{th}).

I.3.3.2.1 Neutron Noise Analysis Before Refuelling

The former peak at 4.2 Hz in the LRP 3 - LRP 4 direction has shifted to 4 Hz (figs. I.3.3/2, I.3.3/3 and I.3.3/4) though the power level is the same as last year.

As for the peak at 5.5 Hz in the LRP 9 - LRP 11 direction it seems have completely disappeared (figs. I.3.3/5, I.3.3/6 and I.3.3/7) but we have not been allowed to use chamber LRP 9 and have had to use LRP 11 instead; now, LRP 10 has the same angular position as LRP 9 but is higher than the latter (fig. I.3.3/1); this probably reduces the signal to noise ratio and prevents from detecting the phenomenon.

I.3.3.2.2 Neutron Noise Analysis After Refuelling

We had two aims for this series of tests:

- Analysis between 1 and 25 Hz as previously, to know the new behaviour of the core in this frequency range.
- Analysis at lower frequencies, i.e. between 0.02 and 2 Hz to detect an eventual peak expected since have been performed experience on a model.

a) Results Obtained Between 1 and 25 Hz

The peak previously obtained at 4 Hz in the LRP 3 - LRP 4 direction has shifted still further to 3.75 Hz (figs. I.3.3/8, I.3.3/9 and I.3.3/10) and corresponds to a displacement peak to peak estimated at about 90 µm. Besides, this 3.75 Hz frequency is also present in the LRP 9 - LRP 11 direction (figs. I.3.3/11, I.3.3/12 and I.3.3/13) and in the LRP 7 - LRP 8 direction.

As a matter of fact, we have not been allowed to use

simultaneously chambers LRP 7 and LRP 8, e.g. the cross-spectrum and autospectra obtained with LRP 7 and LRP 11 show undoubtedly the presence and importance of the 3.75 Hz frequency in the LRP 7 - LRP 8 direction (figs. I.3.3/14, I.3.3/15 and I.3.3/16). The corresponding displacements peak to peak are respectively estimated at 55 μm and 30 μm. We have not been able to perform measurements in the LRP 5 - LRP 6 direction, but there is probably also an oscillation at the same frequency in this direction.

So if the 3.75 Hz frequency were the only one existing the core would describe an elliptical motion (Lissajous' curve with the same frequencies in two perpendicular directions) as indicated in fig. I.3.3/17. In the same figure we show the pendular motion in the LRP 9 - LRP 11 direction at 5.25 Hz whose amplitude peak to peak has been estimated at about 60 μm. We effectively found a peak in this direction (figs. I.3.3/12 and I.3.3/13) and only in this direction, at 5.25 Hz.

Therefore, the former peak at 5.5 Hz has also shifted since last year. The power level has increased from 905 to 950 MW_{th}, but let us call back that the power level had formerly no effect on this peak. This very strange phenomenon is not yet explained.

b) Results Obtained Between 0.02 and 2 Hz

Between LRP 3 and LRP 4, we found a little peak at 0.18 Hz, but it is not very neat even on the $G_{4.4}$ spectrum which is yet the most sensitive (figs. I.3.3/18, I.3.3/19 and I.3.3/20). Between LRP 9 and LRP 11, there are two principle peaks at 0.1 and 0.2 Hz (figs. I.3.3/21 and I.3.3/22).

As shown in fig. I.3.3/22 the phase is almost zero for both peaks; therefore they are not connected with resonance phenomena, contrary to the oscillations at 3.75 Hz and 5.25 Hz.

I.3.3.2.3 Pressure Fluctuations

It was impossible to perform valid measurements at full power because of a leak near our transducer. Nevertheless, in order to test our installation, we had performed preliminary measurements after refuelling, at zero power and found peaks at 2.5 Hz, 5 Hz, 7.5 Hz etc. (figs. I.3.3/23, I.3.3/24 and I.3.3/25).

If we amplify the spectra of neutron noise, we can find again the 7.5 Hz frequency, but the level of the peak is very low and therefore not significant (figs. I.3.3/23, I.3.3/24, I.3.3/25, I.3.3/9, I.3.3/10).

These different peaks, whose nature is not yet explained, seem doubtful and make us think our transducer (piezoelectric) is too sensitive to the accelerations. Tests are being performed to state precisely this point. Let us recall that our transducer was placed on the zero power cooling circuit.

Literature, Section I.3.3

/1/ On-load Surveillance of Nuclear Power Plant Components by Noise and Vibration Analysis
Status Report on work performed for the Commission of the European Communities under Euratom Study Contract No. 043-71-10 ECIC (F), April 1972

Symbols, Used in Figures, Section I.3.3

G_{AA} = auto-power spectrum density of chamber A

G_{AB} = cross-power spectrum density of chambers A and B

G_{--} = auto-power spectrum density of the difference $X_A - X_B$
X_A and X_B being the signals given respectively by chambers A and B

G_{++} = auto-power spectrum density of the sum $X_A + X_B$

γ = coherence function defined by

$$\gamma^2 = \frac{/G_{AB}/^2}{G_{AA}\, G_{BB}}$$

FIG. I.3.3/1: ION CHAMBERS LOCATION

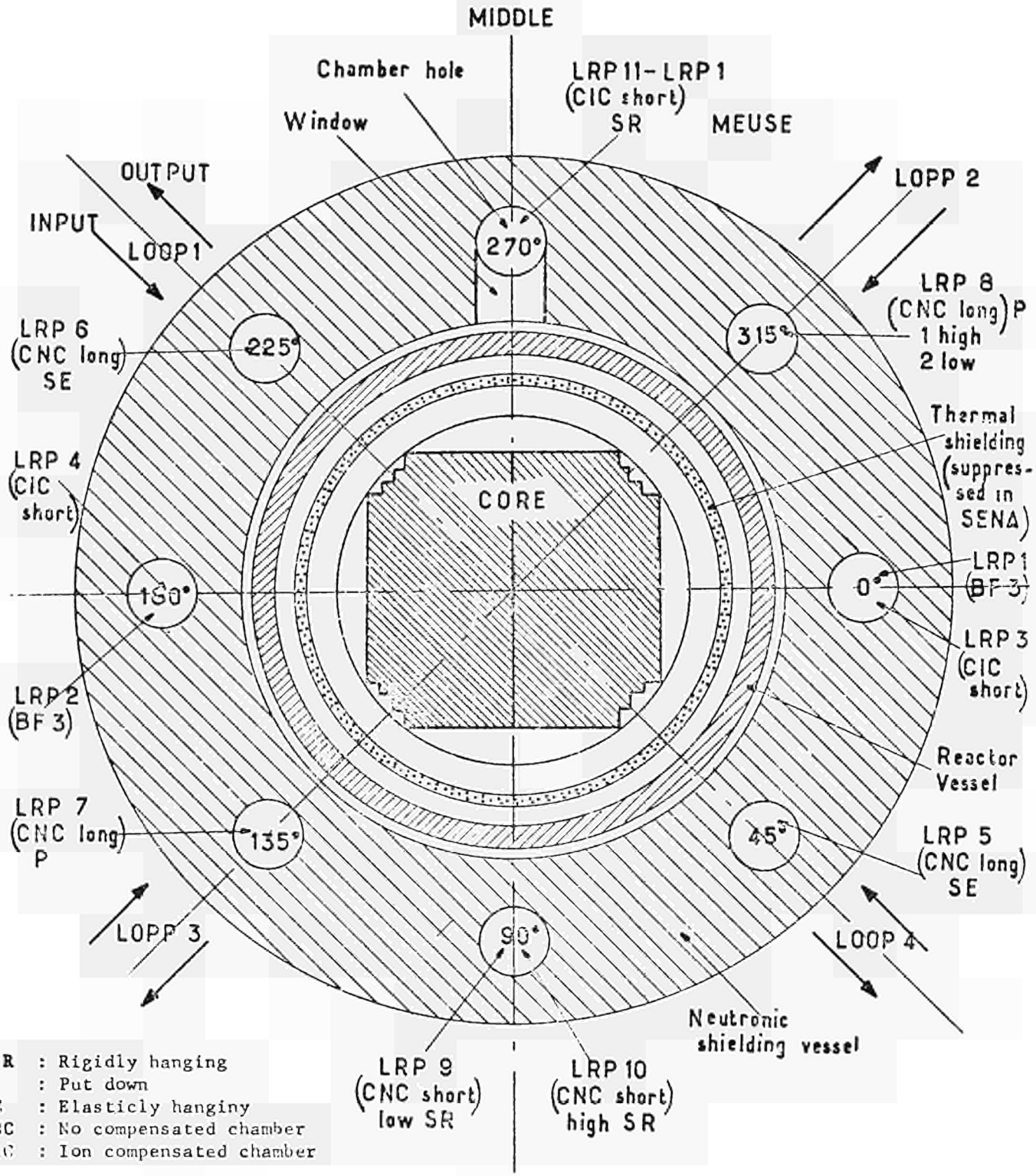

S R : Rigidly hanging
P : Put down
SE : Elasticly hanginy
CNC : No compensated chamber
CIC : Ion compensated chamber

FIG.I.3.3/2 : TEST NO. A1, CHAMBERS LRP 3 and 4

BEFORE REFUELING

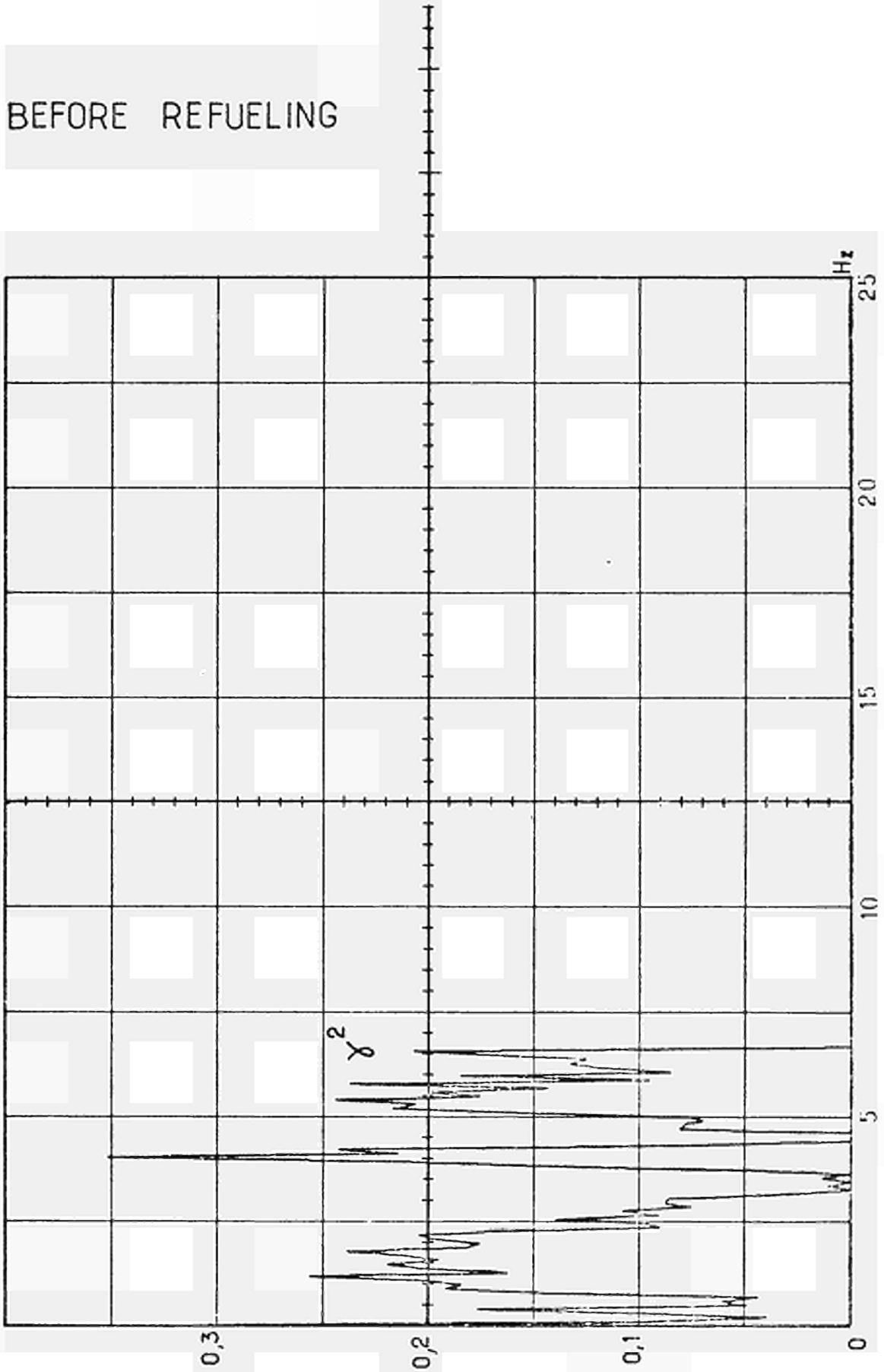

FIG.I.3.3/3a: TEST NO. A1, CHAMBERS LRP 3 and 4

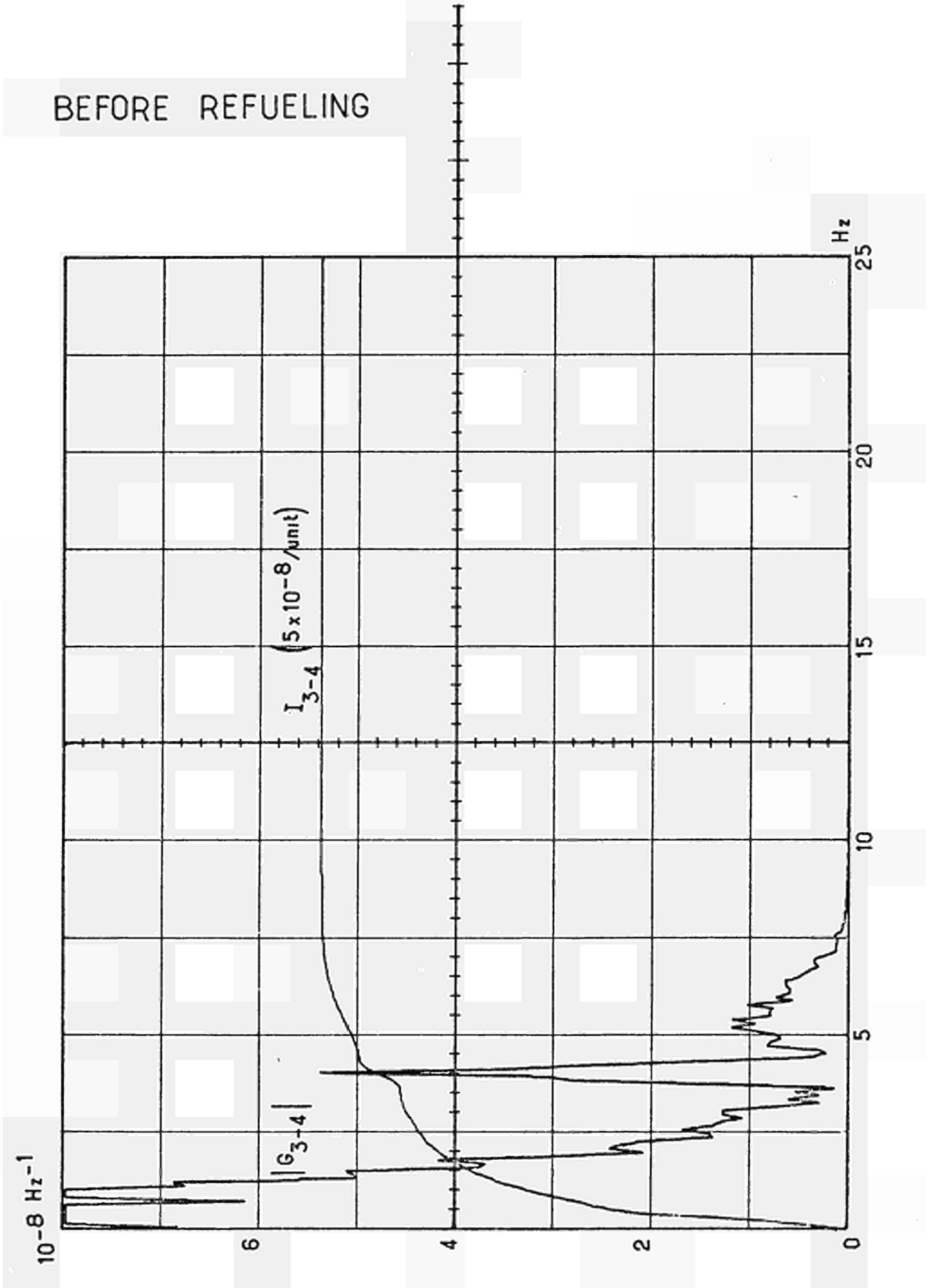

FIG.I.3.3/3b: TEST NO. A1, CHAMBERS LRP 3 and 4

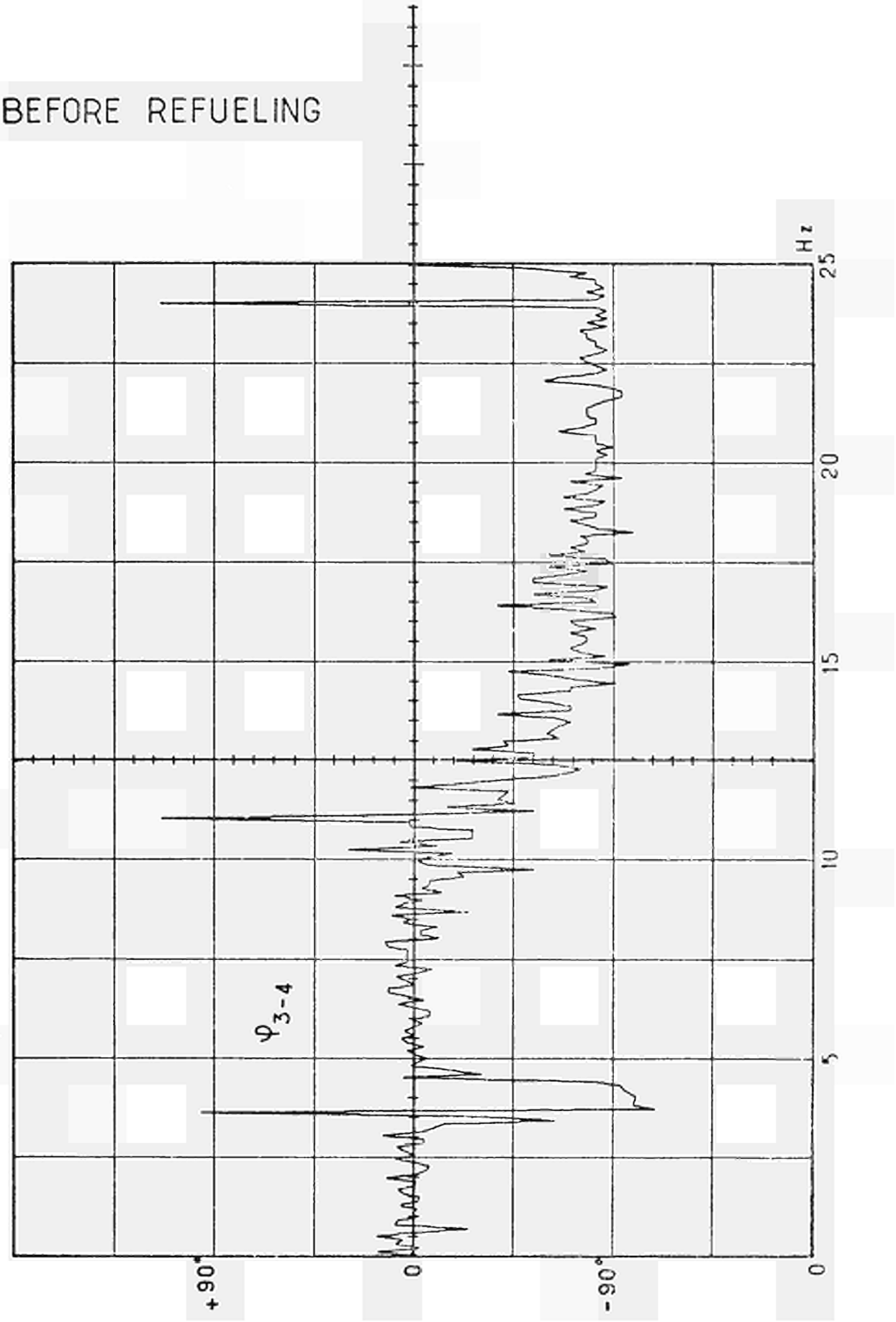

FIG.I.3.3/4 : TEST NO. A1, CHAMBERS LRP 3 and 4

BEFORE REFUELING

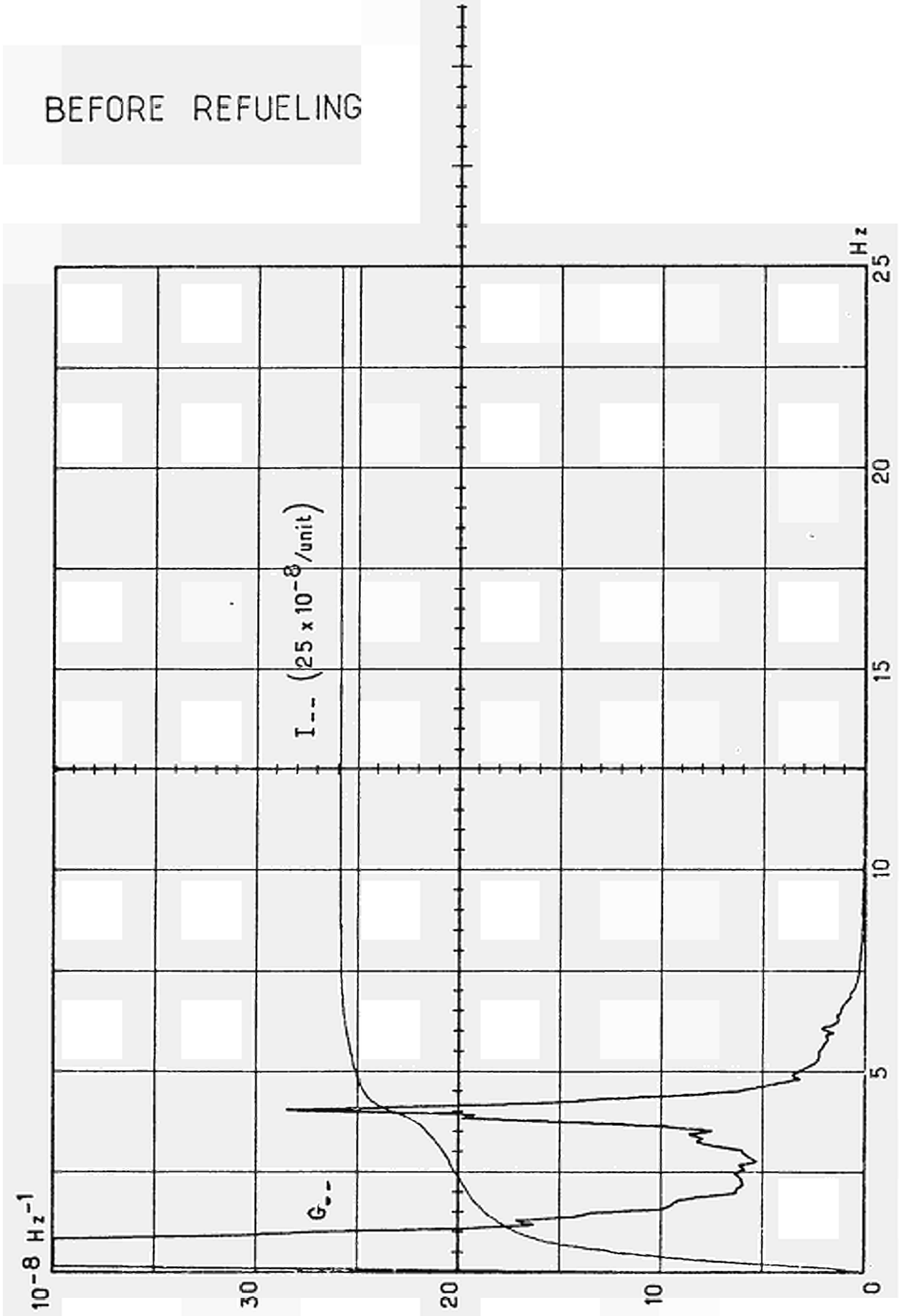

FIG.I.3.3/5: TEST NO. A1, CHAMBERS LRP 10 and 11

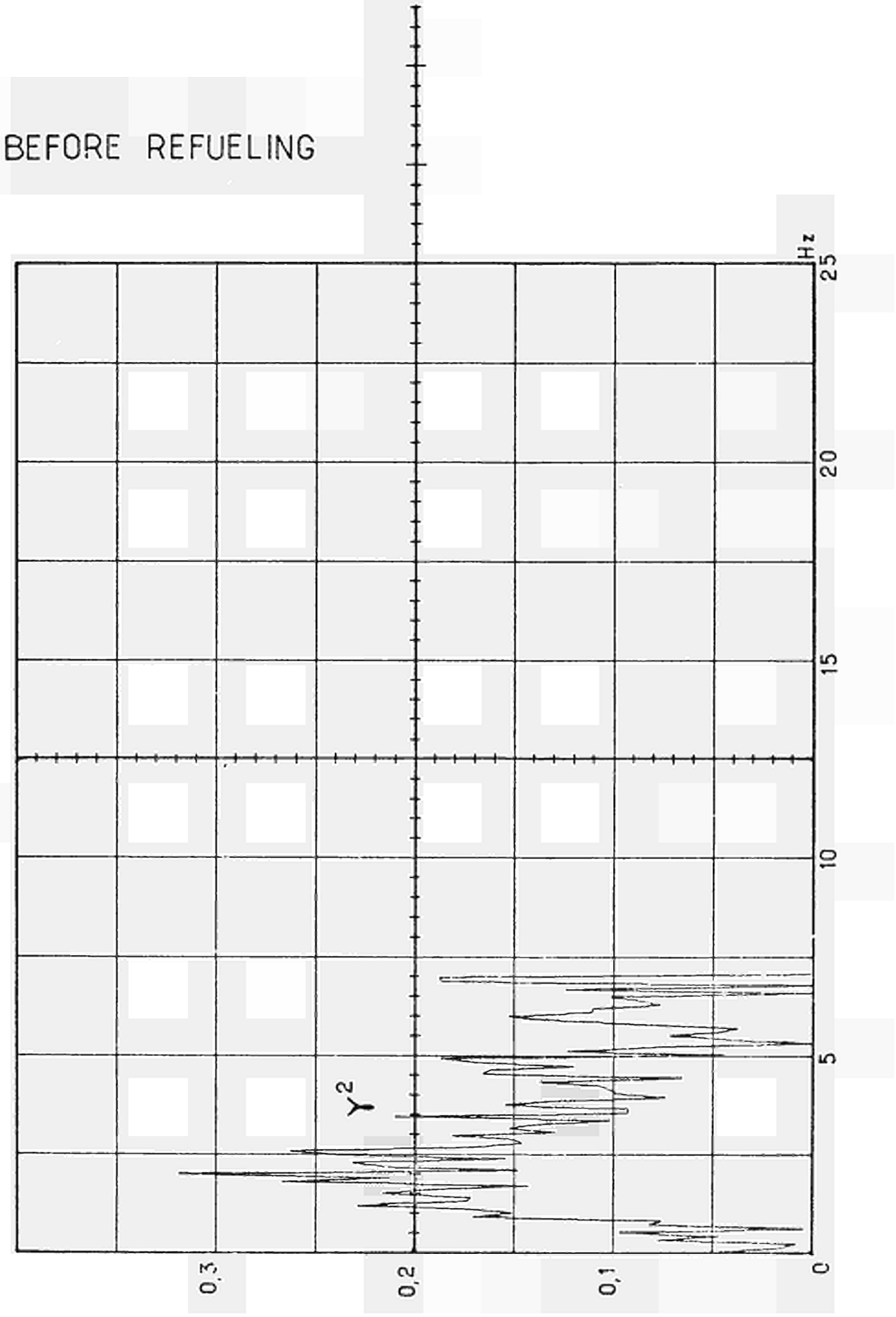

FIG.I.3.3/6 : TEST NO. A1, CHAMBERS LRP 10 and 11

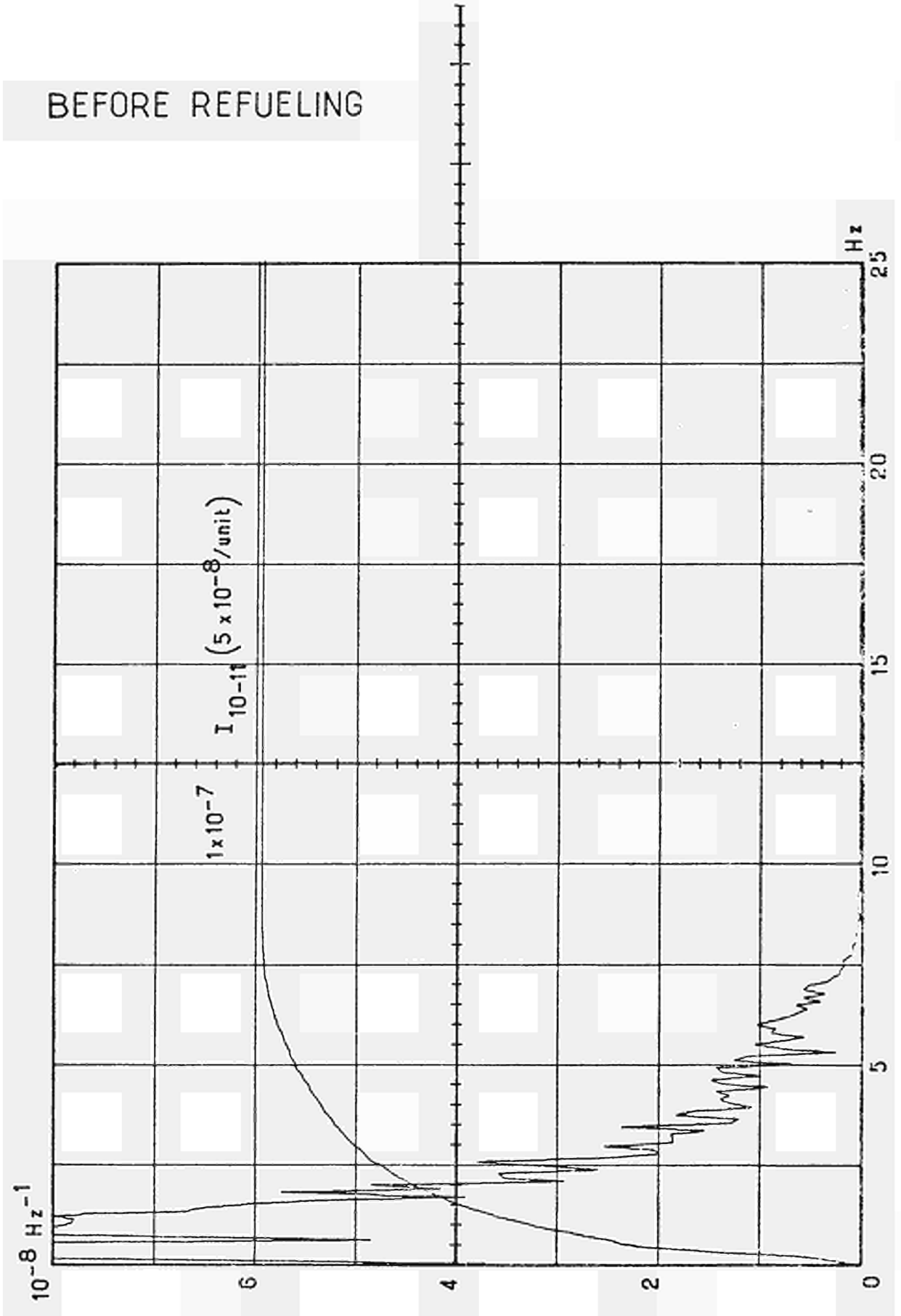

FIG. I.3.3/6a : TEST NO.A1, CHAMBERS LRP 10 and 11

BEFORE REFUELING

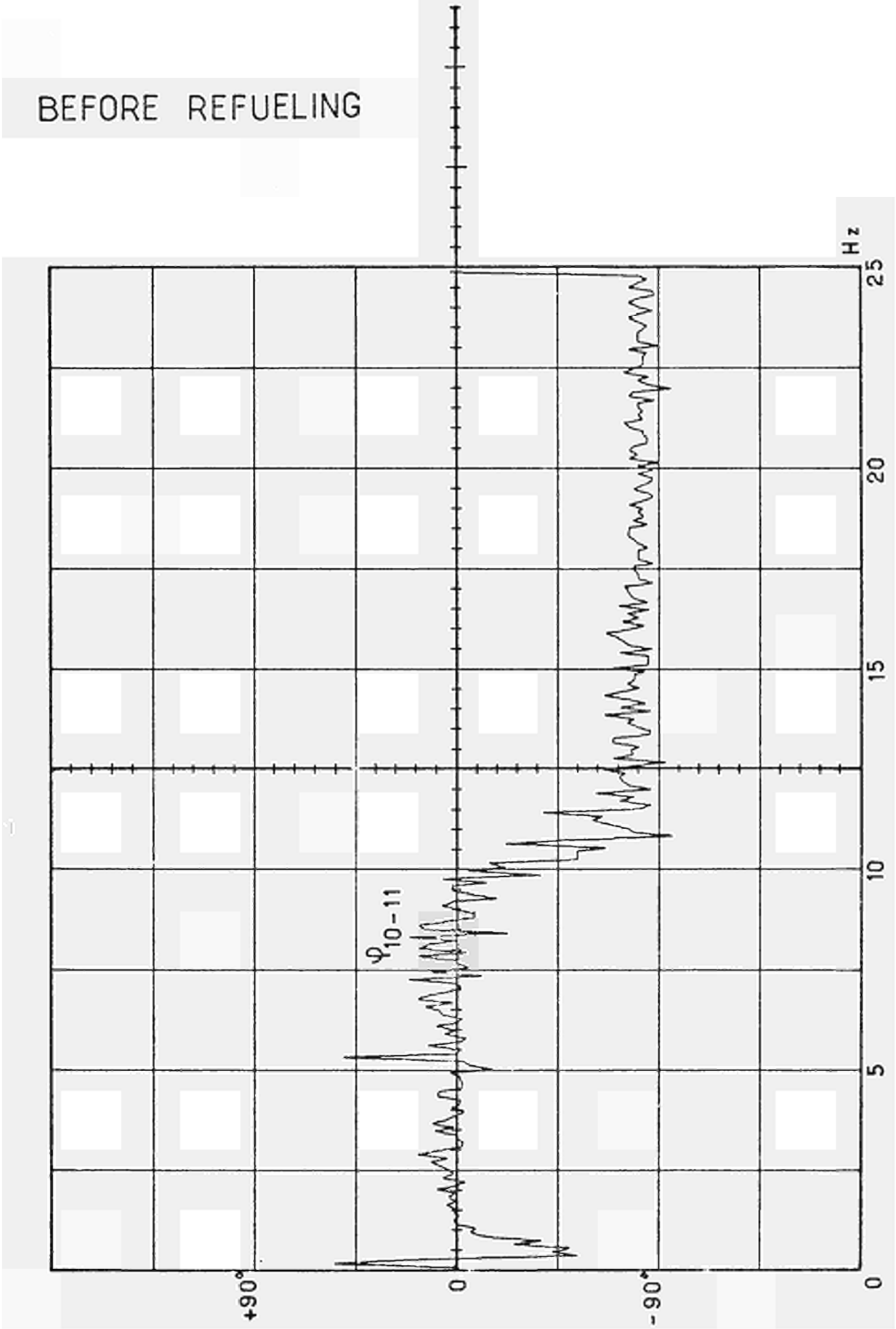

FIG.I.3.3/7: TEST NO. A1, CHAMBERS LRP 10 and 11

BEFORE REFUELING

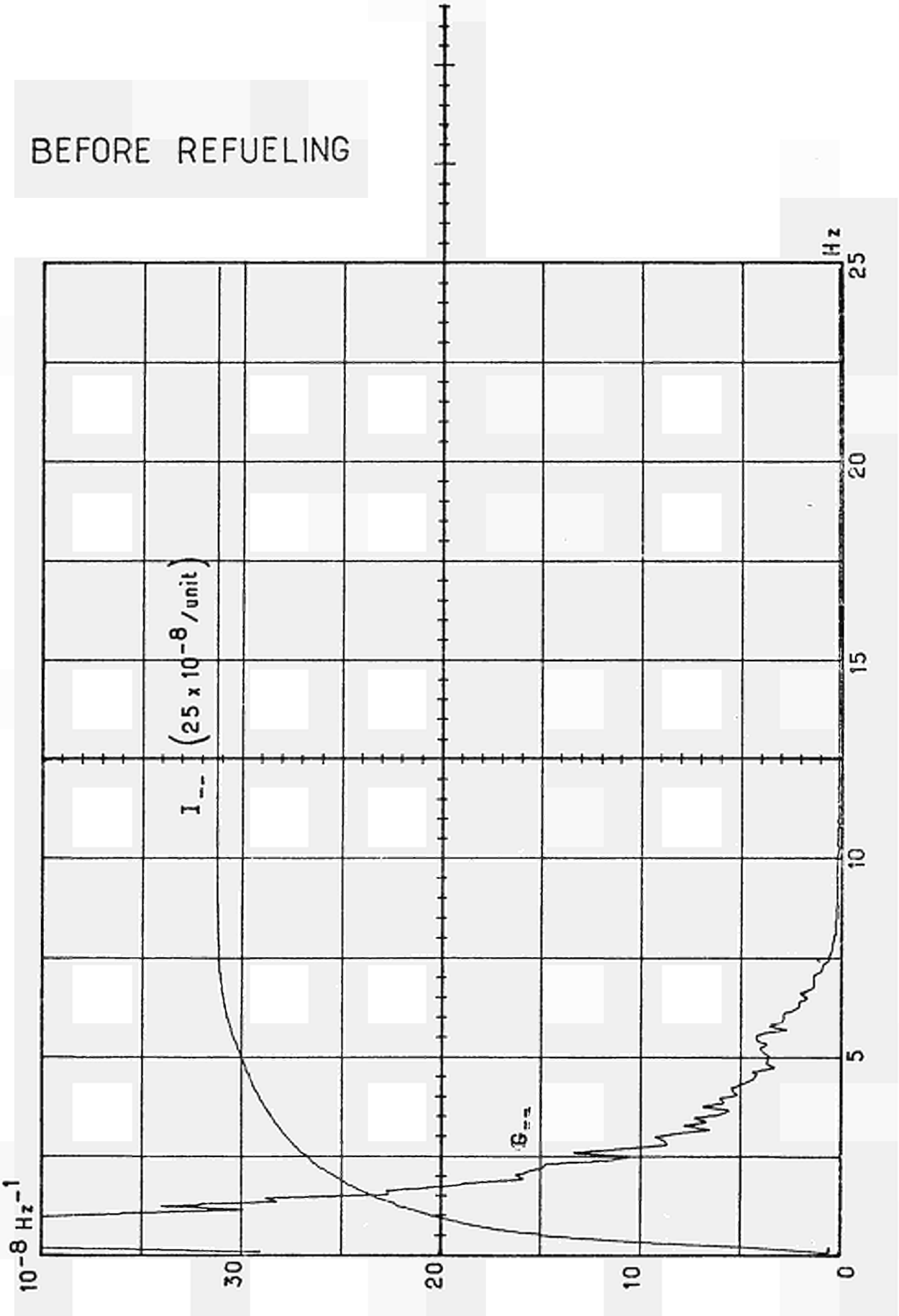

FIG.I.3.3/8: TEST NO. C1, CHAMBERS LRP 3 and 4

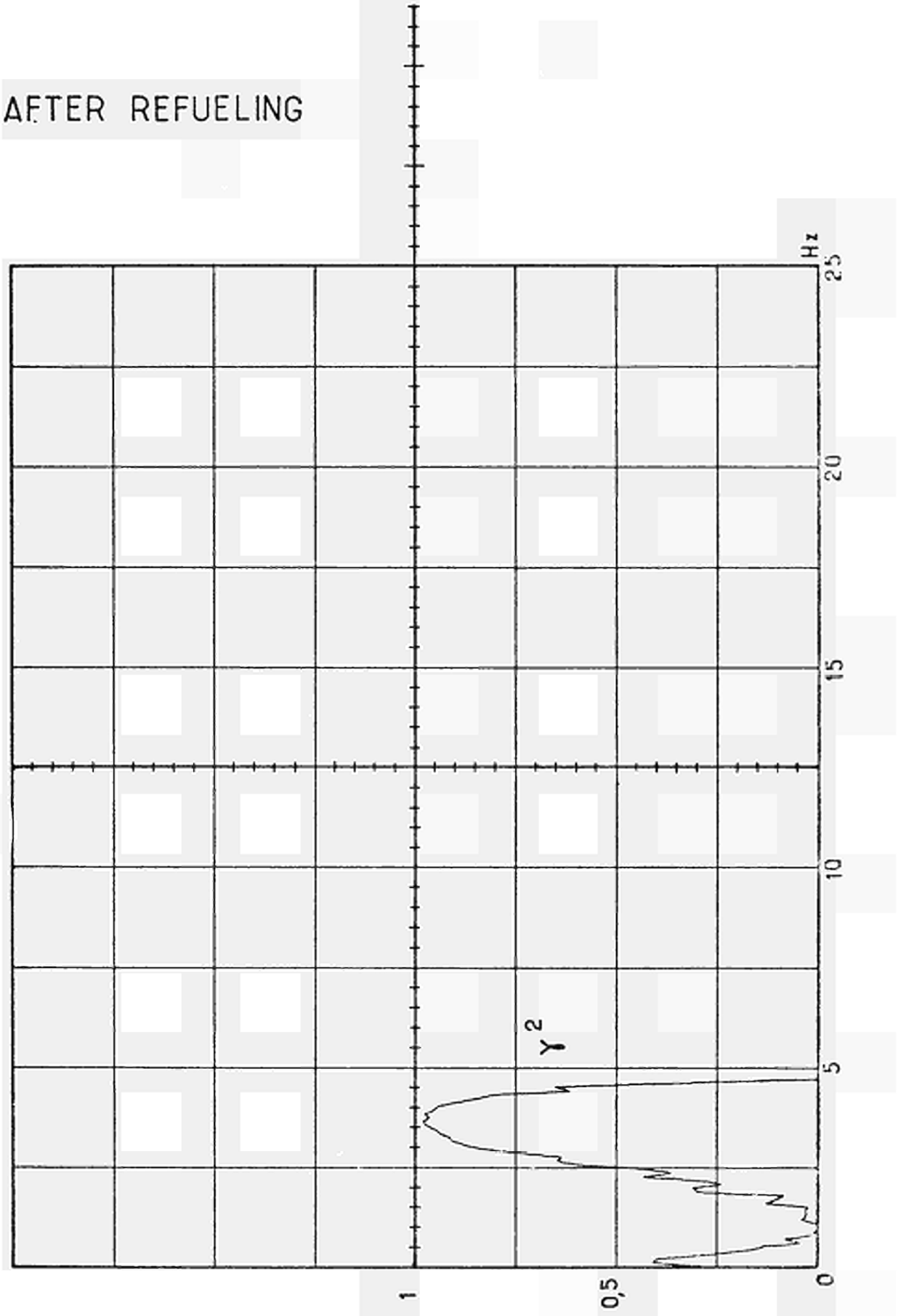

FIG I.3.3/9a: TEST NO. C1, CHAMBERS LRP 3 and 4

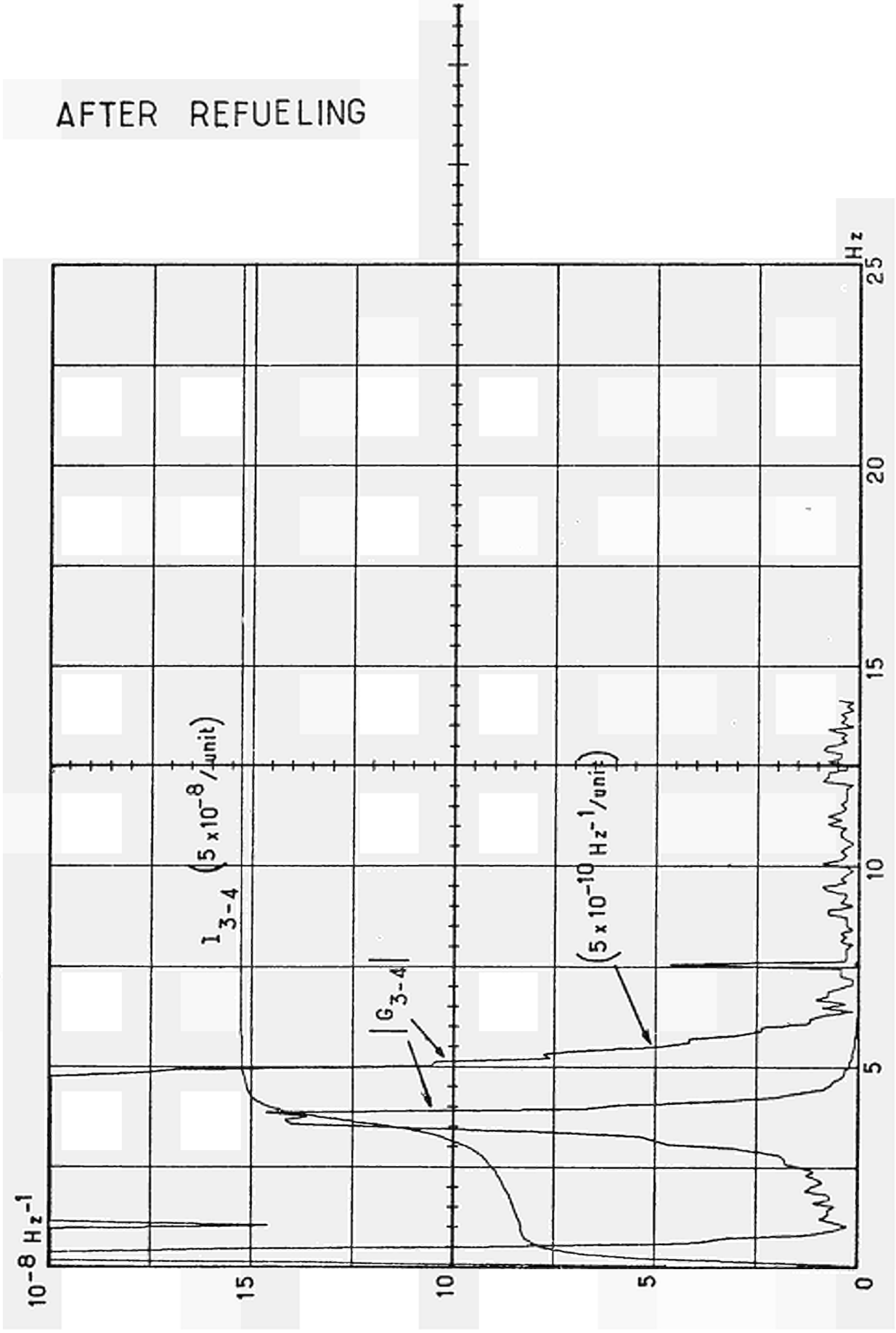

FIG.I.3.3/9b: TEST NO. C1, CHAMBERS LRP 3 and 4

AFTER REFUELING

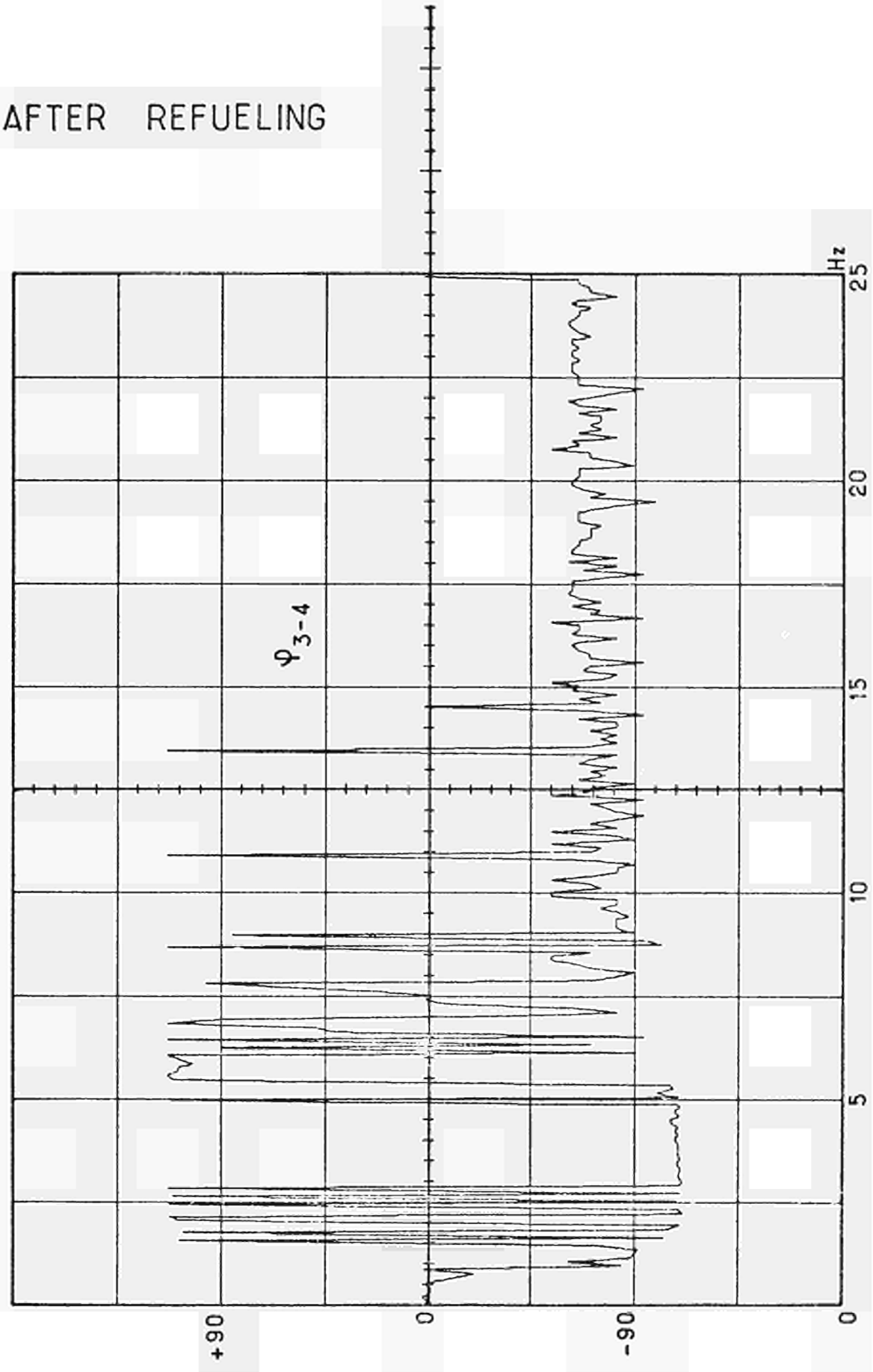

FIG.I.3.3/10: TEST NO. C1, CHAMBERS LRP 3 and 4

AFTER REFUELING

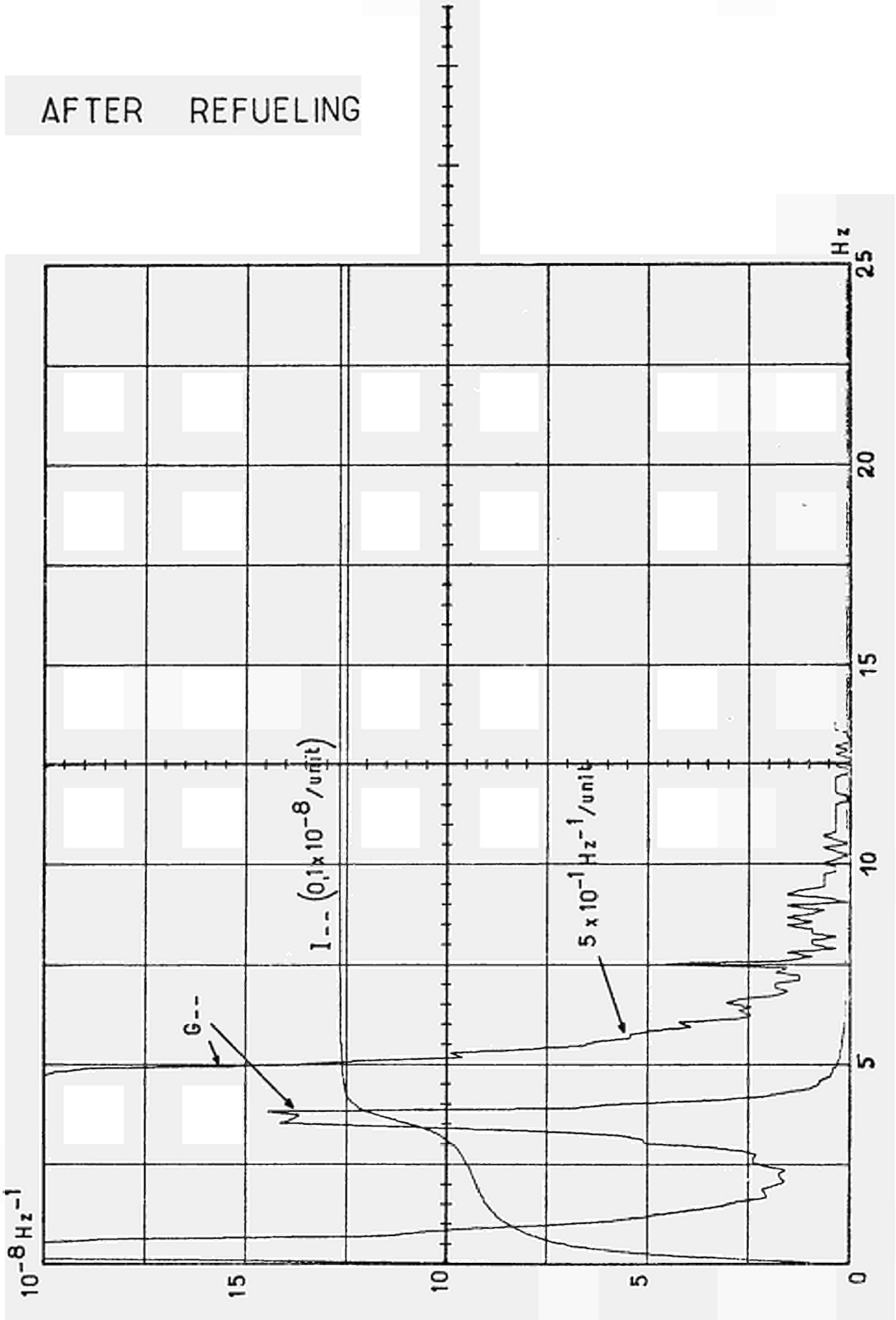

FIG.I.3.3/11: TEST NO. C1, CHAMBERS LRP 9 and 11

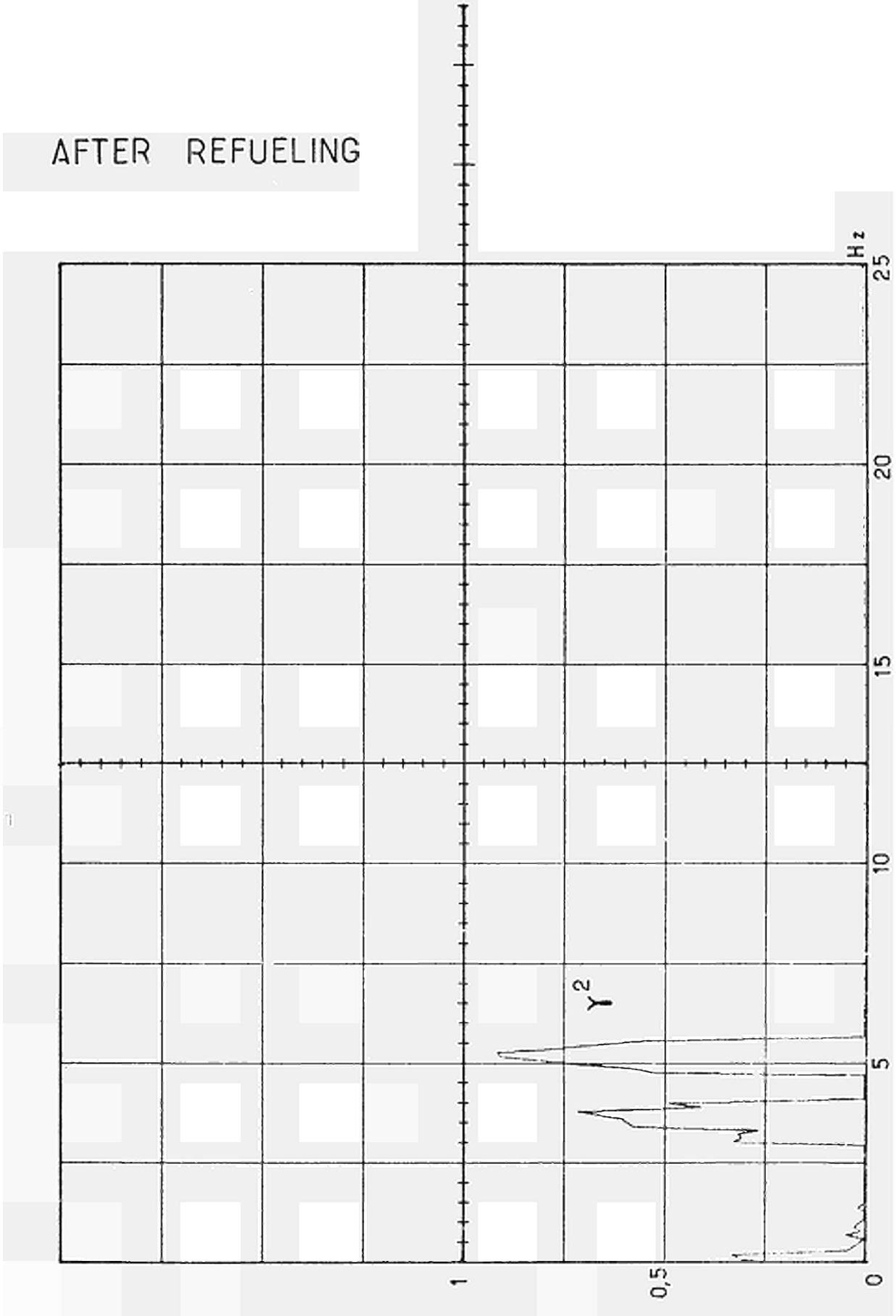

FIG.I.3.3/12a: TEST NO.C1, CHAMBERS LRP 9 and 11

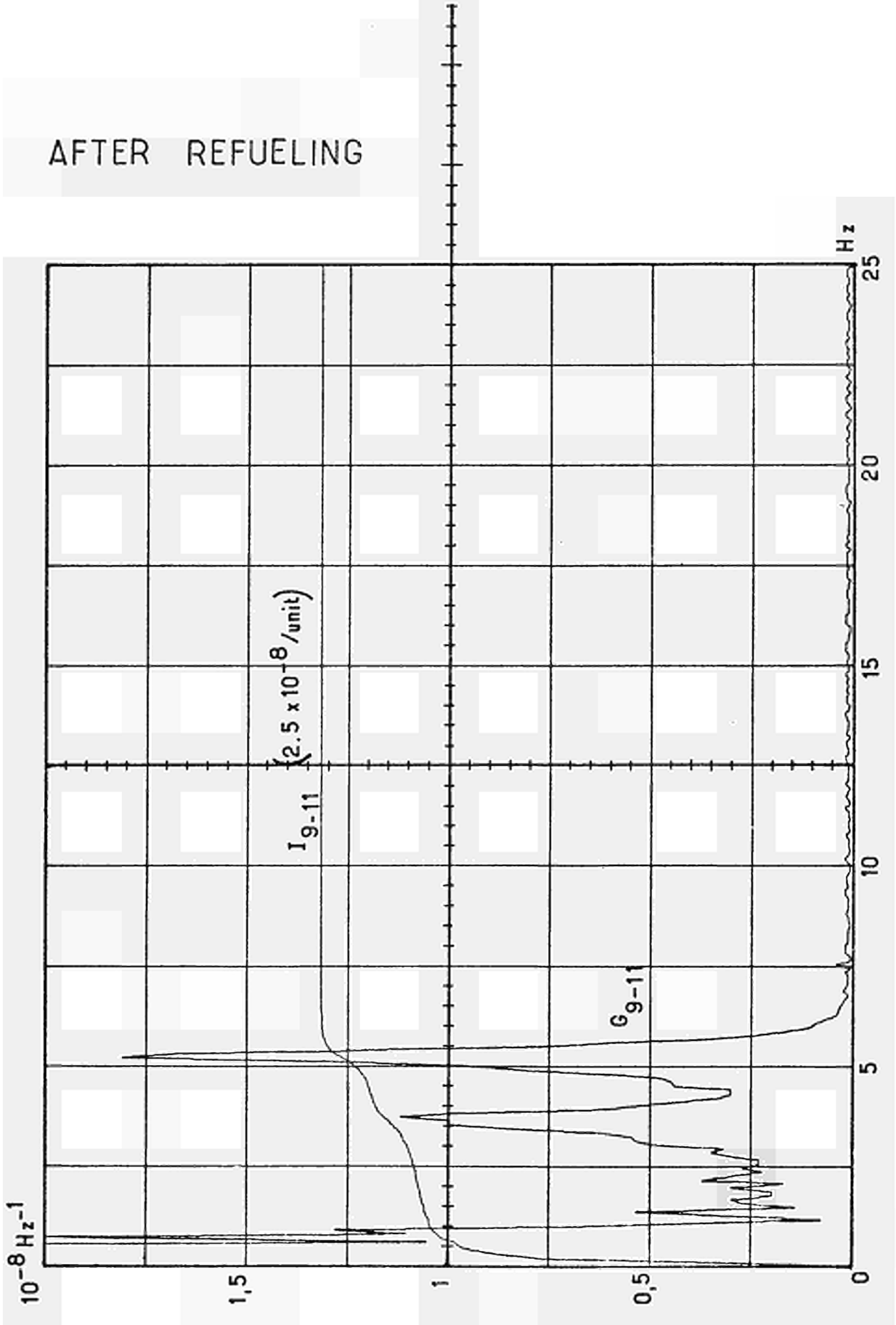

FIG.I.3.3/12b: TEST NO C1, CHAMBERS LRP 9 and 11

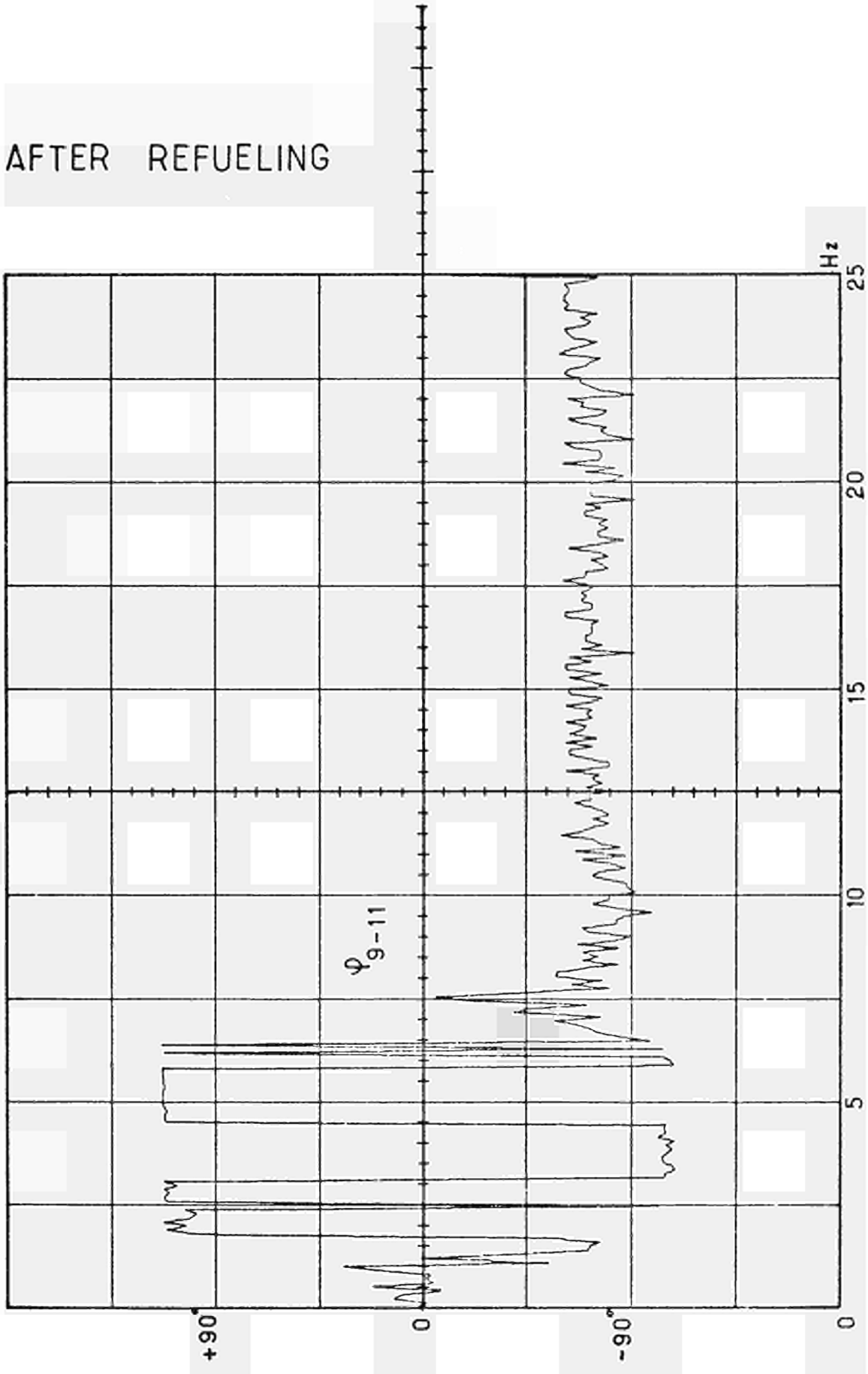

FIG.I.3.3/13: TEST NO.1, CHAMBERS LRP 9 and 11

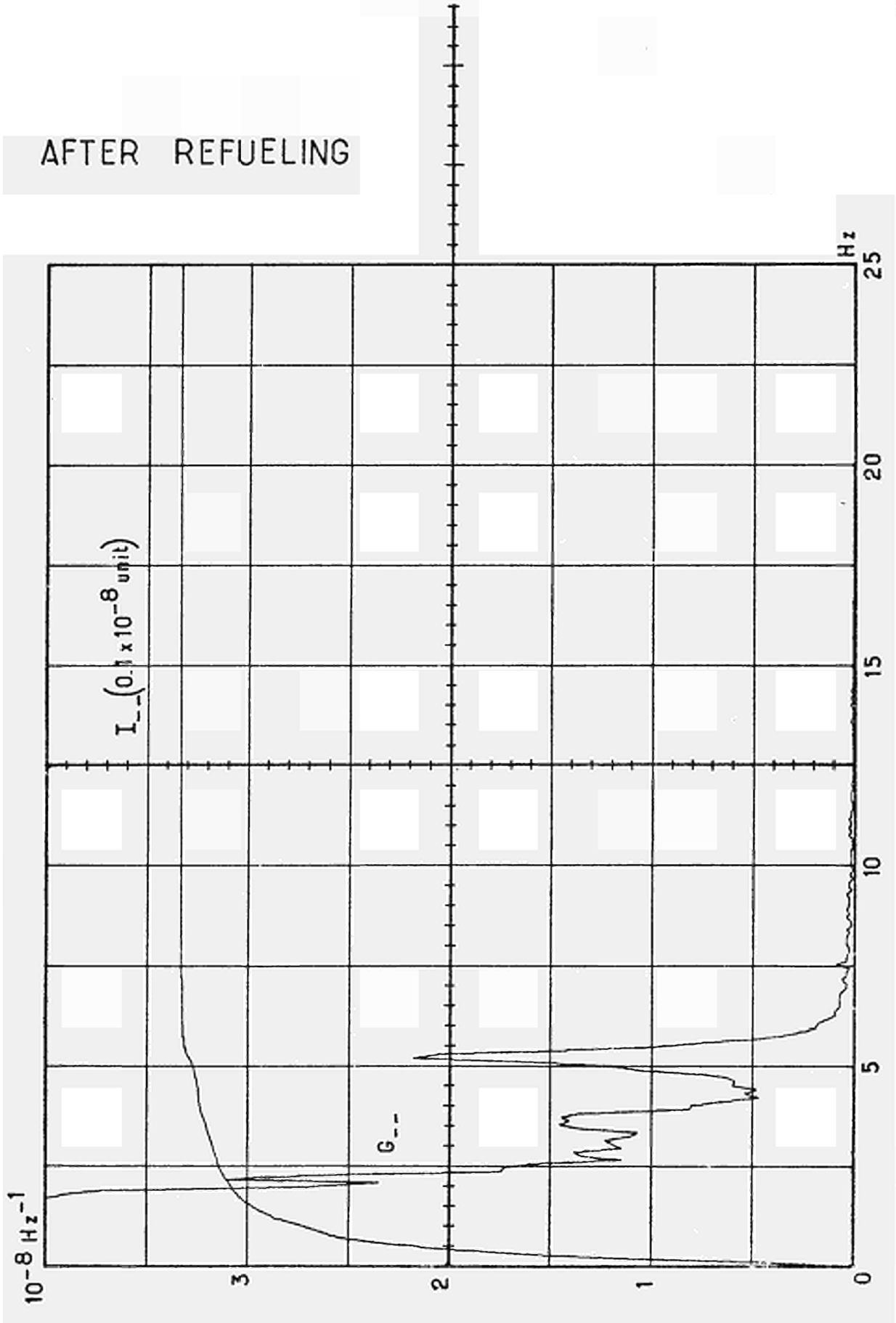

FIG.I.3.3/14: TEST NO. C2, CHAMBERS LRP 7 and 11

AFTER REFUELING

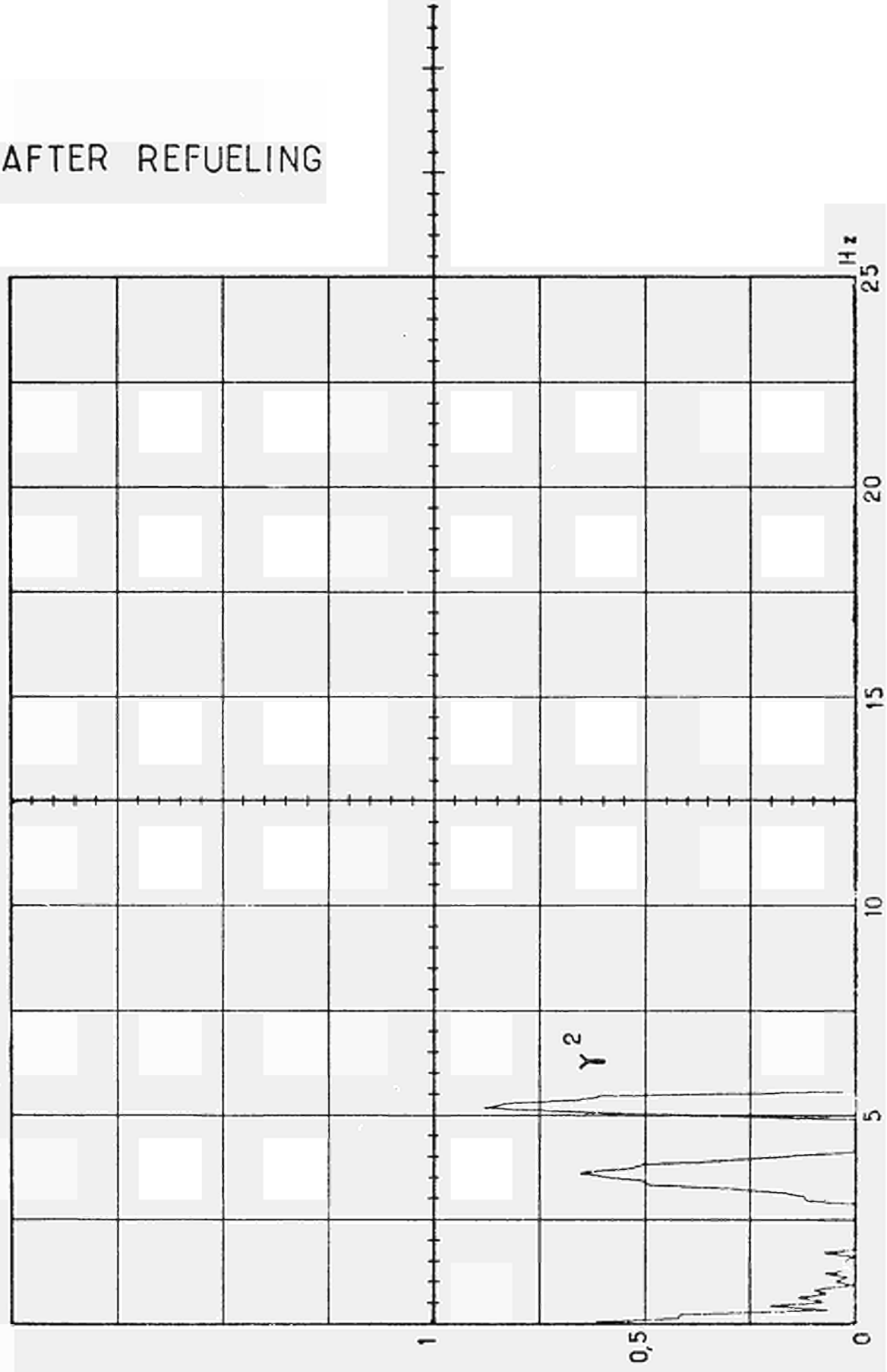

FIG.I.3.3/15: TEST NO.C2, CHAMBERS LRP 7 and 11

AFTER REFUELING

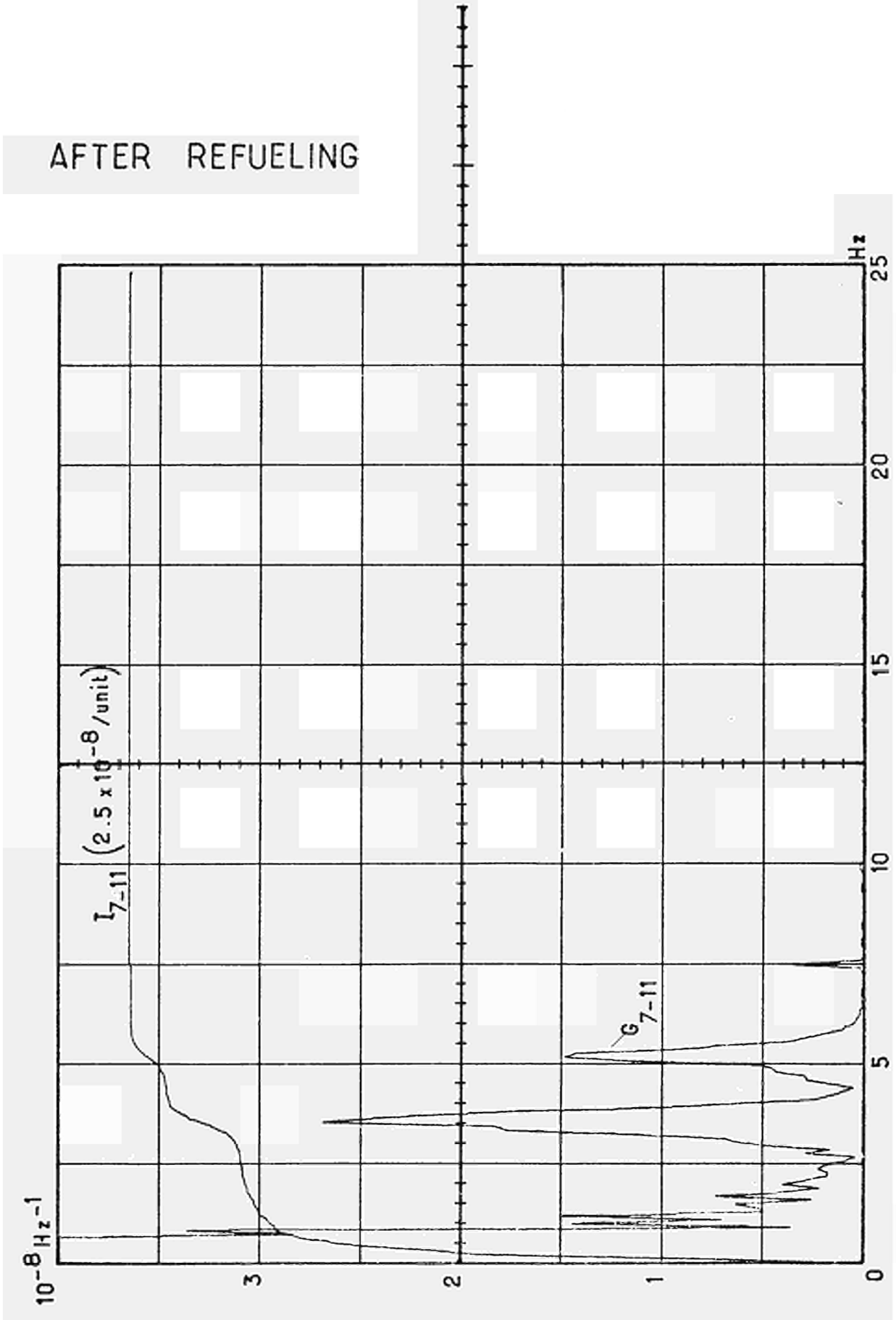

FIG.I.3.3/16: TEST NO. C2, CHAMBERS LRP 7 and 11

AFTER REFUELING

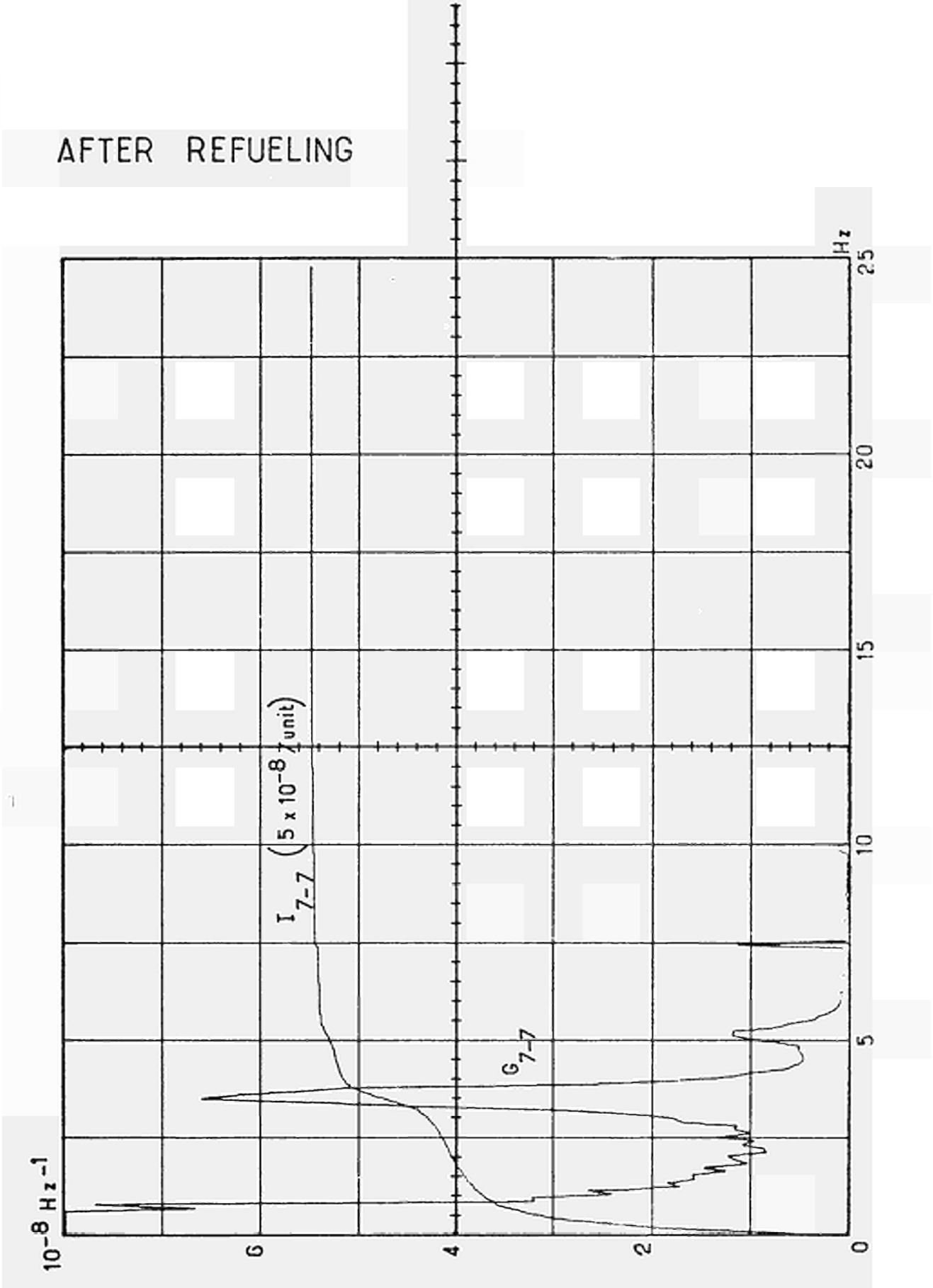

FIG. 2-10

FIG.I.3.3/17:
PENDULAR OSCILLATIONS OF THE CORE AFTER REFUELING

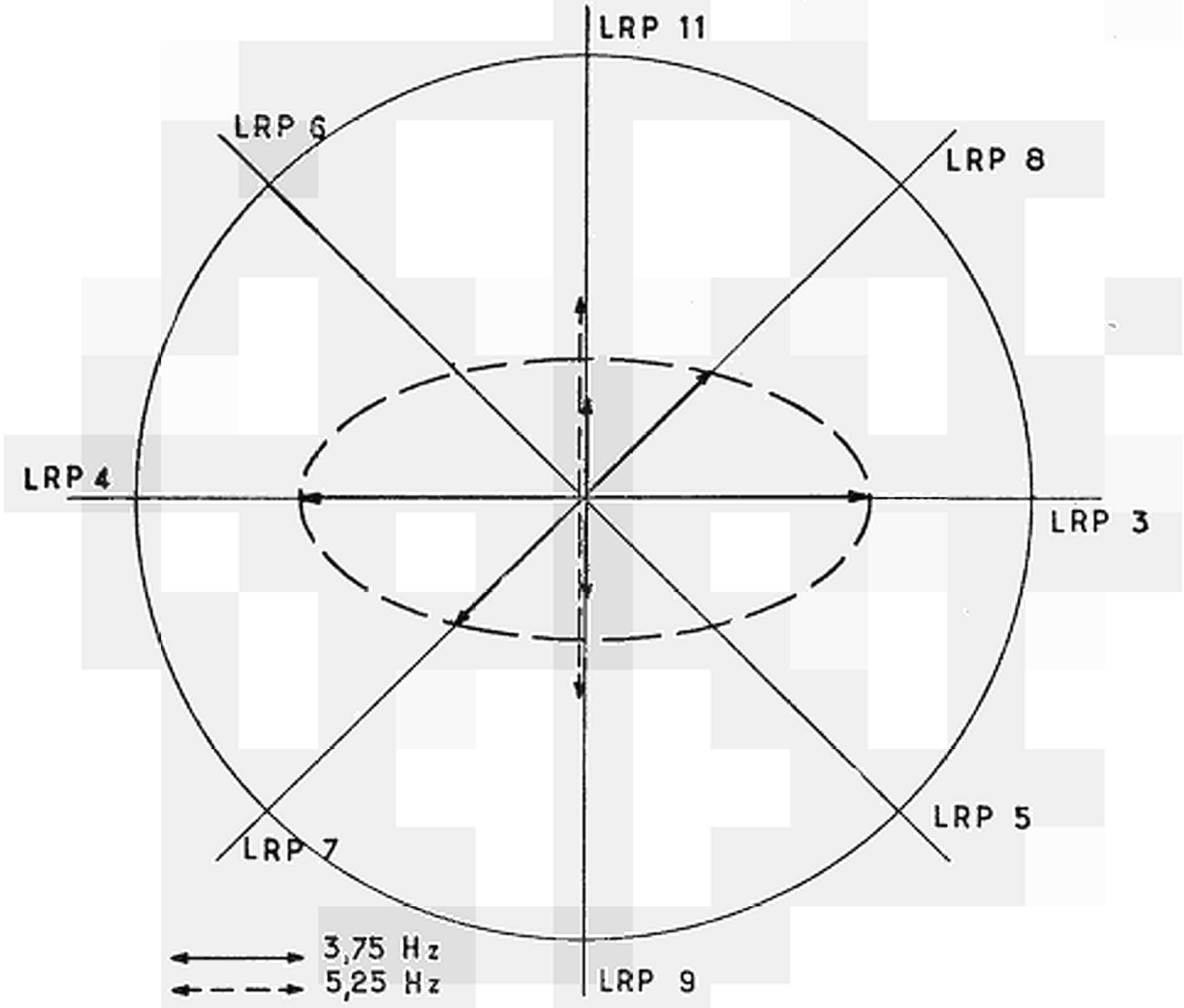

The lengths of the arrows are proportional to the amplitudes of motions

FIG.I.3.3/18: TEST NO. C1, CHAMBERS LRP 3 and 4

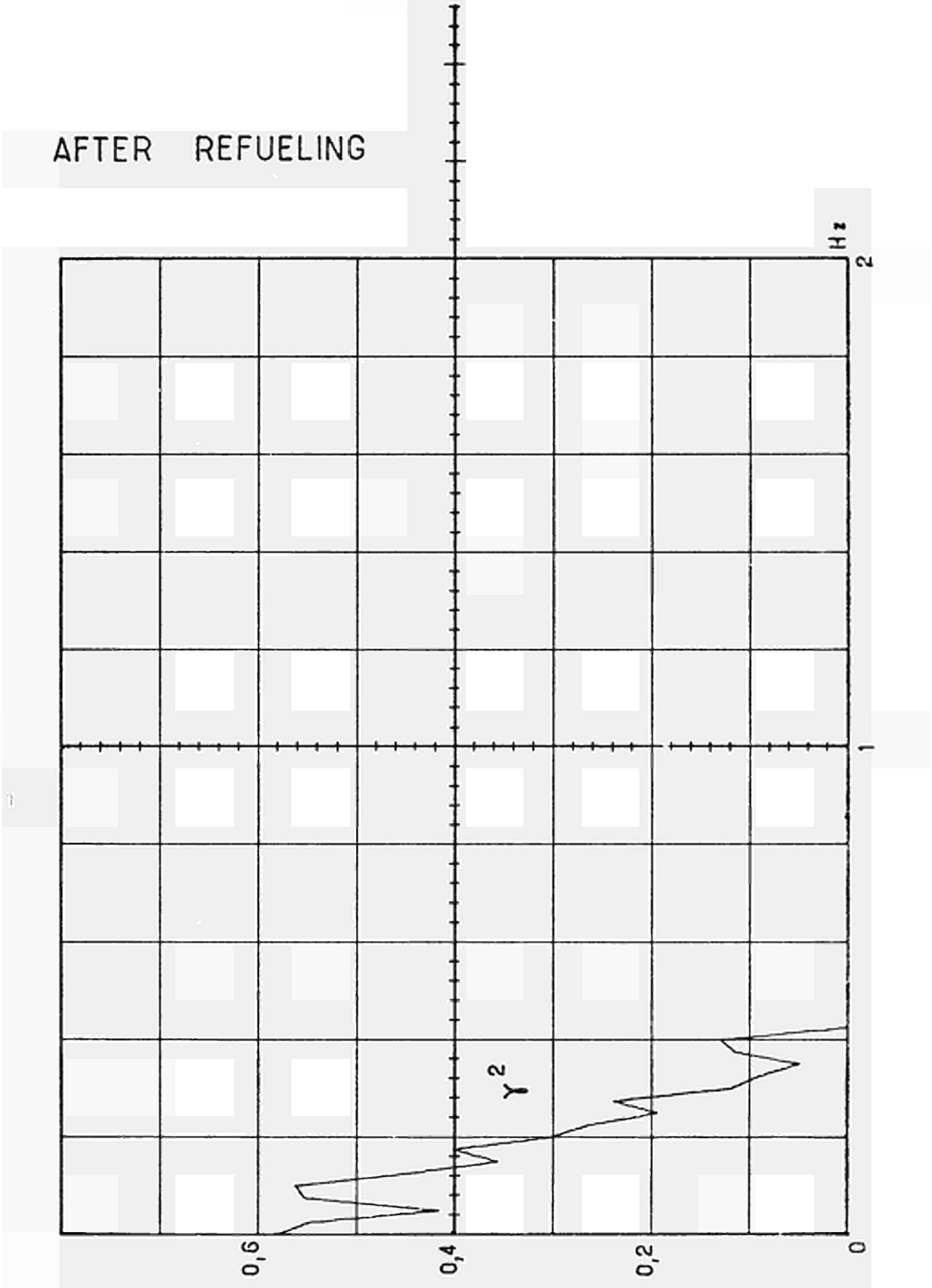

FIG. I.3.3/19 : TEST NO. C1, CHAMBERS LRP 3 and 4

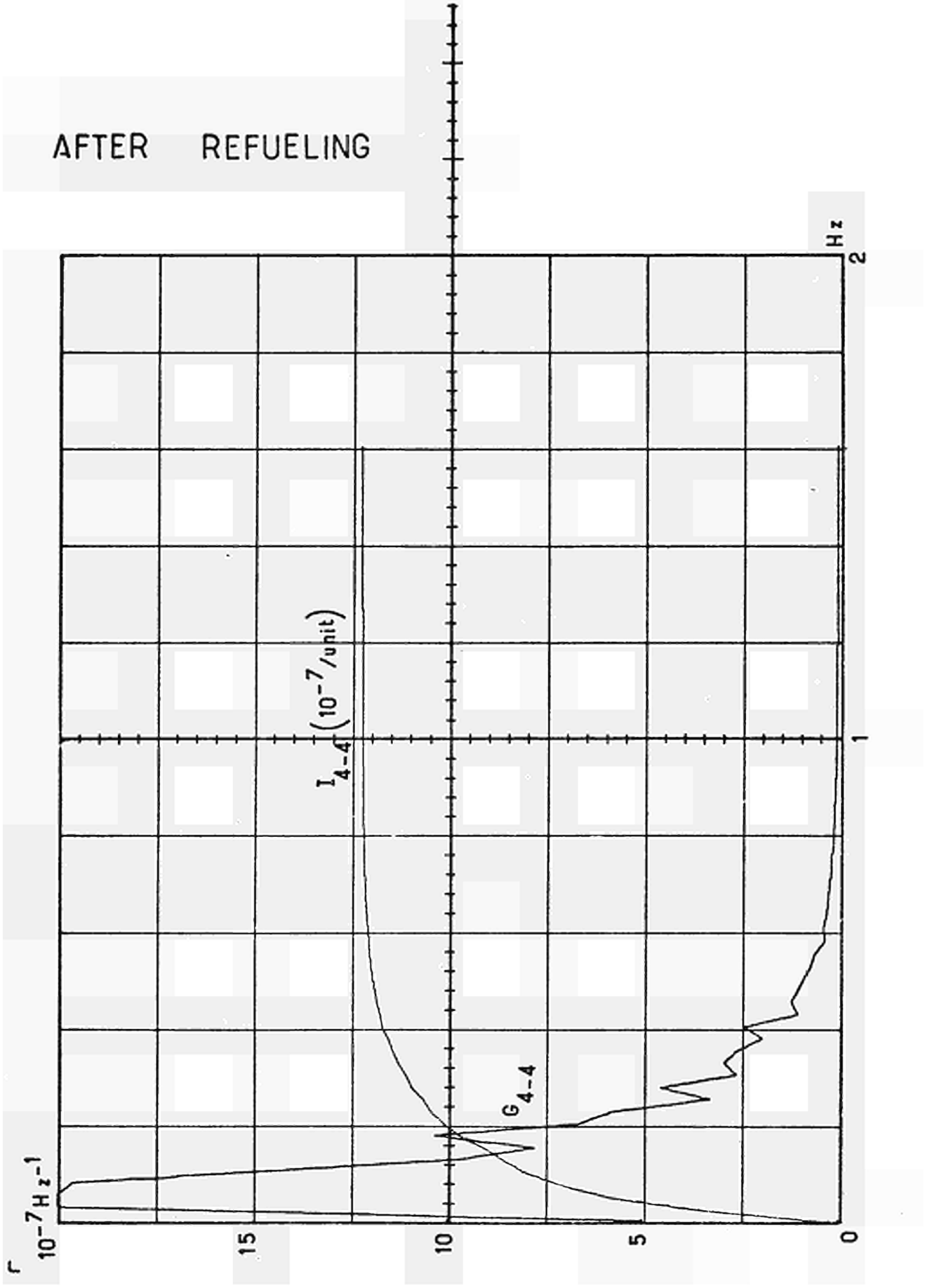

FIG.I.3.3/20a: TEST NO. C1, CHAMBERS LRP 3 and 4

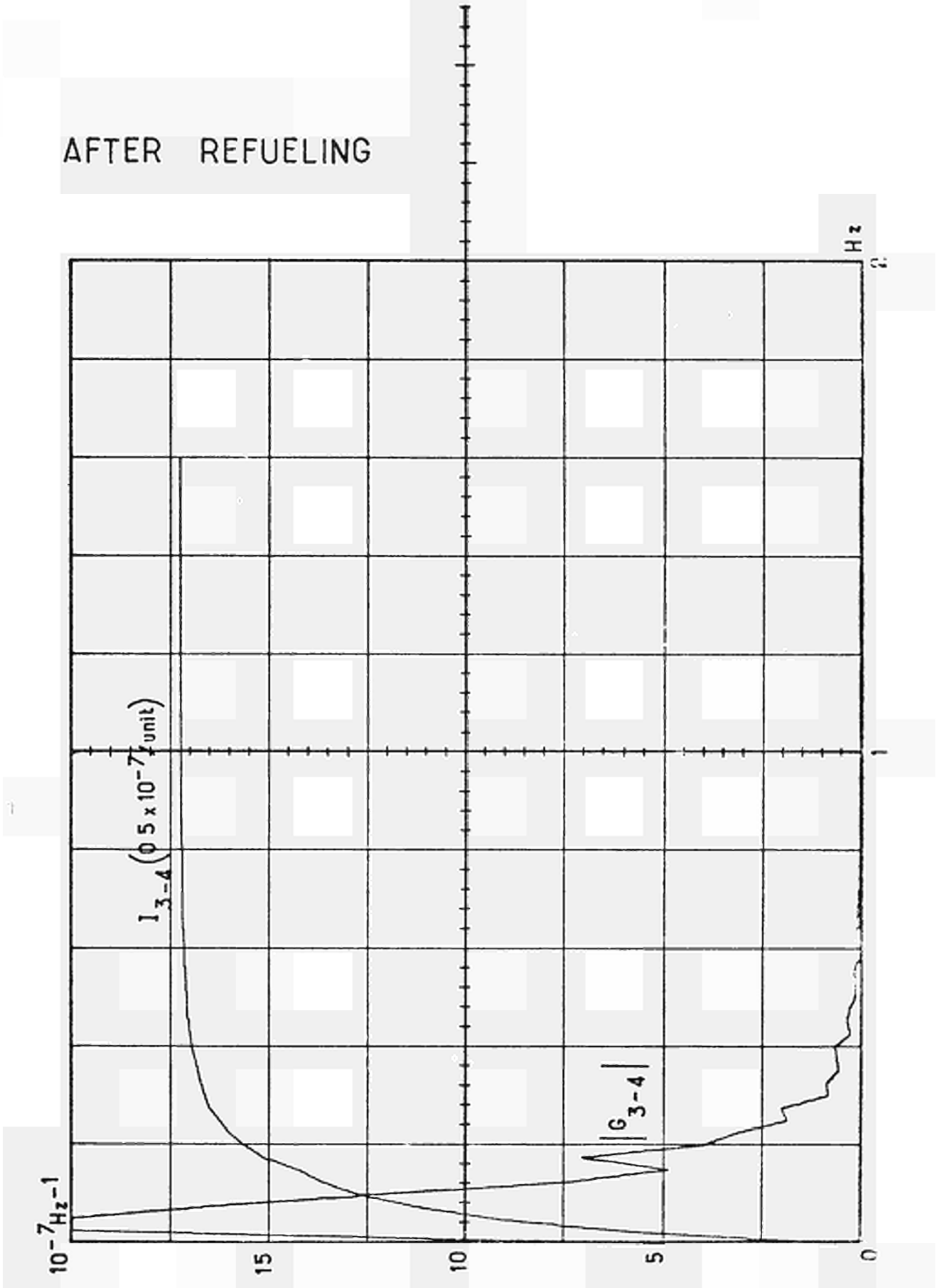

FIG.I.3.3/20b: TEST NO.C1, CHAMBERS LRS 3 and 4

AFTER REFUELING

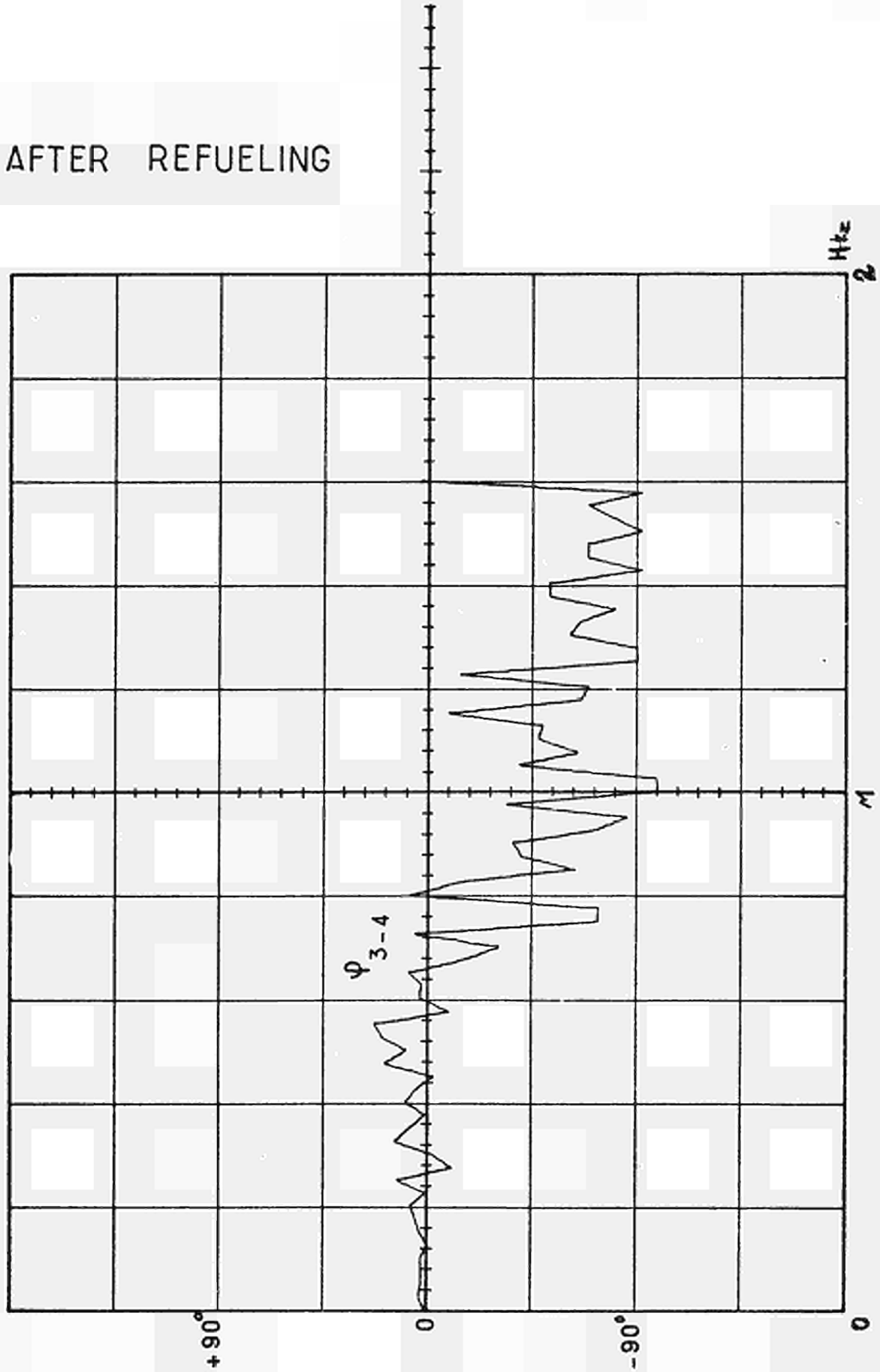

FIG.I.3.3/21: TEST NO. C1, CHAMBERS LRP 9 and 11

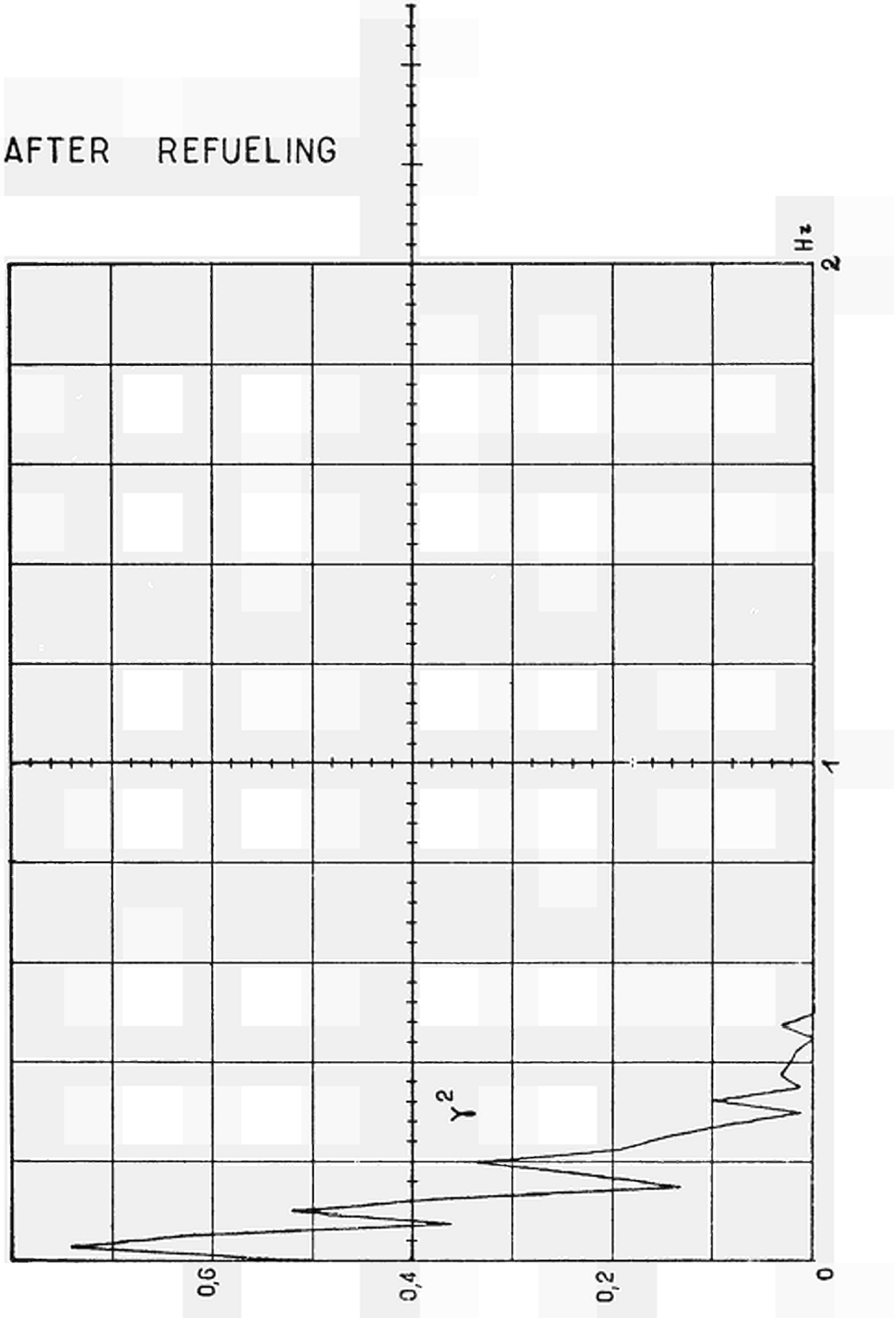

FIG.I.3.3/22a:TEST NO.C1, CHAMBERS LRP 9 and 11

AFTER REFUELING

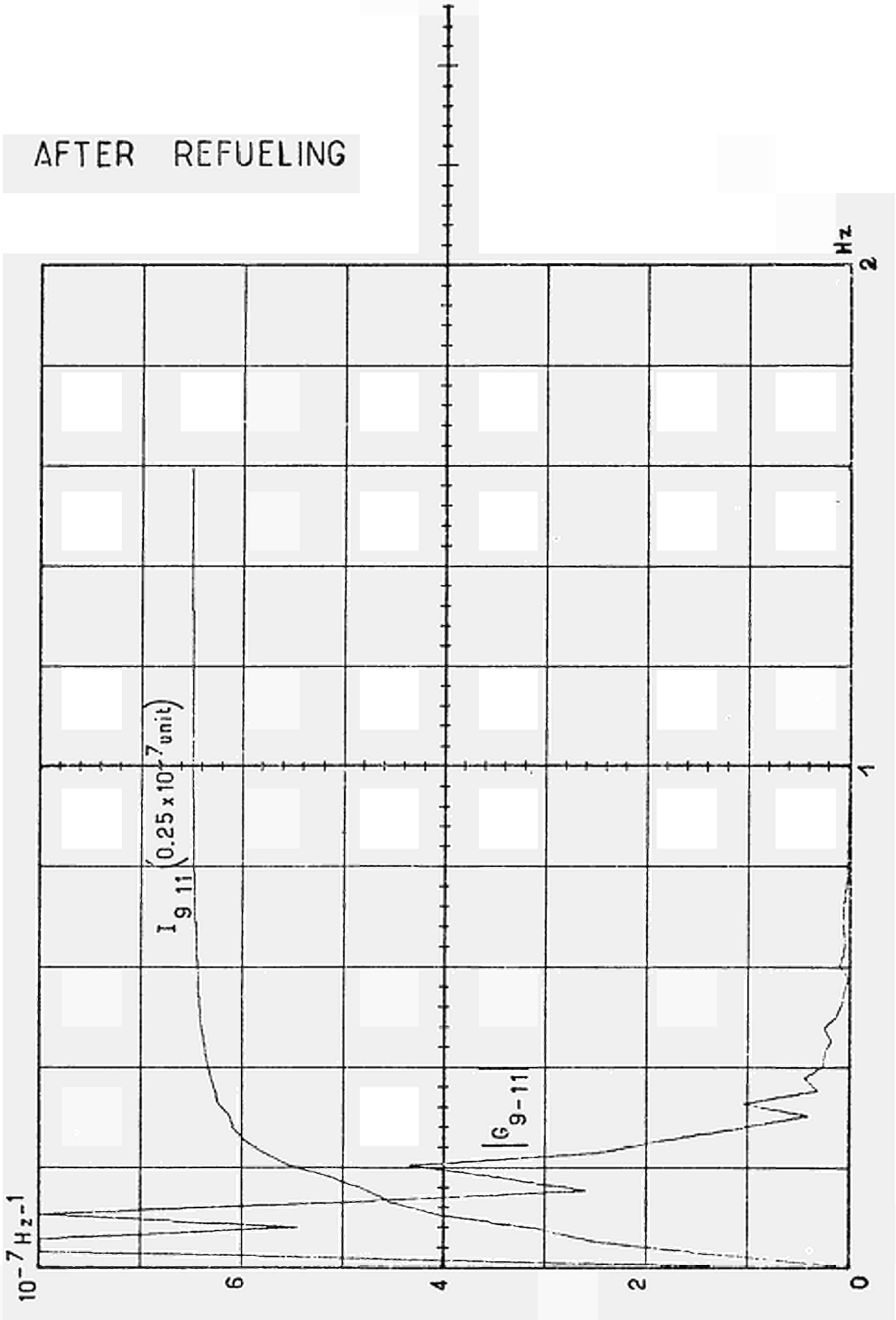

FIG.I.3.3/22b: TEST NO. C1, CHAMBERS LRP 9 and 11

AFTER REFUELING

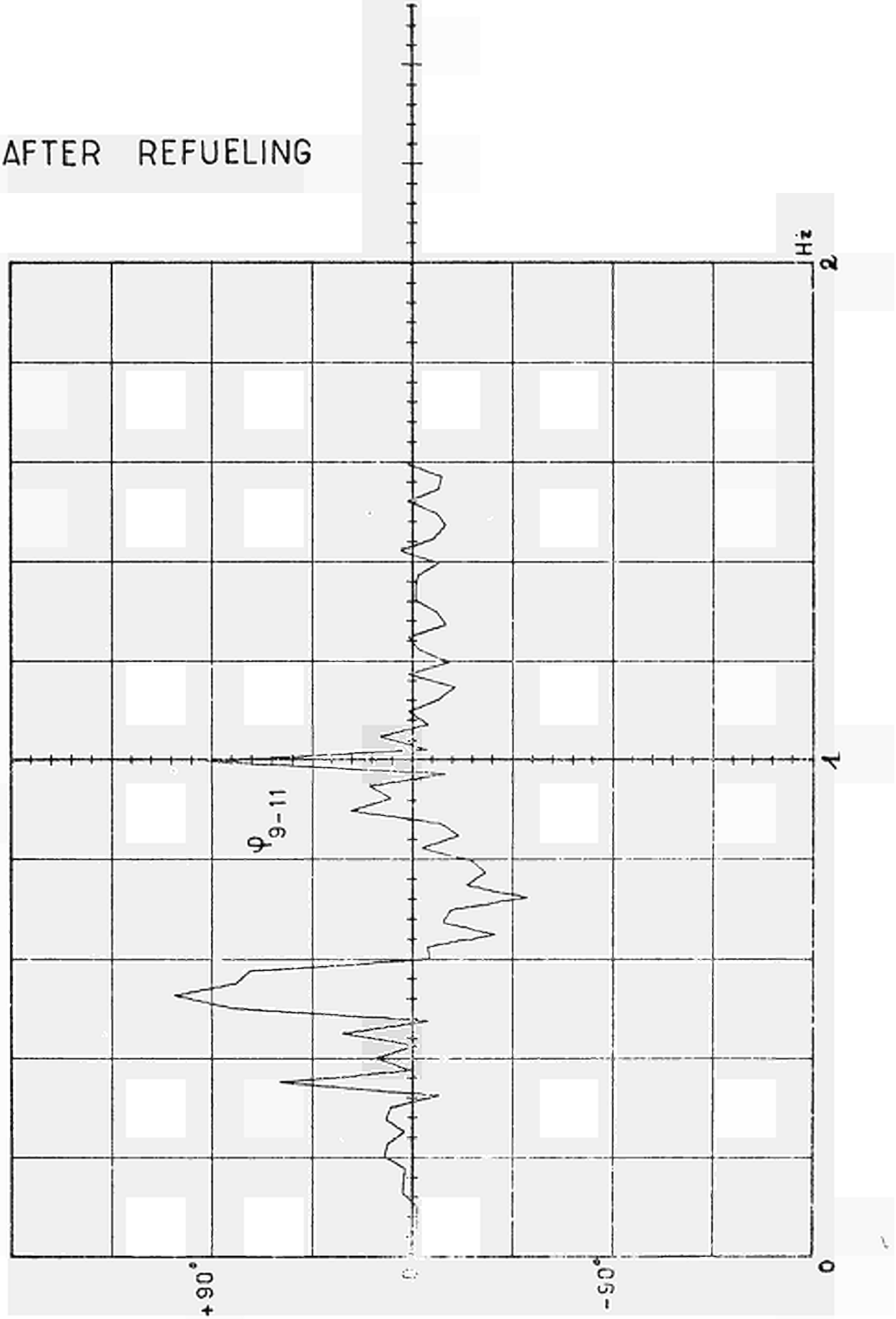

FIG.I.3.3/23: TEST NO. A0, PRESSURE FLUCTUATIONS

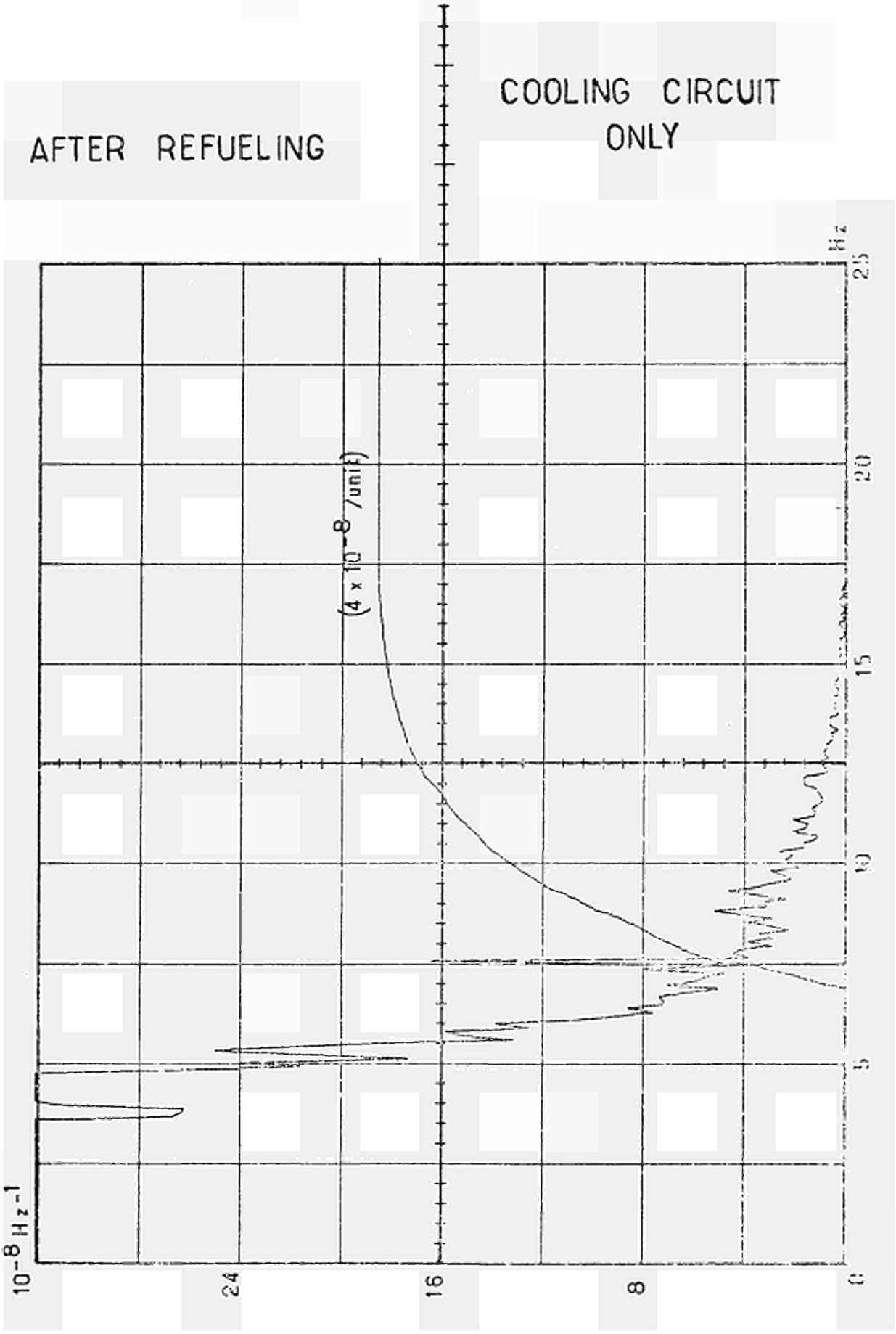

FIG.I.3.3/24 : TEST NO. BO, PRESSURE FLUCTUATIONS

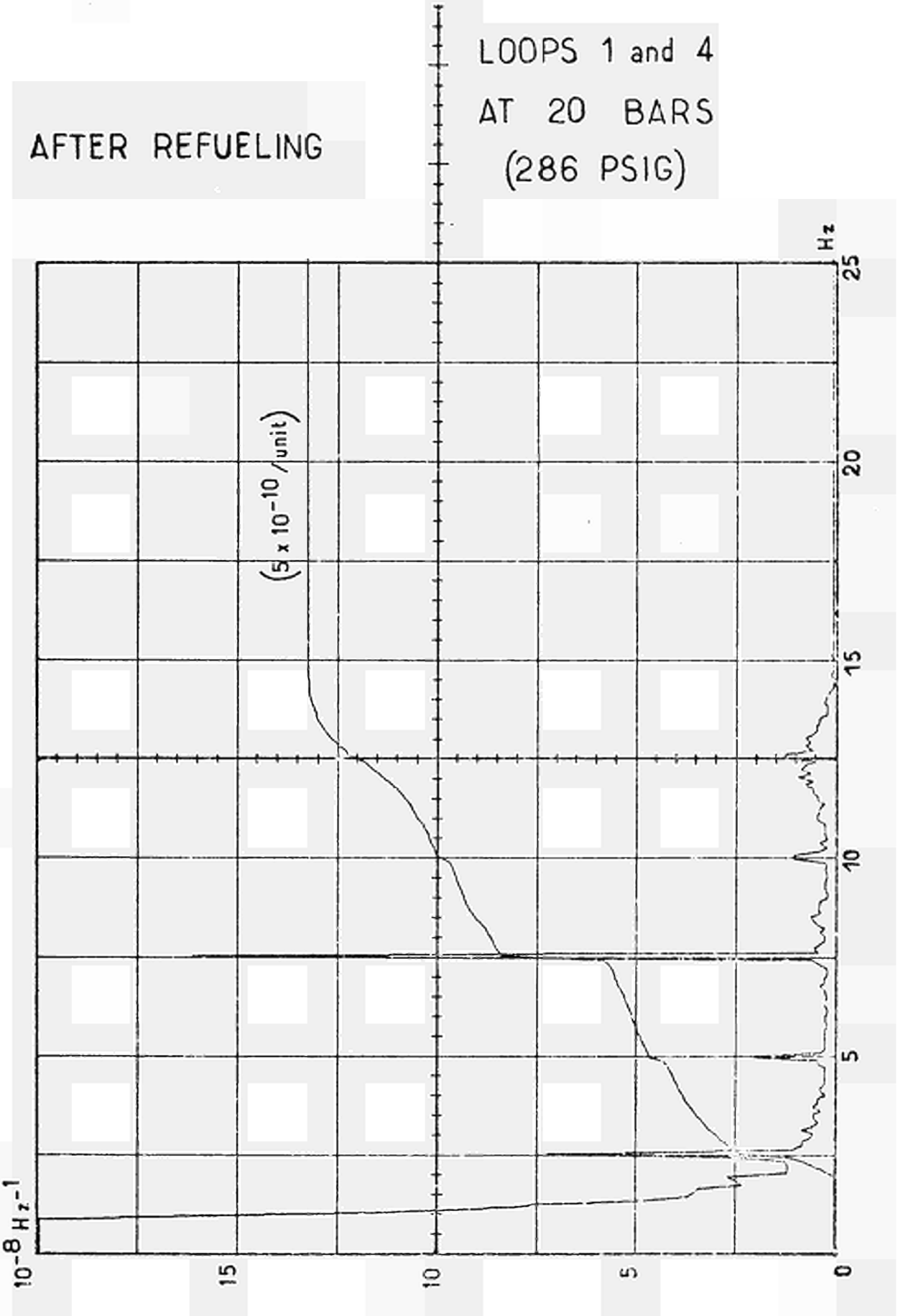

FIG.I.3.3/25: TEST NO. B1 PRESSURE FLUCTUATIONS

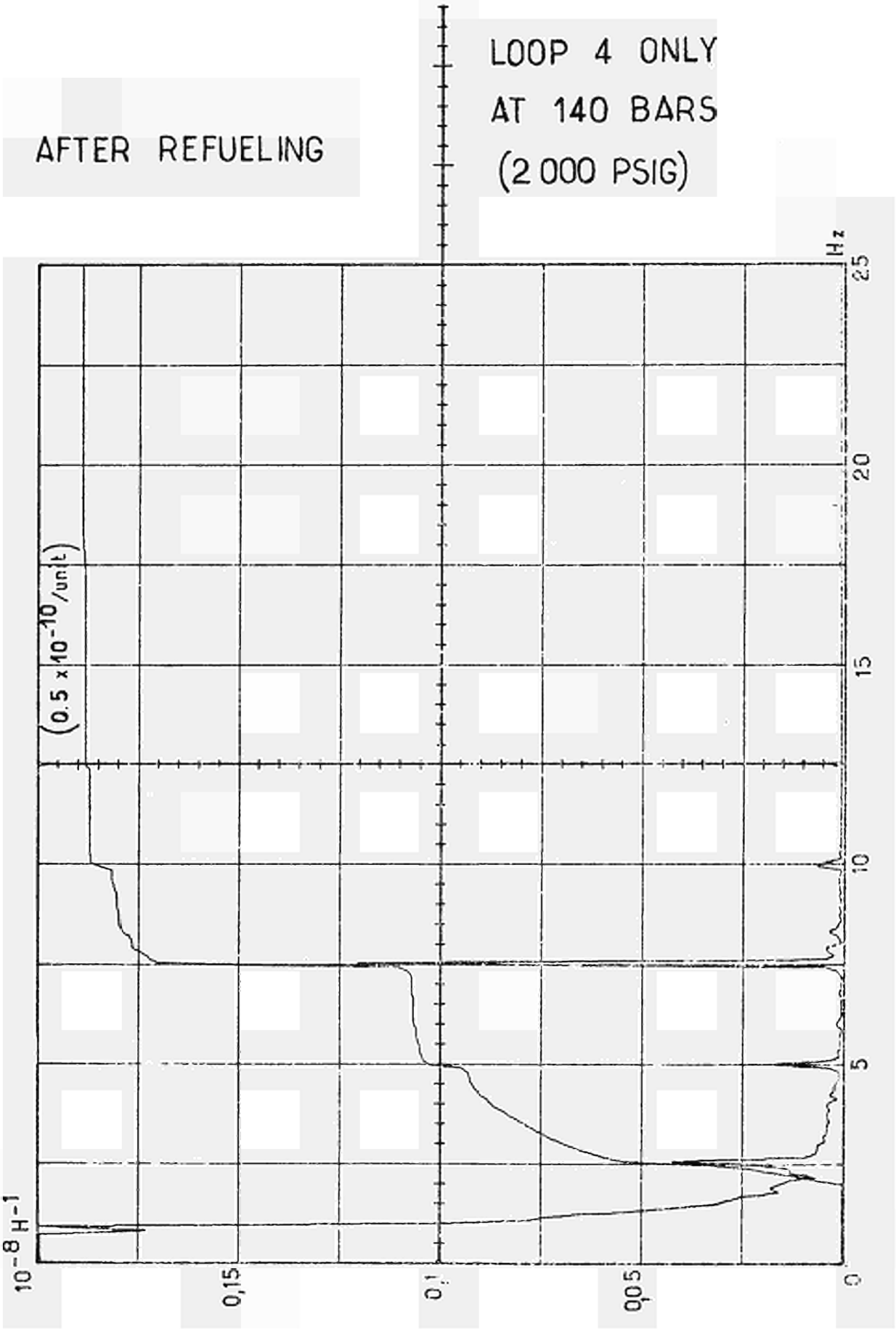

I.3.4 STADE Nuclear Power Plant

I.3.4.1 Measurements

The STADE Nuclear Power Plant (KKS) has a 4 loop configuration and provides an output of 640 MW_{el}.

As indicated in the previous EC-report /1/ successful measurements of the reactor vessel/core barrel pendular behaviour were performed. There it was possible - for the first time - to trace back the vibration of a structure part as represented in a neutron flux signal to the direct measurement of the associated displacement of that part. Thus the final proof was achieved of the adequacy to use ionisation chamber signals for detection of this kind of movement. In this context also the usefulness of displacement measurements outside the vessel was demonstrated, especially when having investigated the spectra during the preop-test phase by means of cross correlation techniques.

The extensive preop-tests demonstrated also the sensitivity and usefulness of pressure signals to measure vibration phenomena. They showed the principle large capability of pressure sensors for the investigation of structure vibrations during normal plant operation. The interpretation of pressure fluctuations during pump switch off tests offered an important possibility to detect vessel internals resonances during plant shut down. It is believed, that this type of measurement will form an important supplement to direct displacement sensors, when performing investigations during a test phase.

In addition the information on pressure fluctuations and vibrations in various positions of the core stimulated the development of theoretical models describing the

dynamic behaviour of the main structure parts. Partly, good agreement could be achieved between the theoretical results and the actual motions and exciting forces as expressed in the measured signals.

Trials were also made to use accelerometers, attached to the pressure vessel wall and the pump housing in several positions, for detection of the various vibration phenomena. This would offer additional measurement information, which is available during plant operation.

I.3.4.2 Analysis

I.3.4.2.1 Reactor Vessel/Core Barrel Pendular Motion Measurements

Fig. I.3.4/1 shows the sensors and their locations. Sensor PO1, PO2 and A12V-A15V can be used also during normal plant operation, the other ones had been dismantled after the preop-tests.

Fig. I.3.4/2 shows the APSD of the displacement sensor R11R measuring the relative distance of the core barrel and the pressure vessel, the peak 13 Hz representing one of the system eigenfrequencies discussed below.

Fig. I.3.4/3 gives the coherence function between two ionisation chambers at opposite positions outside the vessel, fig. I.3.4/4 the phase of the CPSD of these two signals. For the 13 Hz peak we observe that behaviour of the phase, which we would expect for horizontal movements of the core structure (see also /1/). Finally in fig. I.3.4/5 we again detect the resonance peak at 13 Hz showing the good coherence between the neutron flux and the displacement signal. Bearing in mind the peak amplitude of 0.17 mm as measured during the preop-tests with

the sensors R11R/R12R we have a good picture of the sensitivity of neutron flux for measuring this type of structure movement /2/, /3/.

I.3.4.2.2 Investigation of Pressure Signals During Preoperational Tests

When investigating a broad band of frequencies of the pressure signals we observe peaks, which origin from the vibration of other structure parts. In the first instance we have the possibility to search for the sources of the pressure noise by means of investigating the phases of pressure signals measured in various positions (fig. I.3.4/1). Thus we understand better the cause/consequence relations between pressure and motion, because it is very difficult to distinguish, as to what extent the pressure noise signal is created by vibrating parts and as to what extent this signal represents the driving force.

When taking for instance from the cross power density spectra of the various pressure signals the phase shifts as represented in the 75 Hz peak indicated in fig. I.3.4/6 we get a phase diagram as shown in fig. I.3.4/7. (The 75 Hz peak is originating from the recirculation pump.) The distances which can be calculated from this phase diagram based on the sound velocity in water are in rather good agreement with the real average distances of the associated sensors. It is easy to recognize how the pressure waves originating from the pump are distributing in the two directions and are exciting the vibrations of the lower support plate.

The phase shift of the broader peak at 58 Hz originating from random effects is shown in fig. I.3.4/8. In this

case we observe a pressure fluctuation which is created by the reactor vessel itself. There is no doubt that this peak represents a super-position of random exciting forces with the feedback of the vibrating structure on the pressure. This interpretation is especially prooved by the pump-switch-off-tests. In fig. I.3.4/9 we have the momentary pictures of the APSD of PO1 and of the vertical velocity GO4V. It is to be seen very clearly that corresponding to the lowering of the pump speed the peak at 58 Hz is developing in the pressure- and the velocity-signal as well. This behaviour originates from the effect that the falling frequency of the exciting force is arriving at 58 Hz, the resonance frequency of a structure part /4/.

I.3.4.2.3 Calculation of the Pendular Oscillation of the Reactor Vessel/Core Barrel System

The computer code EIGEN described in I.4.2 was used to calculate the double pendulum system as represented by the reactor vessel and the core barrel clamped to the vessel flange by means of the lid or the lid screws respectively. The pressure signal PO4 (fig. I.3.4/1) as measured during the preoperational tests without the core package, was considered to reflect the driving force (input signal) and the oscillation (output signal) as well. From the shape of the pressure spectrum (fig. I.3.4/10) the driving force was assumed to be a band limited white noise as given in fig. I.3.4/11. Based on this assumption the spectrum of the system pendular motion was calculated by means of a double pendulum model. Though other well expressed resonances can be found, a fairly good agreement could be obtained between the calculated spectrum and the measured pressure and movement spectra (the latter one

representing the relative movement between reactor vessel and core barrel). Further details are given in /5/.

I.3.4.2.4 Identification of the Vibrations Performed by the Reactor Vessel/Core Barrel

An attempt was made to investigate the reactor vessel/ core barrel vibrations by means of identification theory. The process model consisted of a double pendulum connected via spring and damping elements. The reactor vessel bearings and its connection to the coolant pipes were verified by additional springs and dampings. In addition to the three dimensional pendular movement also vertical vibration of the vessel and the core barrel was permitted. Based upon the assumption that the vibration of the system is mainly due to hydrodynamic processes of the coolant flow in the vessel, the exciting forces were formulated as linear combinations of the pressure fluctuations and their derivations, as measured at the vessel input and output, and at the lower support grid. The observation model was set up taking into account, that two signals describing the movement of the system and one pressure signal were available. The initial values were estimated by the least square method. For the identification the maximum likelihood- and the maximum a posteriori invariant imbedding algorithm were considered (see also I.4.3).

Though we have already developed the digital codes for this algorithms, their application posed several problems, which are not yet solved. First of all the frequency behaviour of the various instrumentation channels have to be considered, and the correct choice of the sample periods has to be checked. The first results already showed that one would need additional (repeating) measurements.

The investigation of the observability and controllability criteria were rather extensive for the model which was established. Therefore it is necessary to make basic considerations especially with respect to the number and the adequate choice of measurement signals. In order to gain better a priori information it is necessary to get further information by the constructor with respect to the unknown parameters.

Considering the identification algorithm it has to be said, that the standard Kalman-filter has an optimal character only when knowing exactly the mean inital values and co-variances. Hence in practice it would be possible to verify only sub-optimal algorithms. Further problems are the correlation of the noise sources and the non-linearity of the process model when modelling unknown parameters. This problem could be at least theoretically solved by using modified algorithms and by an other choice of optimal filters (extended Kalman-filter, filter of higher order).

For the treatment of identification problems with complicated algorithms and large model dimensions (> 10) very quickly the limit is reached with respect to the computation time and memory space. As a consequence it is necessary to keep the order of the model as low as possible by using the empirical know-how (measurements) of the system. Further on problems of computation accuracy are arising rather quickly, but as a rule they can be handled by applying adequate program techniques.

In order to better overcome the difficulties discussed above it seems to be necessary to start with a much simpler identification problem. Afterwards it should be possible to extent the investigation to a system of the described size.

I.3.4.2.5 Investigation of Accelerometer Signals

Several accelerometers are installed at the pressure vessels, which are resistant to X-rays and to temperatures up to 400°C. 3 transmitters are fixed at the outer wall of the lower range of the pressure vessel and they are shifted 90° to each other around the circumference. Another two transmitters are fixed at the supposing base in the range of the inlet and outlet connection. Each of the recirculating pumps are also equipped with an accelerometer (figs. I.3.4/12, I.3.4/13, I.3.4/14). The whole noise spectrum of solid-borne sound can be divided into three parts /6/:

In the lower frequency range of about 1 cps up to 50 cps one can recognize vibrations of the components and the core barrel. Characteristic peaks of this range are 5 cps, 8 cps, 20 cps, 25 cps and about 37 cps. It is interesting to see that the 20 cps-signal is fluctuating in a wide range (figs. I.3.4/15, I.3.4/16, I.3.4/17). The 25 cps-peak is very sharp and has a constant amplitude. It corresponds to the rotating frequency of the main pumps (1500 rpm). The signal of 37 cps is sometimes shifting to 36 cps. This can result from vibrations of components in the pressure vessel (figs. I.3.4/16 and I.3.4/17).

Middle frequency range: The vibrations in the frequency range of 100 cps up to 2000 cps are concerned with the rotations of the pumps. These peaks can be ordered into a frequency raster with a distance of 75 cps. This raster of 75 cps is a function of the rotation frequency (25 cps) and of the number of the rotating blades (3) of the pumps. The dominant peaks of this range are 300, 525 and 600 cps (fig. I.3.4/18).

Upper frequency range: In this part bursts of rattling noise are dominant. The level and the frequency of these bursts are concerned with the number of the operating pumps. The reason could be the swinging and the butting of the control rod guide tubes within the reactor vessel head or loose particles inside the vessel.

Literature, Section I.3.4

/1/ On-load Surveillance of Nuclear Power Plant Components by Noise and Vibration Analysis
Status Report on work performed for the Commission of the European Communities under Euratom Study Contract No. 043-71-10 ECIC (F), April 1972

/2/ Bastl, W., Dio, W.H., Haas, W., Wach, D.
Nachweis von Pendelbewegungen des Kernbehälters im Neutronenflußrauschen
Atomwirtschaft 5, Mai 1972, S. 263 u. 264

/3/ Bastl, W.
Fortschritte in der Rauschanalyse zur betriebsmäßigen Überwachung von Druckwasserreaktoren
Reaktortagung, Karlsruhe, April 1973

/4/ Bauernfeind, V., Dio, W.H., Pink, W.
Importance and Use of In-core Vibration and Pressure Measurements to Determine Correct Behaviour of Pressure Vessel Internals
IAEA Symposium Nuclear Power Plant Control and Instrumentation, Prague, January 1973

/5/ Österle, B., Kim, J.D.
Experimental and Theoretical Investigations of Flow-Induced Vibrations in Nuclear Components of PWR
International Symposium Vibration Problems in Industry
Keswick, April 1973

/6/ Moravek, I., Raible, B.
Körperschallmessung - ein Weg zur Betriebsüberwachung von Reaktordruckgefäßen
7. Technisches Allianz-Kolloquium, München, Dez. 1973

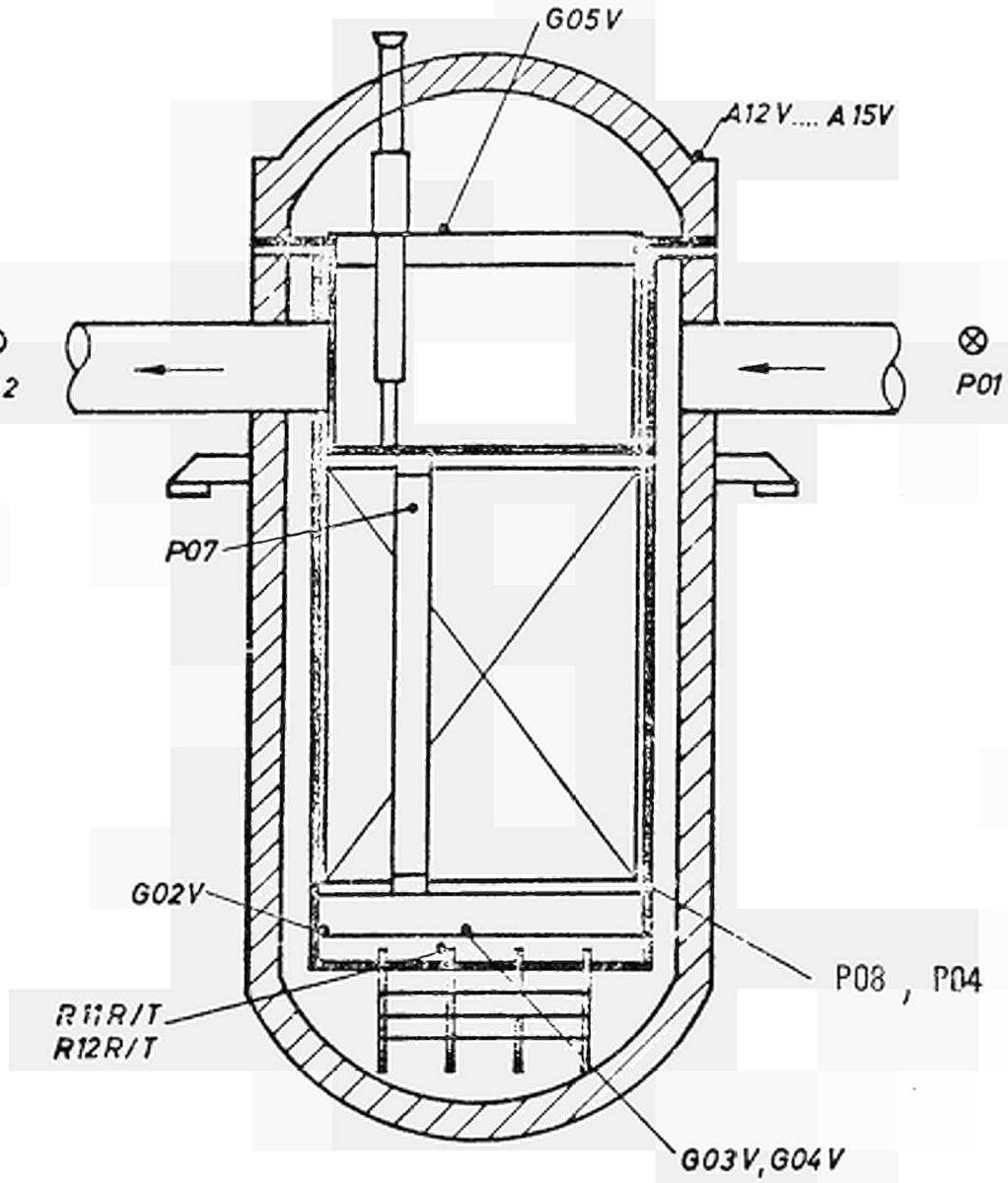

P01...P08	Pressure transducers
G02V..G05V	Vibration velocity sensors of core support structures
A12V...A15V	Absolute displacement sensors pressure vessel
R11R/T, R12R/T	Relative displacement sensors pressure vessel/core barrel

Fig.I.3.4/1: STADE Nuclear Power Plant – position of sensors

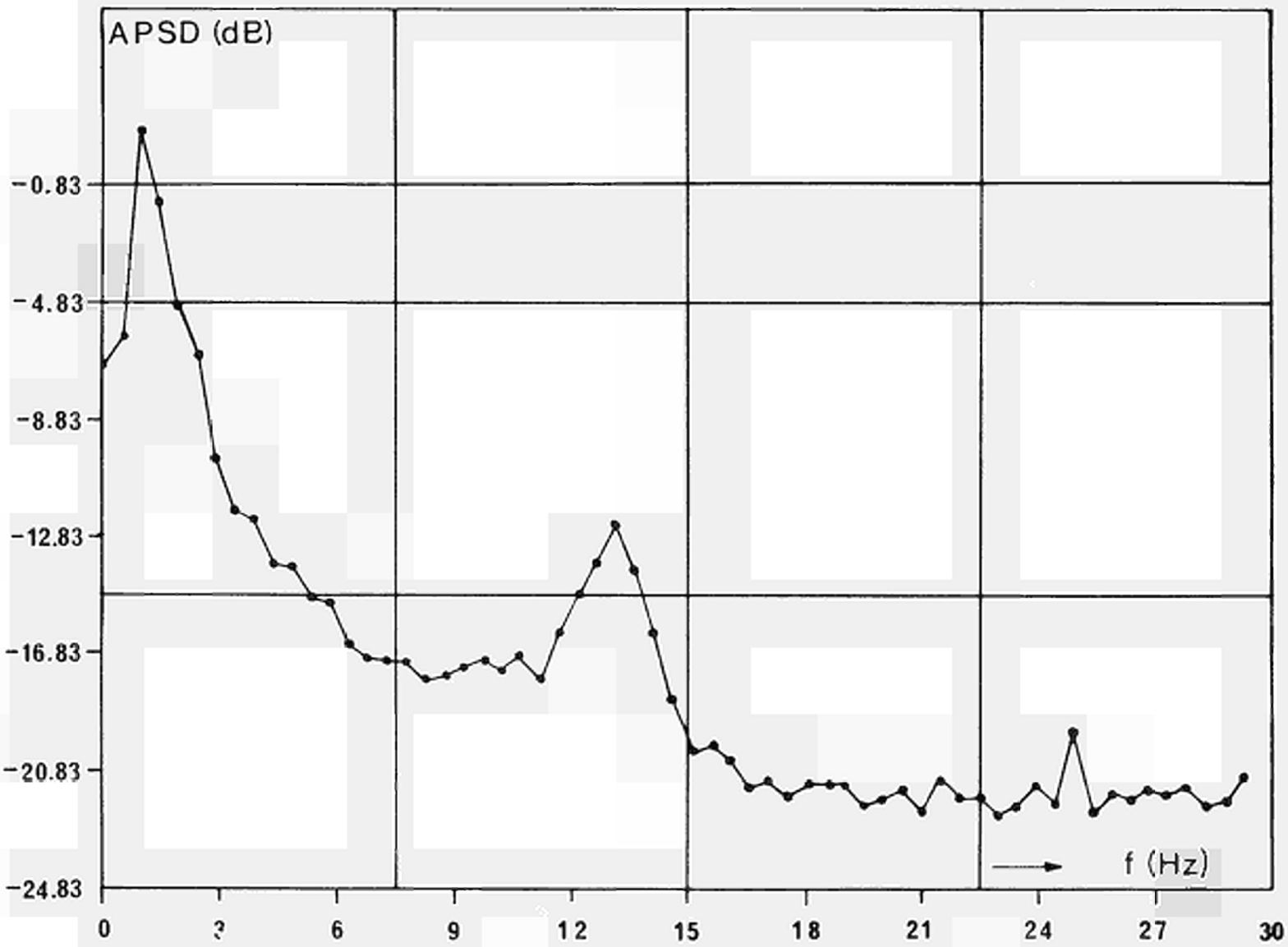

Fig.I.3. 4/2: APSD of sensor R11R as measured during the preop tests (with core) at 260°C and 150 at.

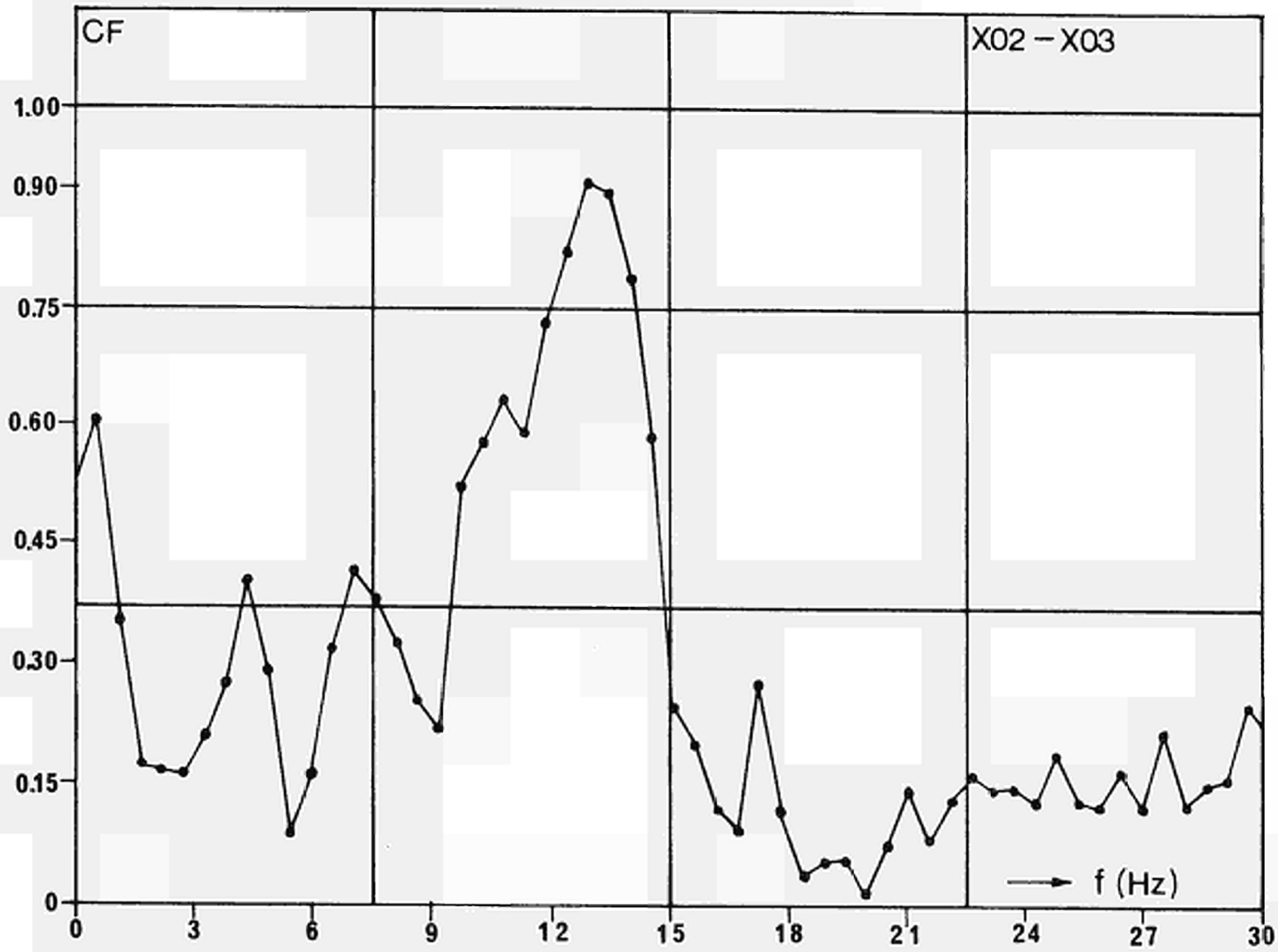

FigI.3.4/3: Coherence function of the signals of 2 opposite ionisation chambers

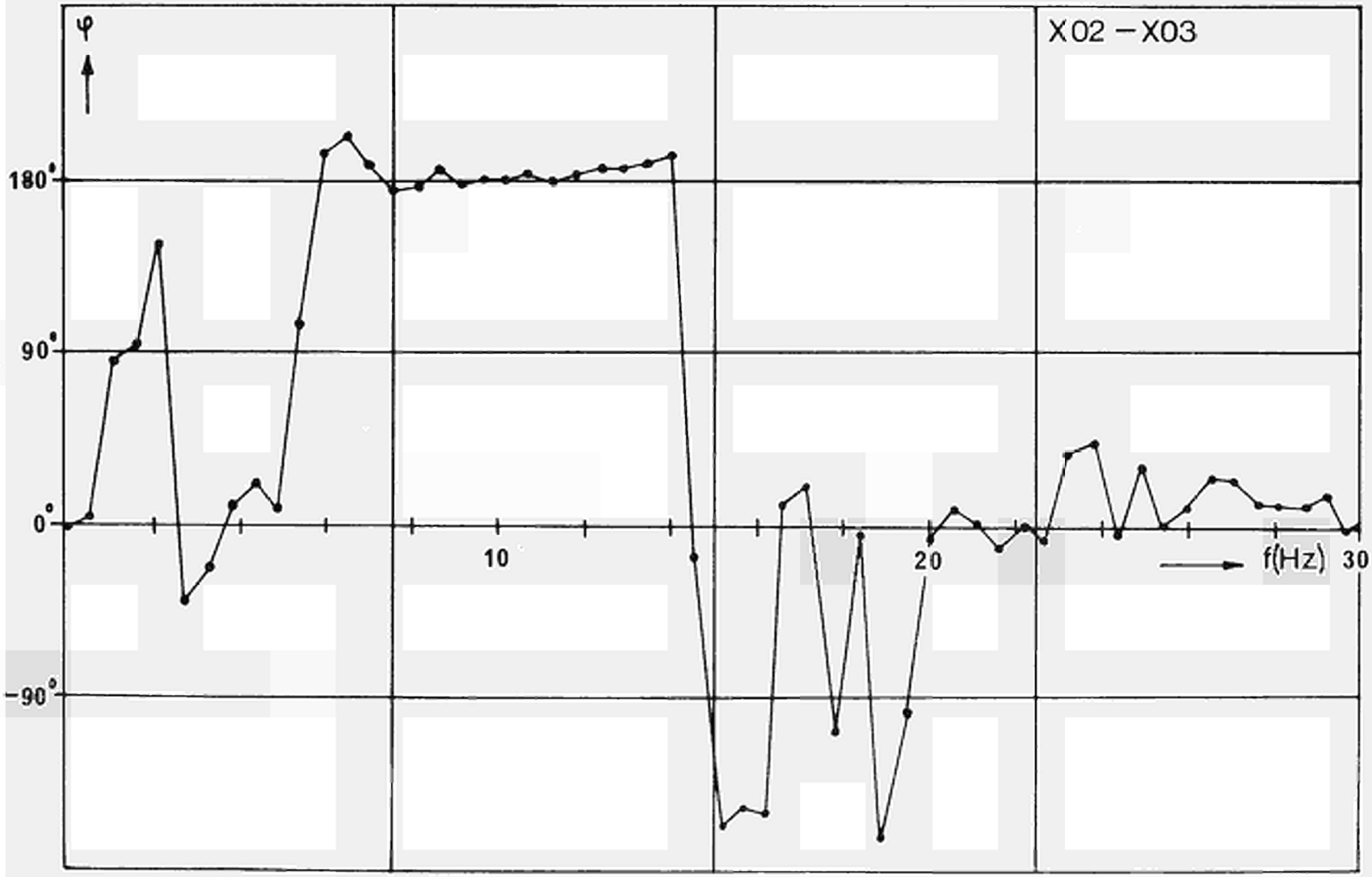

Fig.I.3.4/4: Coherence function (phase) of the signals of 2 opposite ionisation chambers

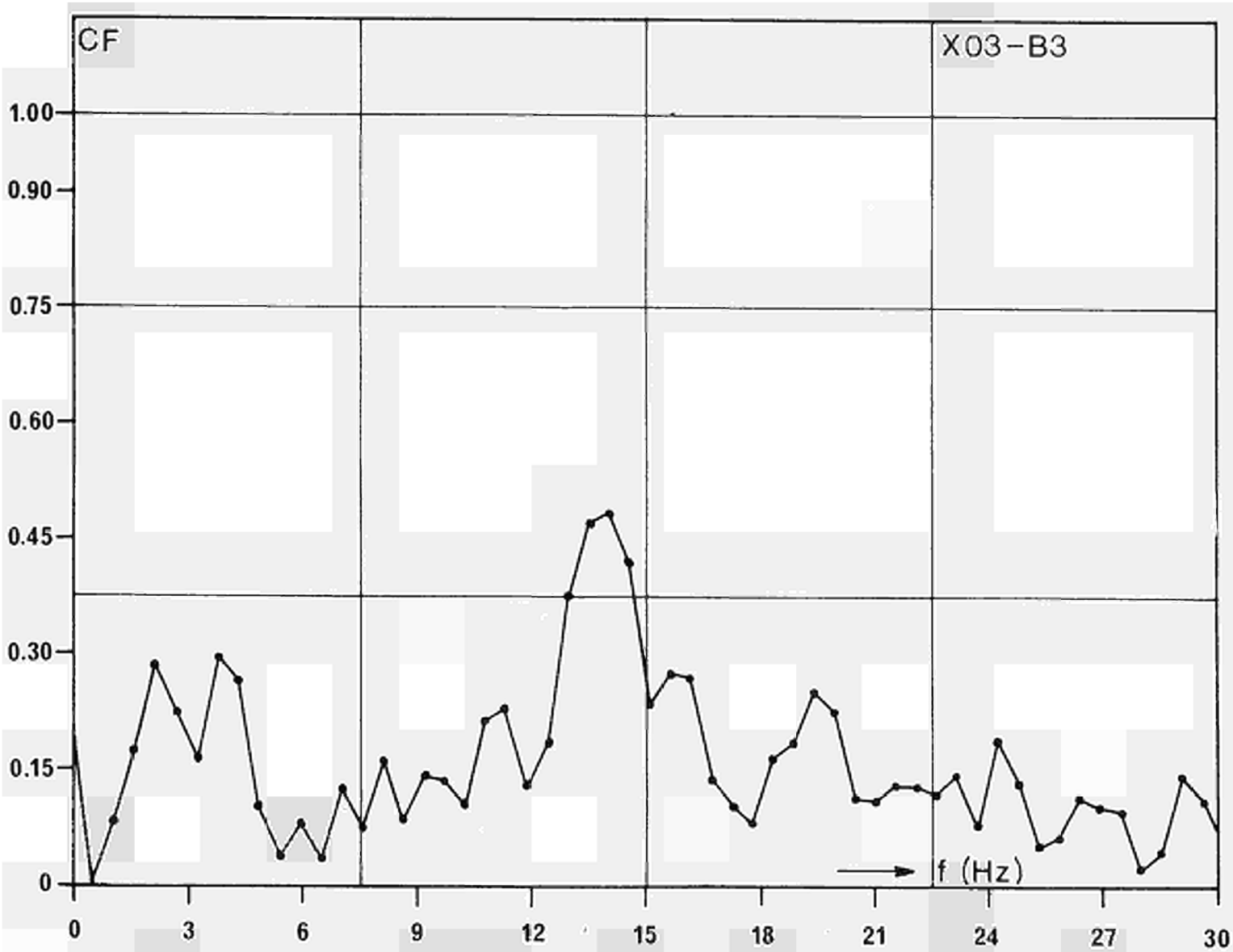

Fig. I.3.4/5 : Coherence function between neutron flux and lid screw movement

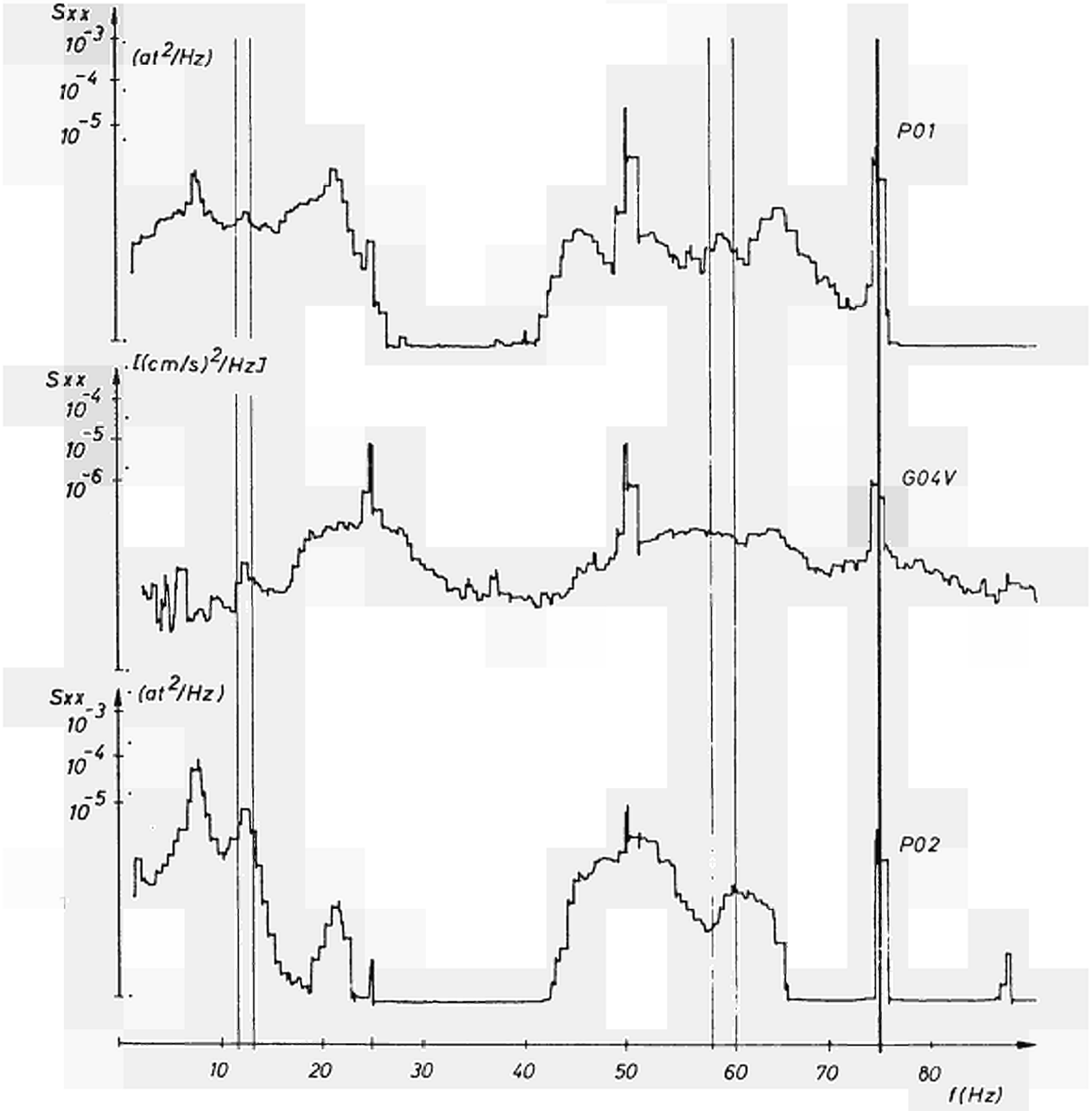

Fig.I.3.4/6: APSDs of pressure signals P01, P02 and of velocity signal G04V as measured during preop tests (with core)

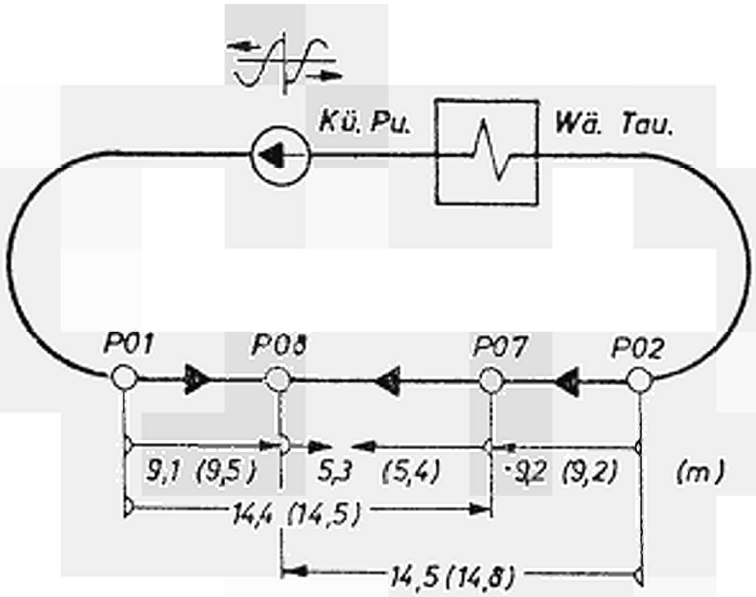

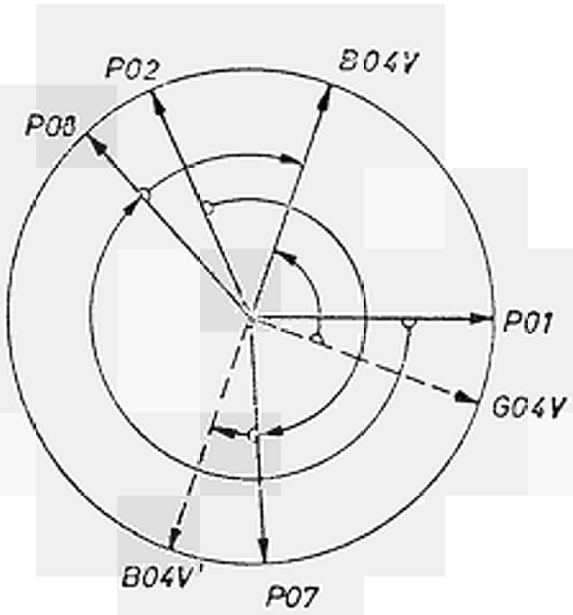

Phase shifts of the pressure signals and their calculation as the distances between the sensors.

Figures in parenthesis mean real sensor distances

P01 P08	9.1 m
P08 B04V	3,3 m
	12,4 m
P01B04V	11,9 m

Fig.I.3.4/7: Propagation of pressure fluctuation at 75 Hz as taken from the results given in Fig.6

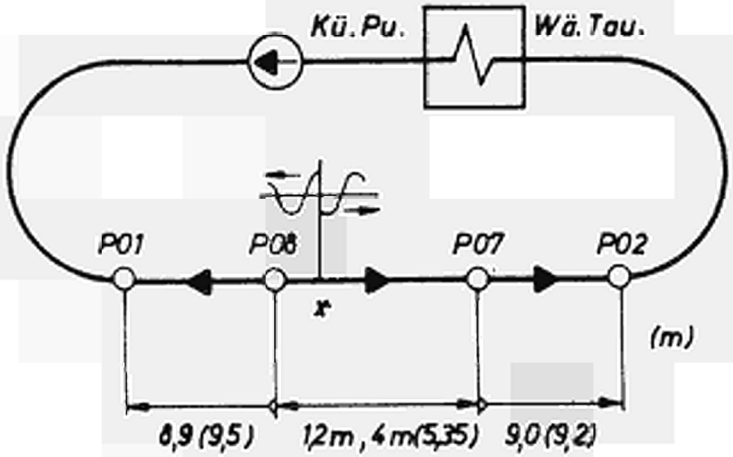

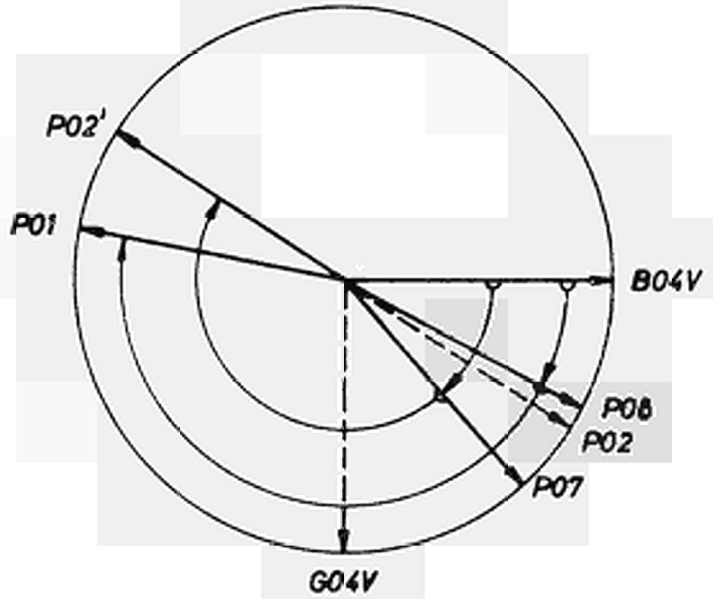

P08 P07 = (5,35m)

P08 x = $\frac{5,35}{2} \pm 1,2 =$ 4 m / 1,6 m

phase = 0°

P08 B40V = 1,4 m

} B04V ≙ x

Phase shifts of the signals and their calculation as the distances bet the sensors.

Figures in parenthesis mean real sensor distances

Fig. I.3.4/8 : Propagation of pressure fluctuations at 58 Hz as taken from the result given in Fig.6

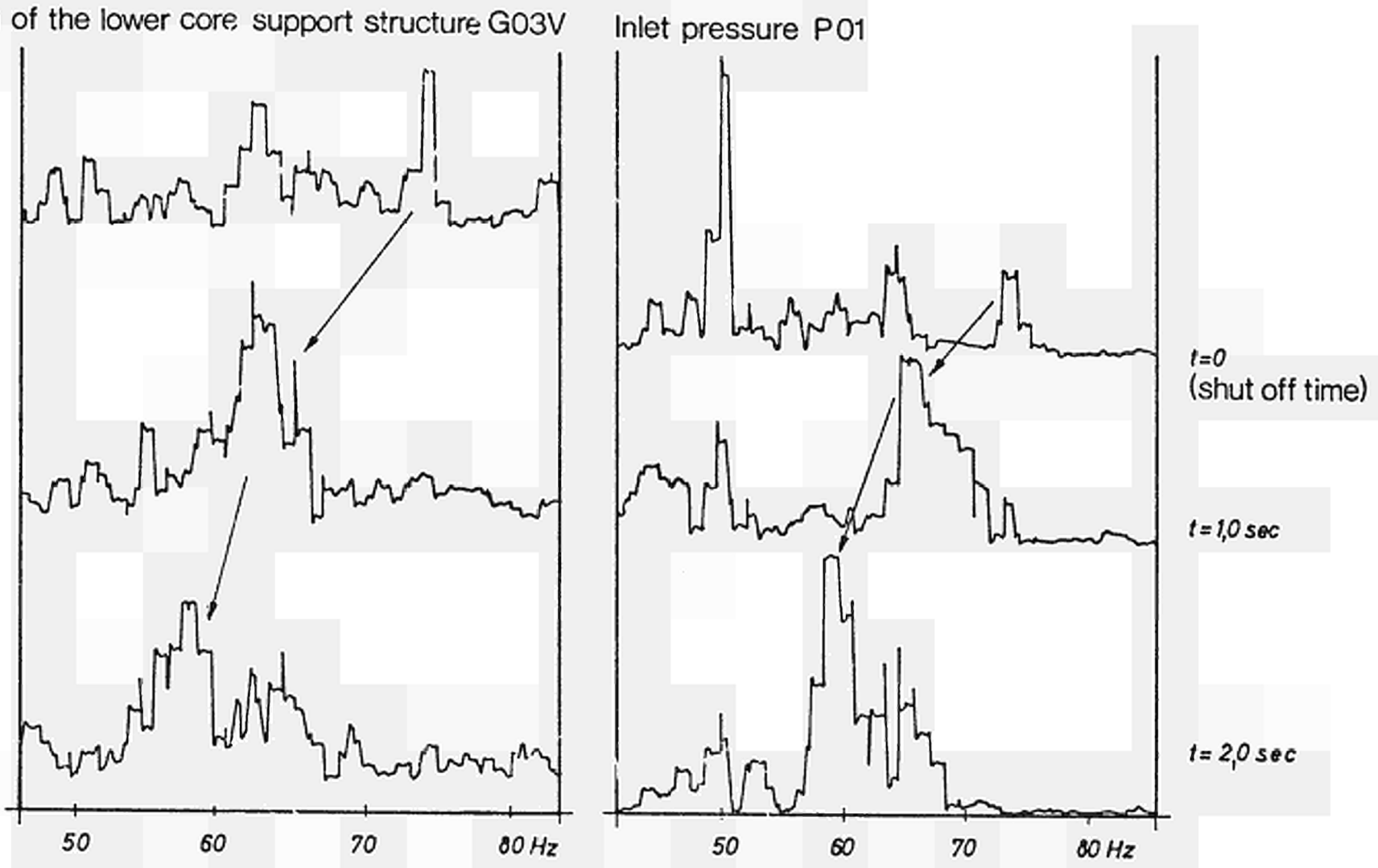

Fig.I. 3.4 /9: APSDs of sensor G03V and P01 as measured during preop tests (four pumps shut down)

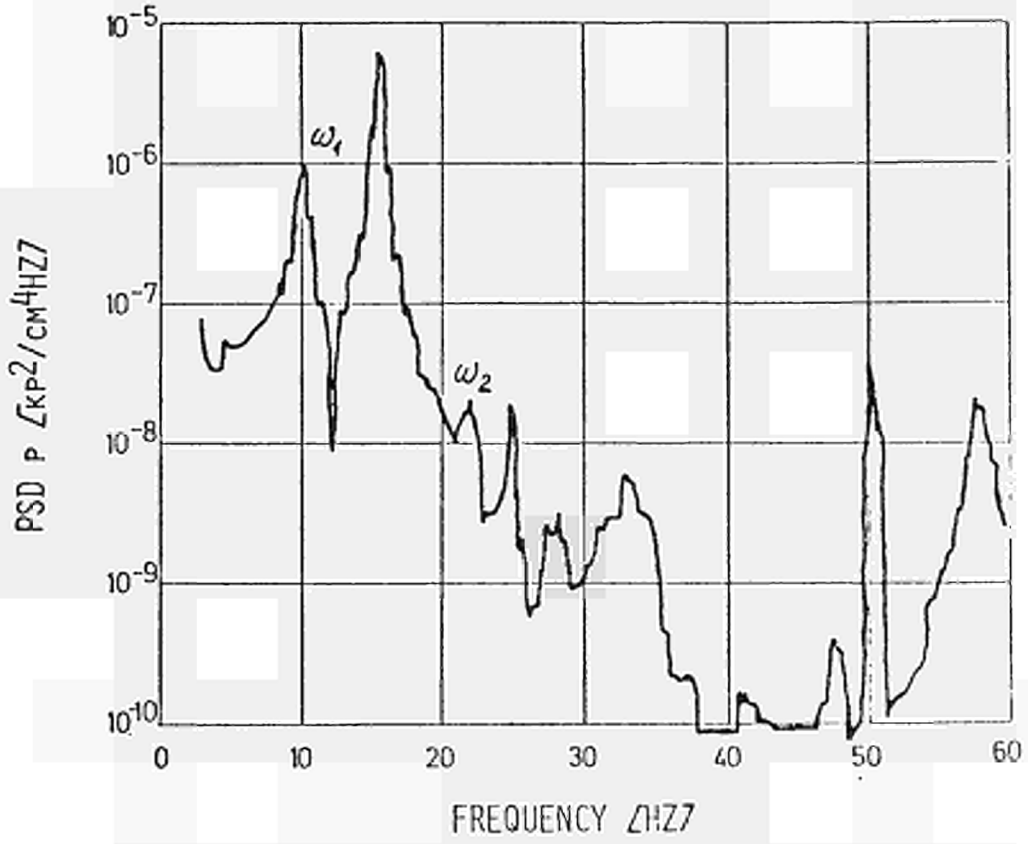

Fig.I.3.4/10: PSDs of pressure and relative motion (measured)

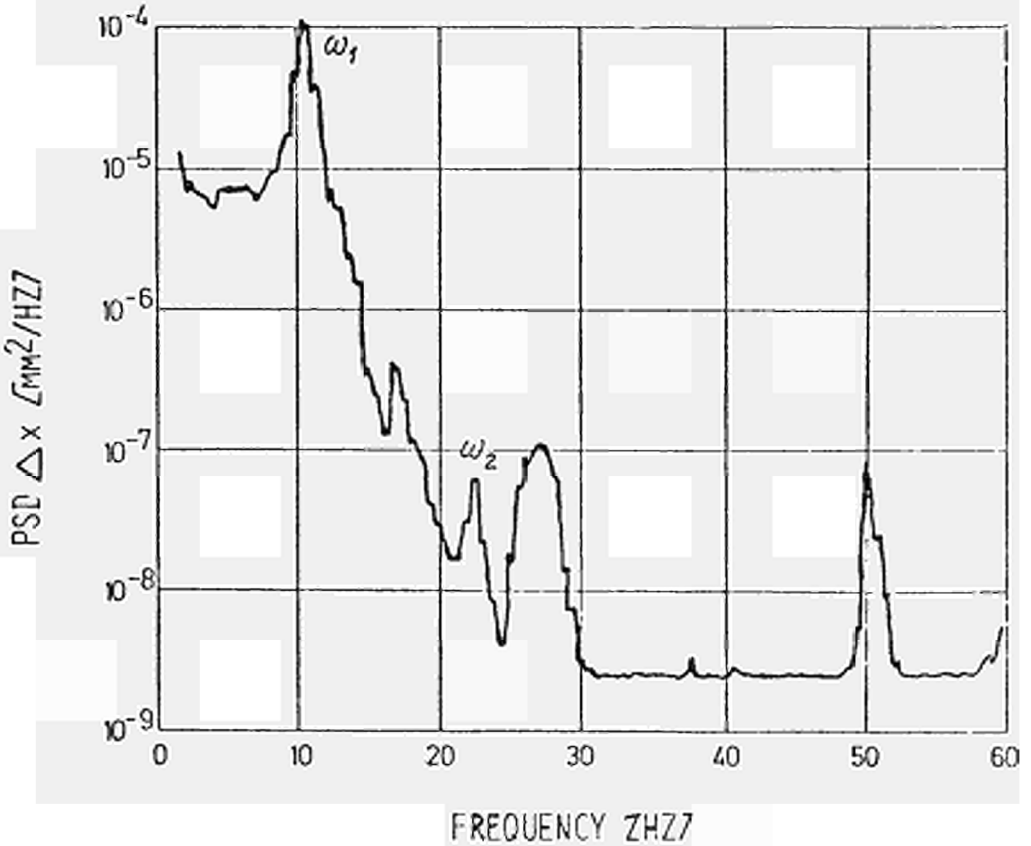

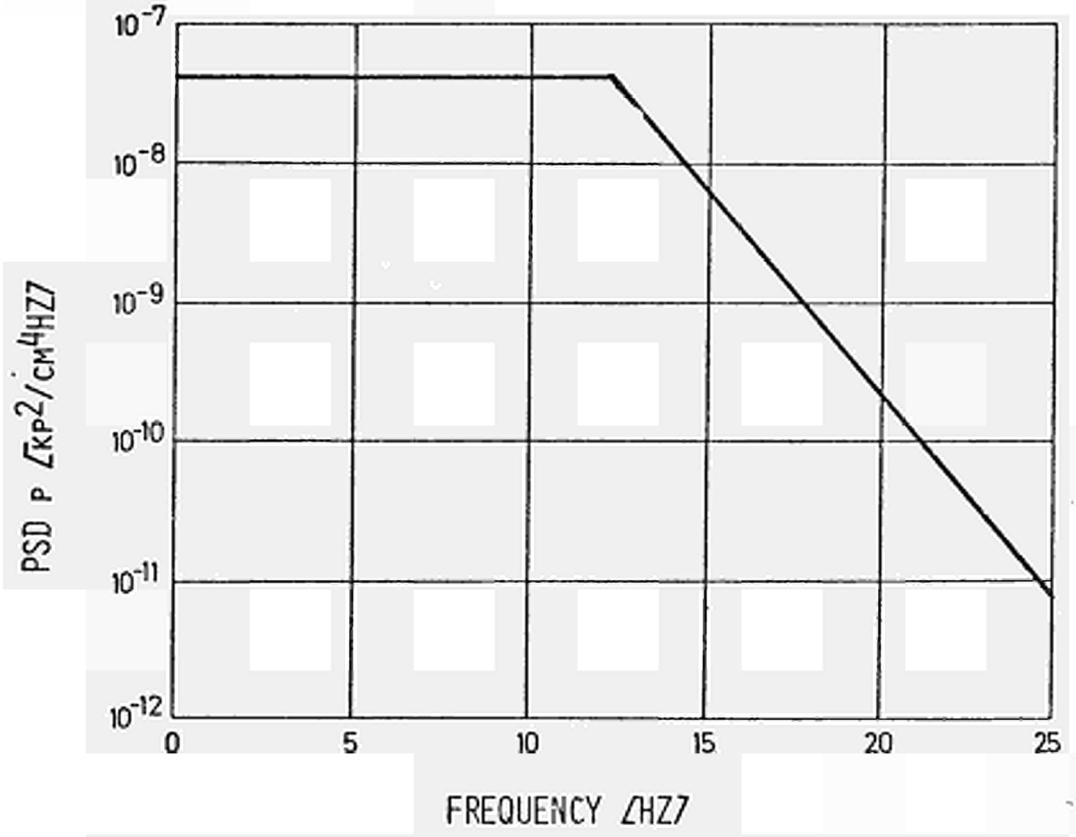

Fig. I. 3.4/ 11: PSDs of pressure and relative motion (calculated)

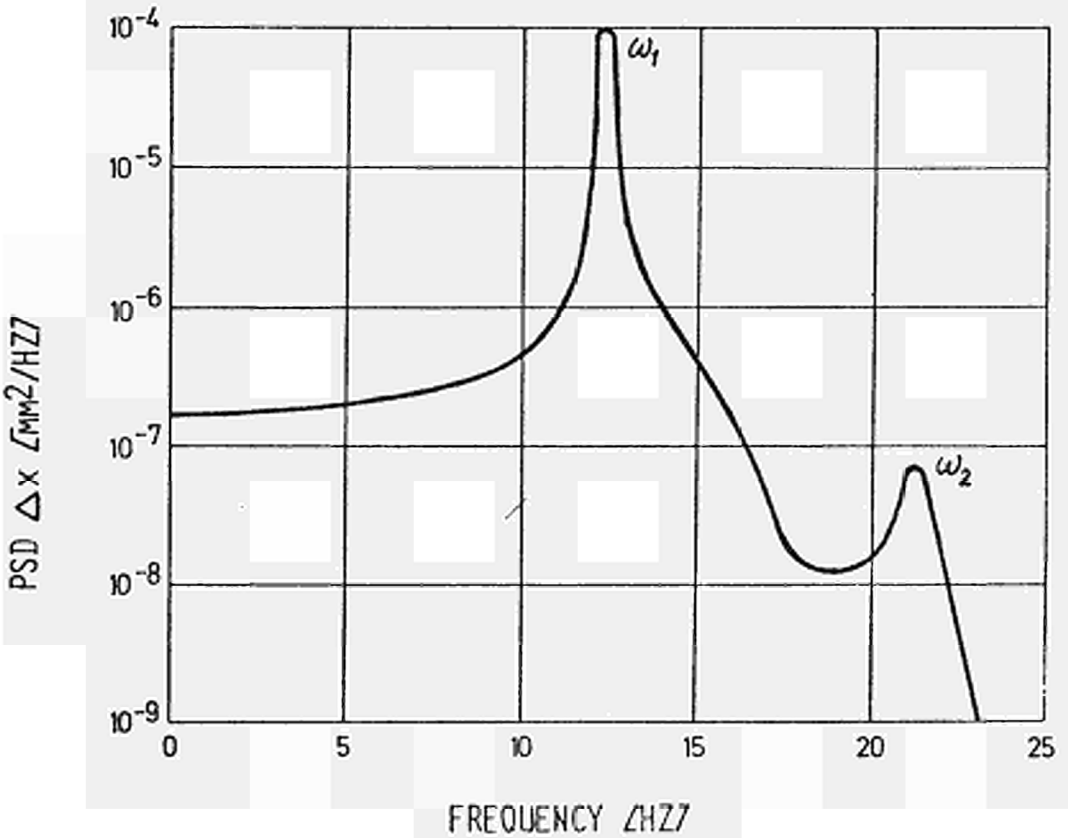

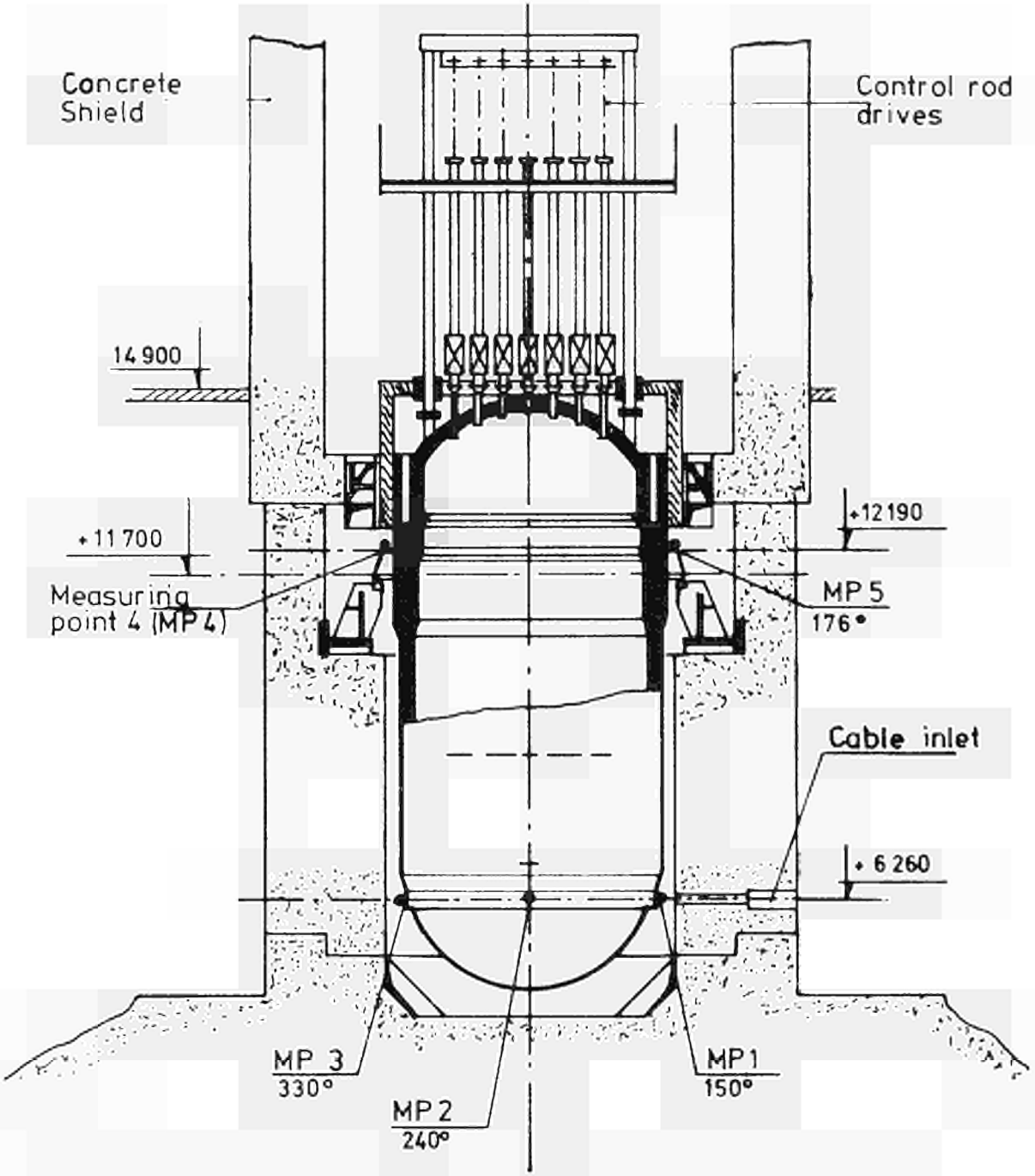

Fig. I.3-4/12 Measuring Points on the Reactor pressure vessel

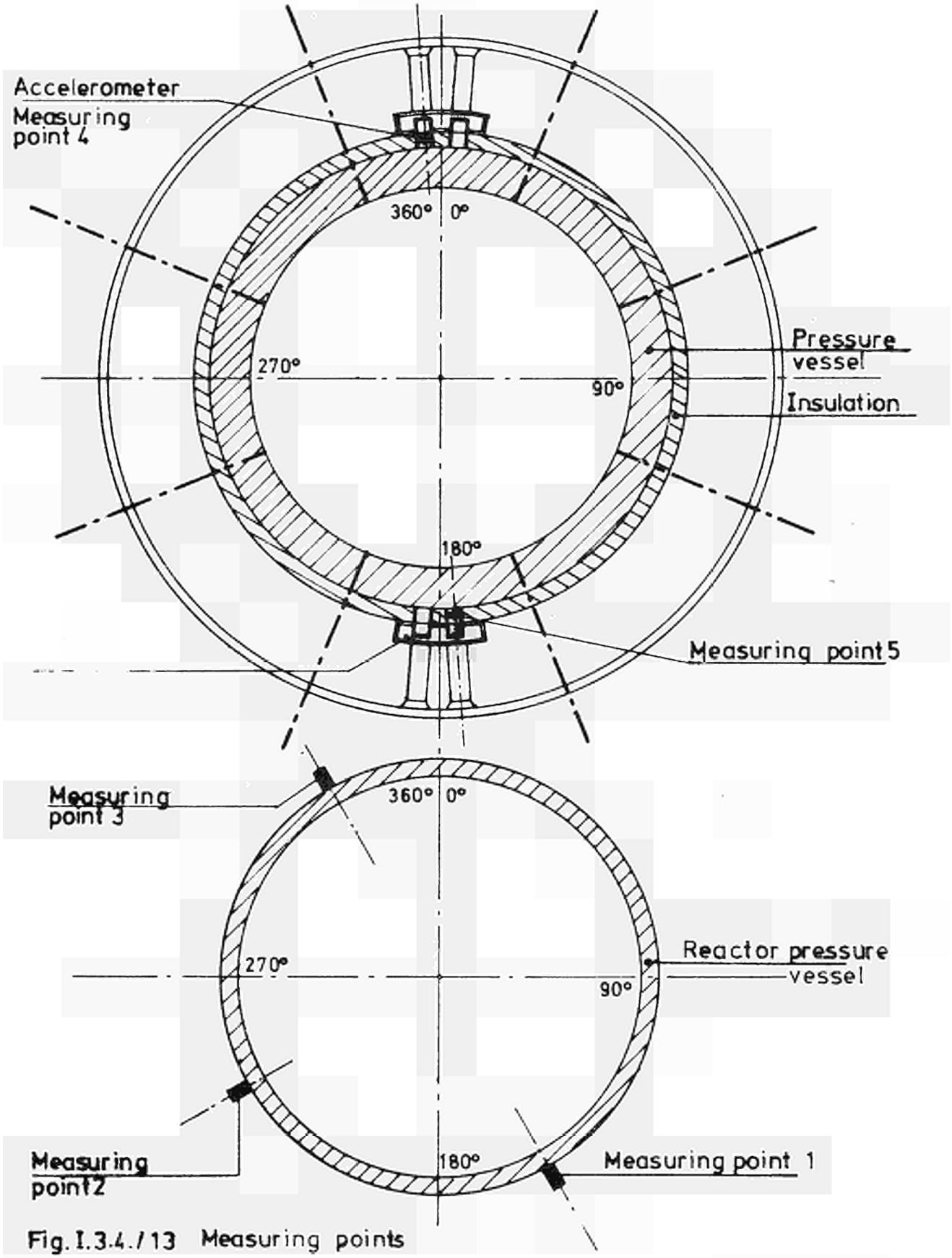

Fig. I.3.4./13 Measuring points

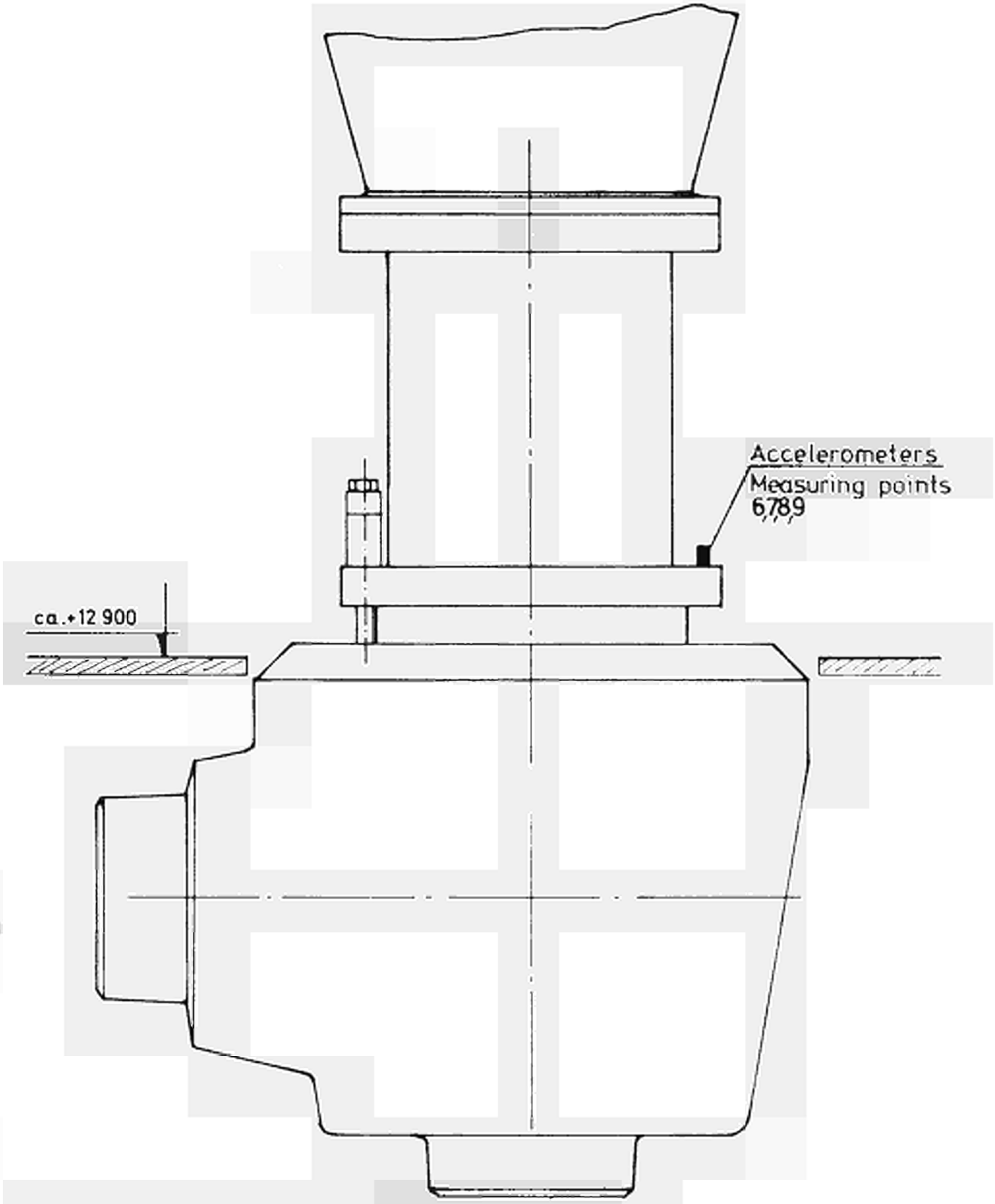

Fig. I.3.4/14 Measuring points on the pumps

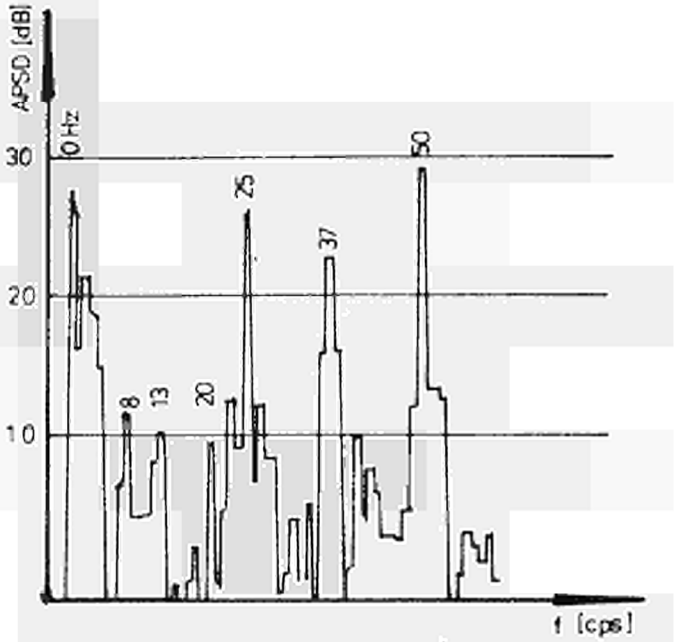

Fig. I.3.4/15 APSD of measuring point 2 (7.16 h)

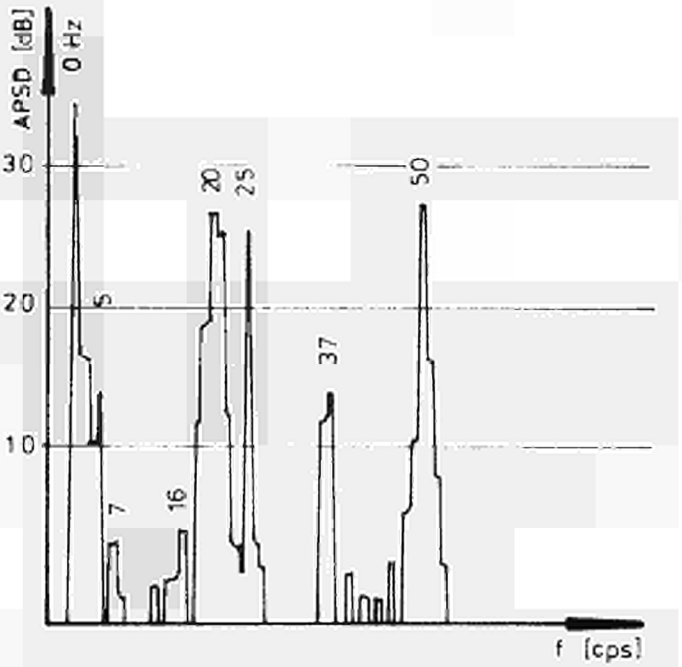

Fig. I.3.4/16 APSD of measuring point 2 (7.20 h)

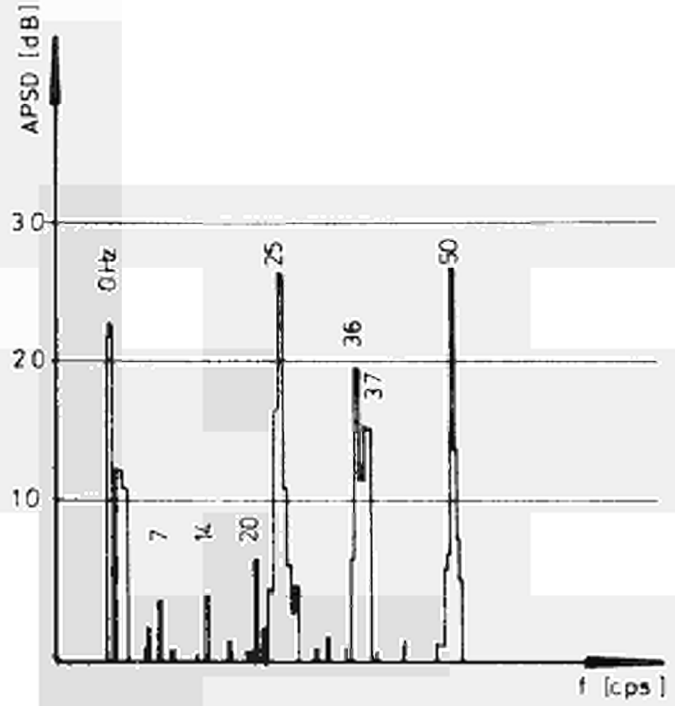

Fig. I.3.4/17 APSD of measuring point 1
(lower frequency range)

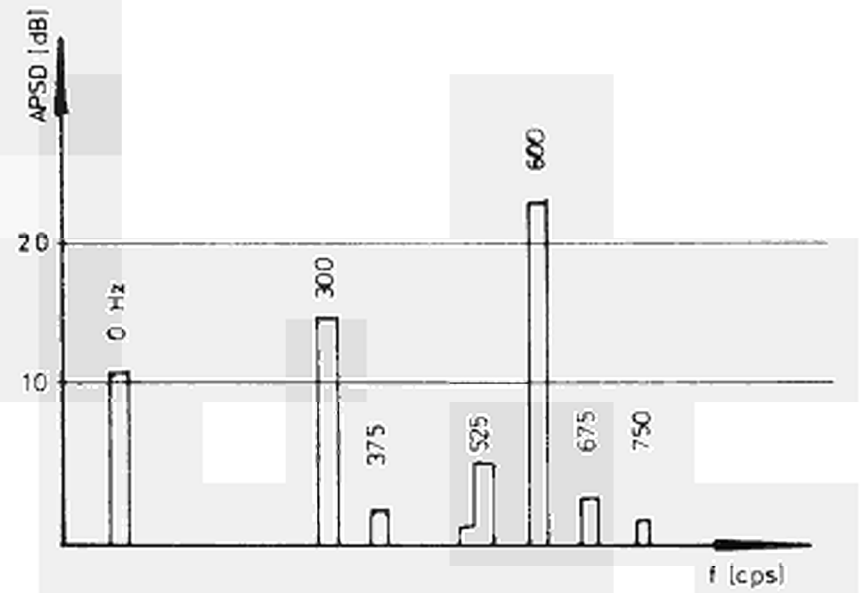

Fig. I.3.4/18 APSD of measuring point 1
(middle frequency range)

I.4 Measurement- and Identification Methods

I.4.1 Self-powered Neutron Detectors in Noise Analysis

A major effort in the framework of investigations which have been performed by the T.U. Hannover since 1970 on the Lingen Boiling Water Reactor (KWL) was concentrated on the application of self-powered neutron (SPN-) detectors for at-power reactor noise investigations in light water reactors. Concerning the results obtained reference is also given to investigations at the Halden Boiling Water Reactor (HBWR) and to some measurements performed by ENEL at the Garigliano Power Plant (see also I.2.1).

The use of SPN-detectors for at power noise measurements is of particular interest, since they are more and more used for control purposes and flux distribution measurements. Hence, it may be possible that these detectors can meet the requirements for both the static flux distribution and noise measurements in view of in-core diagnostics which might be useful for an early warning system.

I.4.1.1 Investigations Using a Prompt Response SPN-Colbalt-Detector

The experimental arrangements and data-reduction system for these experiments will not be repeated here: they are described in detail in /1/ and /4/; only some main results are shown.

A prompt response cobalt SPN detector has been used for a systematic investigation of the space dependent behaviour of the neutronic reactor noise along the axial coordinate. The normalized root mean squared noise amplitudes (NRMS-value) as function of the axial coordinate are shown in fig. I.4.1/1. The horizontal beams indicate the spatial

resolution of the measurements due to the finite length (21 cm) of the commercial cobalt detector (Manufacturer: AB Atomenergi, Sweden). In contrast to the "point reactor" behaviour where the NRMS-value is expected to be constant, here that value increases linearly up to the center of the core and remains constant in the upper half of the core. This behaviour is in agreement with a corresponding measurement on Garigliano reactor mentioned before, and results from enhanced boiling in the upper part of core.

Two characteristic auto correlation functions of the reactor noise in the same reactor core together with their corresponding power spectral density functions are shown in fig. I.4.1/2 in absolute units. The curves which are characteristic for the lower and the upper part of the KWL-core are labeled by detector positions A and B marked in fig. I.4.1/1. The auto correlation functions are measured by means of a real-time correlator (Manufacturer: Hewlett Packard, Mod. 3721 A) and the power spectral densities are gained by Fourier-transforming these functions via a Hanning lag window weighting.

As can be seen in the lower part of fig. I.4.1/2 the shapes of the power spectra change - also in contrast to the "point reactor" model - from a low pass characteristic in the non-boiling zone to a band pass characteristic in the bulk boiling zone. Within the dynamic range of the measurement of more than two decades, in fig. I.4.1/2 no constant noise contribution from uncorrelated neutron events could be observed which means effectively that the detector efficiency of cobalt SPN detectors is high enough to monitor those flux fluctuations resulting from the actual reactor "power noise".

In conclusion, it can be said that prompt response cobalt

detectors used as in-core devices are very well suited to detect the neutronic at-power reactor noise. This fact has also been corroborated by similar measurements with the help of these detectors on the Halden Boiling Water Reactor (HBWR) /1/.

I.4.1.2 Investigations Using Mixed Response SPN-detectors

The aim of noise investigations at HBWR and KWL reactors using self-powered neutron detectors with mixed response was to demonstrate that even these detectors may be used for noise measurements even in high frequency ranges.

A so-called beta-current device, such as the vanadium or rhodium detector, shows a mixed response. The main output current results from β-particles emitted by activated nuclei. The detector response is therefore determined by the decay of the radioisotops in question ($T_{1/2}$ = 42 sec for ^{104}Rh and 3.76 min for ^{52}V, respectively). In addition to this predominant current contribution, however, there exists also a prompt current contribution. This minor prompt contribution appears because prompt capture γ-rays are emitted by the compound nuclei immediately after the absorption of a neutron and these γ-rays generate Compton- and photo electrons by interactions with the emitter material. Since this latter effect works promptly the impulse response function, T(t), of a β-current detector is given by

$$T(t) = W_p \delta(t) + W_d H(t) \quad \text{for } t \geq 0$$

$$= 0 \quad \text{for } t < 0$$

where W_p, W_d = prompt and delayed detector sensitivities in amps/nv

$H(t) = \lambda e^{-\lambda t}$ = normalized impulse response function of delayed component of the considered β-current detector

$\lambda = \ln 2/T_{1/2}$ = decay constant of the β^--active radioisotop
$= 3.072 \times 10^{-3}\ sec^{-1}$ for vanadium-, and
$= 16.50 \times 10^{-3}\ sec^{-1}$ for rhodium detector

The square of the absolute value of the transfer function in frequency domain is obtained by Laplace-transforming eq. (1) to be

$$|T(\omega)|^2 = T^*(\omega)\ T(\omega)$$
$$= W_p^{\,2} + 2W_pW_d\ \mathrm{Re}\ \{H(\omega)\} + W_d^{\,2}|H(\omega)|^2 \qquad (2)$$

with $H(\omega) = \lambda/(\lambda+i\omega)$, since for the Laplace variable s holds in this case $s = \omega i$.

If the last two terms in eq. (2) become small compared to the first one, only the prompt part of the response of the detector is effective. This is the case when

$$\omega >> \omega_c = \lambda\sqrt{\left[\frac{W_d}{W_p}\right]^2 + 2\frac{W_d}{W_p}} \quad 1 \qquad (3)$$

or more simply

$$\omega_c \simeq \lambda \frac{W_d}{W_p} \qquad (4)$$

since the prompt part of the response of a β-current detector is in general small compared to its delayed part, i.e. $W_p << W_d$.

Introducing characteristic values into eq. (3) W_p/W_d = 6.5% and 8% for V and Rh /10/, respectively, it turns out that the critical corner frequencies result to be

$$f_c \simeq 0.008 \text{ Hz for V-detector}$$
$$f_c \simeq 0.035 \text{ Hz for Rh-detector}$$

Fortunately the interesting frequency range of the neutronic reactor noise is beyond these break frequencies. Hence, only the prompt part of the total response of a β-current detector can be used and a measured power spectral density of neutron flux fluctuations is unadulterated provided $f \geq f_c$.

Typical examples are shown in figs. I.4.1/3 and I.4.1/4. In the first figure two spectral densities of the power noise of the HBWR reactor simultaneously recorded by (a) a prompt response cobalt detector and (b) by a mixed response vanadium detector are to be seen one above the other. It is clearly borne out that the vanadium detector delivers a spectral density proportional to that one of the cobalt detector for frequencies higher than about 0.003 Hz. Fig. I.4.1/4 shows three power spectral densities of the flux fluctuations measured with a vanadium and a rhodium detector (commercial types, manufacturer: AB Atomenergi, Sweden) in a nearly central core position. The measurements were made on KWL at two different points of time. The functions shown are obtained by means of a real time correlator/Fourier display system (Manufacturer: Hewlett Packard Mod. 3721 A and 3720 A). Thus, it is also experimentally confirmed that rhodium-detectors, in the same way as vanadium-detectors, can be successfully used to detect the "power-noise" in large water reactors.

Since in most cases the auto correlation function of the actual neutronic reactor noise, $\Psi(\tau)$, can be approximated by a δ-function compared with the impulse response function, $H(\tau)$, of the delayed component of the response of the detector in eq. (1), it can be mathematically shown - when Fourier-transforming eq. (2) - that the normalized auto correlation function, $R(\tau)$, which is measured by means of a mixed response β-current detector, reads

$$R(\tau) = \frac{W_p^2 \frac{\Psi(\tau)}{\Psi(0)} + (2W_pW_d+W_d^2)c\, e^{-\lambda|\tau|}}{W_p^2 + (2W_pW_d+W_d^2)c} \qquad (5)$$

where $\Psi(\tau)/\Psi(0)$ is the (wanted) normalized auto correlation function of the neutron flux fluctuations and $c = \lambda/(4\Delta B)$ is a dimensionless constant depending on the effective bandwidth ΔB (in Hz) of the power spectral density function of the flux fluctuations.

It is seen that for $\tau = 0$, $R(\tau)$ approaches unity due to normalization. For $W_c = 0$, i.e. for a detector with a purely prompt sensitivity, W_p, the above equation yields directly the wanted function $R(\tau) = \Psi(\tau)/\Psi(0)$. For $W_p = 0$, i.e. for a detector with only a delayed sensitivity, W_d, eq. (5) reduces to $R(\tau) = e^{-\lambda|\tau|}$. This expression is nothing else than the normalized auto correlation function of the impulse response function of the delayed component, $H(t)$, and it is seen that this function does not contain any information about the "power noise" of the reactor system.

To visualize the predicted situation in time domain through eq. (5) figs. I.4.1/5 and I.4.1/6 show typical auto-correlation functions measured by means of a vanadium and a rhodium β-current detector, respectively. By subtracting the delayed background, resulting from the delayed part of the detector sensitivity, the (wanted) shapes of the

auto correlation functions of the neutronic flux fluctuations can be gained.

Thus, these two figures in the time-domain approach supplement the frequency-domain results in figs. I.4.1/3 and I.4.1/4 demonstrate very evidently the applicability of mixed response β-current detectors for the analysis of at-power reactor noise.

I.4.1.3 One- and Two-Detector Experiments on KWL Using Neutron and Gamma Sensitive Detectors

The aim of the following one- and two-detector experiments on KWL was twofold: First, different kinds of self-powered detectors, which have been fabricated at the Institut für Kerntechnik, should be tested for both, flux distribution and noise measurements, and secondly, space dependent effects should be investigated by two detector cross correlation measurements including the utilization of reactor gamma ray fluctuations.

The results presented by the following six figures are preliminary and are not yet fully analyzed and understood. Figs. I.4.1/7 to I.4.1/9 show auto power spectral density functions at different axial core positions measured with a prompt response Hf-detector, with a gamma sensitive miniature ion chamber (Mod. WEL 23616) and a mixed response (partly neutron and partly gamma) platinum detector.

Characteristic features of Hf and Pt detectors are described in detail elsewhere /8 - 11/ and other experience gained with both commercial, and predominantly, with self-built SPN-detectors can be found in /9/.

Here, it should be only mentioned that the characteristic property of a hafnium detector is its relatively high sensitivity to fast neutrons. In a typical light water reactor neutron spectrum the ratio of its thermal to its fast sensitivity is /8/

S_{th}/S_{fast} = 1.22 as against 8.6, 17.0 and 5.6 for cobalt, cadmium, and erbium SPN-detectors.

Due to the relatively high atomic number of platinum, these detectors show - besides its neutronic sensitivity - an additional sensitivity to reactor gammas. It could be experimentally shown /10/ that the ratio of the gamma to the neutronic induced mean output current of such a detector ranges between 25% in the lower part of the KWL-core and 35% in its upper part because of the axially increasing void fraction which gives rise to an increased ratio of gamma to neutron flux in the upper part of a BWR-core. Due to their low burn up rates comparable with those of vanadium detectors it is expected that Pt-detectors possess a considerable potential as in-core devices in light water reactors /11/.

The characteristic property of the axially dependent auto power spectral density functions in fig. I.4.1/7, which were measured by a neutron sensitive hafnium detector, is the increasing noise intensity in the upper frequency range for detector positions in the bulk boiling zone. The corresponding curves measured by means of a gamma chamber do not show this behaviour, and in the Pt-detector curves only a slight indication of this effect can be seen. The latter fact is obvious and consistent since the Pt-curves are mixtures of neutron and gamma ray spectra. Thus, as a preliminary conclusion, it can be ascertained that the neutronic noise - detected with a detector with

relatively high fast neutron sensitivity - reveals much better the "boiling noise" than the gamma noise. A theoretical investigation of this boiling noise, which is sometimes also called "slowing down noise" because of distorted removal of the fast neutrons by steam bubbles, is presently underway at the Institut für Kerntechnik.

Figs. I.4.1/10 to I.4.1/12 show results obtained with the same detectors by evaluating cross correlation experiments. Each figure contains the absolute value of the coherence function together with the corresponding phase shift as function of frequency. The accompanying sketch of the KWL-core indicates the labeled detector positions. The first evident fact is the high coherence, even for distant detector positions up to 1 Hz and the sudden break-down of the coherences beyond 1 Hz. This is in contrast to the results of in-core cross correlation measurements at the Garigliano reactor. It is also seen that the dynamic coupling of the gamma field is as strong as for the neutron field.

Based on the results of a recent paper /12/ it can be theorized that the spatial coherence range for the gamma field in axial direction of a cylindrical reactor core in the delayed critical state is at least as high as that one of the neutron field provided

$$\mu >> \left[\frac{\beta}{M^2} + B_r^2\right]^{1/2} \bar{\lambda} << \omega << 1/l \qquad (6)$$

where

μ = effective attenuation coefficient for prompt fission and capture gamma rays within the reactor core, cm^{-1}

M^2 = migration area, cm^2

B_r^2 = $(2.405)^2/R^2$ = transverse buckling of the core, R = radius of core, cm

β = effective fraction of delayed neutrons

$l, \bar{\lambda}$ = thermal neutron life time, sec, and mean decay constant of precursors, sec^{-1}

Assuming a mean gamma energy of ≃ 1 MeV and a mean local void fraction of ≃ 30% the attenuation coefficient for these gamma rays in the KWL-core (including absorption in UO_2-fuel) is $\mu = 0.206\ cm^{-1}$. The numerical value of the right side of the above equation yields ($M^2_{eff} \simeq 91\ cm^2$, $\beta = 0.007$, R = 1.21 m) ≃ $0.0217\ cm^{-1}$.

Hence, the above condition is fulfilled and the high coherence of the gamma noise in fig. I.4.1/11 confirm the predicted behaviour. However, the absolute height of the coherence for all three measuring series and their sudden cut-off at about 1 Hz could not yet be understood. For a spatially constant noise driving force the coherence length in axial direction should be the reziprocal of the right side of the above equation, namely about 46 cm. The observed values in the frequency range f < 1 Hz are too high even if the effects of delayed neutrons are included in this low frequency range /13/.

A similar situation is found with the phase shifts. An equivalent analysis like in Garigliano reactor, concerning local steam velocities, results for the low frequency range in numerical values between 20 and 30 m/sec which are obviously too high (see I.2.2). Therefore, the interest is now focused on the higher frequency range. However, it should be noted, that for the test campaign of the self-powered detectors in KWL reactor it was not possible (due

to mechanical reasons) to measure phase shifts between axially spaced detectors in the same radial positions. Such experiments are planned for the next future.

Due to the high coherences of the neutronic field up to 1 Hz with values nearly unity the KWL-core exhibits in that frequency range with good approximation a point reactor behaviour. May be that this global appearence is only simulated by a mechanism which produces instantaneously a flux perturbation in the whole core as a result of any other perturbation. The pressure-flux interaction is in principle such a possibility and is believed to be responsible for such an effect. Further investigations will be focused also on this point.

Literature, Section I.4.1

/1/ Seifritz, W.
Zur Analyse des Reaktorrauschens in Siedewasserreaktoren
Habilitationsschrift, Technische Universität Hannover
(1972)

/2/ Seifritz, W., Cioli, F.
On-Load Monitoring of Local Steam.
Steam Velocity in BWR Cores by Neutron Noise Analysis
Paper to be presented at the 1973 ANS-Wintermeeting,
San Francisco, Calif., Nov. 11-16 (1973)

/3/ Northern States Power Company, Pathfinder Atomic Power
Plant
Six Month Operating Report, No. 2, p. 561, Minneapolis
(1967)

/4/ Seifritz, W.
An Analysis of the Space Dependent Neutron Flux Density
Fluctuations at the Lingen Boiling Water Reactor (KWL)
by Methods of Stochastic Processes
Atomkernenergie, 19, p. 271 (1972)

/5/ Saxe, R.F.
Survey of Boiling Detection Method in Reactors
Proc. of the Conference on Incipient Failure Diagnosis
for Assuring Safety and Availability of Nuclear Power
Plants, ORNL,
USAEL, Gatlingburg, Tennessee (1967)

/6/ Seifritz, W., Lindmo, T., Roggenbauer, H.
Power Spectral Density Analysis of Sampled Reactor Process
Data Using Heterodyne Digital Filtering Techniques
Submitted for publication in Energia Nucleare (1973)

/ 7/ Seifritz, W.
Measurement of the Ratio of the Prompt to the Delayed Neutronic Response of a Self-Powered Vanadium Detector by Cross-Correlation Techniques
Nucl. Sci. and Eng. 49, pp. 358-369 (1972)

/ 8/ Jaschik, W., Seifritz, W.
Model for Calculating Prompt-Response Self-Powered Neutron Detectors
Paper submitted for publication in Nucl. Sci. and Eng. (1973)

/ 9/ Gebureck, P., Hofmann, W., Jaschik, W., Seifritz, W., Stegemann, D.
Development and Incore-Application of Self-Powered Neutron Detectors
Paper presented at the IAEA Symposium on "Nuclear Power Plant Control and Instrumentation", Prague, January 22-26, 1973

/10/ Seifritz, W., Gebureck, P.
Using a Self-Powered Platinum Flux Detector For In-Core Measurements in a BWR
Summary of paper to be presented at the 1973 ANS-Winter Meeting, San Francisco, November 11-16, Transact. of Am. Nucl. Soc. (1973)

/11/ Shields, R.B.
A Platinum In-Core Flux Detector
IEEE Transactions on Nuclear Science NS-20(1) Feb. (1973)

/12/ Kostic, Lj., Seifritz, W.
The Theory of Space Dependent Reactor Noise Analysis Using Gamma Radiation
Journ. of Nucl. En., 25 pp. 637-655, (1971)

/13/ Seifritz, W.
Some Remarks on the Spatial Correlation Range of the Neutronic Noise in an Infinite Multiplying Medium Including the Effects of Delayed Neutrons
Atomkernenergie 21 (2), pp. 157-158 (1973)

/14/ Seifritz, W., Stegemann, D.
Reactor-Noise Analysis
Atomic Energy Review, Vol. 9, No. 1, pp. 168-172
IAEA, Vienna (1971)

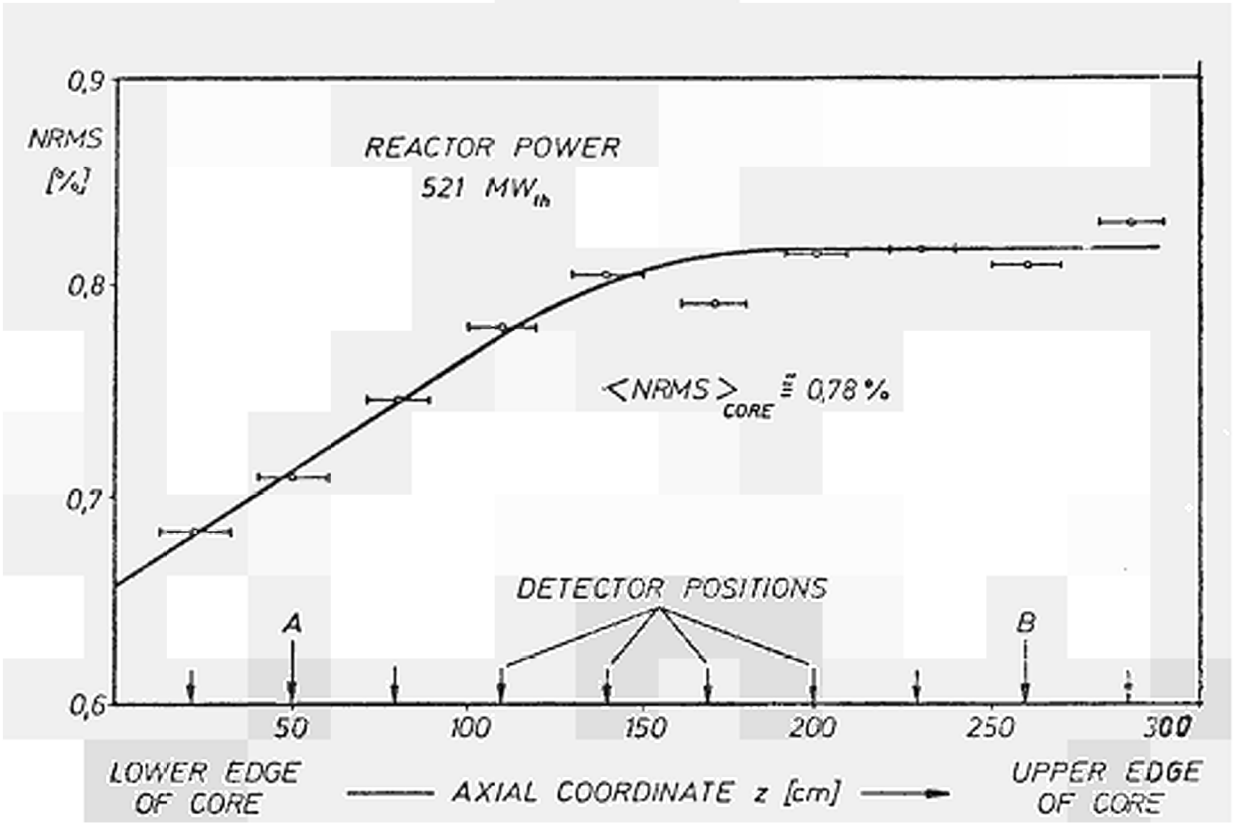

FIG. I.4.1/1 :

Normalized root mean square value (NRMS) of the neutron flux fluctuations in the Lingen BWR as function of the axial coordinate.

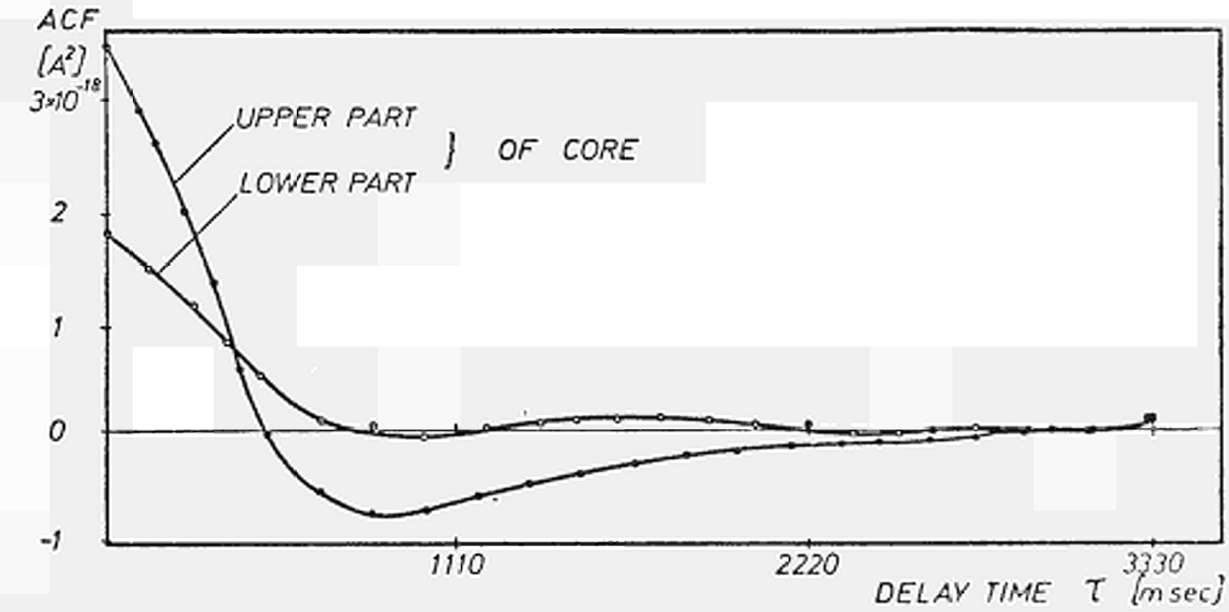

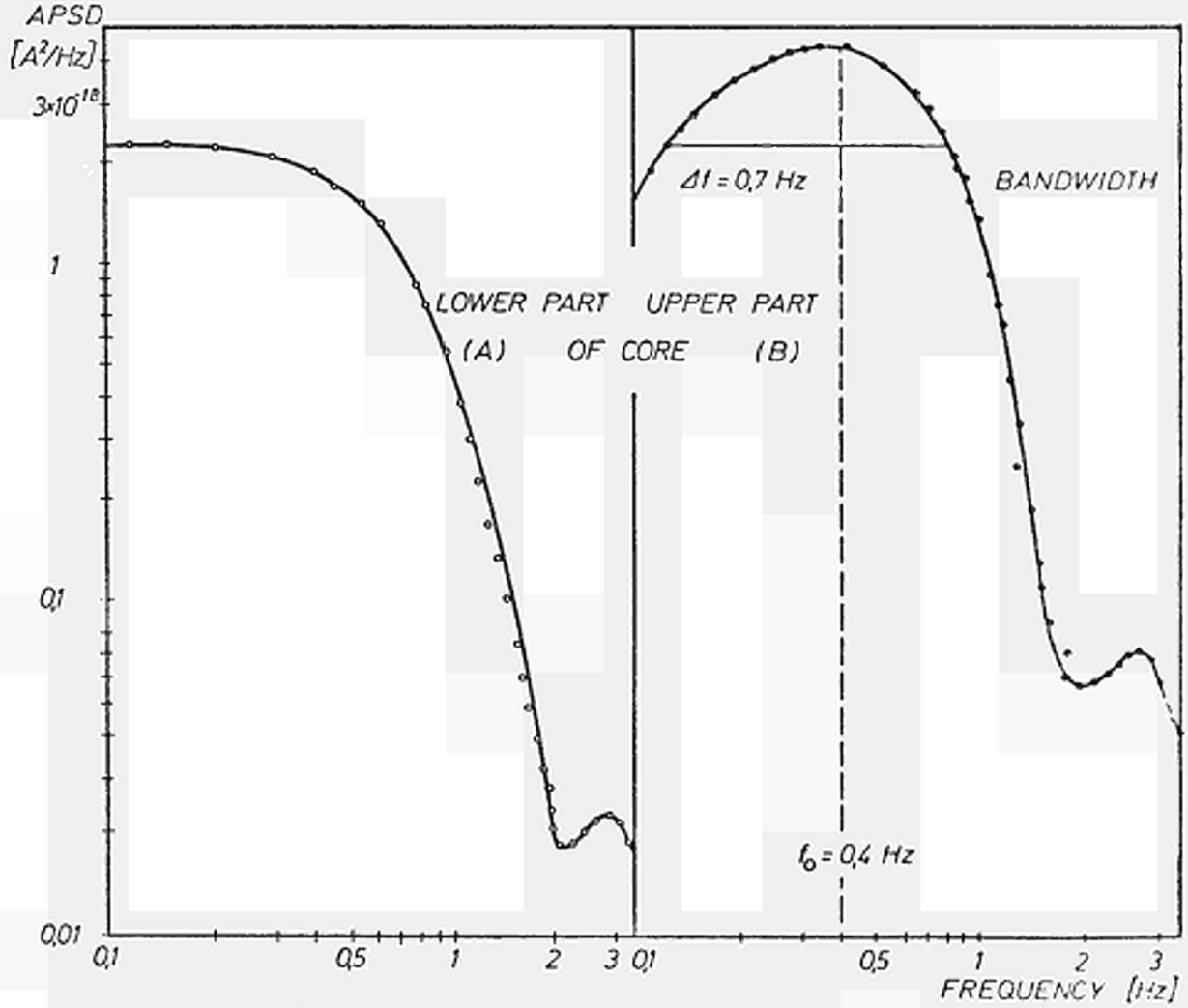

FIG. I.4.1/2 :

Typical auto correlation and auto power spectral density functions of the neutronic reactor noise in the Lingen BWR.

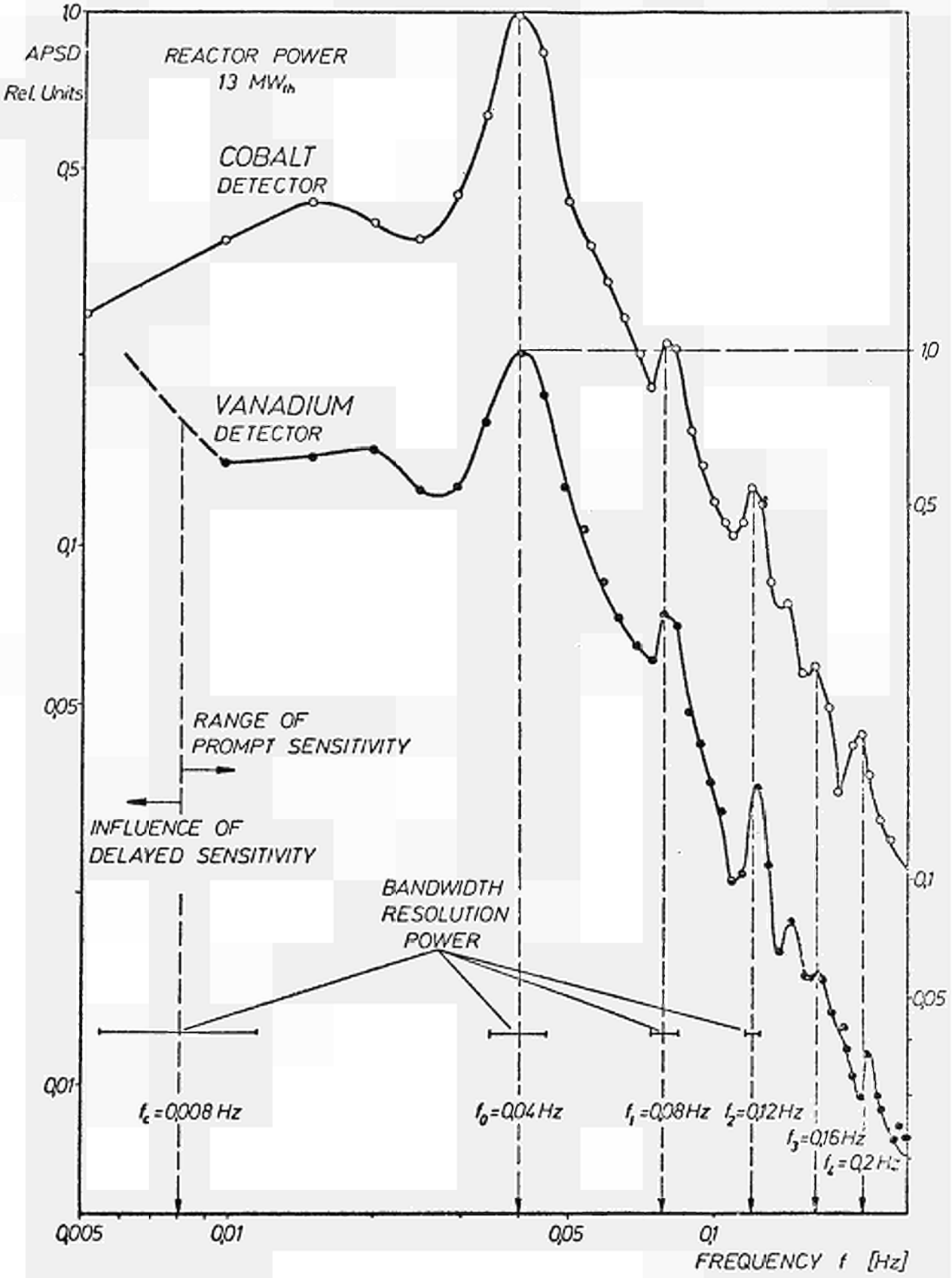

FIG. I.4.1/3 :

Auto power spectral densities of the power noise in the Halden BWR.

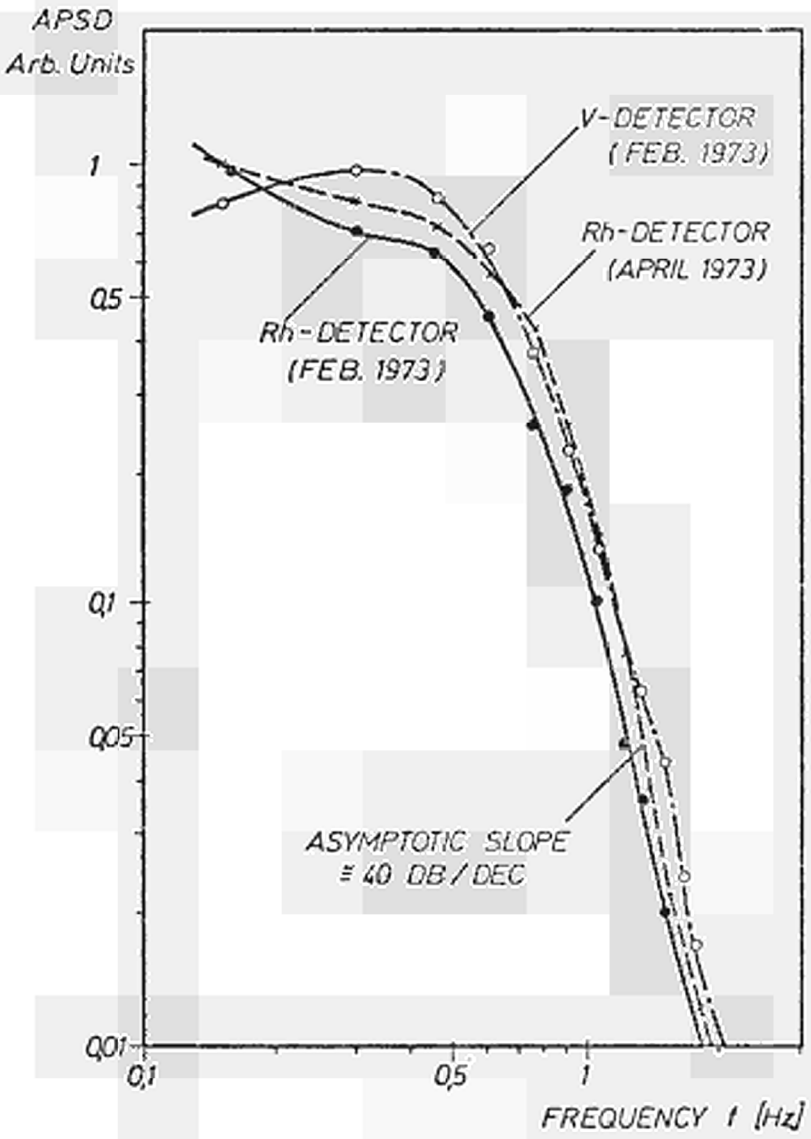

FIG. I.4.1/4 :
Auto power spectral densities of the power noise in the Lingen BWR.

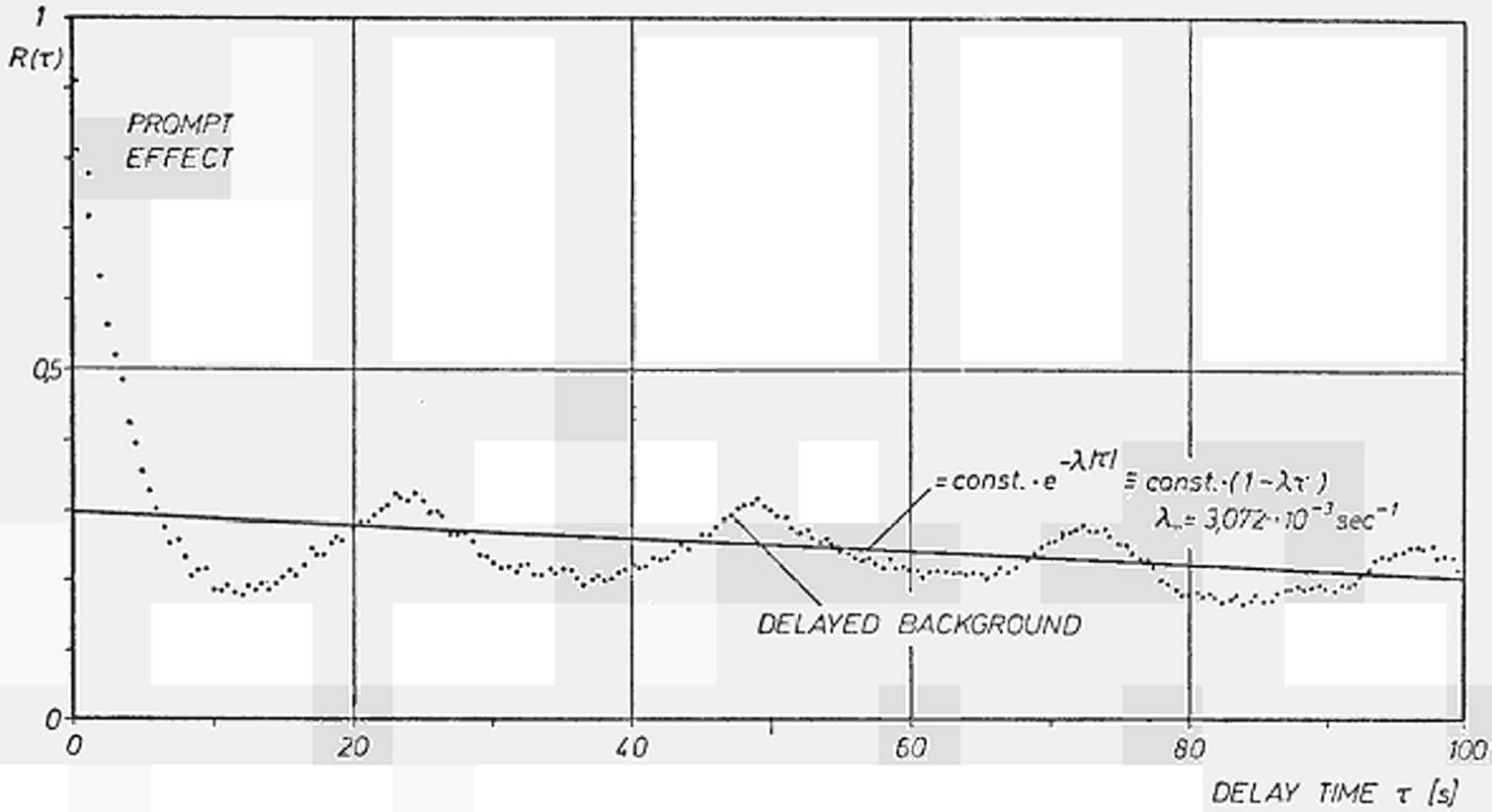

FIG. I.4.1/5 :

Normalized auto correlation function of the Vanadium detector. Halden BWR.

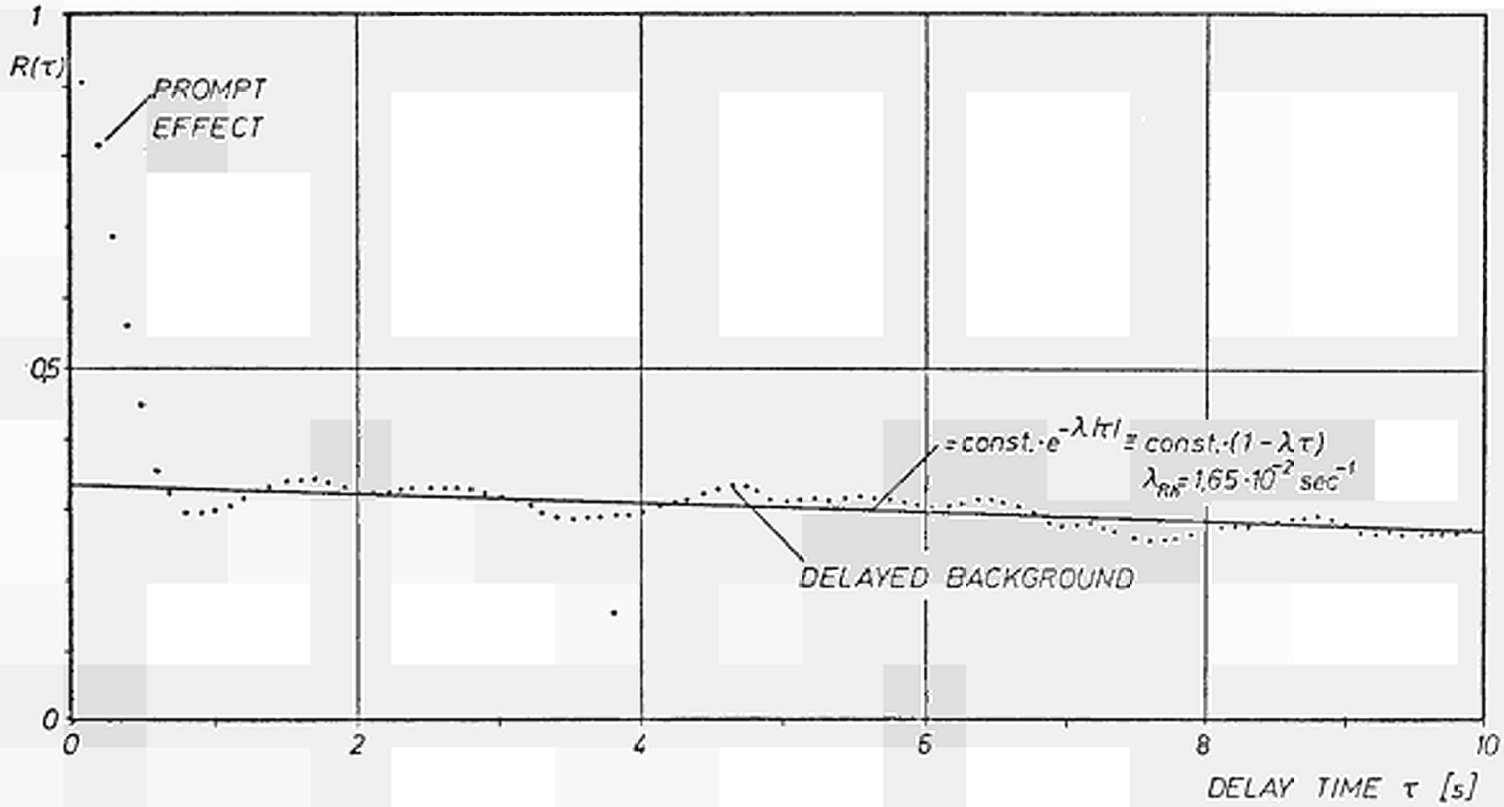

FIG. I.4.1/6 :
Normalized auto correlation function of the Rhodium detector. Lingen EWR.

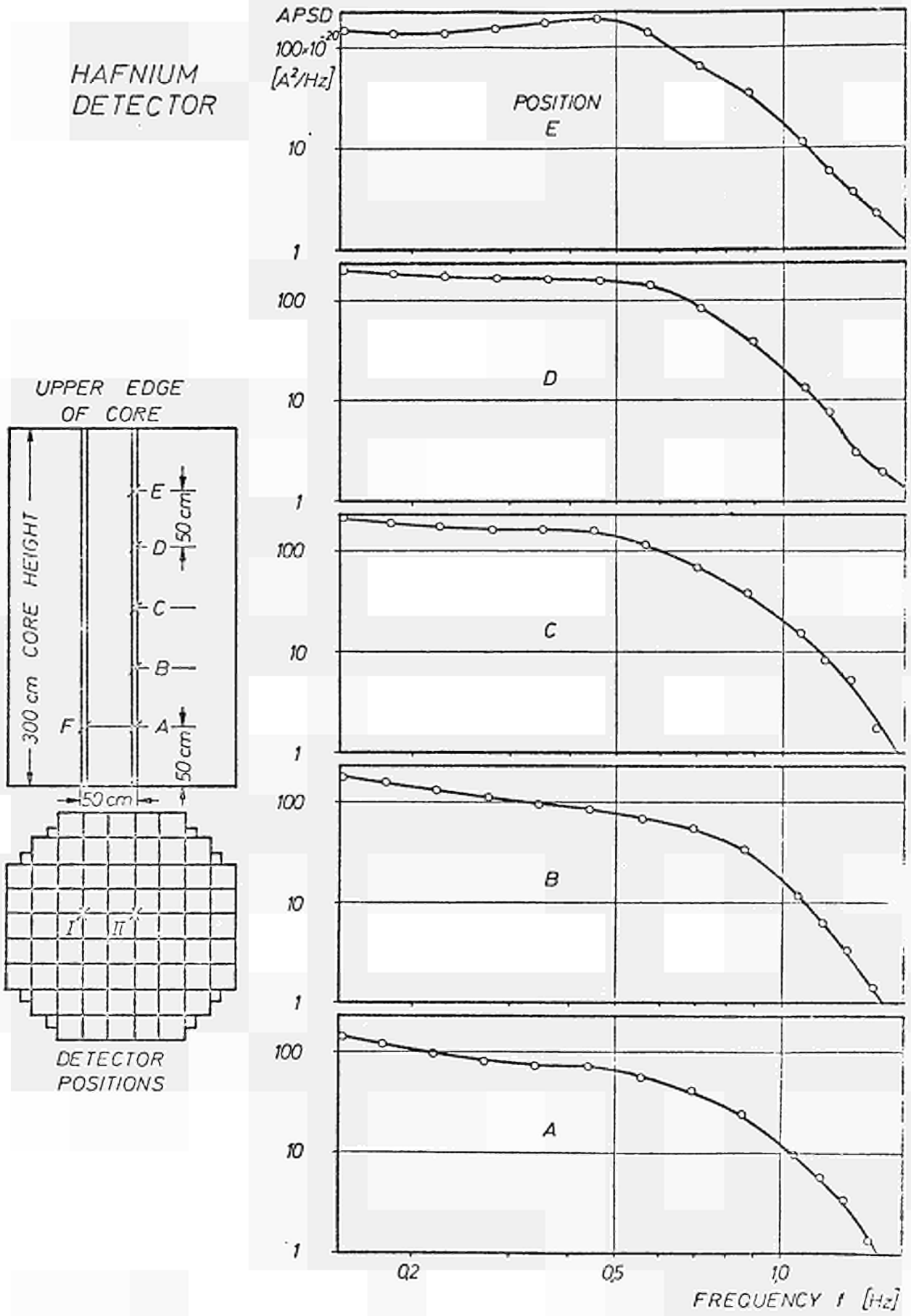

FIG. I.4.1./7 :

Axial dependency of the auto power spectral density function, measured with a Hafnium detector in the Lingen LWR.

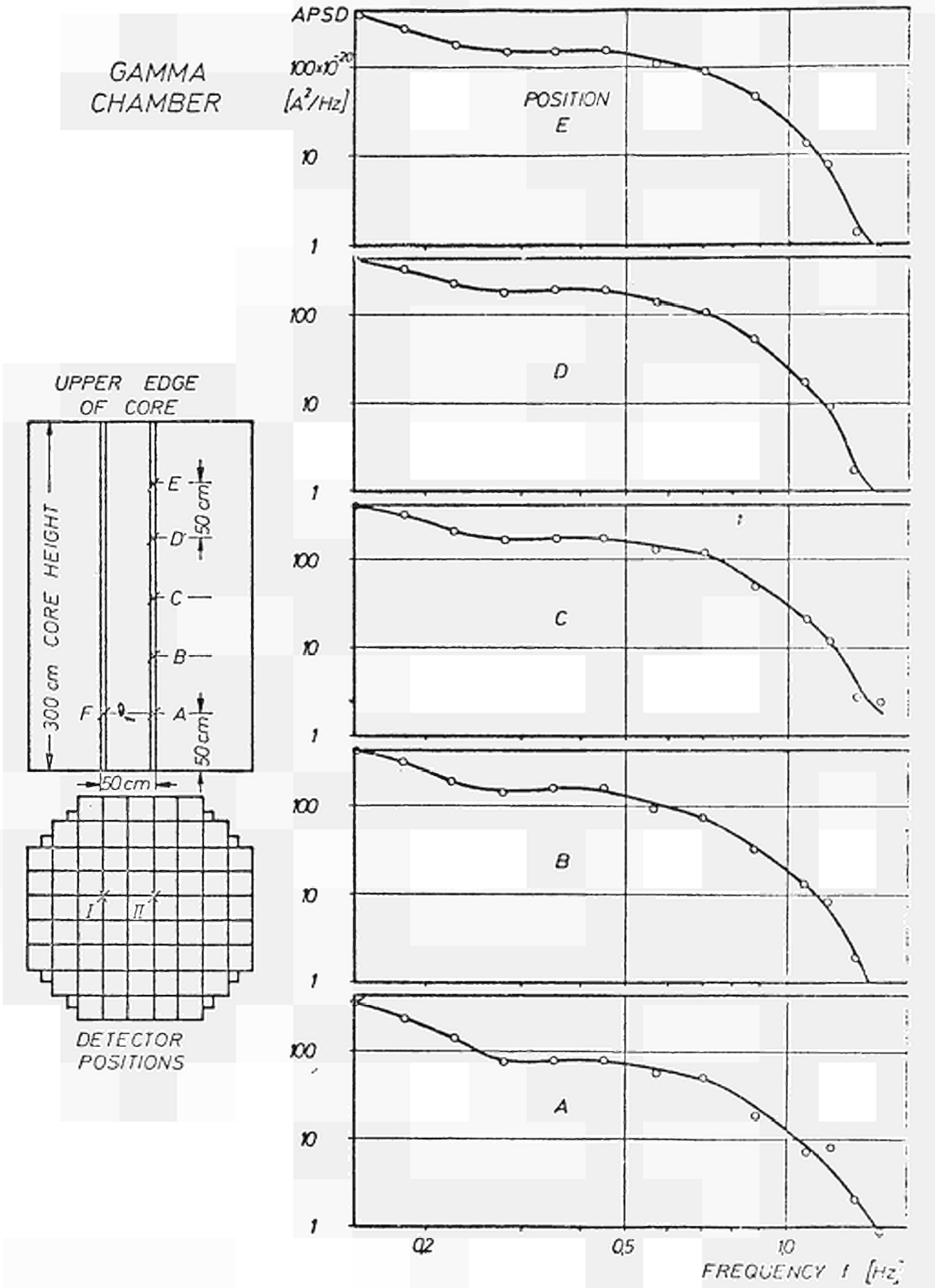

FIG. I.4.1/8 :

Axial dependency of the auto power spectral density function, measured with an in-core gamma chamber in the Lingen BWR.

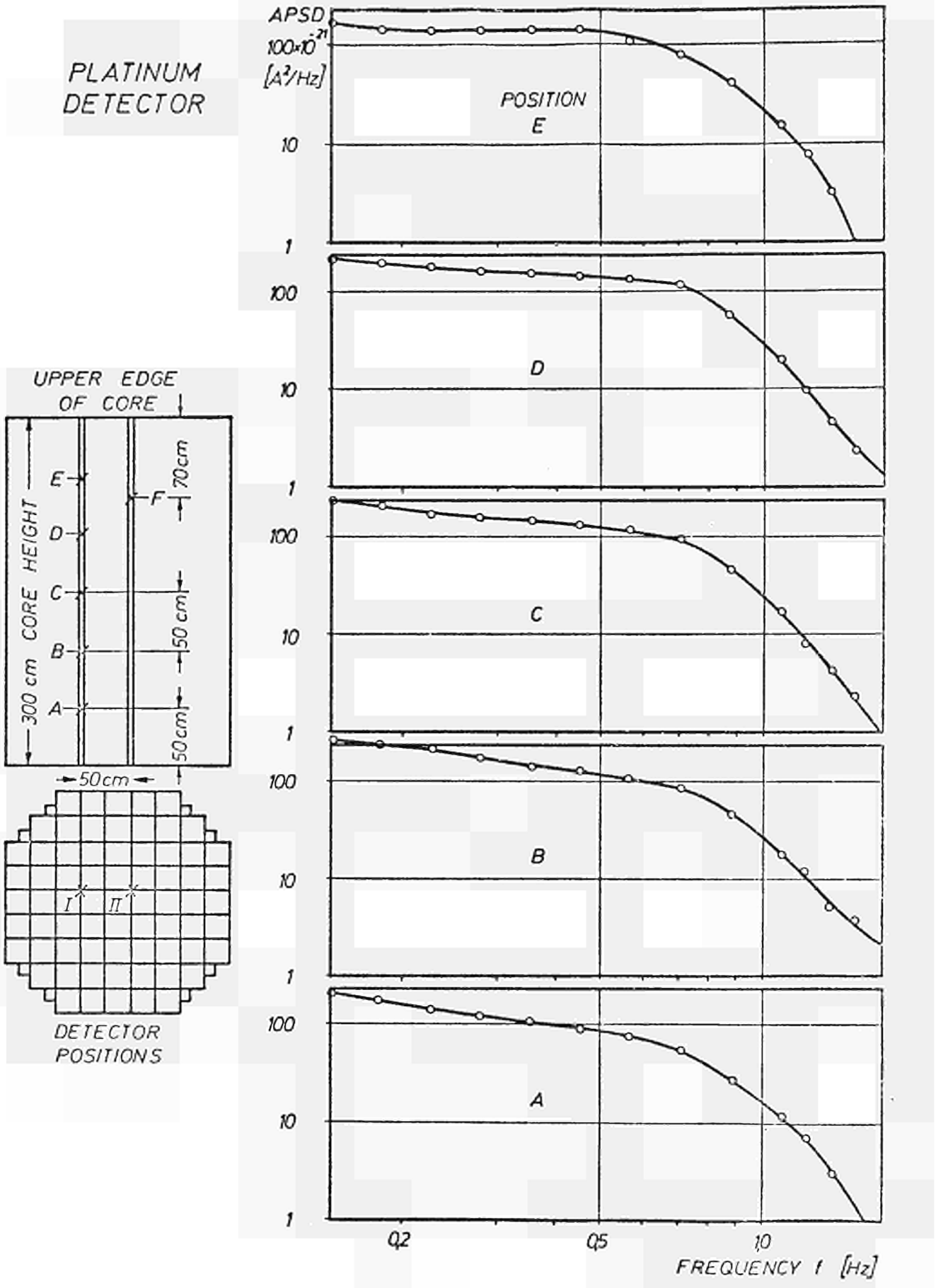

FIG. I.4.1/9 :

Axial dependency of the auto power spectral density function, measured with a Platinum detector in the Lingen BWR.

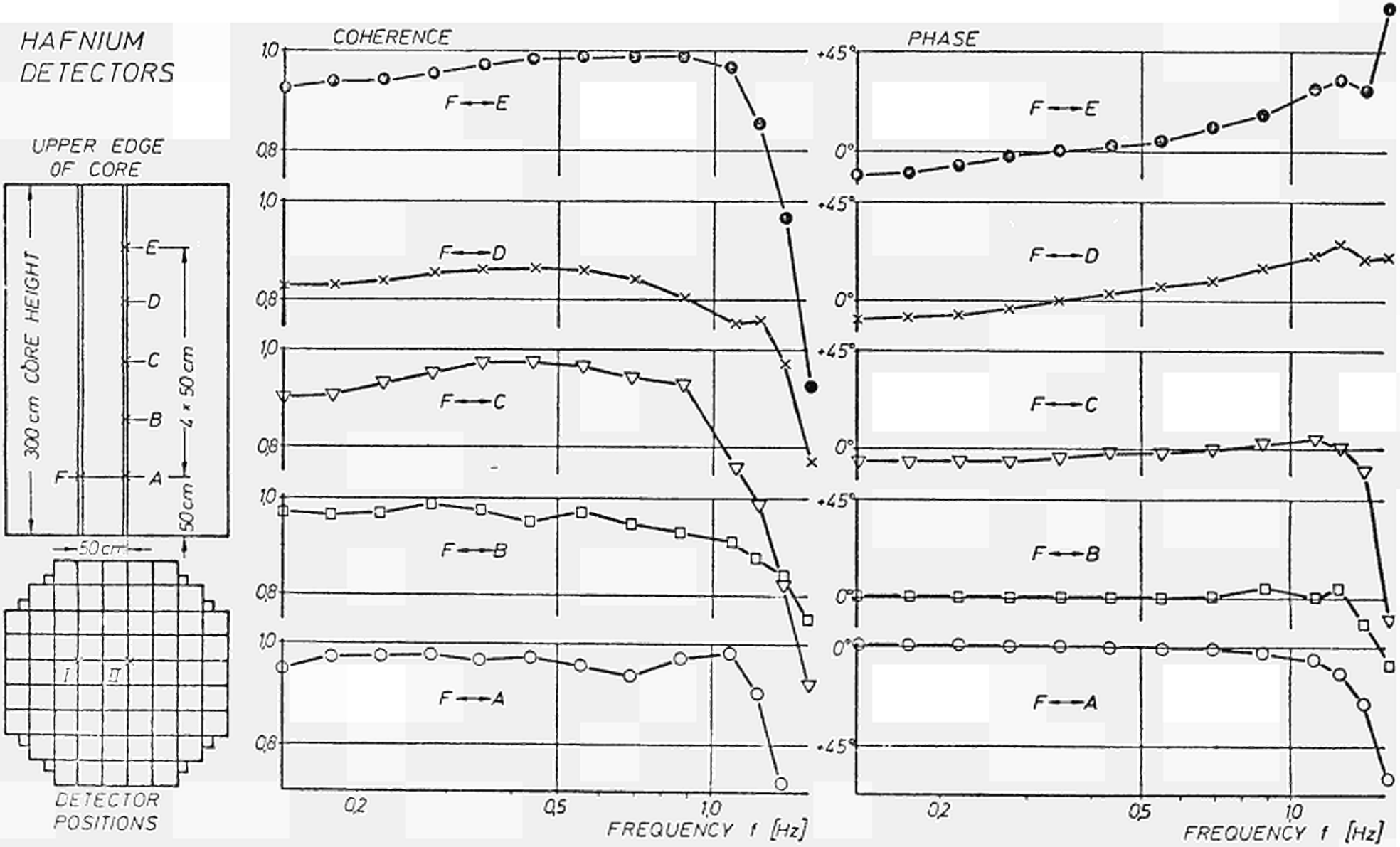

FIG. I.4.1/10 : Coherence and phase for different positions, measured with two Hafnium detectors in the Lingen BWR.

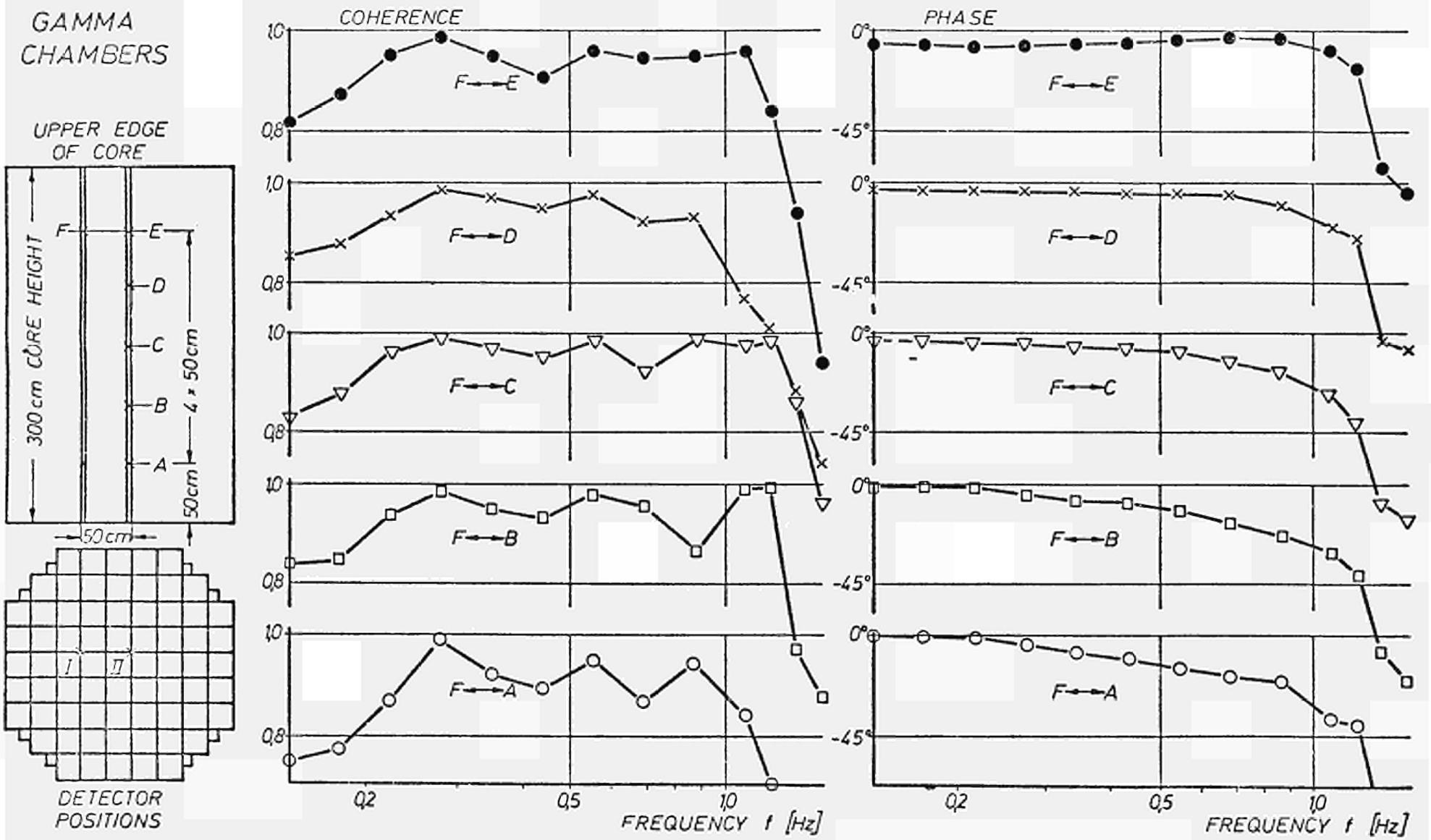

FIG. I.4.1/11 : Coherence and phase for different positions, measured with two in-core gamma chambers in the Lingen BWR.

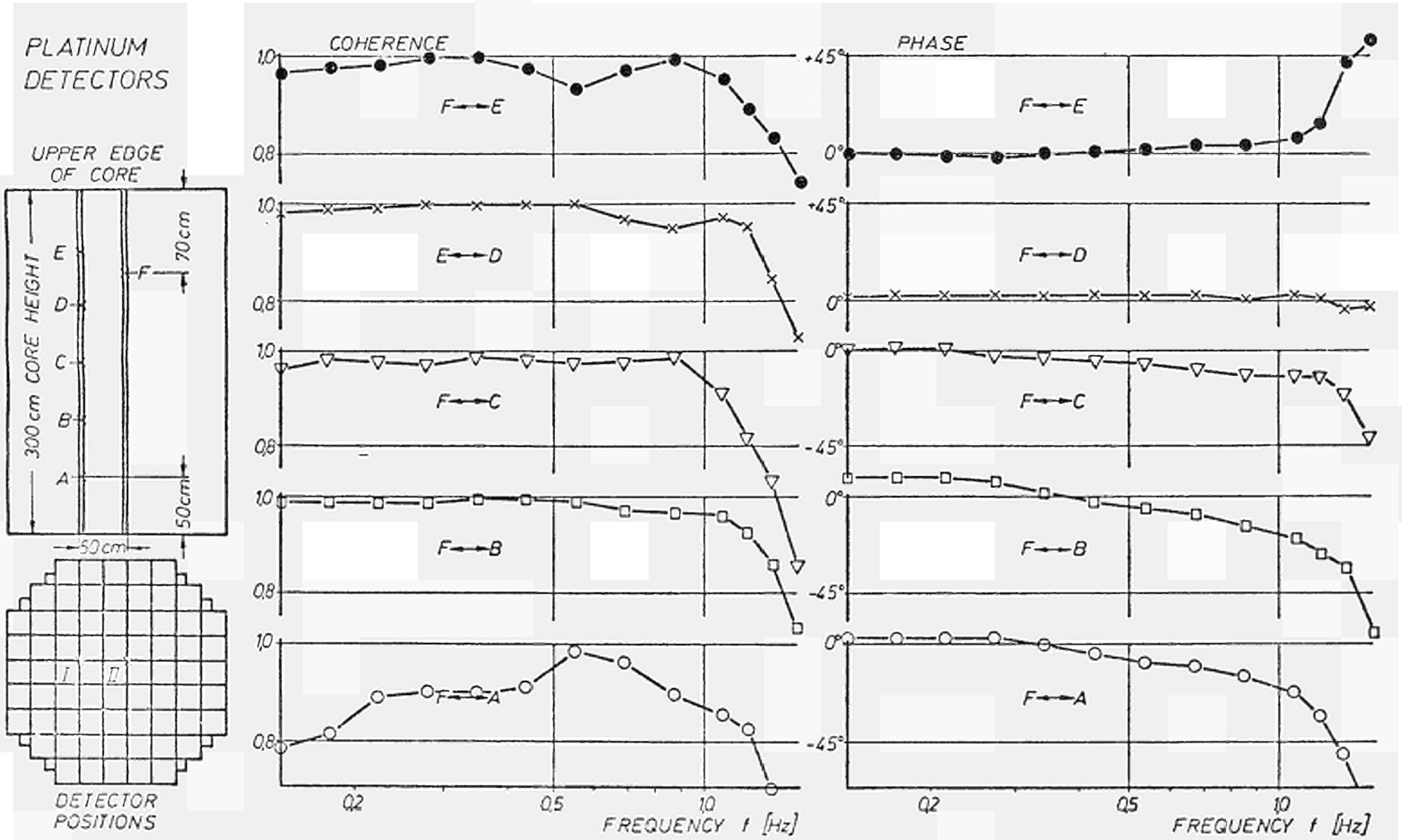

FIG. I.4.1/12 : Coherence and phase for different positions, measured with two Platinum detectors in the Lingen BWR.

I.4.2 Computer Codes for the Prediction of the Vibration Behaviour of Reactor Structures

For the calculation of the dynamic behaviour of structures in the time and frequency domain, there exist various programs, which are partly rather volumenous and complicated (e.g. STARDYNE, ASKA-DYNAM). However, there are no or only few codes of universal character, which are handy and easy to applicate. This posed especially problems when trying to make theoretical studies as a support for the interpretation of noise signals with respect to vibration phenomena. For this reason two programs were developed, which allow to calculate the dynamic behaviour of any structural configuration of not too large size in an universal manner, and which also meet the special requirements for investigations in the context with the loss of coolant accident or earthquake problems. For the latter two purposes the program SWING-R can be preferably used, which takes into account nonlinearities of the structures and friction between the several discrete masses. It calculates the vibrations in the time domain as a consequence of deterministic excitements /1, 2/.

The program EIGEN computes frequency responses of any structures, i.e. the system response as a consequence of deterministic input excitements. However, because of the analogy of the matrix correlations for deterministic and stochastic processes it is also possible to have input signals. It is therefore well suited for the investigation of structure vibrations in power reactors, which are excited by stochastic processes, e.g. pressure fluctuations of the coolant. In addition the presentation of the results in the frequency domain is very practical for comparison with noise measurements, because

they are also given mostly as power density spectra.

I.4.2.1 The Computer Code SWING-R

The program calculates the course of the space-, velocity- and acceleration-coordinates of multi-mass systems with 10 degrees of freedom. The mode of discretisation of the system is not important, e.g. the mass matrix for the simulation of continuously distributed masses can be obtained according to the methods of "lumped-mass representation" or "equivalent-mass matrix" /3/.

The vector differential equation of the entire system

$$[M]\ddot{\underline{x}} + [C]\dot{\underline{x}} + [K]\underline{x} = \underline{f}(t)$$

is transferred in the space of state variables

$$\dot{\underline{Y}} = [A]\underline{Y} + \underline{F}(t);\ [A] = \begin{vmatrix} 0 & I \\ -M^{-1}K & -M^{-1}C \end{vmatrix};\ \underline{F}(t) = \begin{Bmatrix} 0 \\ M^{-1}f(t) \end{Bmatrix}$$

and can then directly be integrated, presumed the vector of the exciting forces is composed of the single exciting forces available in digital form. The solution is /1/, /4/:

$$\underline{Y}_{t+\Delta t} = [\Phi_1]\,\underline{Y}_t + [\Phi_2]\,\underline{F}_t + [\Phi_3]\underline{F}_{t+\Delta t}$$

with the transition matrix $[\Phi_1] = [e^{A\Delta t}]$ and the exciting matrices of the digital power vector (polygonal presentation) $[\Phi_1]$, $[\Phi_2]$, ...

The advantages of this method (time history analysis or matrix exponential method) are:

- for the solution of the equation systems it is not necessary to know the eigenvalues and the eigenvectors

- the dampings which cannot be neglected can be considered exactly without additional expense of calculation.

In order to introduce nonlinearities (the time history analysis is the only method to introduce them with reasonable expense), e.g. nonlinear springs are piece by piece approximated by linear springs, whereby - according to the state of tension of the spring - the calculation is based on the momentary relevant value of the spring stiffness. Friction between two solid masses creates a strong expressed nonlinearity, because it approximately represents a constant extern power during the state of sliding friction, whereas it acts as variable interne power during the state of static friction reducing by one the degrees of freedom of the system.

For the calculation of such processes a formalism was developed for the program SWING-R, which makes possible to determine the momentary state of friction of mass pairs and to determine the transition of the sliding friction to the static friction and vice versa. Those friction processes are of interest for instance for the vibration behaviour of fuel rods.

I.4.2.2 The Computer Code EIGEN

For application in deterministic processes the program calculates the frequency response of linear systems up to 10 degrees of freedom. The vector differential equation of the entire system

$$[M]\ddot{\underline{x}} + [C]\dot{\underline{x}} + [K]\underline{x} = h^{(1)} \cos \Omega t + h^{(2)} \sin \Omega t$$

leads to the input/output relation for the quasi-stationary state

$$\underline{g}(\Omega) = [F(i\Omega)]\,\underline{h}$$

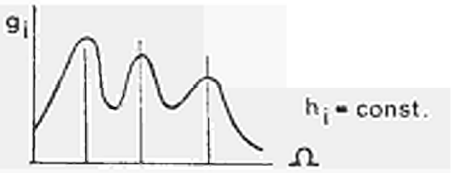

Hence the frequency responses of the outputs g_i with their resonances and interferences can be calculated, when the deterministic input excitement $\underline{h}$ is known. Therefore the frequency behaviour of the system is known without calculating the eigenvalues.

Squaring the equation of the input/output relation according to the rules of the vector analysis by taking the dyadic vector product one achieves:

$$\underline{g} = [F]\cdot\underline{h};\ \underline{g}^T = \underline{h}^T\cdot[F^T];\ \underline{g}\underline{g}^T = [F]\cdot\underline{h}\cdot\underline{h}^T\cdot[F^T]$$

$$[g^*] = [F]\cdot[h^*]\cdot[F^T]$$

The analogy of this expression with the input/output relation for the stochastic excitement

$$[S_{ya}(\Omega)] = [F(i\Omega)]\cdot[S_{ye}(\Omega)]\cdot[F^T(i\Omega)]$$

demonstrates, that the determination of the frequency response for a deterministic excitement can be used also for the calculation of the output auto-power density spectra of a linear system, if the input excitement is given as a power density matrix. The conditions for this kind of calculation are fulfilled, when the input power spectral density matrix is formed by a stochastic process of one source only. Whether a similar analogy can be used for a vibration excitement consisting of several noise sources is still to be checked separately. The code is not yet completely finished.

According to the methods demonstrated above it was tried to perform a model calculation in order to trace back

theoretically the measured pressure fluctuations of the coolant and the measured movements of the pressure-vessel/ core barrel system /5/. The results were promising (see I.3.4).

Literature, Section I.4.2

/1/ Österle, B.
SWING-R, ein digitales Rechenprogramm zur Bestimmung des zeitlichen Verlaufes der Bewegungszeiten von Mehrmassensystemen unter Berücksichtigung von Nichtlinearitäten und Festkörperreibung
MRR 127, Juli 1973

/2/ Österle, B.
SWING-R, ein digitales Rechenprogramm zur Bestimmung des zeitlichen Verlaufes der Bewegungszeiten von Mehrmassensystemen unter Berücksichtigung von Nichtlinearitäten und Festkörperreibung (Programmbeschreibung)
MRR-P-6, Oktober 1973

/3/ Przemieniecki, J.S.
Theory of Matrix Structural Analysis
McGraw-Hill, 1968

/4/ Stoddart, W.C.T.
Transient Response of Linear Elastic Structures Determined by the Matrix Exponential Method
Paper E1/6, First International Conference on Structural Mechanics in Reactor Technology, Berlin 1971

/5/ Österle, B., Kim, J.D., Stölben, H.
Experimental and Theoretical Investigations of Flow-Induced Vibrations in Nuclear Components for Pressurized Water Reactors
Paper 527, International Symposium on Vibration Problems in Industry, Keswick, England, April 1973

I.4.3 Modern Identification Methods for the Investigation of Reactor Structure Part Dynamics

For the analysis of linear dynamic systems with stochastic input and output signals, preferably so called black box identification methods have been used so far. The information on the investigated system was achieved from the measured signals by means of the correlation or the covariance functions, by means of the power spectra, the coherence- and probability density functions, the statistical parameters, etc. /1/, /2/, /3/, /4/, /5/, /6/. However, the results gained with these methods were only suitable for the identification of parameters of simple systems (e.g. single input/output systems) and in addition had, for the most cases, empirical character.

In order to get results on the dynamic behaviour of complicated systems (e.g. multiple input/output systems), and especially of the magnitude of the parameters, it is necessary to establish adequate mathematical models. The modern identification methods are based upon optimal strategies, which are adapting the developed mathematical model to the actual physical system by means of the existing measurements and a certain a priori information on the system. In the ideal case equivalence of the two structures can be achieved. The basic work on these methods was done by R.E. Kalman and R.S. Bucy /7/, /8/ in the years 1960/61.

In the most cases a presentation of the mathematical model in the state space is chosen, because then differential equations of the first order are achieved. In addition recursive calculation methods are available, which permit reasonable solution time and memory size of the digital computer. Depending on the choice of identification algo-

rithms also presentations in the z-space are possible.

An attempt to applicate the modern identification methods to the vibration behaviour of the reactor vessel/core barrel system of the STADE Nuclear Power Plant was made in /9/, /10/. The model was based upon the knowledge of the pendular behaviour of these structure parts. It described pendular movements in any radial direction and in addition separate vertical movements of the vessel and the barrel (fig. I.4.3/1). However, the practical application mainly suffered from the fact, that there were not available sufficient measurement signals. A special difficulty was also posed by the calculation of the exciting forces from the measured pressure signals.

All these problems are briefly discussed in I.3.4.2. The analysis is going on, the next step being to define a simpler case, e.g. in order to avoid restrictions by lacking measuring signals. The process model and the observation model developed so far are given below, whereby an introductionary part shortly outlines the basic problem posed when identifying system-states and parameters.

I.4.3.1 Identification of System States and Parameters Basic Problem

I.4.3.1.1 Modelling of the System

The global structure of the investigated system is given by the physical-mathematical equations. However, it is basically no trivial task to establish the model equations. Generally these are nonlinear, time variant or/and partial differential equations.

Having set up adequate model equations they are lineari-

zed and reduced (see fig. I.4.3/2). The state space presentation of the dynamic system is described by the linear stochastic vector differential equation

$$\dot{\underline{x}}(t) = F(t)\underline{x}(t) + G(t)\ \underline{w}(t) \qquad (1)$$

$\underline{x}(t)$	n x 1	state vector
$\underline{w}(t)$	r x 1	noise vector (process noise)
$F(t)$	n x n	system matrix
$G(t)$	n x r	input matrix

Further on the following statistical parameters are assumed to be known:

$$E\left\{\underline{w}(t)\right\} = \underline{0}$$

$$E\left\{\underline{w}(t)\underline{w}^T(\tau)\right\} = Q(t)\,\delta_D(t-\tau)$$

$$E\left\{\underline{x}(t_o)\right\} = \underline{x_o}$$

$$E\left\{(\underline{x}(t_o)-\underline{x_o})\ (\underline{x}(t_o)-\underline{x_o})^T\right\} = P_o$$

$$E\left\{\underline{w}(t)\underline{x}^T(t_o)\right\} = 0$$

$Q(t)$ is a (rxr) symmetrical positive semidefinite matrix, whose elements are representing the covariances of the process noise. P_o is the (nxn) variance matrix of the state vector, for $t = t_o$.

Approximating the continuous process model one gets the discrete model; i.e. the difference equation

$$\underline{x}(k+1) = \Phi(k)\underline{x}(k) + \Gamma(k)\ \underline{w}(k) \qquad (2)$$

with the following approximative correlations:

$$\Phi(k) \simeq I+F(t_k)\Delta t \qquad \text{(transition matrix)}$$

$$\Gamma(k) \simeq G(t_k)\Delta t$$

$$Q(k) \simeq \frac{Q(t_k)}{\Delta t}$$

I.4.3.1.2 Modelling of the Observation (Measurement) Model

Besides the development of the process model it is also necessary to verify the observation model. The corresponding model equation is a linear combination of the state variables and the measurement noise:

$$\underline{z}(t) = H\underline{x}(t) + \underline{v}(t) \qquad (3)$$

$\underline{z}(t)$	m x 1	measurement vector
$\underline{v}(t)$	m x 1	noise vector (measurement noise)
H	m x n	observation matrix

$$E\left\{\underline{v}(t)\right\} = \underline{0}$$

$$E\left\{\underline{v}(t)\underline{v}^T(\tau)\right\} = R(t)\ \delta_D(t-\tau)$$

$$E\left\{\underline{w}(t)\underline{v}^T(t)\right\} = 0$$

$$E\left\{\underline{x}(t)\underline{v}^T(t)\right\} = 0$$

The (mxm) covariance matrix R(t) of the measurement noise is positive definite.

In discrete presentation we get

$$\underline{z}(k) = H\underline{x}(k) + \underline{v}(k)$$

The observation matrix H contains a priori information on the properties of the whole measurement chain (sensors, amplifiers, etc). It may be necessary to perform an adequate

management of the measurement data in order to compensate the various influences of the measurement chains. Of course this presupposes the knowledge of the dynamic behaviour of the various measurement devices (e.g. the frequency response).

I.4.3.1.3 Observability, Controllability, Stability and Identifiability of the Process- and Observation Model

Suppositions for the regularity - especially the asymptotic behaviour - of the optimal filter and the accompaning Riccati-equation are the observability and the controllability of the system /11/. Necessary conditions for the regular behaviour are:

a) Q and P_o positive semidefinite

b) R positive definite

c) F(t), G(t), H, Q(t), R(t) restricted steady functions (Lipschitz-condition)

The system /F(t), H/ is equally and completely R-observable when the information matrix

$$I(t,t_o) = \int_{t_o}^{t} \Phi^T(\tau,t_o) H^T(\tau) R^{-1}(\tau) H(\tau) \Phi(\tau,t_o)\, d\tau \qquad (4)$$

is positive definite, with the transition matrix $\Phi(\tau,t_o)$.

For time invariant systems the condition of the observability can be replaced by the following simpler form

$$\text{rank}\ (Q_B) = n \qquad (5)$$

with

$$Q_B = \left[H^T \mid F^T H^T \mid F^T{}^2 H^T \mid \ldots \mid F^T{}^{n-1} H^T \right] \qquad (6)$$

and n ... dimension of the state vector

The fundamental importance of the equations (4), (5) is demonstrated by the fact, that the variance of the estimation errors of all state variables can be only reduced by means of the measurements, if the system is completely observable.

The question of the filter stability and of the Riccati-equation is strongly linked to the controllability of the process through $\underline{w}$. Assuming all preceeding suppositions (regularity, R-observability) are fulfilled, a sufficient experimental asymptotic stability of the algorithm is the Q-controllability of the /F(t), G(t)/-system.

$$C_Q(t_o,t_1) = \int_{t_o}^{t_1} \Phi(t_1,\tau) G(\tau) Q(\tau) G^T(\tau) \Phi^T(t_1,\tau) d\tau > 0 \qquad (7)$$

consequently we get for time invariant matrices

$$\text{rank} \quad (Q_s) = n \qquad (8)$$

$$\text{with} \qquad Q_s = \left[G \mid FG \mid F^2G \mid \ldots \mid F^{n-1}G \right] \qquad (9)$$

When the process model is stable, it is not necessary to demonstrate the Q-controllability. Condition (7) means, that the noise $\underline{w}$ is contributing to the stability of the optimal filter. Hence, for small noise contributions and additional modelling errors, the optimal filter need not be necessary stable. The proof of the filter stability and of the Riccati-equation can be performed by means of the Ljapunov function of the quadratic type /12/.

The criteria of local identifiability of linear dynamic systems with a set of unknown parameters are dealing with the questions, if such a set of parameters is at all identifiable. For more details it is referred to literature /13/, /14/.

I.4.3.1.4 A priori Information

For many of the known identification algorithms it is necessary to have an a priori information on the initial conditions of the states and parameters, and on the covariance matrices of the process- and measurement noise and of the variance matrix of the state estimation error. This is important especially in context with the amount of iteration steps and with the eventually only sub-optimal filter behaviour. Therefore it seems reasonable to gain those informations by means of "classical" methods (correlations, statistical parameters, etc.).

For the pre-estimation of parameters in general least square methods are used besides the know-how of the designer of the investigated system. An additional important question is the adequate choice of the system order. For this various process procedures can be used (polynomial test, statistical F-test, etc.), and the proof, that the innovations of the Kalman-filter represent white noise /15/.

I.4.3.1.5 Identification Algorithms

From the literature many state estimation algorithms are known. However, up to now it is not possible, to find general information on the choice and the quality of the various algorithms for general systems. The best known algorithms are:

- Least square estimation (LS)
- Generalized LS estimation (GLS)
- Instrumental variable method (IV)
- Maximum likelihood algorithm (ML)
- Maximum a posteriori algorithm (MAP), (Bayes updating)
- Monte Carlo methods

In order to gain the estimation values, it must generally be distinguished between: prediciton, filtering, smoothing. In this report we deal only with filtering problems.
In addition the following conditions should be fulfilled for the estimation algorithms:

- unbiased estimator
- consistent estimator
- efficient estimator
- sufficient estimator

The choice of the algorithm is dependent on the system size and on the other considerations with respect to cost and expense (computation time etc.). It can be also necessary to apply several algorithms in parallel.

In the context with the least square (LS), the maximum likelihood (ML) and other methods the problem of minimization of a quality criterion for the parameter estimation is arising. Besides the gradient procedures of the 1st and 2nd order the following methods can be used /16/, /17/, /18/:

- Conjugate gradient method (and modifications /18/)
- Newton-Raphson method
- Modified Newton-Raphson method
- etc.

and:

- Direct search techniques
- Random search techniques
- etc.

The identification task can be devided into two parts, the a priori knowledge on the structure and the a posteriori knowledge on the measurements. Fig. I.4.3/2 shows the basic identification procedure.

I.4.3.2 Dynamic Model of the Vibrating Reactor Vessel Internals of the STADE Nuclear Power Plant

I.4.3.2.1 The Process Model

In this chapter a dynamic model is developed, which describes in the state space the pressure vessel and the core barrel vibrations. These structure parts connected via the clamping on the lid flange represent the coupled two-mass-system. For the description of the movement the Lagrange-formulism is used. The Lagrange-equations of the 2nd type are:

$$\frac{d}{dt}\frac{\partial L}{\partial \dot{q}_i} - \frac{\partial L}{\partial q_i} = Q_i \qquad (10)$$

$$i = 1(1)n$$

$$L = T - V - D \qquad (11)$$

T ... kinetic energy
V ... potential energy
D ... dissipative energy
Q ... exciting forces
q_i and $\dot{q}_i$ are the general coordinates, the special ones are introduced according to fig. I.4.3/3

Assuming small amplitudes we get for the

Kinetic Energy

$$T = \frac{1}{2}\theta_{db}(\Delta\dot{\alpha}^2+\Delta\dot{\beta}^2) + \frac{1}{2}\theta_{kb}\left[(\Delta\dot{\alpha}+\Delta\dot{\gamma})^2 + (\Delta\dot{\beta}+\Delta\dot{\delta})^2\right] + \frac{1}{2}M_{db}\Delta\dot{Z}_d^2 + \frac{1}{2}M_{kb}(\Delta\dot{z}_k+\Delta\dot{z}_d)^2 \qquad (12)$$

M_{db}, M_{kb} ... masses of the pressure vessel and core barrel

θ_{db}, θ_{kb} ... moments of inertia of the pressure vessel and the core barrel with respect to the axis 0_d, 0_k

Potential Energy

The amplitudes $s_{d,i}$ and $s_{k,i}$ are in the plain

$$s_{d,i} = \Delta\alpha x_i + \Delta\beta y_i + \Delta z_d$$
$$s_{k,i} = \Delta\gamma x_i + \Delta\delta y_i + \Delta z_k$$

For the potential energy we get

$$V = -\frac{1}{2}\sum_{i=1}^{N} c_{d,i}\,(\Delta\alpha x_i+\Delta\beta y_i+\Delta z_d) - \tag{13}$$
$$-\frac{1}{2}\sum_{i=1}^{N} c_{k,i}\,(\Delta\gamma x_i+\Delta\delta y_i+\Delta z_k)$$

$c_{d,i}$ $c_{k,i}$ ... spring constants

N ... number of springs

x_i, y_i ... coordinates of the springs

Dissipative Energy

Assuming that for small amplitudes, x_i, y_i are independent from time, we get for the dissipative energy

$$D = -\frac{1}{2}\sum_{i=1}^{N} d_{d,i}(\Delta\dot{\alpha} x_i+\Delta\dot{\beta} y_i+\Delta\dot{z}_d)^2 - \tag{14}$$
$$-\frac{1}{2}\sum_{i=1}^{N} d_{k,i}(\Delta\dot{\gamma} x_i+\Delta\dot{\delta} y_i+\Delta\dot{z}_k)^2$$

$d_{d,i}$ $d_{k,i}$ ... damping constants

Exciting Forces

For the excitement of the pressure vessel and core barrel vibrations, especially hydrodynamic processes have to be considered. Therefore it seems reasonable to formulate the exciting forces as linear combination of the pressure fluctuations and their derivations, measured at the inlet and the outlet of the vessel and at the lower support grid.

The exciting forces are formulated as follows (fig. I.4.3/4):

$$\underline{Q} \equiv \begin{bmatrix} Q_{d,x} \\ Q_{d,y} \\ Q_{d,z} \\ Q_{k,x} \\ Q_{k,y} \\ Q_{k,z} \end{bmatrix} = \begin{bmatrix} A_d \\ A_k \end{bmatrix} \cdot \begin{bmatrix} \Delta p_1 \\ \Delta p_2 \\ \Delta p_3 \end{bmatrix} + \begin{bmatrix} B_d \\ B_k \end{bmatrix} \cdot \begin{bmatrix} \dot{\Delta p}_1 \\ \dot{\Delta p}_2 \\ \dot{\Delta p}_3 \end{bmatrix} \qquad (15)$$

whereby the matrices A_d, A_k, B_d, B_k are considered as unknowns.

The equation (15) is valid only when assuming the pressure deviations Δp_1, Δp_2, Δp_3 and their derivations deliver sufficient information about the exciting forces. For the quasi stationary case we write according to the action-reaction-principle:

$$A_d = -A_k \qquad B_d = -B_k$$

After using the equations (15), (14), (13) and (12) in connection with the initial equation (10), performing algebraic reconfiguration and making the assumption,

that the time behaviour of vector $\underline{\Delta p}$ can be described by a system of 2nd order differential equations, we get the following stochastical vector differential equation

$$\underline{\dot{x}}(t) = F\underline{x}(t)+G\underline{w}_n \tag{16}$$

with $\underline{x}$ as the state vector

$$\underline{x} \equiv \begin{bmatrix} \underline{\Delta\omega_d} \\ \underline{\Delta\omega_k} \\ \underline{\Delta\varphi_d} \\ \underline{\Delta\varphi_k} \\ \underline{\delta\Delta p} \\ \underline{\Delta p} \end{bmatrix}$$

with the correlations

$$\underline{\Delta\varphi_d} \equiv \begin{bmatrix} \Delta\alpha \\ \Delta\beta \\ \Delta z_d \end{bmatrix} \qquad \underline{\Delta\varphi_k} \equiv \begin{bmatrix} \Delta\gamma \\ \Delta\delta \\ \Delta z_k \end{bmatrix} \qquad \underline{\Delta\omega_d} \equiv \begin{bmatrix} \Delta\dot{\alpha} \\ \Delta\dot{\beta} \\ \Delta\dot{z}_d \end{bmatrix}$$

$$\underline{\Delta\omega_k} \equiv \begin{bmatrix} \Delta\dot{\gamma} \\ \Delta\dot{\delta} \\ \Delta\dot{z}_k \end{bmatrix} \qquad \underline{\Delta p} \equiv \begin{bmatrix} \Delta p_1 \\ \Delta p_2 \\ \Delta p_3 \end{bmatrix} \qquad \underline{\Delta\dot{p}} \equiv \begin{bmatrix} \Delta\dot{p}_1 \\ \Delta\dot{p}_2 \\ \Delta\dot{p}_3 \end{bmatrix} = \delta\Delta p$$

System matrix F:

$$F \equiv \begin{bmatrix} M_1^{-1}D_d & M_{12}^{-1}D_k & M_1^{-1}C_d & M_{12}^{-1}C_k & M_1^{-1}B_d + M_{12}^{-1}B_k & M_1^{-1}A_d + M_{12}^{-1}A_k \\ M_{12}^{-1}D_d & M_2^{-1}D_k & M_{12}^{-1}C_d & M_2^{-1}C_k & M_{12}^{-1}B_d + M_2^{-1}B_k & M_{12}^{-1}A_d + M_2^{-1}A_k \\ I & 0 & 0 & 0 & 0 & 0 \\ 0 & I & 0 & 0 & 0 & 0 \\ 0 & R_\omega & 0 & Q_\varphi & R_\delta & Q_p \\ 0 & 0 & 0 & 0 & I & 0 \end{bmatrix}$$

Input matrix G and white noise vector $\underline{w}_n$:

$$G \cdot \underline{w}_n = \begin{bmatrix} \underline{0} \\ \underline{0} \\ \underline{0} \\ \underline{0} \\ \underline{w} \\ \underline{0} \end{bmatrix} = \begin{bmatrix} 0 & & & & & \\ & 0 & & & 0 & \\ & & g_{13,13} & & & \\ & & & g_{14,14} & & \\ & 0 & & & g_{15,15} & \\ & & & & & 0 \end{bmatrix} \cdot \begin{bmatrix} \underline{0} \\ \underline{0} \\ \underline{0} \\ \underline{0} \\ \underline{w_n} \\ \underline{0} \end{bmatrix}$$

2nd order differential equations for $\underline{\Delta p}$:

$$\delta \Delta p = R_\delta \delta \underline{\Delta p} + R_\omega \underline{\Delta \omega_k} + Q_p \underline{\Delta p} + Q_\varphi \underline{\Delta \varphi_k} + \underline{w} \qquad (17)$$

with

$$\underline{\delta \Delta p} = \underline{\Delta \dot{p}} \qquad \underline{w} = \begin{bmatrix} w_1 \\ w_2 \\ w_2 \end{bmatrix} \qquad \underline{\Delta \omega_k} = \begin{bmatrix} \Delta \dot{\gamma} \\ \Delta \dot{\delta} \\ \Delta \dot{z}_k \end{bmatrix} \qquad \underline{\Delta \varphi_k} = \begin{bmatrix} \Delta \gamma \\ \Delta \delta \\ \Delta z_k \end{bmatrix}$$

R_δ, R_ω, Q_p, Q_φ are the model matrices for the presentation of $\underline{\Delta p}$

The following definitions are used:

M (M_1, M_2, M_{12}) - mass matrix containing the moments of inertia and masses

D (D_k, D_d) - damping matrix containing the products and sums of the damping constants and the amplitudes

C (C_k, C_d)	-	spring matrix containing the products and sums of the spring constants and of the amplitudes
A (A_k, A_d)	-	input matrix, see equ. (15)
B (B_k, B_d)	-	input matrix, see equ. (15)
I	-	identity matrix

Discretisation of the Process Model

Assuming the vector $\underline{w}_n(t)$ becomes constant in the intervall $k\,\Delta t$, $(k+1).\Delta t$, we get as the solution of equation (16) the transformation equation:

$$\underline{x}(k+1) = \Phi(\Delta t)\underline{x}(k)+\Gamma(\Delta t)\underline{w}_n(k) \qquad (18)$$

$\Phi(\Delta t)$ and $\Gamma(\Delta t)$ according to the relations in equ. (2).

Because the vector $\underline{w}_n(k)$ is white noise, equation (18) represents the Markoff-process model.

I.4.3.2.2 The Observation Model

The relation between the measurement variables and the state variables are described by the observation model. Assuming, only the deviations $\Delta\varphi_d$, $\Delta\varphi_k$ and Δp were measured we get for the observation model:

$$\underline{z}(k) = H\underline{x}(k) + \underline{v}(k) \qquad (19)$$

with

$$\underline{z}(k) = \begin{bmatrix} \underline{\Delta\varphi_d} \\ \underline{\Delta\varphi_k} \\ \underline{\Delta p} \end{bmatrix}$$

$$H = \begin{bmatrix} 0 & 0 & I & 0 & 0 & 0 \\ 0 & 0 & 0 & I & 0 & 0 \\ 0 & 0 & 0 & 0 & 0 & I \end{bmatrix}$$

$$\underline{v}(k) = \begin{bmatrix} \underline{v}_1 \\ \underline{v}_2 \\ \underline{v}_3 \end{bmatrix}$$

I.4.3.2.3 Identification Methods

In equation (16) we find the time invariant block matrices F and G, which contain, from the point of view of system identification, the unknown parameters. The unknown elements of the block matrices F, G are the matrices C, D, A, B, R, Q, G. The mass matrix M can be obtained from the geometry and the masses of the structure.

The identification problem is formulated as follows: Based upon the measurement signals of the vectors $\underline{\Delta\varphi}_d$, $\underline{\Delta\varphi}_k$, $\underline{\Delta p}$ a consistant and asymptotic-efficient estimation of the elements of the matrices C, D, A, B, R, Q, G is to be done. As already indicated in I.4.2.2 an adequate start model (a priori information) is the supposition for the convergence of the ML- and MAP-estimation procedures. For the estimation of the initial values the LS-method is used beginning with equation (17). For the estimation we get

$$\hat{\underline{u}} = (L^T L)^{-1} L^T y_M^*$$

whereby

$$L = \Psi S_N$$

$$y_M^* = \Psi y_N$$

with

$$\Psi = \begin{bmatrix} \alpha I & 0 & 0 \\ 0 & \alpha I & 0 \\ 0 & 0 & \alpha I \end{bmatrix} \qquad \alpha > 1$$

weighting matrix

and after rearrangement of equation (17)

$$\begin{bmatrix} M_1 & M_{12} & 0 \\ M_{12} & M_2 & 0 \\ 0 & 0 & I \end{bmatrix} = \begin{bmatrix} U_{\Delta\omega_d} & 0 & U_{\Delta\varphi_d} & 0 & \tilde{U}_{\delta\Delta p} & 0 & \tilde{U}_{\Delta p} & 0 & 0 & 0 & 0 & 0 \\ 0 & U_{\Delta\omega_K} & 0 & U_{\Delta\varphi_K} & 0 & \tilde{U}_{\delta\Delta p} & 0 & \tilde{U}_{\Delta p} & 0 & 0 & 0 & 0 \\ 0 & 0 & 0 & 0 & 0 & 0 & 0 & 0 & \tilde{U}_{\Delta\omega_K} & \tilde{U}_{\Delta\varphi_K} & \tilde{U}_{\delta\Delta p} & \tilde{U}_{\Delta p} \end{bmatrix} \cdot \underline{u} + \begin{bmatrix} \underline{0} \\ \underline{0} \\ \underline{w} \end{bmatrix}$$

$$\underline{y} = S\underline{u} + \underline{\varepsilon} \qquad (21)$$

Because equation (21) shall be valid for any instant of time $t = k\Delta t$ one gets the following vector differential equation

$$\begin{bmatrix} \underline{y}(1) \\ \vdots \\ \underline{y}(N) \end{bmatrix} = \begin{bmatrix} S(1) \\ \vdots \\ S(N) \end{bmatrix} \cdot \underline{u} + \begin{bmatrix} \varepsilon(1) \\ \vdots \\ \varepsilon(N) \end{bmatrix}$$

$$\underline{y}_N = S_N\underline{u} + \underline{\varepsilon}_N \qquad (22)$$

The structure of equation (17) is to be considered only as a hypothesis. Therefore it is possible that one obtains the matrix $V_\varepsilon = E\left\{\underline{\varepsilon}\ \underline{\varepsilon}^T\right\}$ not in the diagonal shape. This means we get $\underline{\varepsilon}$ as coloured noise. In this case it is necessary to modify the structure of equation (17), e.g. by enlarging the order of the equation and hence bringing V_ε to a diagonal shape.

First of all, the ML identification algorithm shall be used for the solution of the identification problem. Because the process and the estimation model are linear this algorithm is identical to the standard Kalman-filter /11/, /18/, /19/. In order to minimize the cost functions, i.e. in order to gain the unknown parameters, the methods given in I.4.3.1.5 can be applied.

The vector of the unknown parameters is

$$\underline{u}^T = [c_{d,xx}, \ldots, c_{d,zz}, d_{d,xx}, \ldots, d_{d,zz}, c_{k,xx}, \ldots, c_{k,zz},$$
$$b_{d,11}, \ldots, b_{d,33}, a_{d,11}, \ldots, a_{d,33}, \ldots, g_{13}, g_{14}, g_{15}] \quad (23)$$

The calculation algorithm of the ML identification is shown in table I.4.3/1. In fig. I.4.3/5 the structure of the Kalman-filter is presented.

Another possibility for identification is given by modelling the time invariant unknown parameters, i.e. by formulating the difference equation.

$$\underline{u}(k+1) = \underline{u}(k) \quad (24)$$

and by extending the state vector by means of the vector $\underline{u}$. Then the process model gets the following shape

$$\underline{x}'(k+1) = \begin{bmatrix} \underline{x}(k+1) \\ \underline{u}(k+1) \end{bmatrix} = \underline{\Phi}(\underline{x}(k),\underline{u}(k),k)+\Gamma\underline{w}(k) \quad (25)$$

For the identification the invariant imbedding maximum a posteriori (MAP) algorithm according to Sage, Melsa /18/ is used. Then we gain the advantage, that together with the state variables the unknown parameters can be identified directly. A disadvantage is the enlargement of computation expense. In addition it is necessary to have a sufficient a priori information about the parameters which are to be estimated. The invariant imbedding -MAP algorithm is shwon in table I.4.3/2. As demonstrated there, the algorithm is working like the Kalman-filter, however, we find the derivation of the transition vector Φ with respect to the state estimator within the expression for the error variance P(k+1) (Riccati-equation).

For the discussed identification algorithms (ML, MAP) a general applicable digital program was developed. Up to now the dynamic model for the vessel internals (as shown in I.3.4) could not be calculated with one of the two filter algorithms, because still additional investigations are necessary, e.g. the dynamic behaviour of the instrumentation chains, the adequateness of the available measurement signals, the suitability of the pressure signals as a measure for the input sources, etc.

Summarizing it is to be stated, that so far it was only possible to show some global problems when applying modern identification procedures for system analysis and synthesis. It turned out that the required expense is rather large and that it can be reduced only to a certain extent for each new problem. Again we have to remember the difficulties starting with the measurements, the modelling, the model structures and the application of the algorithms. Further on it can be concluded, that even for comparably simple practical problems a rather redundant working procedure is necessary (repeating of measurements, various algorithms, improved model structures). Inspite of these difficulties the possibilities inherent in these methods have to be seen optimistic especially in the light of the identification problems which have been solved already, e.g. in the aircraft and space field. In addition considerable progress to be expected in computer techniques and application theories (e.g./22/).

Literature, Section I.4.3

/1/ Bastl, W., Wach, D., Dio, W.H., Haas, W.
Nachweis von Pendelbewegungen des Kernbehälters im Neutronenflußrauschen
Atomwirtschaft-Atomtechnik, 5. Mai 1972

/2/ Höld, A.
TUMX92 - A Computer Code for Sectional Spectrum Estimation of Large Time Series
MRR 87, Aug. 1972

/3/ Sädtler, E.
Statistische Kennfunktionen und -parameter multipler Input/Output-Systeme (TUMX68)
MRR 134, Febr. 1974

/4/ Wach, D.
Der Informationsgehalt der Rauschsignale von Druckwasserreaktoren im Hinblick auf das Schwingungsverhalten der Druckgefäßeinbauten
MRR 111, April 1972

/5/ Sädtler, E.
DIGCHN - Ein Programm zur Berechnung von Wahrscheinlichkeitsdichtefunktionen und statistischen Parametern stochastischer Signale
MRR-Bericht in Vorbereitung

/6/ Hawickhorst, W.
Auswertung von Schwingungsmessungen an einem Druckwasserreaktor mit einem hybriden Rechenprogramm
LRA Garching (Diplomarbeit)

/7/ Kalman, R.E.
A New Approach to Linear Filtering and Prediction Problems
Journal of Basic Engineering, Vol 82 D, 1960

/8/ Kalman, R.E., Bucy, R.S.
New Results in Linear Filtering and Prediction Theory
Journal of Basic Engineering, Vol 83 D, 1961

/9/ Martancik, J.,
Identifikation des Schwingungsmodells des DWR Stade
Interner Bericht des LRA, Dezember 1972

/10/ Sädtler, E.
Ein allgemeines Rechenprogramm zur Systemidentifikation mit Hilfe des Maximum-Likelihood- und Maximum-a-posteriori Algorithmuses
MRR-Bericht in Vorbereitung

/11/ Kortüm, W.
Lineare Zustandsschätzung
Vortrag auf dem Lehrgang "Grundlagen und Anwendung der Kalman-Filterung"
CCG. e.V., Februar 1973, Oberpfaffenhofen

/12/ Bucy, R.S., Joseph, P.D.
Filtering for Stochastic Processes with Applications to Guidance
Interscience Publ., 1968

/13/ Glover, K., Williams, J.C.
On the Identifiability of Linear Dynamical Systems
Preprints 3rd IFAC Symposium, The Hague, June 1973
"Identification and System Parameter Estimation Part 2"

/14/ Berntsen, H.E., Batchen, J.G.
Identifiability of Linear Dynamical Systems
Preprints, 3rd IFAC Symposium, The Hague, June 1973

/15/ Unbehauen, H., Göhring, B.
Application of Different Statistical Tests for the Determination of the Most Accurate Order of the Model in Parameter Estimation
Preprints, 3rd IFAC Symposium, The Hague, June 1973

/16/ Larson, R.E.
Applications of Nonlinear Filtering Techniques to Aerospace Vehicle Tracking and Parameter Identification
Nato Summer School, Toulouse, July 1972

/17/ Analyse und Synthese dynamischer Systeme
- Optimierung stochastischer Systeme
Kursmaterialien zur Automatisierung, TU Berlin Nr. 17

/18/ Sage, A.P., Melsa, J.L.
System Identification
Academie Press, New York, 1971

/19/ Sage, A.P., Melsa, J.L.
Estimation Theory with Applications to Communications and Control
McGraw-Hill Book Company, New York, 1971

/20/ Bauernfeind, V., Dio, W.H., Pink, W.
Importance and Use of In-core Vibration and Pressure Measurements for Determination of Correct Behaviour of Pressure Vessel Internals
IAEA-Symposium IAEA/SM-168/A-4, Prague, Jan. 1973

/21/ Young, P.C.
Lectures on Parameter Estimation
Nato Summer School, Toulouse, July 1973

/22/ Identification and System Parameter Estimation Part 1 and 2
3rd IFAC Symposium, The Hague, June 1973

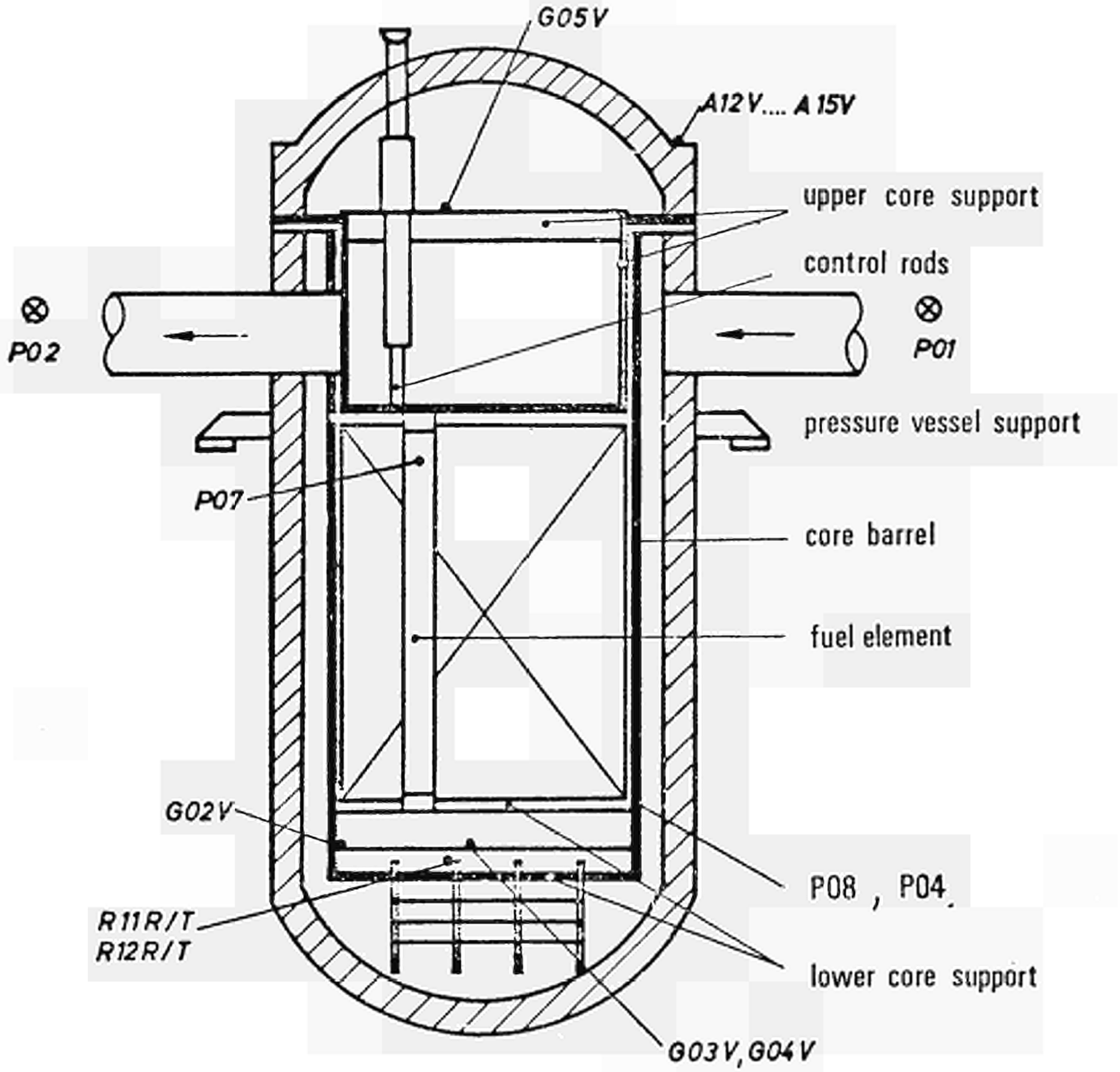

P01...P08	Pressure transducers
G02V...G05V	Vibration velocity sensors of core support structures
A12V...A15V	Absolute displacement sensors pressure vessel
R11R/T, R12R/T	Relative displacement sensors pressure vessel/core barrel

Fig. I.4.3/1: STADE Nuclear Power Plant, Main Structure Parts and Position of Sensors

message model	$\underline{x}(k+1) = \Phi \underline{x}(k) + \Gamma \underline{w}(k)$
observation model	$\underline{z}(k) = H\underline{x}(k) + \underline{v}(k)$
prior statistics	$E\{\underline{w}(k)\} = \underline{0}$ $\quad cov\{\underline{w}(k), \underline{w}(j)\} = V_w(k)\delta_K(k-j)$ $E\{\underline{v}(k)\} = 0$ $\quad cov\{\underline{v}(k), \underline{v}(j)\} = V_v(k)\delta_K(k-j)$ $E\{\underline{x}(0)\} = \underline{x}_0$ $\quad var\{\underline{x}(0)\} = V_{x_0}$ $\quad j \geq k$ $cov\{\underline{w}(k), \underline{v}(k)\} = cov\{\underline{x}(k), \underline{v}(k)\} = cov\{\underline{x}(k), \underline{w}(j)\} = 0$
filter algorithm	$\hat{\underline{x}}(k+1, \underline{u}) = \hat{\underline{x}}(k+1\|k, \underline{u}) + K(k+1)\left[\underline{z}(k+1) - H\hat{\underline{x}}(k+1\|k, \underline{u})\right]$
one-stage prediction algorithm	$\hat{\underline{x}}(k+1\|k, \underline{u}) = \Phi \hat{\underline{x}}(k, \underline{u})$
filter gain algorithm	$K(k+1) = V_{\tilde{x}}(k+1, \underline{u}) H^T V_v^{-1}(k+1)$
filter prior error variance algorithm	$V_{\tilde{x}}(k+1\|k, \underline{u}) = \Phi V_{\tilde{x}}(k, \underline{u}) \Phi^T + \Gamma V_w(k) \Gamma^T$
filter error variance algorithm	$V_{\tilde{x}}(k+1, \underline{u}) = V_{\tilde{x}}(k+1\|k, \underline{u}) - V_{\tilde{x}}(k+1\|k, \underline{u}) H^T \left[H V_{\tilde{x}}(k+1\|k, \underline{u}) H^T + V_v(k)\right]^{-1} H V_{\tilde{x}}(k+1\|k, \underline{u})$
maximum likelihood identification cost function	$J = \frac{1}{2} \sum_{k=k_1}^{k_f} \left[\ln \det V_{\underline{z}}(k\|k-1, \underline{u}) + \left\| \underline{z}(k) - H\hat{\underline{x}}(k\|k-1, \underline{u}) \right\|^2_{V_{\underline{z}}^{-1}(k\|k-1, \underline{u})} \right]$ $V_{\underline{z}}(k\|k-1, \underline{u}) = V_v(k) + H V_{\tilde{x}}(k\|k-1, \underline{u}) H^T$
filter initial conditions	$\hat{\underline{x}}(0\|0, \underline{u}) = x_0$ $V_{\tilde{x}}(0\|0, \underline{u}) = V_{x_0}$

Table I.4.3/1: Discrete Kalman-filter algorithm

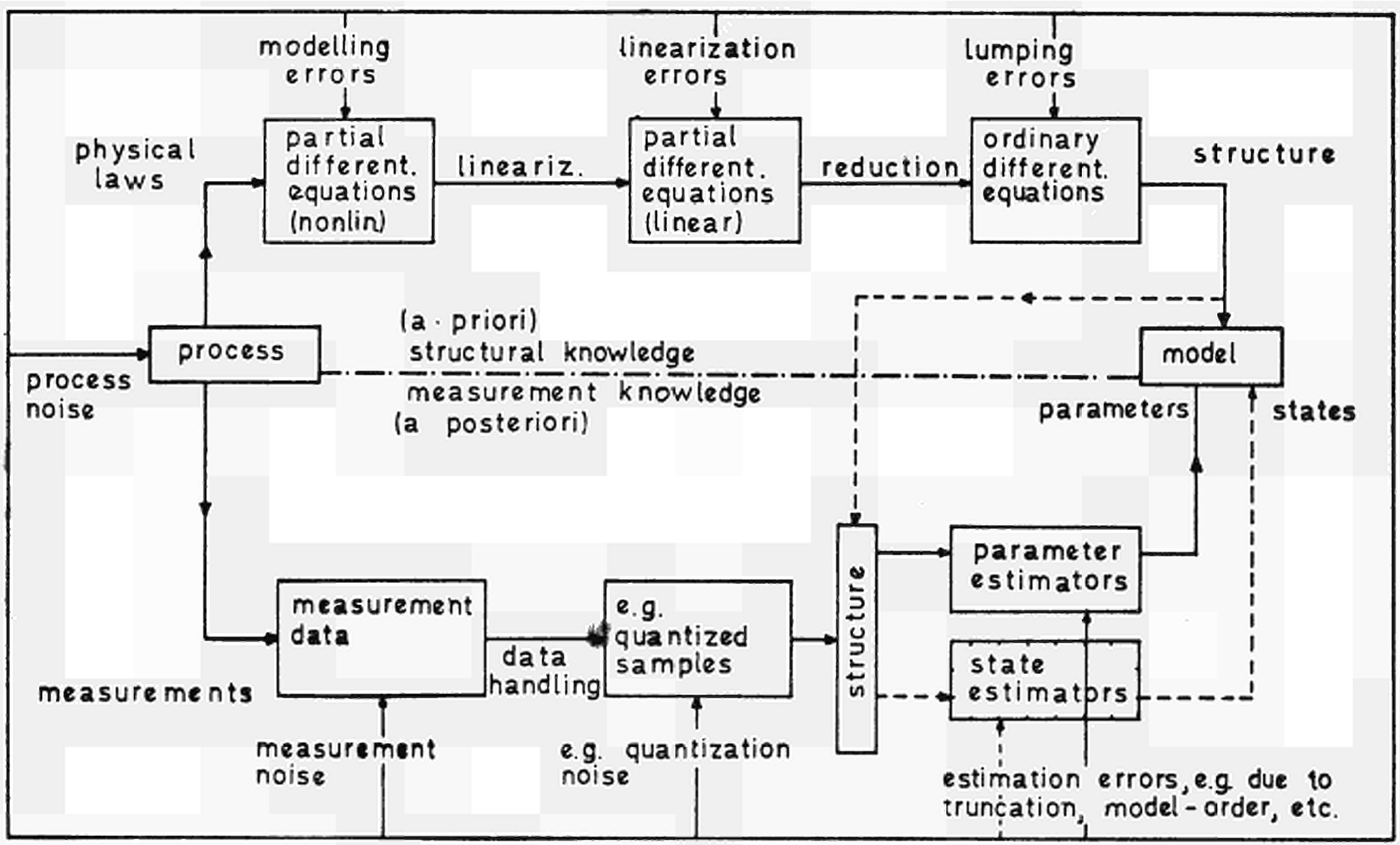

Fig.I.4.3/2: Identification Task according to P. Eykhoff, Tutorials 3rd IFAC Symposium, The Hague, June 1973

system model	$\underline{x}(k+1) = \phi[\underline{x}(k),k] + \Gamma[\underline{x}(k),k]\,\underline{w}(k)$
observation model	$\underline{z}(k) = H(k)\,\underline{x}(k) + \underline{v}(k)$
statistical parameters	$E\{\underline{x}(k_o)\} = \underline{x}_o \qquad \mathrm{var}\{\underline{x}(k_o)\} = V_{x_o}$ $E\{\underline{w}(k)\} = \underline{0}$ $E\{\underline{v}(k)\} = \underline{0}$ $\mathrm{cov}\{\underline{w}(k), \underline{w}(j)\} = V_w(k)\,\delta_K(k-j)$ $\mathrm{cov}\{\underline{v}(k), \underline{v}(j)\} = V_v(k)\,\delta_K(k-j) \qquad j \geq k$
one-stage predictor	$\hat{\underline{x}}(k+1\|k) = \phi[\hat{\underline{x}}(k),k]$
filter algorithm	$\hat{\underline{x}}(k+1) = \hat{\underline{x}}(k+1\|k) + K(k+1)\left[\underline{z}(k+1) - H(k+1)\hat{\underline{x}}(k+1\|k)\right]$ $K(k+1) = P(k+1)\,H^T(k+1)\,V_v^{-1}(k+1)$
prior variance algorithm	$P(k+1\|k) = \Gamma[\hat{\underline{x}}(k),k]\,V_w(k)\,\Gamma^T[\hat{\underline{x}}(k),k] + \frac{\partial\phi[\hat{\underline{x}}(k),k]}{\partial\hat{\underline{x}}(k)}\,P(k)\,\frac{\partial\phi^T[\hat{\underline{x}}(k),k]}{\partial\hat{\underline{x}}(k)}$
error variance algorithm	$P(k+1) = P(k+1\|k) - P(k+1\|k)\,H^T(k+1)\left[H(k+1)P(k+1\|k)H^T(k+1) + V_v(k+1)\right]^{-1} \cdot H(k+1)\,P(k+1\|k)$
initial conditions	$\hat{\underline{x}}(k_o) = \underline{x}_o$ $P(k_o) = V_{x_o}$

Table I.4.3/2: Discrete invariant imbedding-MAP algorithm

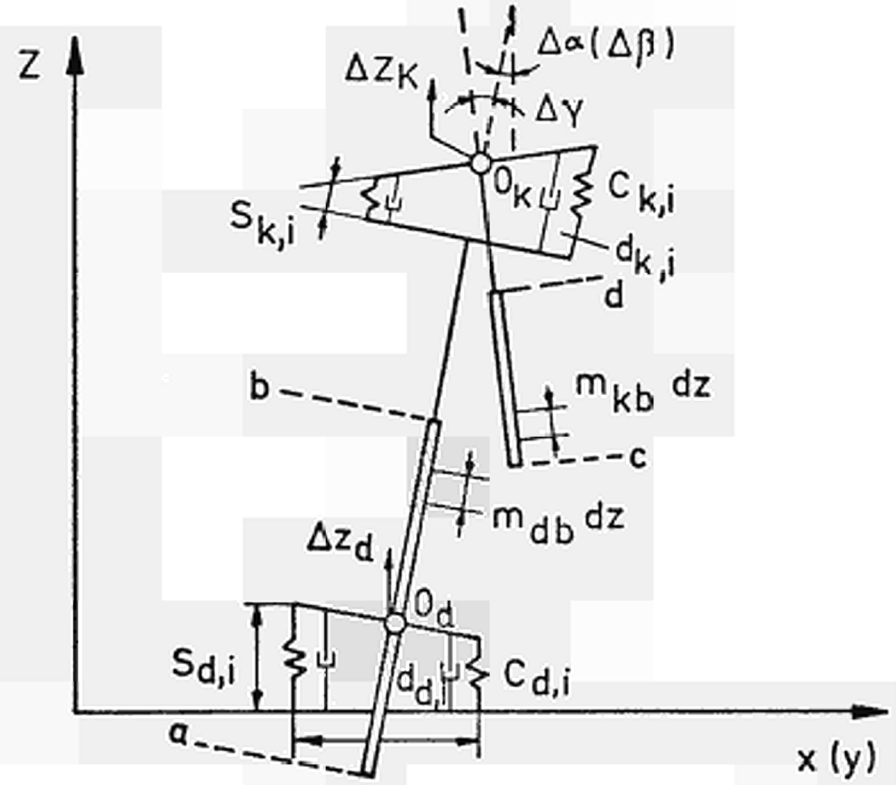

$\Delta\alpha$, $\Delta\beta$ – deviations of the angles of the pressure vessel in tangential (0°) and radial direction

Δz_d – deviation of the pressure vessel in vertical direction

$\Delta\gamma$, $\Delta\delta$ – deviations of the angles of the core barrel in tangential and radial direction (relative to the pressure vessel)

Δz_K – deviation of the core barrel in vertical direction (relative to the pressure vessel)

Fig.I.4.3/3: Formulation of Movements

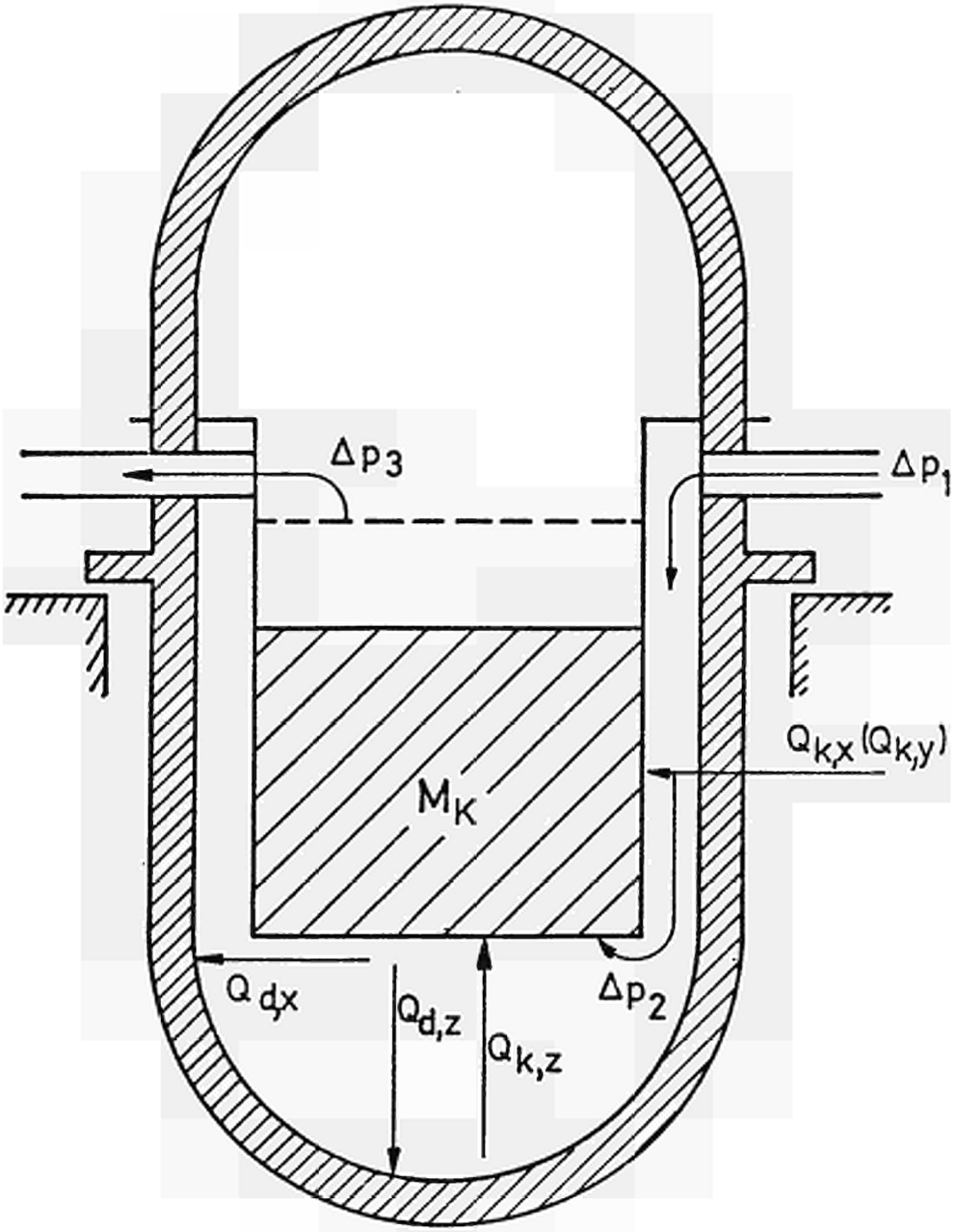

Fig. I.4.3/4: Formulation of Exciting Forces

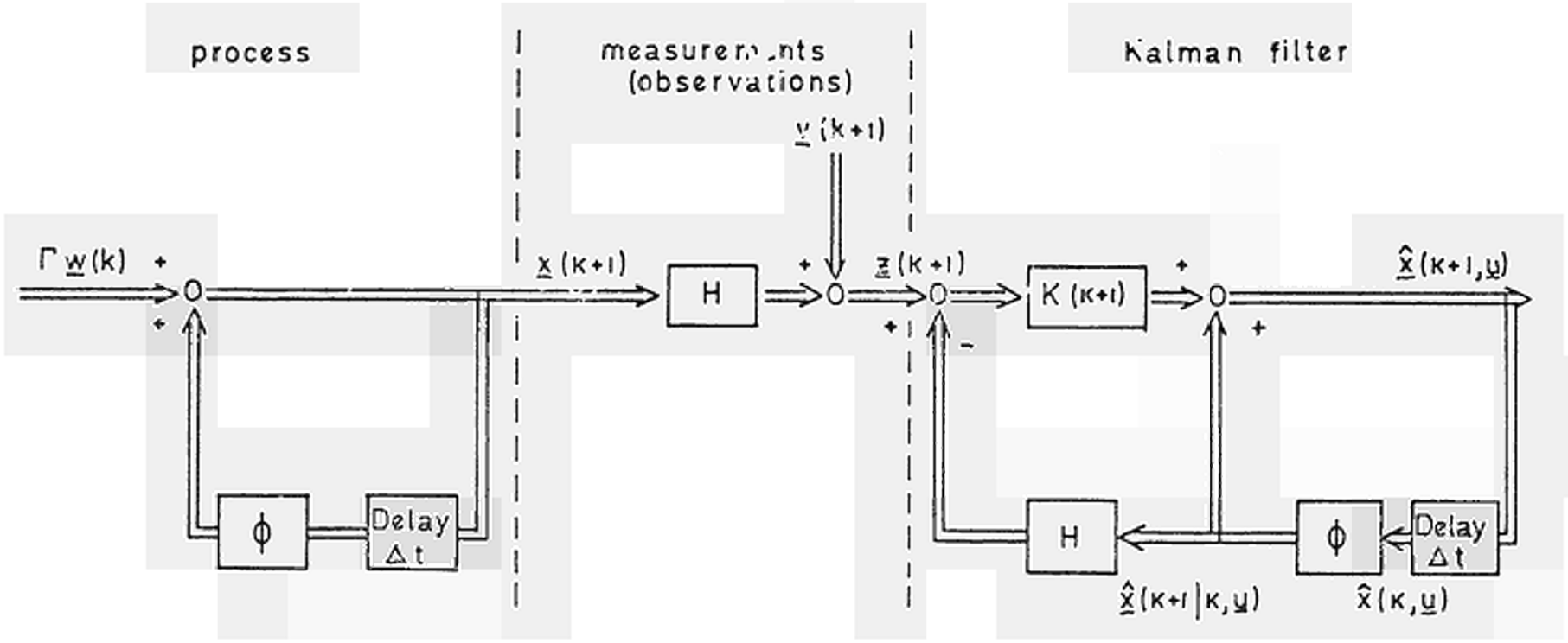

Fig.I.4. 3/5: Identification by means of a Kalman-filter

I.5 Summary and Conclusion

In PWRs of the investigated type the analysis of neutron flux as measured outside the core can be used to monitor the vibrational behaviour of the reactor vessel/core barrel system. This result was proved by preoperational vibration measurements, by correlation between vibration and neutron flux signals and by comparison with theoretical models describing the mechanical structure. Displacement gauges and accelerometers mounted to the surface of the pressure vessel wall even may provide information on alterations of the vibrational behaviour of internal structure parts. Refinement and extension of the models and additional investigations during the preoperational phase would certainly enable the finding of further possibilities to supervise selected structure parts. The application of identification theory for matching the models to the actual vibrations still need further investigation. Analysis of pressure noise (measured along the coolant path) and displacement signals during the preoperational tests permit insight in the hydrodynamic behaviour of the coolant and of the random forces acting on the structure.

For BWRs so far no significant influence of vibrations on the neutron flux signal was experienced. The overall noise as created by the boiling process seem to be too dominant. Various promising results were gained when using accelerometers. Incore ion chambers positioned one above the other in the coolant channel are suitable to measure mean local steam velocities. They can be certainly used to monitor coolant channel blockages.

Intensive investigations of various type of self-powered detectors showed their suitability to measure neutronic

at-power noise. This holds for the prompt response and for the mixed response detectors as well.

Summarizing it can be stated that the vibration and noise analysis being now in the state to enter practical application and to provide help for various cases where on-load surveillance is envisaged. Loose particle monitoring systems are being installed more and more in the large power plants. Measuring of core barrel vibration by means of the neutron flux again demonstrated its usefulness on the occasion of the Palisades incident. The first permanent installations of vibration monitoring systems are on the way. In general a certain trend can be observed to better utilize the possibilities for monitoring on-line the mechanical state of the overall plant in order to avoid possible propagating of defects, to judge on the right moment of repair and thus rising the availability and safety of the plant.

PART II: TURBINES

Table of Contents

II.1 Introduction

In the light of increasing power demands and economic considerations, it has become necessary to construct and put into operation considerably larger turbo-sets than in the past. The higher rating per unit, however, results in substantially higher financial losses per incident of damage than hitherto, in addition to which surveys and inspections also entail higher costs.

It is therefore obvious that endeavours must be made to monitor the mechanical state of the machine during operation in such manner that breakdowns resulting from damage, and shut-down periods occasioned by inopportune inspection intervals, are restricted to a minimum. The present methods of monitoring are, in this respect, in need of revision and improvement.

The study referred to in the foreword furnishes a review of the efforts made in the past within the European Community to procure information on the mechanical state of a turbine by means of noise and vibration measuring, without having to take the turbine out of operation. This revealed that at present no really informative results are obtainable from noise measuring. Better, but by no means satisfactory results have sofar only been achieved in the field of vibration measuring.

In the course of the subsequent study, which is the subject of this report, the following objectives were pursued:

1. In view of the fact that the hitherto applied "global" procedure in the field of noise measuring has not led to the desired results, its limitations as regards the early detection of damage should be determined by specific application to certain endangered components (e.g. blade carriers, valves, etc.).

2. The experience sofar available in the field of vibration monitoring should be made accessible to operators to enable them to furnish accurate data on the mechanical state of the rotor and the bearings of a turbine. In this connection, the measuring prerequisites, which must first be fulfilled, are elucidated.

3. Further investigation should be made into whether the early detection of damage by means of noise and vibration measuring can be improved by additional investigation of mechanical and thermodynamic parameters.

Tests carried out by EdF on the Arrighi 8 MW turbine as per Section 1 have sofar been unsuccessful, due to reasons connected with the Vibracoax pick ups, which were employed for the first time. The tests are being continued. No conclusive results can, however, be expected within the contract period.

An example of noise analysis successfully conducted by LABORELEC within the meaning of Section 1 is dealt with in Chapter II.5.

The criterions for qualitative assessment referred to under Section 2 are set-out in Chapter II.6. Chapter II.3 deals with the measuring prerequisites.

The work in connection with Section 3 is still in progress. Insofar as concrete results are available, these are dealt with in Chapter II.6.

In Chapters II.2 - II.4 the basic fundamentals of noise and vibration monitoring and diagnosis are summarised, based on the experience gained by the contract partners through various means. This furnishes pointers on future development work in this field.

II.2 MECHANICAL STATE OF HEALTH OF A TURBINE

Definition of monitoring and diagnosis

The operation of a machine generally involves the coming into play of forces, some of which can be considered as causing a deformation of the structure of the machine. They are the provocative forces, some of which are static and some dynamic.

For instance, putting a condenser under vacuum produces a static force which acts on the foundation of the turbine; the lack of balance of a rotor results in a dynamic force that acts on its bearings.

These provocative forces impose on the structures involved a deformation that can be a combination of a static deformation (displacement) and a dynamic deformation (movement). This reaction of the structure to the stress is the physical phenomenon the occurrence of which is most easily brought to notice because it is easily accessible to measurement, or even to human perception (touch, sight, hearing).

One could also easily imagine the shape of a deformation resulting from the two types of provocative forces already mentioned as examples.

But the fact should immediately be stressed that the deformation of a structure has no virtue of its own. It is but an accessible intermediary between the cause (provocative forces) and the effect (resulting mechanical stresses).

Knowledge of these mechanical stresses is the basic element that will determine judgment that can be passed on the state of health of the machine. This judgment is expressed in "probable duration of life" which combines the nature, location,

main directions, size and frequency of the determinative mechanical stress, i.e. the one leading to the maximum action on the material.

But it would be illusive to claim reaching thorough knowledge of the determinative mechanical stress, in the case of a machine as complex in structure as a turbine, for which the parameters of operation have futhermore considerable action on the provocative forces, as well as on the identification of the structure itself.

It will therefore be possible to characterize the mechanical state of a turbine, only by assessment of the physical quantities easily accessible to measurement, i.e. the deformation (displacement, movement) and from the interpretation that can be given to the data thus gathered.

This interpretation will be based more especially on the assumption that there are univocal relations between forces, deformation and stresses, and that the core of these relations is the identification of the structure. In other words, we assume that identical forces create identical deformations and then identical mechanical stresses.

Since we are unable to base our assessment of the state of health of a turbine on absolute knowledge of the determinative mechanical stress correlated to operation of the turbine under know working conditions, we shall assess this state of health from deformation measurement (displacement, movement) on the turbine. This first hypothesis is shown on figure II.2/1.

It is obvious that the provocative forces and the mechanical structure identification are under constant influence of what are called the parameters of operation.

What is less evident is how to determine what such parameters are, and the way each acts on the operational behaviour of the turbine.

In most cases, however, experience tells us that a given setting for the parameters we can control leads to an operation of the turbine that does not overstep a certain boundary.

Taking into account the normal range of settings for the controlled parameters of a given turbine in normal state of health, we can define limits within which all deformations, hence all measurements for parts of this turbine must stay, and reciprocally.

This leads to a way of monitoring parts in a turbine, as shown on figure II.2/2.

According to figure II.2/2, Monitoring is then passing a permanent judgment on the state of health of some parts of a turbine, in order to take a decision leading to immediate action on the operating conditions of the monitored turbine.

For instance, the decision to stop operation of a turbogenerator when the vibrations of a bearing have overstepped a predetermined threshold, comes under monitoring.

But monitoring considers only the necessary evidence to pass its judgment - it can take into account the way the events have been evolving previously, and the way they are expected to evolve later, but it does not try to analyze the reasons for such an evolution.

Diagnosis, on the other hand, is then passing a judgment on the mechanical state of a turbine, at a given time, and concerning its probable future evolution. This judgment in turn

can lead to a decision of a deferred action on the conditions of operation and maintenance of the turbine.

For instance, judging that there is a thermal unbalance on the rotor of a turbine and taking the decision to reduce the load, in order not to take the machine apart before a planned deadline date, come within diagnosis.

Diagnosis, to be justified, needs a second hypothesis according which the mechanical state of a machine, at a given time, can be deduced from comparison between measurements made at that time, and measurements previously made. In other words, this hypothesis means that there is a strong correlation between significant measurements and the mechanical state of a turbine. This in turn is shown on figure II.2/3.

From the foregoing, it can be stated the points of difference between monitoring and diagnosis:

- monitoring consists especially in a comparison between a momentary situation, its development in the immediate future, and the values that experience and the statistics of incidents on other machines lay down as limits,

- diagnosis consists especially in the comparison of the momentary situation with similar situations noted in the past on the same machine,

- monitoring must be a reliable means at the permanent disposal of the operational personnel. It should apply the methods and devices that meet the imperatives of industrial operation,

- diagnosis should be a means adaptable to the special case of each machine. It can apply the methods and devices of specialized testing.

For these reasons, monitoring and diagnosis are each the object of a separate description in what follows.

II.3 VIBRATIONAL MONITORING OF TURBINES

II.3.1 Object

The object of vibrational monitoring of a turbine is to give permanent concrete form to a decision that may be one of the three that follow:

- operation of the turbine is authorized under the existing conditions;
- operation of the turbine is authorized, but running conditions involve the risk of mechanical damage (alarm);
- the turbine must stop running in the shortest possible time (stoppage).

II.3.2 Method

Judgment of the state of mechanical health of the turbine is reached by comparison of the amplitudes of the vectors representing the vibratory quantities measured at certain points of the turbine (shaft, bearings) with predetermined values of these amplitudes ("alarm" threshold, "stoppage" threshold).

II.3.3 Measurement points

It is desirable that sensors be available on all the bearings of the turbine. However, in the case of a turbo-generator, one bearing out of two for each rotor will suffice, except for the HP rotor, which must have instruments on the two bearings.

A typical arrangement is shown in figure II.3.3/1 the positions considered indispensable are marked by thick strokes.

Each measurement point has to be instrumented to provide signals permitting determination of the absolute vibrations of bearings and shaft.

Furthermore, it is advisable to get a phase marking on the rotating parts.

II.3.4 Sensors and their associated equipment

II.3.4.1 Vibrations of bearings

The quantity to be measured is the absolute vibration of the bearing. Its basic component corresponds to the speed of rotation of the machine. The sensor is therefore preferably of the seismic mass type and with an axis of reference (maximal sensitivity).

The place where the sensor is attached is chosen as near as possible to the bearing proper, for instance on the cap of the bearing.

The orientation of the sensor reference axis is chosen in such manner as to best represent the bearing vibrations according to the various operating conditions of the machine. The total bandpass of the sensor unit plus its associated electronic equipment must cover at least the interval 2o - 2oo % of the rated rotation frequency of the machine. In any case, it is desirable that it should correspond to the ISO standard.

It is desirable that the sensor, or its associated electronic equipment permit an electric analog output to be available, independent of the circuit intended for monitoring, which would

eventually enable connection to be made with the measurement circuit, without disturbing the monitoring in any way.

It should further be noted that the location of the sensor is likely to be difficult of access and that in that case any operation involving it may require stopping the turbine.

Consequently, it is desirable not only that the sensor be able to operate without failure for at least 1o,ooo hours but also that it be possible to make a check without needing to take it apart.

II.3.4.2 Shaft vibrations

The quantity to be measured is the relative shaft/bearing bibration. Its basic component corresponds to the speed of rotation of the turbine. It is therefore preferable to use a pair of sensors, of the contactless type, which measure the relative shaft/bearing displacement according to two mutually orthogonal directions and orthogonal to the shaft as shown in figure II.3.4.2/1.

The position of the sensors is chosen as near as possible to the middle of the bearing.

The orientation chosen for the sensors is preferably following the vertical and the horizontal transverse.

The total band-pass of the sensor unit plus the associated electronic equipment must cover at least the interval 2 - 2oo % of the rated rotational frequency of the turbine. It is desirable to be able to measure the DC component (measurement of the static rise of the shaft).

As already stated, it is desirable that the sensors, or their associated electronic equipment, permit an electric analog output to be available, independent of the circuit intended for monitoring.

It is also desirable that it be possible to check on their operation without taking them apart.

II.3.5 Treatment of signals, information sought

Still remaining within the setting of monitoring, two complementary forms of treatment can be given to the vibratory signals:

- As long as the turbine is at variable speed, in any case not at its rated speed of rotation, and in order to avoid complicating the monitoring device, it is desirable to disregard the fact that it is a rotating machine and to consider solely the value of the amplitude of the r.m.s. vibrational velocity.

- When the turbine is running at its rated speed of rotation, it is desirable that the signals emitted by the sensors be treated in such manner as to furnish:

  a) as above, the amplitude of the r.m.s. value of the vibratory velocity (all components);

  b) the amplitude of the component at the rotation frequency (unbalance);

  c) the amplitude of the component at double the rotation frequency (disalignment);

  d) the amplitude of the component at half the rotation frequency (whipping).

II.3.6 Presentation of vibration data

Monitoring consists essentially in comparing vibration data with the limit values of alarm or of stoppage. It

is however desirable that judgment be weighted by examination of the past situation, and the development trends that it may be possible to define therefrom.

The simple process in most general use consists in recording the vibration quantities on a multi-track graphic recorder that can be consulted by operating personnel.

A more elaborate procedure consists in recording only the vibration values that reach certain thresholds or that show a certain trend of development.

Furthermore, a visualization on a multi-oscilloscope of Lissajous figures corresponding to each pair of sensors gives information simultaneously on the rise of the shaft in the bearing and the critical velocities of the machine. It is desirable that this information should be displayed on a console, in the control room, together with additional information, for each bearing, as to antifriction metal temperatures and oil pressures.

II.3.7 Deciding device

The electronic device making instantaneous comparison of the vibration information and the limit values (alarm, stoppage), must, in accordance with what is stated above, have for each incoming signal a stage taking into account the amplitude of the signal and a stage discerning the speed of variation of the amplitude. The corresponding limit values have to be adjusted to the special characteristica of the machine monitored, account taken of ISO standards.

II.4 VIBRATORY DIAGNOSIS OF THE TURBINES

II.4.1 Object

The aim of the vibratory diagnosis of a turbine is to pass a judgment on the state of health of this turbine, at a given moment, and for assumed known values of its mechanical parameters, so as to take a decision concerning its more or less long-term future.

Such a decision can assume three forms:

- This turbine doesnt seem to be affected in the integrity of its structure, and its behaviour is similar to the one of a turbine in new condition.

  Consequently this turbine can perform at its nominal power, irrespective of its working conditions, and some maintenance operations can even be postponed.

- This turbine seems to be affected in the integrity of its structure - the corresponding damaged or abnormally worn parts are located, and their damage defined - but on the other hand, its global behaviour is still comparable to that of a turbine in new condition.

  Consequently, this turbine can perform at its nominal power, without noticeable restriction with regard to its working conditions, and some maintenance operations can be planned.

- This turbine seems to be affected in the integrity of its structure - the corresponding damaged or abnormally worn parts are located, and their damage is defined - besides, its global behaviour is different from that of a turbine in new condition.

  Consequently, this turbine can perform only at a fraction of its nominal power, under restricted working conditions, and some maintenance operations have to be planned.

II.4.2 Method

The judgment of the state of health of a turbine is reached by collecting significant signals from typical points on this turbine, then by treating these signals so as to exract the information they enclose, and lastly by identifying this information (that is by comparing it to typical shapes and values), and by studying its evolution.

II.4.3 Measurement points

It is not conceivable to define measurement points as accurately as it was done for the vibratory monitoring (see II.4), and each model of turbine, if not each turbine, needs special investigation.

However, some general indications can be given:

II.4.3.1 Measurements on the surface of the turbine

The measurement points are provided with fixing devices which allow, when needed, the setting of sensors.

These devices ensure the fixing of the corresponding sensors so that measurements be made according to some reference axis, and the mechanical transfer function of the fixing device with the greatest fidelity.

The typical layout is shown on figures II.4.3/1:

II.4.3.2 Measurements inside the turbine

The measurement points are provided with permanently fixed sensors.

There is no typical layout.

For instance, the auscultation of a turbine rotor involves the insertion of sensors in the mount of the stator blades; the auscultation of a turbine foundation involves embedding strain gauges in the concrete beams, bars, etc...

II.4.4 Sensors and their associated equipment

As expressed above, it is a matter of assessing the evolution of the deformation of a turbine structure.

Such an evolution being worked out by processing collected signals, the sensors and their connected equipment must, above all, be particularly reliable.

This reliability, besides, involves accurate knowledge of their behaviour according to their environment (temperature, pressure, magnetic field, etc...).

Finally, the deformation which is to be measured generally consists of static and dynamic deformations. Each measurement point must then be provided with different kinds of sensors so as to obtain, by overlapping, the whole frequency range it is desired to explore.

II.4.5 Treatment of signals - Information sought

It is obvious that the choice of a treatment of the signals depends on an option on the information sought.

Since we know that we are dealing with a rotating machine, assuming, so to speak, that the main part of the implemented physical phenomena is correlated to the rotation of the turbine, it is natural to select a priori a vectorial frequential treatment - which implies that the information sought comes mainly from stationary signals involving components at frequencies that are multiples

or submultiples of the rotation frequency. This line of argument is similar to the one given above in the case of the vibratory monitoring. It leads to completing and broadening the corresponding field.

Because of its systematic appearance, and the use of a filing system displaying results of the treatment, it is given the name of "vibratory card diagnosis". It is described further on.

But thougt the vibratory card diagnosis supplies information on the main part of the behaviour of a turbine, the latter has some functional components that put into action provocative forces which can be correlated only in a partial or null manner to the movement of the rotors. It must then be necessary, should occasion arise, to complete the above - mentionned vectorial frequential treatment by other treatments, of various kinds, adapted for each case to the way in which the physical phenomena to be identified are imagined. Such processes are described below under the name of "tracking-down diagnosis".

II.4.6 Vibratory card diagnosis

Such a diagnosis deals more particularly with the shaft of the turbine. For that, the information obtained from an eventual treatment of the signals is displayed from two viewpoints:

- slow or quasi-static evolution:
  - . values of the working parameters of the turbine (steam pressures and temperatures, oil pressures and temperatures, power, etc...).
  - . values of the static deflections (flatness of the supporting table, alignment of the bearings, rise of the shaft in each bearing, etc...).

- dynamic data:

  . values of the dynamic deflections (vibratory vectors - amplitude and phase - with respect to the components at frequencies that are multiples or submultiples of the rotation frequency, spectral analysis, etc...).

Each vibratory card gathers this information concerning a chosen turbine at a particular instant chosen to collect the information. A file is set up for each turbine.

Treatment of the information consists in looking for trends in the evolution of each frequential component, according to the variations of the slow or quasi-static parameters.

Judgment is passed by correlating the established trends.

For instance, when the components at the rotation frequency, and twice this frequency, of the vibratory vector (shaft as well as bearing) are increasing in steps as time elapses, it can mean that a crack is developing in the shaft of the turbine.

II.4.7 TRACKING-DOWN DIAGNOSIS

Such a diagnosis completes and explicits the previous one with regard to the turbine shaft. Moreover, ist deals with the turbine organs the operation of which does not set in action provocative forces bound to the movement of the rotors. Finally it deals with non-periodic vibratory signals (such as shocks).

The guiding idea remains the search for development trends

in and of their identification to typical shapes and values assessed from computation or experience.

The judgment is rendered by correlation of the established trends.

For instance, the evidence is that the working of an H.P. inlet valve is accompanied by a whirring noise for a certain setting of the poppet.

Moreover, a variation in the steam temperature at the inlet is correlated with a frequency variation of the pure tone radiated by the valve.

It is then plausible that the pressure fluctuations occuring as the steam is circulating between the poppet and the seat will cause an acoustical cavity or a pipe to resonate.

II.5 Characteristic Noise Phenomena due to Faults and Damages

As was stated on page II.2 we did not succeed up to this day in finding the right way to survey steam turbines by means of noise measuring. So it is not yet possible to describe common noise phenomea characterizing faults or damages.

Only one example of noise propagation on a turboalternator due loosening of core laminations may be mentioned. It shows that further efforts on this scope can give efficient results.

Not long after a normal inspection of the machine, in July 1971, an abnormal noise appeared during the normal service of the 125 MW Baudour alternator in Belgium. The noise, which was intermittent during short or long periods of time, looked like a "compressor noise" or a "hammering noise" according to different workers. This noise appeared at several times during the summer, disappeared during the winter, and came back in the following summer.

Different tests have shown that the noise had no correlation with the power level or other electrical characteristics (voltage or current), but that other factors as frequency (rotation speed) and temperature of the cooling fluid (hydrogen) had certain relation with the phenomenon.

It appeared that the noise was radiated by the casing and that a very good image of the phenomenon was given by the signal of an accelerometer fixed on the middle of the alternator casing.

When the state of the machine was normal, the spectrum of the accelerometer signal included all the normal harmonics of the magnetic core's vibrations: 1oo - 2oo - 3oo - 4oo Hz, and so on up to 15oo Hz.

When the machine was "noisy", several of these harmonics were accompanied by two side-bands at plus and minus 13 Hz of the normal frequency, i.e. as examples:

187 - 2oo - 213 Hz
787 - 8oo - 813 Hz
1287 - 13oo - 1313 Hz

Although, the vibration amplitude was very small, the noise was disagreeable and disquieting.

The same side-bands were noticed on three signals which were recorded simultaneously on a multi-track magnetic band:

- acoustic noise
- acceleration of the alternator casing
- acceleration of the 2 alternator bearings,

but these side-bands were not present on other signals as

- vibration of the shaft
- dynamic pressure of the bearing oil
- voltage and current in the stator.

The annexes give excerpts of some of the recorded spectrums:

fig. II.5/1 + 2: normal and abnormal spectrum of the casing acceleration: o - 5oo Hz

fig. II.5/3 + 4: idem: o - 1ooo Hz

fig. II.5/5 : abnormal spectrum of a bearing acceleration (normal harmonics with side-bands around 2oo - 3oo - 4oo Hz among others)

fig. II.5/6 : acceleration of the casing: harmonics 8oo and 13oo Hz, without and with abnormal noise.

The alternator ran in that state during a year and was then opened.

It was established, at that time, that some of the stator core laminations were losse, mainly in the central part of the core, where the noise was generated. It is supposed that these loose parts were vibrating at one of their resonance frequencies and that this induced an amplitude modulation of the normal vibrations of the core.

The phenomenon disappeared after proper fixing of the core laminations.

It seems that, in that case, a "noise analysis" technique is useful for detecting the cause of an imperfect mechanical state of the machine.

II.6 Characteristic Vibration Phenomena due to Faults and Damage

Vibration measuring normally has two functions to fulfil:

1. To indicate any critical vibrational state of the turbo-set, to enable measures to be instituted to prevent rubbing or bearing damage.

2. To reveal changes in normal vibrational behaviour, which are characteristic of certain types of failure or damage in the machine.

The first-mentioned monitoring function thus primarily serves the prevention of damage, whilst the second lends itself to damage diagnosis or, generally, to assessing the mechanical state of the rotor and bearings. It thus already becomes apparent, here, that vibration measuring is subject to natural physical limitations as regards the early detection of damage. Only those types of damage, namely, are detectable which proximately influence the normal state of balance and the alignment of the shafting.

Vibration measuring thus does not indicate a reaction until the damage has already occurred. Strictly speaking, the objective of detecting damage in its evolutionary stage is not thereby attainable by means of vibration measuring. Experience has, however, shown that it is to date the only measuring procedure capable of indicating the changes mentioned, so that at least consequential damage - the cost of which often considerably exceeds that of the primary damage - can be avoided.

Basically speaking, the bearing block vibration and the shaft vibration measurements should both reveal changes in the balance and alignment of a turbine rotor in the same manner. It has, however, been revealed that direct measurements on the rotor, that is to say shaft vibration readings, have the greater informative value; for the oil film damping and the bearing elasticity influence the bearing block vibration very strongly as regards amplitude, this resulting in the lower degree of sensitivity observed from the bearing block vibration reading.

The main applicational field of shaft vibration measuring is during normal operation, that is to say when the turbine is

under load. Valuable data can, however, also be gained by measuring carried out at other operating points.

In turning gear operation, for example, the excentricity can be monitored relatively easily if the shaft vibration measuring system also permits measuring at low speeds. This primarily applies in the case of thermal turbo-machinery, where the rotors can suffer thermal distortion between shutting-down and complete colling-off. Concentric measuring always proves particularly expedient in cases where turning gear operation has to be stopped for some reason before the warm start-up of a turbo-set.

Even in cases, however, where thermal influences play little or no role at all, concentric control checks assist in early detection of the displacement and deformation of rotors, casings and bearings.

Shaft vibration measuring during running up to speed serves in reducing the rubbing risk in over-critical rotors when traversing the critical bending speed ranges.

The recording of resonance step-up during traversing of the critical speed ranges - particularly when shutting down - aids, when compared with earlier measurements, in locating damage which has brought about a change in balance or alignment.

During normal operation, the indication of an already existing or - better still - an evolving critical vibrational state is the primary monitoring function of shaft vibration measuring. This is designed to eliminate the possibility of the rotor rubbing against fixed parts or of dynamic overloading of the bearing or rotationg components.

In the majority of all cases, increased shaft vibration amplitudes are due to failures or damage caused by a gradual or sudden change in balance and/or alignment. These are so-called forced vibrations.

Less numerous, but by no means less dangerous, are those cases in which major shaft deflections are caused by self-excited vibrations. The characteristic feature here is a complete change in the character of vibratory movement, as the normally dominant rotation frequential vibration is superimposed by a vibration, the frequency of which roughly corresponds to the natural flexural frequency (usually the lowest) of the rotor in question. Self-excitid vibrations, based on present-day experience, are:

1. The oil whip, a hydrodynamic vibration stimulated by the oil film. It occurs primarily when the rotation frequency of the rotor attains a value greater than double the natural flexural frequency (usually the lowest) of the rotor in question.

   In this case (the so-called resonance vortex) the prerequisites for instability are present in certain types of bearing construction, where a minor failure intensifies of its own accord.

2. Gap excitement, an aerodynamic excitement caused by unsymmetric flow of the medium in the machine. This affects rotors, whose operating frequency is greater than one of its natural flexural frequencies. Gap excitement is dependent on load and can occur in steam turbines at as low as 25 % of the design flow rate. Much points to the fact that, in the majority of all cases of self-excited vibrations, aerodynamic excitement is the cause. In more seldom cases, excitement caused by shrink-fit friction of fitted parts is observed. This occurs at the speed at which the shrink is lost. The possibility also exists of rotation frequent alien vibrations occuring as a result of subharmonic resonance in the event of non-linearities in the spring tension and damping force.

In the field of damage diagnosis - the second monitoring function - shaft vibration measuring is subject to natural physical

limitations. Normally - as already mentioned - the rotor motion is subject to the influence of centrifugal force. This means that only such damage is ascertainable by means of shaft vibration measuring which affects the normal balance and the alignment of the shafting, namely:
Blade fractures, shroud band breads, as a result of which a sudden change in shaft vibration occurs, whereby this is by no means always a deterioration.

Rotor distortion by radial rubbing due to the displacement of inner casings or blade carriers or the deformation of inner and outer casings.

Rotor distortion by axial rubbing due to the buckling of intermediate bottoms by exceeding of the permissible relative dilatation.

Rotor distortion caused by the in-break of water from the main steam or cold feed and bleed lines of steam turbines. Rotor cracks, whereby a change in balance and consequently a change in the shaft vibration amplitude gradually increases with the propagation of the fatigue crack.

Rotor disc cracks, whereby the change in balance occurs very late, namely upon the lifting of a section of the disc or upon loss of the shrink-fit.

Loosening of the shrink-fitted sealing rings of radial shaft seals, glands for labyrinth packings, coupling haves and thrust bearing discs, whereby at the commencement of loosening strongly scattered shaft vibration impulses occur - primarily in the case of inconstant temperature equalisation processes in the machine - which can disappear during constant settled operation following temperature equalisation. The possibility of self-excited vibration occurring as a result of such loosening has already been referred to.

Breakage or displacement of composite parts.

Changes in alignment, e.g. in the case of bearing damage. Influence on shaft vibration is, however, only measurable if a sharp change in the bearing geometry - usually in the lower bearing bushing - has occurred.

Changes in unbalance causes by uneven deposits or abrasion.

Expansion hindrance of bearing blocks by base plate displacement, whereby again a clear change in the original deflection line of the rotor extrusion must occur, primarily in the double bearing assembly, due to tensioning of the rotor in the closely adjacent bearing.

Incidents of damage, which have been the subject of vibration measuring in the past, are listed in the following table. The illustrations to which reference is made may be regarded by and large as generally valid in respect of qualitative content.

No.	characteristic vibratory feature	thermal and mechanical feature	cause	operating safety
1	dominant vibration frequency = n_k $n^+ > 2\ n_k{}^{++}$ (fig. II.6/1 + 2)	linked with the rotor speed	rotor instability due to oil whip	endangered
2	dominant vibration frequency = n_k $n > n_{shrinkage}$ (fig. II.6/1	linked with the rotor speed	elastic hysteresis due to a loose shrunk joint	endangered
3	dominant vibration frequency = n_k (fig. II.6/3	linked with the operational power	rotor instability due to steam leakage in the clearances of the sealing glands and rotor blades	endangered
4	dominant vibration frequency = n sudden change of the vibration amplitudes (fig. II.6/4) and/or change in the unbalance vector position	fractures of several blades cause arising of the interstage pressure and temperature	blade fractures shroud band breaks, etc.	endangered
5	dominant vibration frequency = n gradual rise in the vibration amplitude (fig. II.6/5		increasing rotor bowing	possibly endangered

$^+$ n (s^{-1}) rated rotor speed

$^{++}n_k$ (s^{-1}) critical rotor speed

No.	characteristic vibratory feature	thermal and mechanical feature	cause	operating safety
6	dominant vibration frequency = n and/or 2 n gradual increase, in steps, in the vibration amplitude (fig. II.6/6-8)	sometimes linked with the operational power	chrack propagation in the shaft	endangered
7	dominant vibration frequency = n steep but not sudden rise in the vibration amplitude (fig. II.6/9)	arising oil or white metal temperature	damage of journal bearing	endangered
8	dominant vibration frequency = n steep but not sudden rise in the vibration amplitude (fig. II.6/10-11) and rotation of the unbalance vector		rotor rubbing	endangered
9	dominant vibration frequency = n steep and/or sudden rise in the vibration amplitude (generally scattering), especially before equalization of temperature		loose shrunk joint of sealing rings, bushes coupling halfs, etc.	possibly endangered

II.7 Summary and Conclusion

The investigations conducted in connection with Study Contract 47-72-12 ECIC have shown that a stage of development has been reached in the field of vibration measuring, which at present leaves little scope for further efforts. One must, however, ensure that the equipment of major turbo-sets, with the measuring systems available, are accepted as the technical standard.

More or less concrete conceptions exist in the interpretation of vibration phenomena. A limited catalogue of characteristic damage features was listed in Chapter II.6. It would be expedient if the ecperience gained by the operators of vibration measuring systems were to be further compiled and made available to interested circles.

In the field of noise measuring, there are still a number of problems to be overcome. Efforts in this direction are worthwhile, for it has in individual cases been shown that noise measuring can also be employed for diagnosis purposes in respect of steam turbine.

As regards the evaluation of noise analysis results, the same applies here as in respect of vibration measuring.

On the basis of the comments set-out in Chapters II.2 and II.3, endeavours will also be necessary to render possible long-term diagnoses on the mechanical state of steam turbines, based on the correlation of vibration and noise signals.

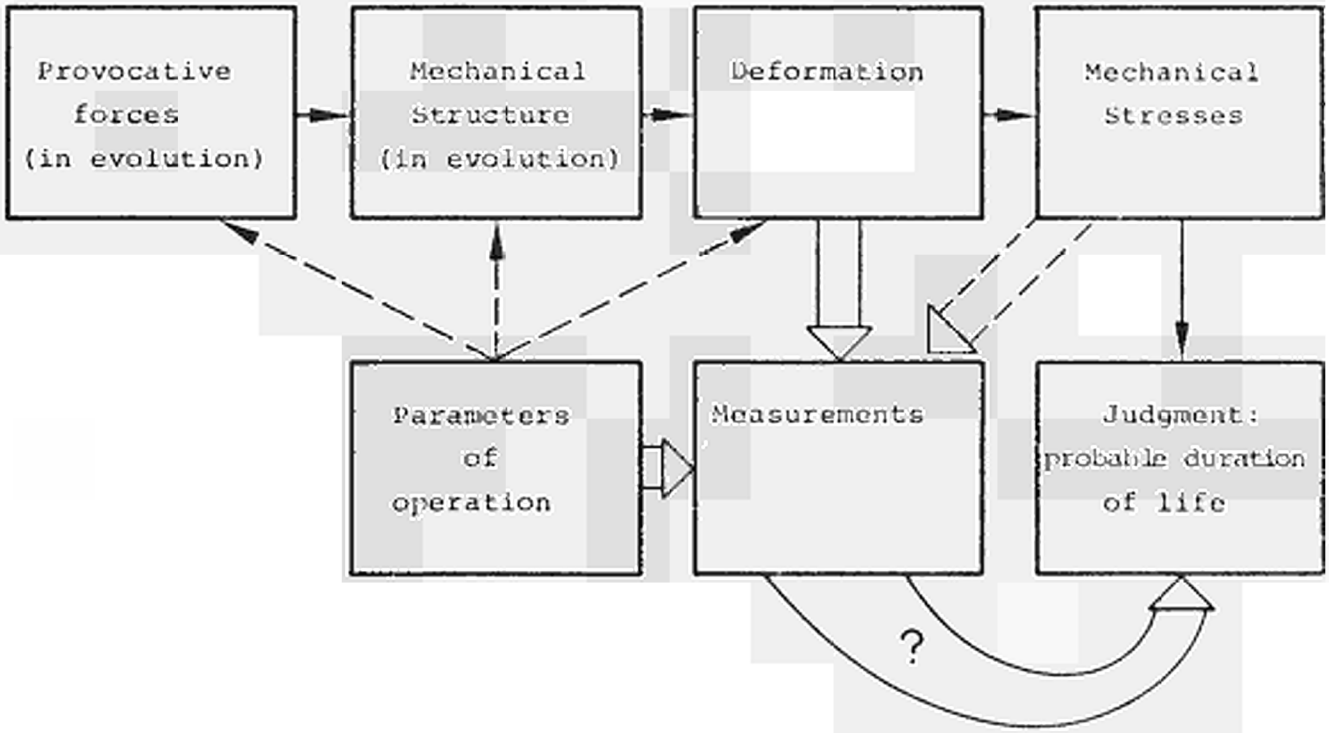

Fig. II.2/1: 1st hypothesis: Correlation measurements/probable duration of life

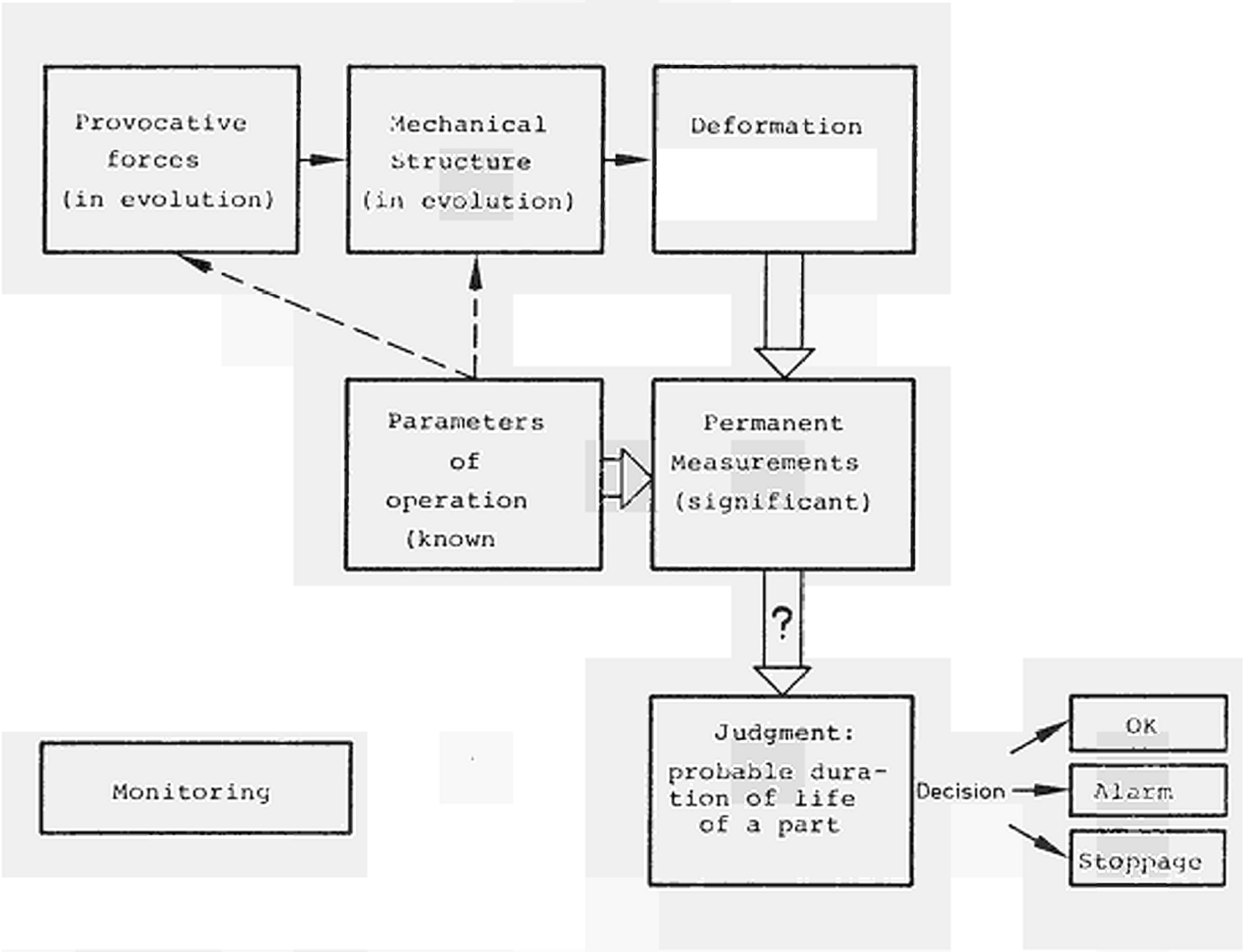

Fig. II.2/2: 1st Hypothesis bis: Correlation significant measurements/ duration of life of a part

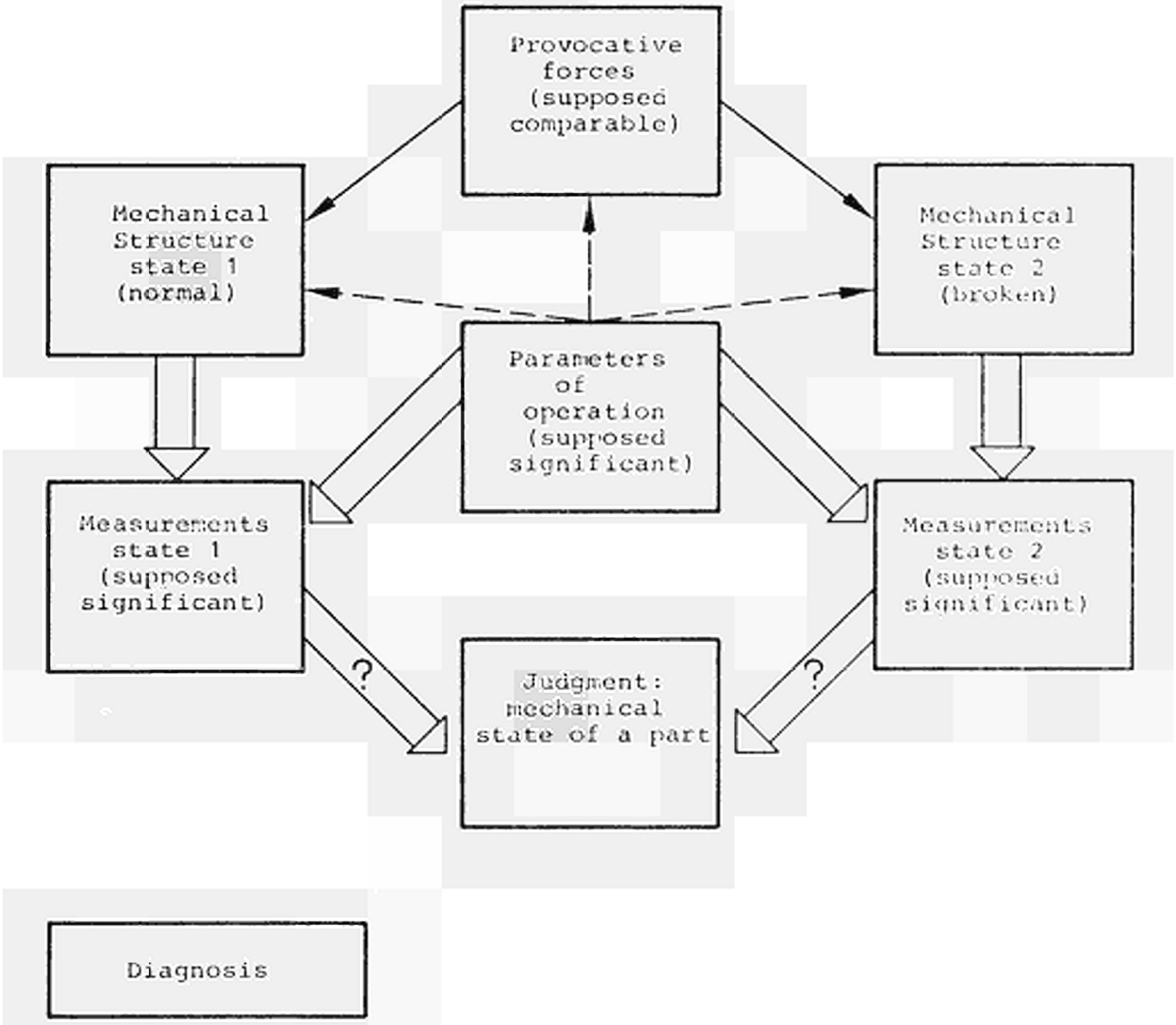

Fig. II.2/3: 2[d] Hypothesis: Correlation significant measurements/ mechanical state

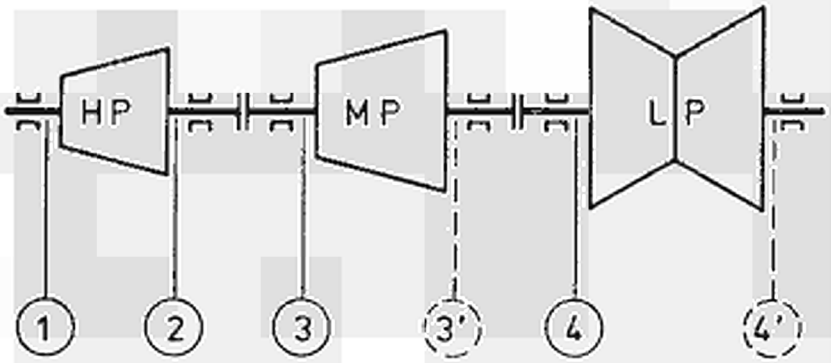

Fig. II.3.3/1

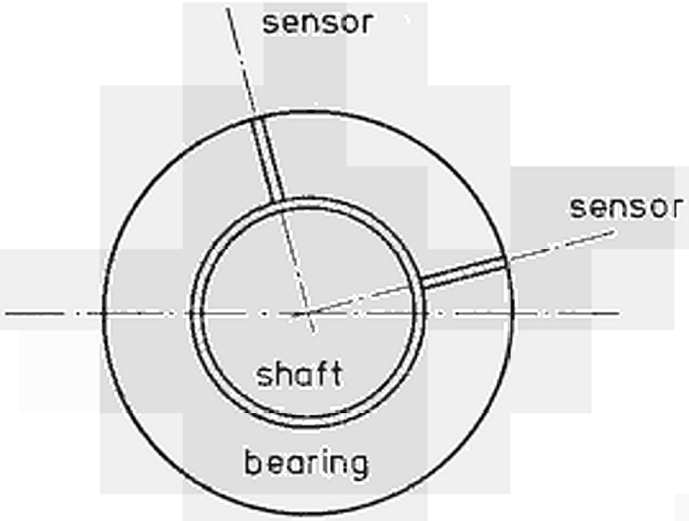

Fig. II.3.4.2/1

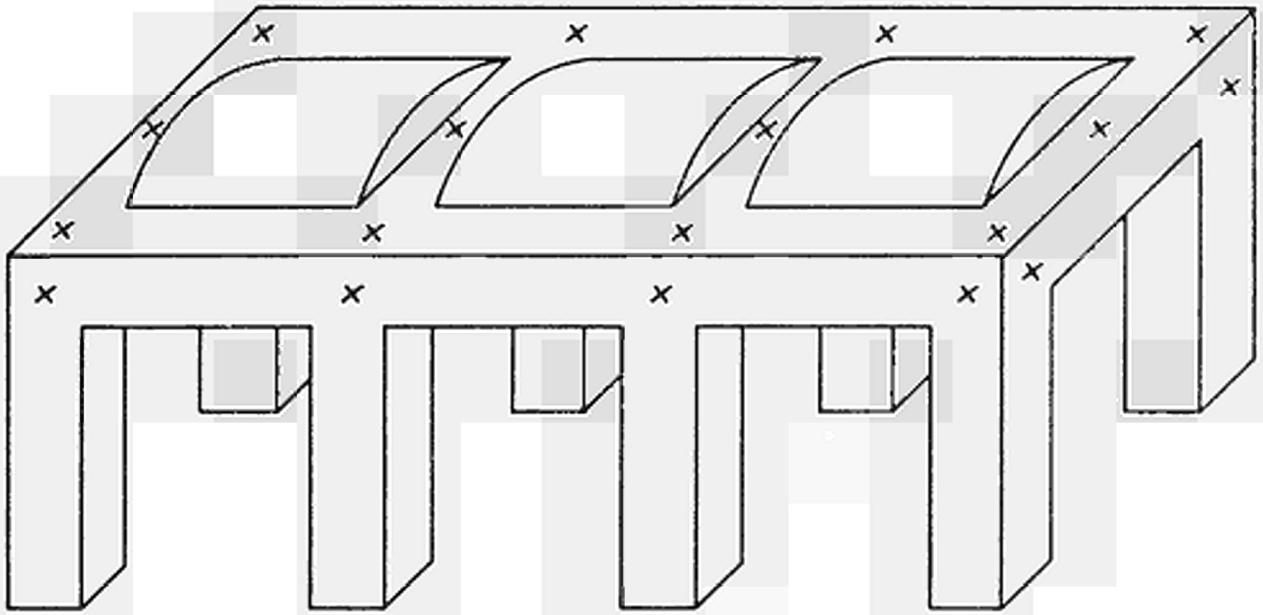

Fig. II.4.3/1

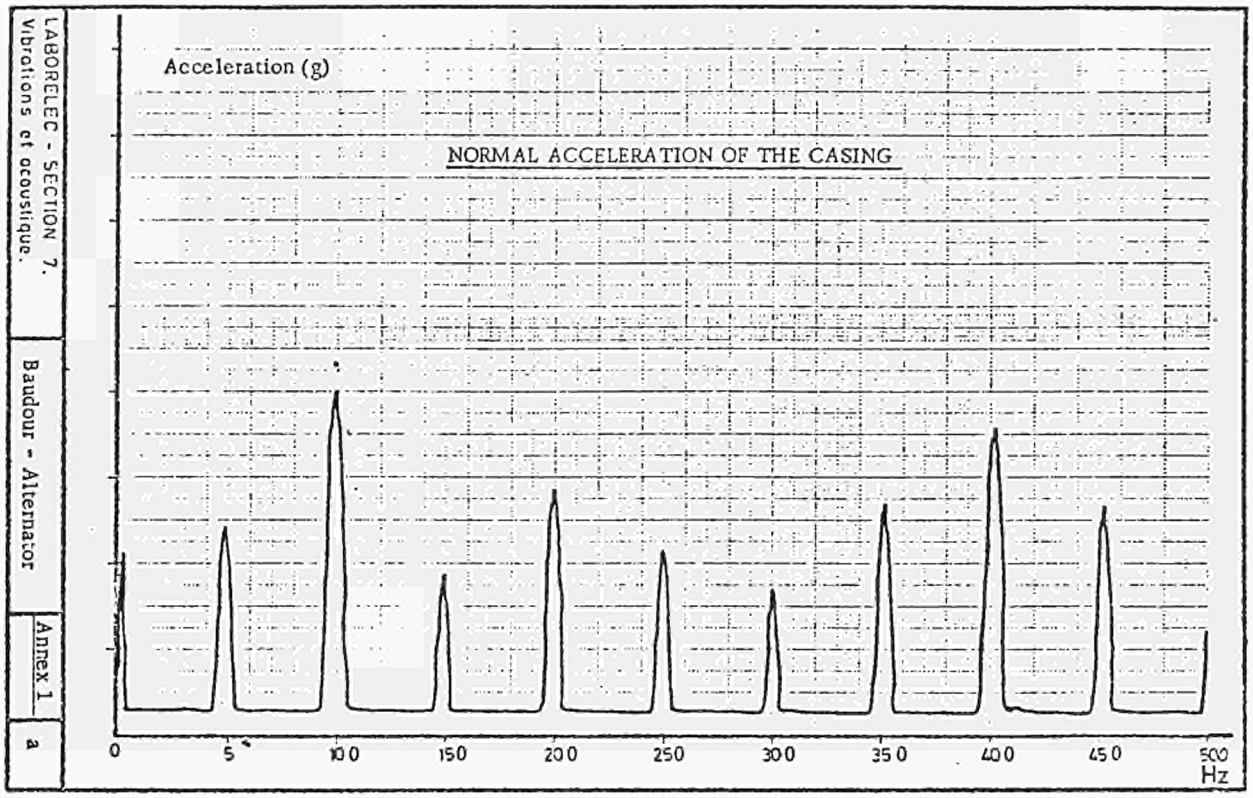

Fig. II.5/1

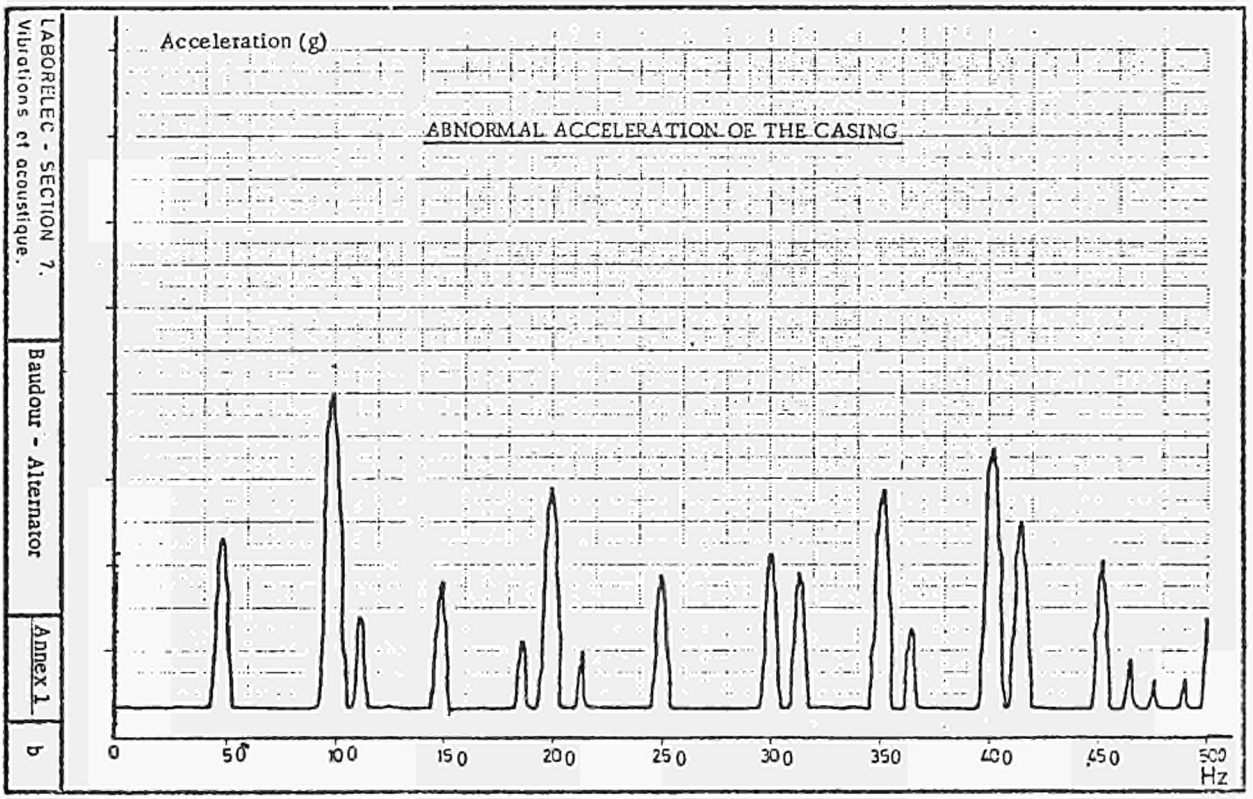

Fig. II.5/2

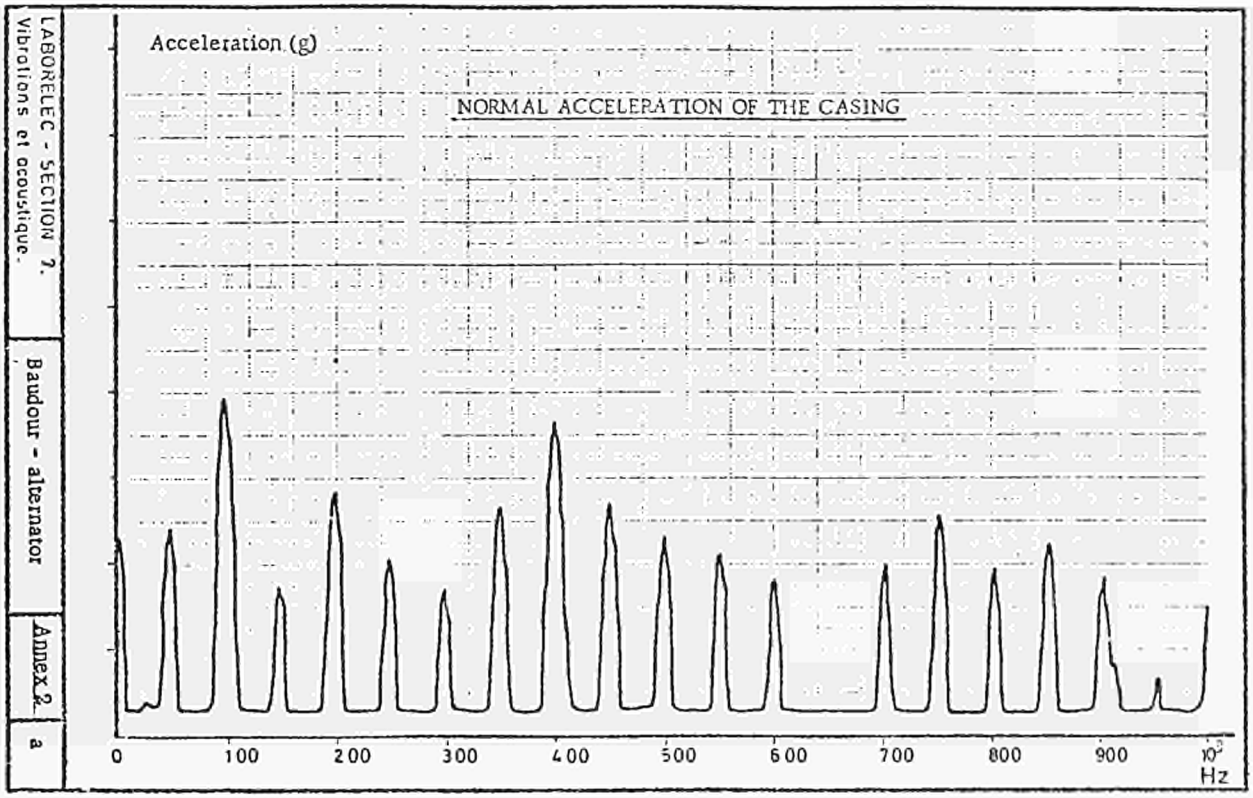

Fig. II.5/3

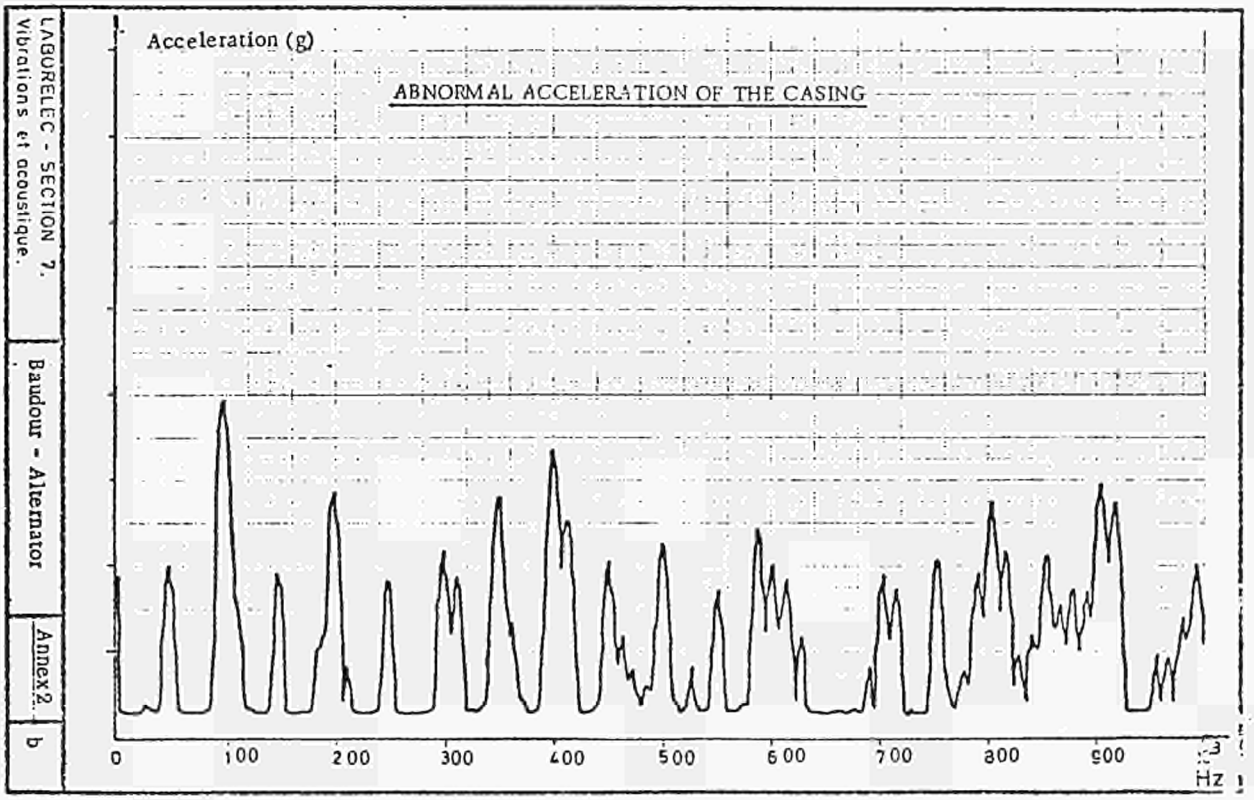

Fig. II.5/4

ALTERNATEUR DE BAUDOUR

Vibrations du Palier côté excitatrice (accélération)
Analyse des vibrations de 50 à 1000 Hz

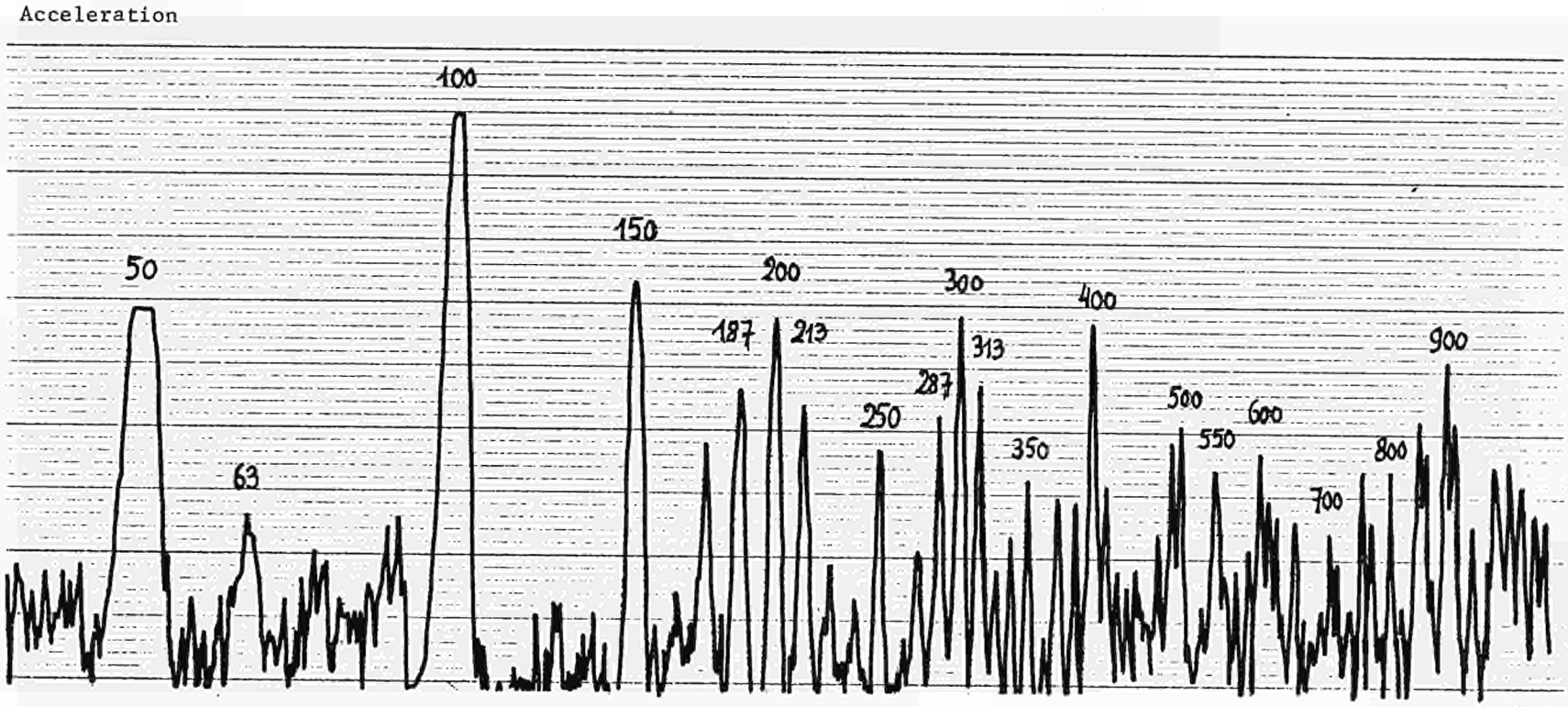

Baudour Alternator - Abnormal spectrum of a bearing acceleration

Fig. II.5/5

Annex 3

Normal state

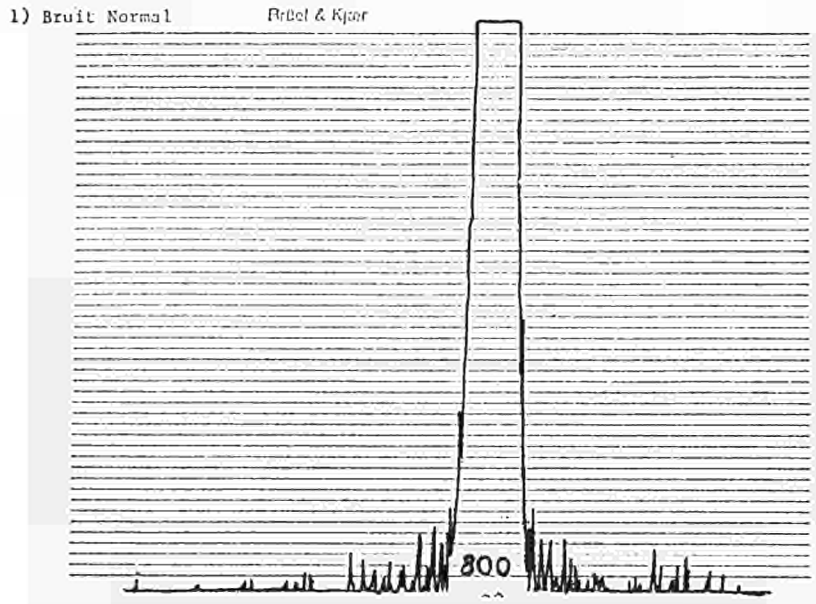

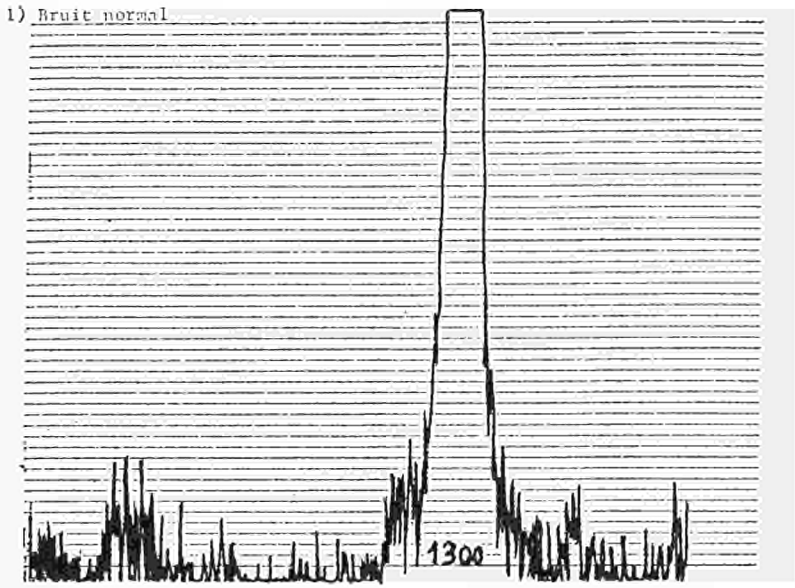

Abnormal state (noise)

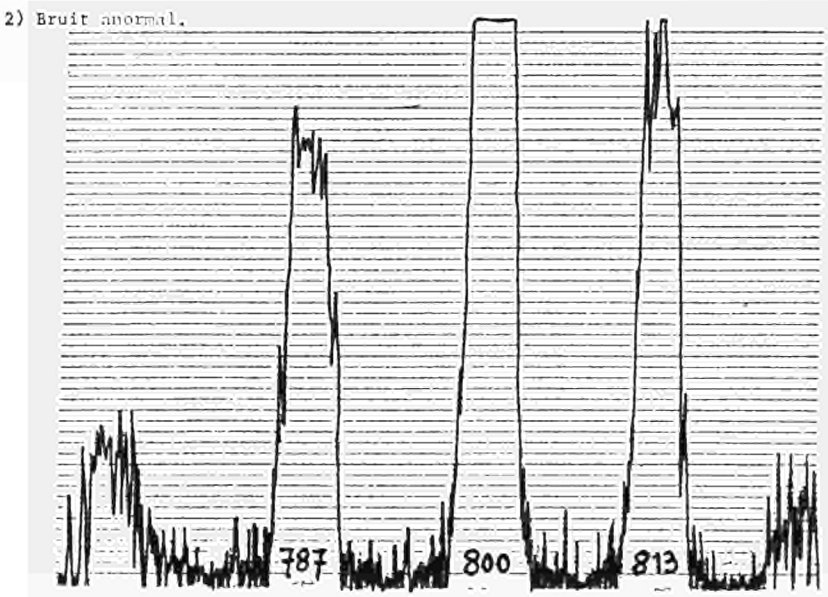

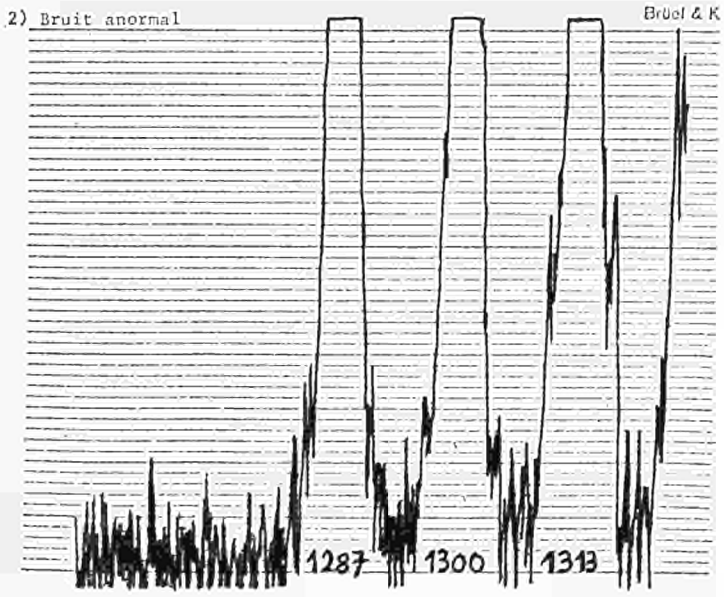

Baudour Alternator - Acceleration of the casing : harmonics 800 and 1300 Hz
Fig. II.5/6

Annex 4

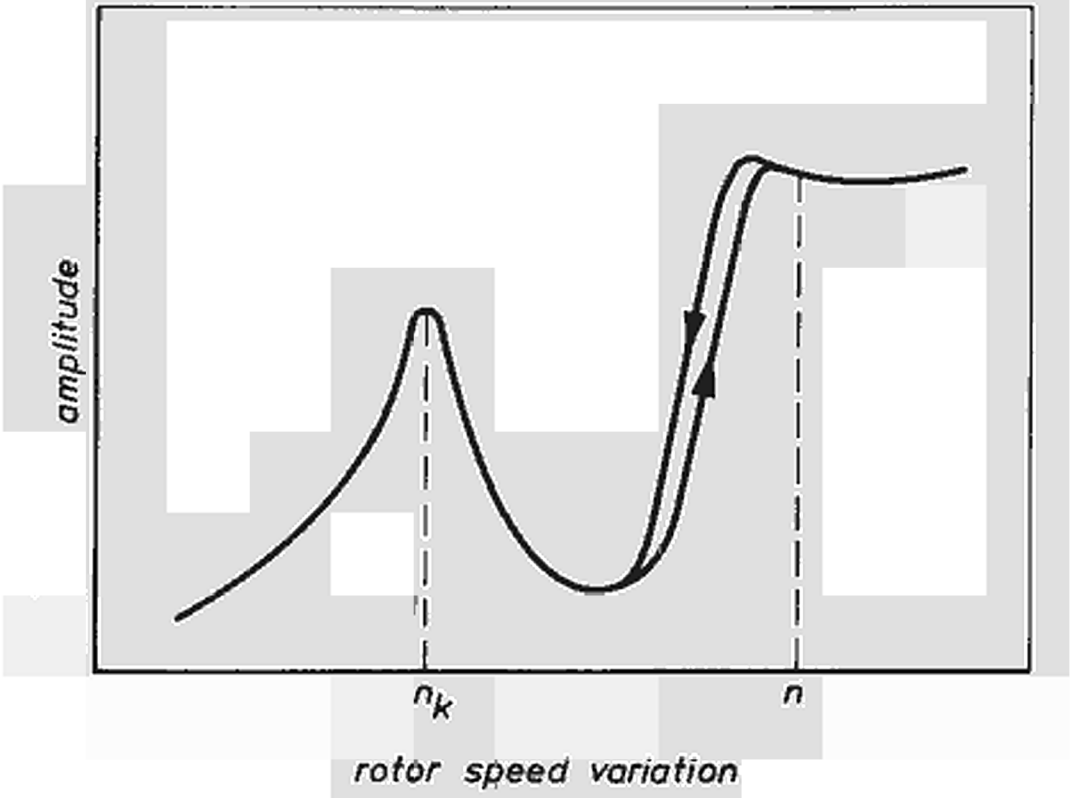

Fig. II.6./1

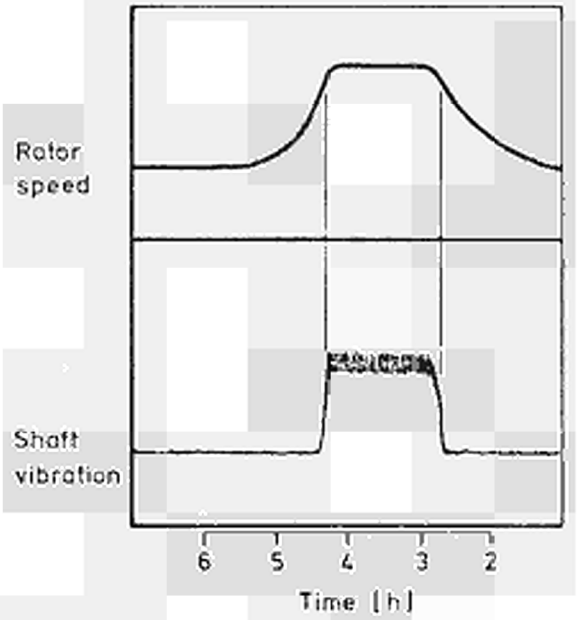

Fig. II.6/2

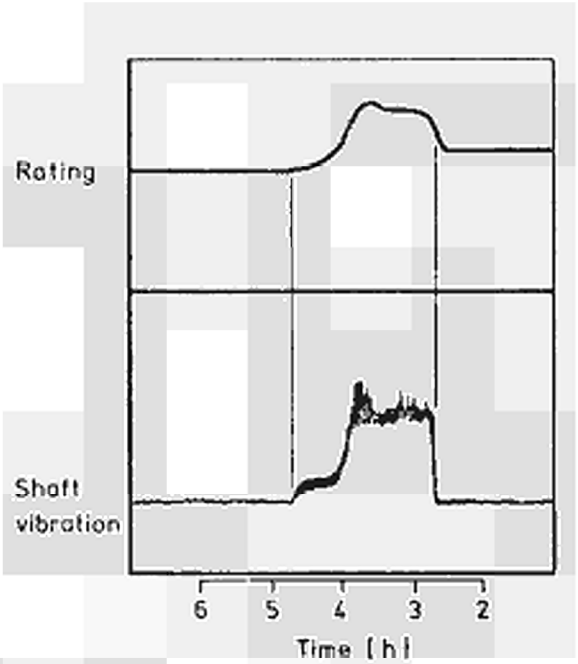

Fig. II.6/3

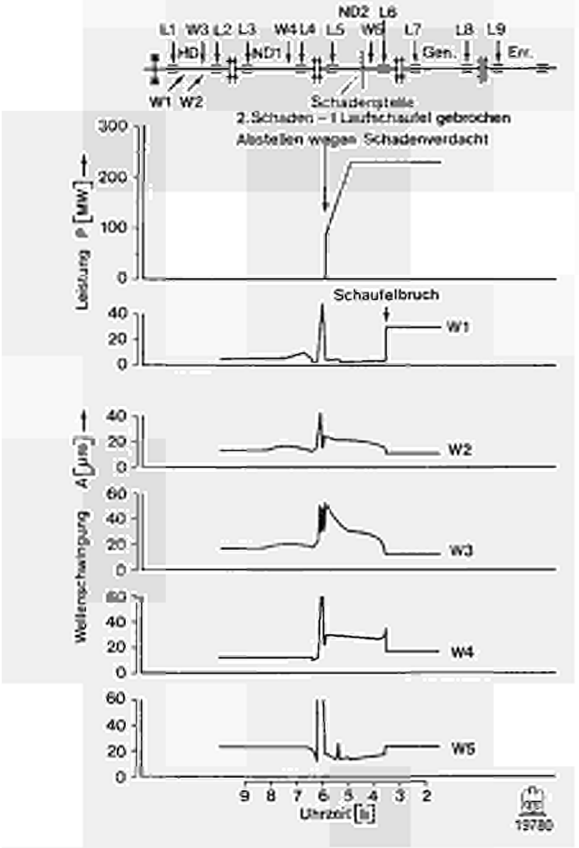

Fig. II.6/4

Schadenstelle ≙ Damage location

2. Schaden - 1 Laufschaufel gebrochen ≙ 2. Damage - 1 blade fractured

Abstellen wegen Schadenverdacht ≙ Shut-down due to suspected damage

Schaufelbruch ≙ Blade fracture

Uhrzeit ≙ Time

Wellenschwingung ≙ Shaft vibration

Leistung ≙ Rating

Vergleich der 5o Hz-Amplituden an Meßebene HD vorne horizontal und vertikal bei 29o MW

Comparison of 5o Hz amplitudes on measuring plane HP front horizontal and vertical at 29o MW

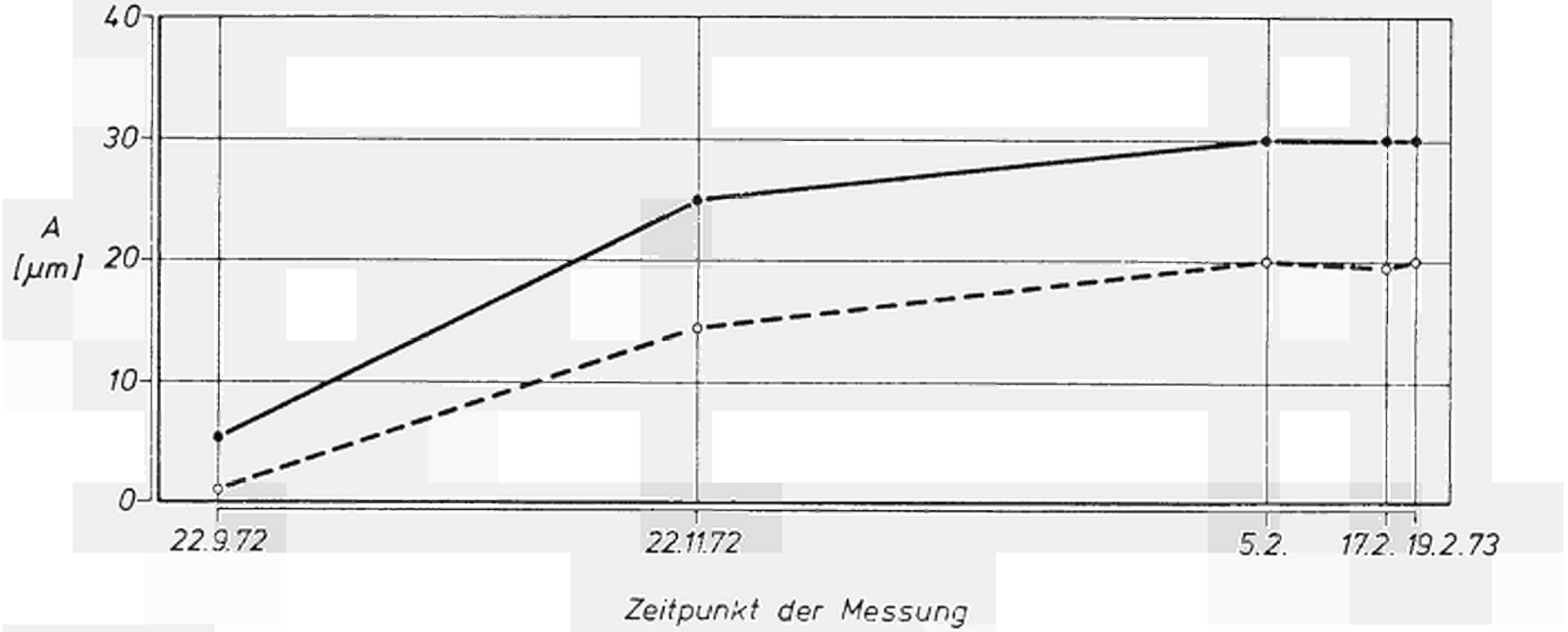

Fig. II.6/5

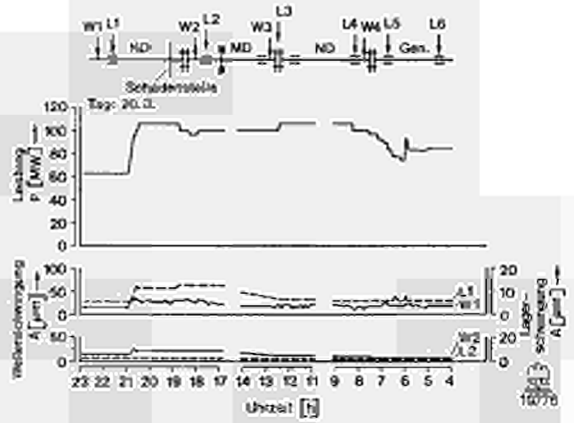

Schwingungsverhalten fünf Tage vor dem Abstellen der Turbine wegen Wellenanriß. (Dia-Nr.: 2.3.0./10)

Fig. II.6/6

Schwingungsverhalten fünf Tage vor dem Abstellen der Turbine wegen Wellenanriß ≙ Vibration behaviour five days befor shut-down of the turbine due to shaft crack

Schadenstelle ≙ Damage location

Tag: 2o.3. ≙ Date: 2o.3.

Uhrzeit ≙ Time

Wellenschwingung ≙ Shaft vibration

Leistung ≙ Rating

Lagerschwingung ≙ Bearing vibration

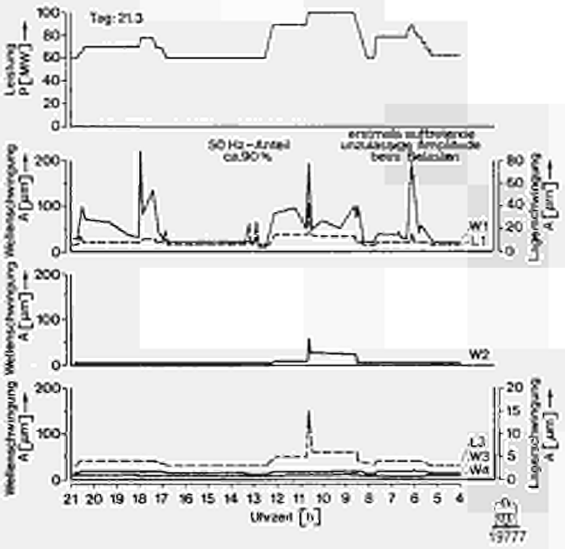

Schwingungsverhalten bei Wellenanriß am Betriebstage vor dem endgültigen Abstellen einer Turbine. (Dia-Nr.: 2.3.0./11)

Fig. II.6/7

Schwingungsverhalten bei Wellenanriß am Betriebstage vor dem endgültigen Abstellen einer Turbine ≙ Vibration behaviour in the case of shaft crack on the day before final shut-down of a turbine

Tag: 21.3. ≙ Date: 21.3.

5o Hz-Anteil ca. 9o % ≙ 5o Hz share approx. 9o %

Erstmals auftretende unzulässige Amplitude beim Belasten ≙ Initial occurrence of undue amplitude under load

Uhrzeit ≙ Time

Wellenschwingung ≙ Shaft vibration

Leistung ≙ Rating

Lagerschwingung ≙ Bearing vibration

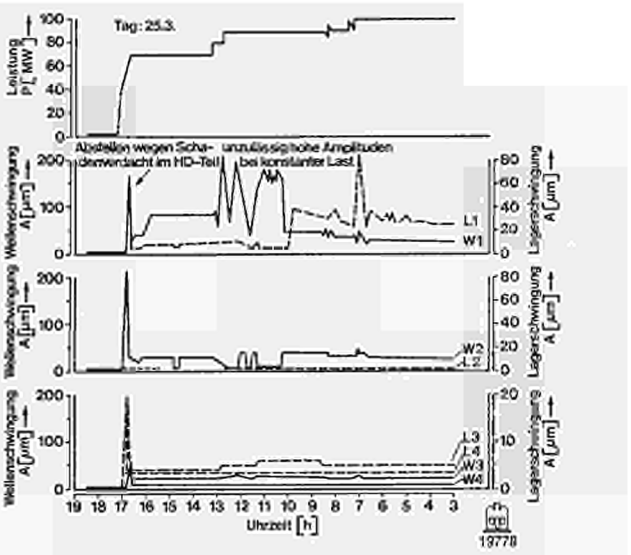

Schwingungsverhalten bei weit fortgeschrittenem Wellenanriß.
(Dia-Nr.: 2.3.0./12)

Fig. II.6/8

Schwingungsverhalten bei weit fortgeschrittenem Wellenanriß ≙ Vibration behaviour in the case of advanced shaft crack

Tag: 25.3. ≙ Date: 25.3.

Abstellen wegen Schadenverdacht im HD-Teil ≙ Shut-down due to auspected damage in HP stage

Unzulässig hohe Amplituden bei konstanter Last ≙ Undue amplitudes at constant load

Uhrzeit ≙ Time

Wellenschwingung ≙ Shaft vibration

Leistung ≙ Rating

Lagerschwingung ≙ Bearing vibration

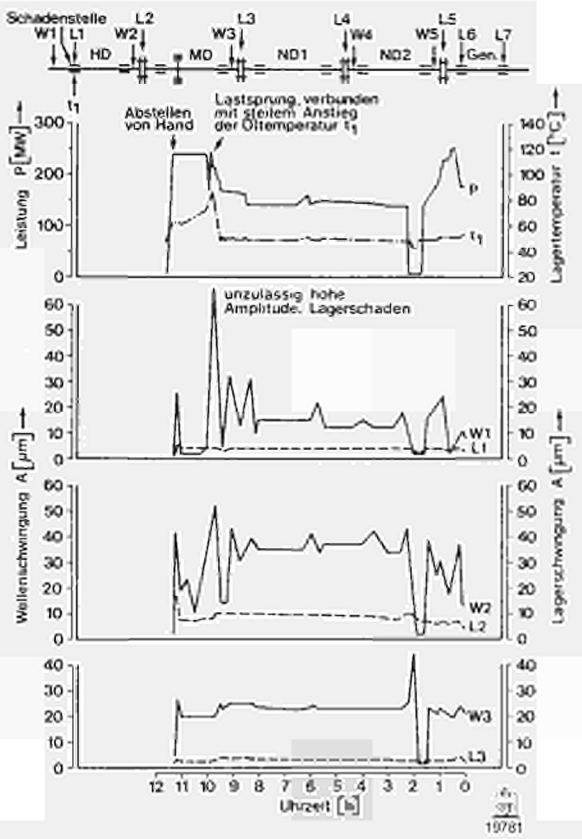

Schwingungsverhalten bei einem Schaden an einem Radiallager. (Dia-Nr.: 2 3.0./06)

Fig. II.6/9

Schwingungsverhalten bei einem Schaden an einem Radiallager ≙ Vibration behaviour in the case of damage to a radial bearing

Schadenstelle ≙ Damage location

Abstellen von Hand ≙ Manual shut-down

Lastsprung, verbunden mit steilem Anstieg der Öltemperatur ≙ Load jump with steep increase in oil temperature

Unzulässig hohe Amplitude, Lagerschaden ≙ Unduly high amplitude, bearing damage

Uhrzeit ≙ Time

Wellenschwingung ≙ Shaft vibration

Leistung ≙ Rating

Lagerschwingung ≙ Bearing vibration

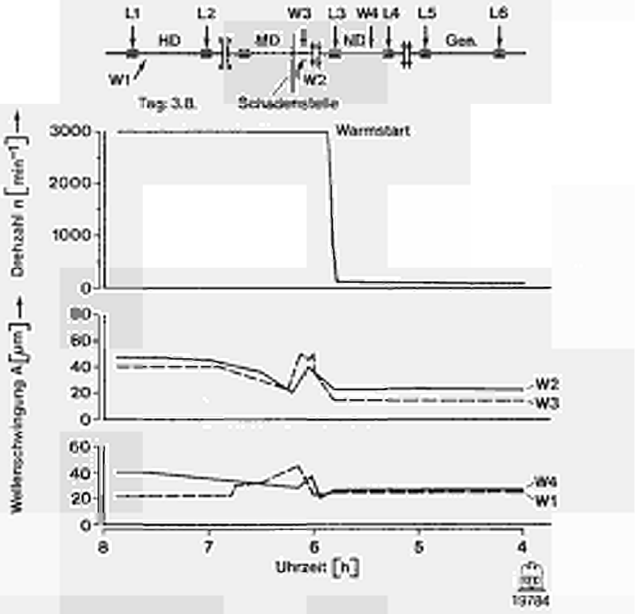

Schwingungsverhalten bei Warmstart, 24 Stunden vor dem Auftreten eines Anstreifschadens. (Dia-Nr.: 2 3 0 /04)

Fig. II.6/1o

Schwingungsverhalten bei Warmstart, 24 Stunden vor dem Auftreten eines Anstreifschadens ≙ Vibration behaviour during warm start-up, 24 hours before the occurrence of rubbing damage

Tag: 3.8. ≙ Date: 3.8.

Schadenstelle ≙ Damage location

Warmstart ≙ Warm start-up

Uhrzeit ≙ Time

Wellenschwingung ≙ Shaft vibration

Drehzahl ≙ Speed

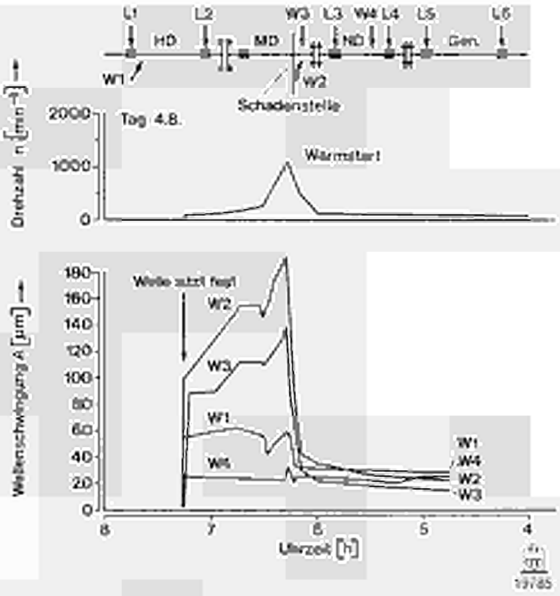

Schwingungsverhalten bei Warmstart mit Anstreifschaden im MD-Teil. (Dia-Nr. 2.3.9.-05)

Fig. II.6/11

Schwingungsverhalten bei Warmstart mit Anstreifschaden im MD-Teil ≙ Vibration behaviour during warm start-up with rubbing damage in the MP stage

Tag: 4.8. ≙ Date: 4.8.

Schadenstelle ≙ Damage location

Warmstart ≙ Warm start-up

Welle sitzt fest ≙ Shaft stuck

Uhrzeit ≙ Time

Wellenschwingung ≙ Shaft vibration

Drehzahl ≙ Speed

NOTICE TO THE READER

All scientific and technical reports published by the Commission of the European Communities are announced in the monthly periodical **"euro-abstracts".** For subscription (1 year : B.Fr 1 025,—) or free specimen copies please write to :

Office for Official Publications
of the European Communities
Boîte postale 1003
Luxembourg
(Grand-Duchy of Luxembourg)

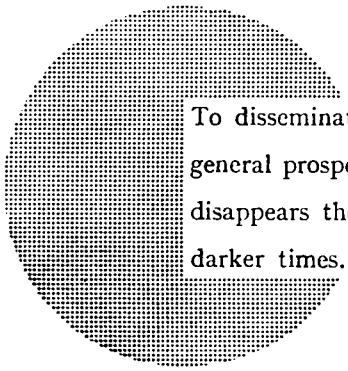

To disseminate knowledge is to disseminate prosperity — I mean general prosperity and not individual riches — and with prosperity disappears the greater part of the evil which is our heritage from darker times.

Alfred Nobel

SALES OFFICES

The Office for Official Publications sells all documents published by the Commission of the European Communities at the addresses listed below, at the price given on cover. When ordering, specify clearly the exact reference and the title of the document.

UNITED KINGDOM

H.M. Stationery Office
P.O. Box 569
London S.E. 1 — Tel. 01-928 69 77. ext. 365

BELGIUM

Moniteur belge — Belgisch Staatsblad
Rue de Louvain 40-42 — Leuvenseweg 40-42
1000 Bruxelles — 1000 Brussel — Tel. 512 00 26
CCP 50-80 — Postgiro 50-80

Agency :
Librairie européenne — Europese Boekhandel
Rue de la Loi 244 — Wetstraat 244
1049 Bruxelles — 1049 Brussel

DENMARK

J.H. Schultz — Boghandel
Møntergade 19
DK 1116 København K — Tel. 14 11 95

FRANCE

Service de vente en France des publications des Communautés européennes — Journal officiel
26, rue Desaix — 75 732 Paris - Cédex 15e
Tel. (1) 306 51 00 — CCP Paris 23-96

GERMANY (FR)

Verlag Bundesanzeiger
5 Köln 1 — Postfach 108 006
Tel. (0221) 21 03 48
Telex: Anzeiger Bonn 08 882 595
Postscheckkonto 834 00 Köln

GRAND DUCHY OF LUXEMBOURG

Office for Official Publications of the European Communities
Boîte postale 1003 — Luxembourg
Tel. 4 79 41 — CCP 191-90
Compte courant bancaire: BIL 8-109/6003/200

IRELAND

Stationery Office — The Controller
Beggar's Bush
Dublin 4 — Tel. 76 54 01

ITALY

Libreria dello Stato
Piazza G. Verdi 10
00198 Roma — Tel. (6) 85 08
CCP 1/2640

NETHERLANDS

Staatsdrukkerij- en uitgeverijbedrijf
Christoffel Plantijnstraat
's-Gravenhage — Tel. (070) 81 45 11
Postgiro 42 53 00

UNITED STATES OF AMERICA

European Community Information Service
2100 M Street, N.W.
Suite 707
Washington, D.C. 20 037 — Tel. 296 51 31

SWITZERLAND

Librairie Payot
6, rue Grenus
1211 Genève — Tel. 31 89 50
CCP 12-236 Genève

SWEDEN

Librairie C.E. Fritze
2, Fredsgatan
Stockholm 16
Post Giro 193, Bank Giro 73/4015

SPAIN

Libreria Mundi-Prensa
Castelló 37
Madrid 1 — Tel. 275 51 31

OTHER COUNTRIES

Office for Official Publications of the European Communities
Boîte postale 1003 — Luxembourg
Tel. 4 79 41 — CCP 191-90
Compte courant bancaire: BIL 8-109/6003/300

OFFICE FOR OFFICIAL PUBLICATIONS OF THE EUROPEAN COMMUNITIES
Boîte postale 1003 — Luxembourg 6790

CDNA05294ENC